

**DISASTER RISK ASSESSMENT AND ROCK MASS
CHARACTERIZATION OF STATE HIGHWAY FROM
CHAMPHAI TO ZOKHAWTHAR, CHAMPHAI DISTRICT,
MIZORAM**

**A THESIS SUBMITTED IN PARTIAL FULFILLMENT OF THE
REQUIREMENTS FOR THE DEGREE OF DOCTOR OF
PHILOSOPHY**

LALLAWMSANGA

MZU REGISTRATION NO.: 2100107

Ph.D. REGISTRATION NO.: MZU/Ph.D./1889 of 19.08.2021



**CENTRE FOR DISASTER MANAGEMENT
SCHOOL OF EARTH SCIENCES AND NATURAL RESOURCES
MANAGEMENT**

JUNE, 2025

**DISASTER RISK ASSESSMENT AND ROCK MASS
CHARACTERIZATION OF STATE HIGHWAY FROM
CHAMPHAI TO ZOKHAWTHAR, CHAMPHAI DISTRICT,
MIZORAM**

By

LALLAWMSANGA
CENTRE FOR DISASTER MANAGEMENT

NAME OF SUPERVISOR

Dr. LALDINPUIA

Submitted

In partial fulfillment of the requirement of the Degree of Doctor of
Philosophy in Disaster Management of Mizoram University, Aizawl

CENTRE FOR DISASTER MANAGEMENT
SCHOOL OF EARTH SCIENCES AND NATURAL RESOURCES
MANAGEMENT



MIZORAM

UNIVERSITY

SUPERVISOR'S CERTIFICATE

This is to certify that **Lallawmsanga**, a Ph.D. scholar having MZU Registration No. **2100107** and Ph.D. Registration No. **MZU/Ph.D./1889 of 19.08.2021** has completed a thesis entitled **“Disaster Risk Assessment and Rock Mass Characterization of State Highway from Champhai to Zokhawthar, Champhai District, Mizoram”** under my supervision and the same has been submitted to the Mizoram University, Aizawl, Mizoram, for the degree of Doctor of Philosophy.

To the best of our knowledge, this thesis as a whole has not been submitted earlier to any other institution for any degree.

(Dr. LALDINPUIA)

Supervisor

CENTRE FOR DISASTER MANAGEMENT
SCHOOL OF EARTH SCIENCES AND NATURAL RESOURCES
MANAGEMENT



MIZORAM

UNIVERSITY

DECLARATION

I, **Lallawmsanga**, hereby declare that the subject matter of this thesis is the record of work done by me, that the contents of this thesis did not form basis of the award of any previous degree to me or to do the best of my knowledge to anybody else, and that the thesis has not been submitted by me for any research degree in any other University/Institute.

This is being submitted to the Mizoram University for the Degree of Doctor of Philosophy in Disaster Management.

(LALLAWMSANGA)

(Prof. BENJAMIN L. SAITLUANGA)

(Dr. LALDINPUIA)

Head

Supervisor

ACKNOWLEDGEMENT

I express my sincere gratitude to the almighty God for providing me the opportunity and bestowing upon me the capability to proceed successfully with this thesis entitled “Disaster Risk Assessment and Rock Mass Characterization of State Highway from Champhai to Zokhawthar, Champhai District, Mizoram” and all his blessings for giving me good health and precious time.

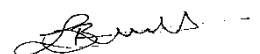
I am heartily thankful to all the Departmental Research Committee, Department of Geography and Resource Management, Mizoram University for accepting my research work.

I express my sincere gratitude to my Supervisor Dr. Laldinpuia, Associate Professor, Centre for Disaster Management, Mizoram University. This thesis would not have been completed without his guidance.

I extend my sincere gratitude to Lalremruati, Zosangliana Ralte, Lalhmingsangi, Benjamin Roluahpuia, Lalramngheta and K. Zoramthanga who in one way or another contributed their valuable assistance in the preparation and completion of this study.

I sincerely thank the Department of Geology, Pachhunga University College for generously allowing me to use their Geotechnical Laboratory without charge. I sincerely thank the Centre for Disaster Management, Mizoram University for allowing me to conduct my research under their esteemed institution. I extend my sincere gratitude to the DST-SHRI Project (DST/TDT/SHRI-19/2021) for support in carrying out this research.

I render my sincere thanks to my lovely parents Pu Lalnghakliana and Pi Lalthapuii, and my siblings Malsawmzuali and Vanlaldampaia for their unconditional love and support. I thank them for inculcating me the dedication, and discipline and for being the foundation of this achievement.



(LALLAWMSANGA)

TABLE OF CONTENTS

CHAPTER	PAGES
SUPERVISOR CERTIFICATE	i
DECLARATION	ii
ACKNOWLEDGEMENTS	iii
TABLE OF CONTENTS	iv
LIST OF FIGURES	viii
LIST OF TABLES	xiii
LIST OF EQUATIONS	xvi
LIST OF ABBREVIATIONS	xvii

CHAPTER 1	INTRODUCTION		1-23
	1.1	General Introduction	1
	1.2	Climate and Rainfall	6
	1.3	Geology of Mizoram	7
		1.3.1 Regional Geology	7
		1.3.2 Barail Group	10
		1.3.3 Surma Group	11
		1.3.4 Tipam Group	12
	1.4	History of the Study Area	15
	1.5	Location and Accessibility of the Study Area	18
	1.6	Scope of the research	21
	1.7	Objective of the research	23
CHAPTER 2	METHODOLOGY		24-55
	2.1	Atterberg Limit Test	24
		2.1.1 Soil Sampling	25
		2.1.2 Natural Moisture Content (NMC)	25
		2.1.3 Liquid Limit	26
		2.1.4 Plastic Limit	28
		2.1.5 Plasticity Index (P.I.)	29
		2.1.6 Liquidity Index (L.I.)	29
		2.1.7 Consistency Index (C.I.)	30
	2.2	Proctor Compaction Test	30
	2.3	Direct Shear Test	32
	2.4	Slake Durability Test (S.D.I.)	33
	2.5	Limit Equilibrium Method (L.E.M.)	35
	2.6	Rock Mass Rating (R.M.R.)	36
		2.6.1 Uniaxial Compressive Strength (U.C.S.)	37

		2.6.2	Rock Quality Designation (R.Q.D.)	38
		2.6.3	Condition of Discontinuities	39
		2.6.4	Joint Spacing	39
		2.6.5	Groundwater Condition	40
	2.7	Geological Strength Index (G.S.I.)		44
	2.8	Kinematic Analysis		46
		2.8.1	Slope Geometry and Failure Surfaces	46
		2.8.2	Block Analysis	47
		2.8.3	Discontinuity Characterization	47
		2.8.4	Block Movement Assessment	47
		2.8.5	Risk Assessment and Mitigation Measures	47
	2.9	Slope Mass Rating (S.M.R.)		48
2.10	Rockfall Hazard Rating System		50	
2.11	Analysis of Rainfall		53	
CHAPTER 3	LITERATURE REVIEW			55-71
CHAPTER 4	RESULTS AND DISCUSSIONS			72-176
	4.1	Field Observations		72
	4.2	Determination of Atterberg Limit		78
		4.2.1	Natural Moisture Content (NMC)	78
		4.2.2	Liquid Limit	79
		4.2.3	Plastic Limit	83
		4.2.4	Plasticity Index	84
		4.2.5	Liquidity Index (L.I.) and Consistency Index (C.I.)	85
	4.3	Analysis using Proctor Compaction		86
	4.4	Direct Shear Test		92
	4.5	Analysis of Slope Stability using Limit Equilibrium Method (L.E.M.)		97

		4.5.1	LS1	98
		4.5.2	LS2	103
		4.5.3	LS3	109
		4.5.4	LS4	114
		4.5.5	LS5	119
		4.5.6	LS6	124
	4.6	Slake Durability Test		131
	4.7	Rock Mass Rating (R.M.R.) Method		131
	4.8	Determination of Geological Strength Index (G.S.I.)		133
	4.9	Kinematic Analysis		136
	4.10	Determination of Slope Mass Rating (S.M.R.)		140
	4.11	Rockfall Hazard Rating		142
		4.11.1	Numerical Simulation	149
		4.11.2	Bounce Height and Run-out Distance	157
		4.11.3	Total Kinetic Energy and Translational Energy	158
	4.12	Analysis of Champhai District Rainfall Data		160
	4.13	Hazard Zonation		164
4.14	Discussions		166	
CHAPTER 5	CONCLUSION AND RECOMMENDATIONS			166-1
	5.1	Conclusion		169
	5.2	Mitigation Suggesstions		171
	5.3	Limitations		174
APPENDICES	Photographs – Field and laboratory			177-186
REFERENCES				187-210
BRIEF BIO-DATA				211-214
PARTICULARS OF THE CANDIDATE				215

LIST OF FIGURES

Fig. No.	Title of Figures	Page
1.1	Geological Map of Mizoram	14
1.2	Map showing Champhai to Zokhawthar road and realignment	16
1.3	Landslides in three different locations	16
1.4	Location Map of the Study Area	20
2.1	Flowchart of Atterberg Limit Test	25
2.2	G.S.I. Chart	45
4.1	Collapsed Road and Landslides	74
4.2	Landslide along the Road	74
4.3	Road and Retaining Wall Collapsed	75
4.4	Slope Failure	75
4.5	Collapsed Retaining Wall	76
4.6	Bedding Plane	77
4.7	Road Subsidence	77
4.8	Liquid Limit of LS1	80
4.9	Liquid Limit of LS2	81
4.10	Liquid Limit of LS3	81
4.11	Liquid Limit of LS4	82
4.12	Liquid Limit of LS5	82
4.13	Liquid Limit of LS6	83
4.14	Moisture Content Vs. Dry Density for LS1	87

4.15	Moisture Content Vs. Dry Density for LS2	88
4.16	Moisture Content Vs. Dry Density for LS3	89
4.17	Moisture Content Vs. Dry Density for LS4	90
4.18	Moisture Content Vs. Dry Density for LS5	91
4.19	Moisture Content Vs. Dry Density for LS6	92
4.20	Shear Stress at Failure for LS1	94
4.21	Shear Stress at Failure for LS2	94
4.22	Shear Stress at Failure for LS3	95
4.23	Shear Stress at Failure for LS4	95
4.24	Shear Stress at Failure for LS5	96
4.25	Shear Stress at Failure for LS6	96
4.26	Field Photographs of LS1	98-99
4.27	GLE/ Morgenstern-Price method of LEM Analysis for LS1	100
4.28	Janbu Simplified method of LEM Analysis for LS1	101
4.29	Bishop Simplified of LEM Analysis for LS1	102
4.30	Ordinary/ Fellenius method of LEM Analysis for LS1	103
4.31	Field Photographs of LS2	104-105
4.32	GLE/ Morgenstern-Price method of LEM Analysis for LS2	106
4.33	Janbu Simplified method of LEM Analysis for LS2	107
4.34	Bishop Simplified of LEM Analysis for LS2	108
4.35	Ordinary/ Fellenius method of LEM Analysis for LS2	109
4.36	Field Photographs of LS3	110

4.37	GLE/ Morgenstern-Price method of LEM Analysis for LS3	111
4.38	Janbu Simplified method of LEM Analysis for LS3	112
4.39	Bishop Simplified of LEM Analysis for LS3	113
4.40	Ordinary/ Fellenius method of LEM Analysis for LS3	114
4.41	Field Photographs of LS4	115
4.42	GLE/ Morgenstern-Price method of LEM Analysis for LS4	116
4.43	Janbu Simplified method of LEM Analysis for LS4	117
4.44	Bishop Simplified of LEM Analysis for LS4	118
4.45	Ordinary/ Fellenius method of LEM Analysis for LS4	119
4.46	Field Photographs of LS5	120
4.47	GLE/ Morgenstern-Price method of LEM Analysis for LS5	121
4.48	Janbu Simplified method of LEM Analysis for LS5	122
4.49	Bishop Simplified of LEM Analysis for LS5	123
4.50	Ordinary/ Fellenius method of LEM Analysis for LS5	124
4.51	Field Photographs of LS6	125
4.52	GLE/ Morgenstern-Price method of LEM Analysis for LS6	126
4.53	Janbu Simplified method of LEM Analysis for LS6	127
4.54	Bishop Simplified of LEM Analysis for LS6	128
4.55	Ordinary/ Fellenius method of LEM Analysis for LS6	129
4.56	LEM Analyses using different methods	130
4.57	G.S.I. Rating for each study sites	135
4.58	Stereographic Projection showing the potential for direct toppling	137

	failure at S1	
4.59	Stereographic Projection showing the potential for direct toppling failure at S2	137
4.60	Stereographic Projection showing the potential for wedge failure at S3	138
4.61	Stereographic Projection showing the potential for direct toppling failure at S4	138
4.62	Stereographic Projection showing the potential for wedge failure at S5	139
4.63	Stereographic Projection showing the potential for wedge failure at S6	139
4.64	Stereographic Projection showing the potential for wedge failure at S7	140
4.65	Field Photographs	147-149
4.66	Simulation of Rockfall trajectories detached from R1	151
4.67	Simulation of Rockfall trajectories detached from R2	152
4.68	Simulation of Rockfall trajectories detached from R3	153
4.69	Simulation of Rockfall trajectories detached from R4	154
4.70	Simulation of Rockfall trajectories detached from R5	155
4.71	Simulation of Rockfall trajectories detached from R6	156
4.72	Bouncing Height obtained from falling rocks after hitting the ground for each Slopes	157
4.73	Kinetic Energy obtained from falling rocks for each Slopes	158
4.74	Translational Velocity obtained from falling rocks for each Slopes	159

4.75	Monthly Rainfall of Chmphai District in 2021	160
4.76	Daily rainfall data of Champhai District in 2021	163
4.77	Hazard Zonation Map of study sites	165

LIST OF TABLES

Table No.	Title of Tables	Page
1.1	Generalized Geological Succession in Mizoram	9
1.2	Stratigraphic succession of Surma basin	11
2.1	Datasheet for determining Natural Moisture Content (NMC)	26
2.2	Datasheet for Liquid Limit	28
2.3	Datasheet for Plastic Limit	29
2.4	Datasheet for Proctor Compaction Test	31
2.5	Datasheet for Direct Shear Test	33
2.6	Datasheet for Cohesion and Angle of Friction	33
2.7	Sub-Division of Slake-Durability Scale	35
2.8	Ratings for Uniaxia Compressive Sttrength of Rockmass	37
2.9	R.Q.D. classification and rating	38
2.10	Classification of Volumetric Joint Count (Jv)	38
2.11	Joint Separation and Rating	39
2.12	Discontinuity Spacing Classification	40
2.13	Ground Water Condition and Rating	40
2.14	R.M.R. Classification on the characteristics of rock mass	41
2.15	Slope Mass Rating Adjustment Factor	48
2.16	Rockfall Hazard Rating System of India	51
4.1	Sampling sites and slopes under investigations for rock mass characterization	73

4.2	Calculations for Natural Moisture Content (NMC)	78
4.3	Calculations of liquid limit for each soil sample	79
4.4	Results of plastic limits for each soil sample	83
4.5	Plasticity index for different location	84
4.6	Liquidity Index and Consistency Index and their classification	85
4.7	Standard Proctor Test for LS1	86
4.8	Standard Proctor Test for LS2	87
4.9	Standard Proctor Test for LS3	88
4.10	Standard Proctor Test for LS4	89
4.11	Standard Proctor Test for LS5	90
4.12	Standard Proctor Test for LS6	91
4.13	Direct shear test value for each location	92
4.14	Input Parameters of soil properties for different study sites	97
4.15	Factor of Safety for each study site	130
4.16	Slake Durability Index for each cycle	131
4.17	Rock Mass Rating for different locations	132
4.18	RMR Classification for different selected locations of slopes	133
4.19	GSI Rating based on Structural Rating and Surface Condition Rating	134
4.20	Rock attitudes for kinematic analysis	136
4.21	Slope Mass Rating for each location	140
4.22	Detailed Scoring of Rockfall Hazard Rating System for Slope	143

4.23	Detailed Scoring of Rockfall Hazard Rating System for Climate	143
4.24	Detailed Scoring of Rockfall Hazard Rating System for Geology (Sedimentary Rock)	144
4.25	Detailed Scoring of Rockfall Hazard Rating System for Traffic	145
4.26	Detailed Scoring of Rockfall Hazard Rating System for Rock History/ Frequency	146
4.27	Cumulative Score for Rockfall Hazard Rating System	146
4.28	Coefficient of Restitution for surface type	150
4.29	Champhai District Rainfall (in mm) in 2021	160
4.30	Rainfall data of Champhai District in 2021	162
4.31	Remedial Measures based on field observations and laboratory analyses	172

LIST OF EQUATIONS

Eqn. No.	Equation
2.1	$W = \{(W2 - W3) / (W3 - W1)\} \times 100$
2.2	$P.I. = L.L. - P.L.$
2.3	$\frac{\text{Natural moisture content of the soil} - \text{Plastic limit of the soil}}{\text{Plasticity Index of the soil}}$
2.4	$CI = (LL - W) / (LL - PL)$
2.5	$\gamma_{wet} = (M2 - M1) / V$
2.6	$\gamma_d = (100 \gamma_{wet}) / (100 + w)$
2.7	$Id1 = \frac{B - D}{A - D} 100$
2.8	$Id2 = \frac{C - D}{A - D} 100$
2.9	$FOS = \frac{\Sigma \text{Resisting forces}}{\Sigma \text{Driving forces}}$
2.10	$R.Q.D. = 115 - 3.3 J_v \text{ (For flat and long blocks)}$
2.11	$R.Q.D. = 110 - 2.5 J_v \text{ (For cubic shaped blocks)}$
2.12	$SR = -17.5 \ln (J_v) + 79.8$
2.13	$SCR = R_r + R_w + R_l$
2.14	$SMR = RMR_B + F1.F2.F3 + F4$

LIST OF ABBREVIATIONS

ADT	Average Daily Traffic
AVR	Average Vehicle Risk
CI	Consistency Index
COR	Coefficient of Restitution
DSD	Decision Sight Distance
et al.	Et alia (and others)
GSI	Geological Strength Index
G.S.I.	Geological Survey of India
IS	Indian Standard
Jv	Volumetric Joint Count
LL	Liquid Limit
LS	Lawmsanga (<i>Study sites named after candidate</i>)
NMC	Natural Moisture Content
PL	Plastic Limit
PI	Plasticity Index
PWD	Public Works Department
RMR	Rock Mass Rating
R	Rockfall
RQD	Rock Quality Designation
SMR	Slope Mass Rating
SDI	Slake Durability Index

CHAPTER 1

INTRODUCTION

1.1. GENERAL INTRODUCTION

Disasters interrupt the daily routines of affected communities and halt developmental initiatives, as funds intended for new projects are diverted to response, relief, and rehabilitation activities (Collins, 2018; Ray et al., 2021). A comprehensive and proactive risk management approach includes both risk assessment and risk evaluation (Aven, 2015). It encompasses risk identification, risk reduction, and risk transfer (Rodriguez et al., 2018). Technically, a hazard does not become a disaster until it is triggered by a natural or human-made agent (Kumar & Srivastava, 2022). Experts in engineering and management estimate the probability of a disaster occurring and the potential losses using the technical concept of risk (Munier, 2014; Saulnier et al., 2020; Omidvar & Shirazi, 2023; Inan et al., 2023). While the term "risk" is sometimes used synonymously with "hazard," risk more accurately refers to the likelihood of a particular hazard occurring (Zakaria, 2009). Risk is often generated by the excessive use of resources, leading to significant environmental degradation (Saulnier et al., 2020; Kaiser, 2021).

Disaster risk refers to the likelihood of a community experiencing losses in terms of people, property, and essential services (Perry, 2018). Such losses may occur when complex conditions interact with human-made or natural hazards (Rahman, 2022). Risk assessment involves determining the probability that these interactions will result in negative consequences (Zakaria, 2009; Inan et al., 2023).

Risk assessment is the process of identifying the type and magnitude of risk by examining potential hazards and evaluating existing vulnerabilities (Bobrowsky, 2013; Rovins et al., 2015). These risks may endanger people, their livelihoods, and the environment upon which they depend (Zakaria, 2009; Rovins et al., 2015). Risk

evaluation involves analyzing the effectiveness of proposed risk reduction strategies from a cost-efficiency perspective (Cardona et al., 2012; Jespen, 2016). Hazard, exposure, and susceptibility are considered key factors that influence disaster risk (Olusegun, 2024; Cardona et al., 2012; Dar & Alam, 2020).

A hazard is a potential threat—an activity, process, or phenomenon—that has the capacity to harm people, communities, and the environment (White, 1973; UNDRO, 1980; Cardona et al., 2012). A hazard becomes a disaster when a natural event with destructive potential is actualized, resulting in significant damage to property and loss of human life (UNDDR & Dadvar, 2020). A disaster occurs when a hazard interacts with a vulnerable situation within a community or human settlement (Basyah et al., 2023).

Disasters cause severe harm to individuals and result in significant losses of infrastructure and human life (Sahrif, 2020; Khan et al., 2023). They disrupt everyday life, throwing social systems out of equilibrium and severely affecting regulatory and developmental governance practices (Schlitz et al., 2023). The economic, social, and psychological impacts of disasters also negatively affect the surrounding environment (Arcaya et al., 2020). A disaster is a hazard that escalates into a catastrophe in response to a triggering stimulus, whether natural or human-made (Singh, 2020; Rahman, 2022).

A landslide is the rapid flow of Earth's materials down a slope—whether rock, soil, plant matter, debris, or a combination of these—caused by gravity and triggered by natural forces, human activities, or both (Cruden & Varnes, 1996; Nemčok et al., 1972; Varnes, 1954; Geertsema et al., 2009; Turner, 2018; Anbalagan et al., 2015). A stable slope is a condition in which all slope-forming materials remain undisturbed and experience no displacement (Chaudhary et al., 2010). A slope is considered stable when the inclined rock mass or soil can withstand the tendency for downward movement (Laldinpuia et al., 2013).

Under the influence of gravity, the soil beneath a slope tends to move outward or downhill (Gutiérrez & Gutiérrez, 2016). The slope remains stable if the shear strength of the soil is sufficient to resist this movement; otherwise, a landslide occurs (Kumar et al., 2020; Tiwari & Ajmera, 2023).

Over time, various classification systems for landslides have been developed, considering factors such as the type and nature of deposits, the age of the deposits, the shape of the sliding surface, the mode and speed of movement, and external triggers like precipitation (Li & Mo, 2019; Bin Masood & Yuzuak, 2021; Laldinpuia, 2013, 2019). The major types of landslides include falls, topples, slides, lateral spreads, flows, and complex movements (Sarkar et al., 2012; Hungr et al., 2014). Landslides are commonly classified based on the materials involved, such as earth, soil, rock, or debris.

Different types of landslides move at varying rates. Flows tend to move faster, whereas slides generally move more slowly (Cruden, 2013). Falls and topples occur almost instantly and are typically associated with cliffs or steep slopes (Gutiérrez & Gutiérrez, 2016). The rate of movement during slope failure is primarily determined by the type of slope-forming material and the nature of the slip surface (Gajamer & Kumar, 2023; Asthana & Sah, 2007; Bhambri et al., 2017). For slopes composed of brittle materials, the movement may accelerate significantly when ground stresses exceed the strain at which peak ground strength occurs (Nichol et al., 2011; Hoeg, 2013). Slope-forming materials, including clays, may experience almost complete strength loss when remolded, increasing their susceptibility to slope failure (Thakur et al., 2017).

Human activities and rainfall are the primary triggers for landslides in Mizoram. Inadequate consideration of slope characteristics, material properties, and other contributing factors account for most landslide hazards (Alcantara-Ayala & Sassa, 2023). The design of stable slope angles, especially where deep cuts are involved, is rarely based on comprehensive stability analysis (Dinpuia, 2019; Kumar et al., 2022). However, with careful design and proper planning, these issues can be

mitigated or even prevented, and appropriate precautions can be taken to maintain slope stability (Alcantara et al., 2023; Munier, 2014; Rovins et al., 2015).

A rockfall is one of the most damaging natural events in mountainous terrain, significantly affecting slope stability (Ansari et al., 2016). A rockfall can result from toppling, sliding, wedging, or falling, and involves a fragment of rock or block detaching from the slope. It then falls vertically or sub-vertically, rolling down a debris slope or bouncing along various trajectories (Ansari et al., 2013; Sissakian et al., 2021). These rock fragments can vary in size, ranging from small pieces to massive blocks spanning several cubic meters.

The initial evidence of a fall is the separation of rock from an upward slope along a surface where little to no shear displacement has occurred (Verma et al., 2018). The material typically falls by bouncing, rolling, or dropping. Rockfalls occur when rock, soil, or both break from cliff walls or steep slopes. Bouncing usually happens when falling fragments hit the lower slope at angles less than the angle of descent (Ansari et al., 2016). The falling mass may begin to roll when it reaches a steeper slope, continuing to roll until the ground flattens. If not, it may shatter upon impact.

Due to challenging topographical features, roadways in hilly areas are often narrower than those in flat regions, which can cause several problems when rockfall occurs. Multiple factors, including lithology, the degree of interbedded rock, the orientation and condition of discontinuities, slope steepness, and other geomechanical properties of the rock mass, contribute to rockfall occurrence (Piteau, 1993). It is well-known that different types of rock and variations in rock composition have different strengths (Cheng et al., 2023). The quality of rock is determined by its geomechanical properties (Aydan et al., 2014). The physical properties of a rock mass can be assessed through both laboratory studies and on-site inspections (Muralha & Lamas, 2022).

Rock mass characterization refers to determining a matrix composed of rock discontinuities and other related attributes (Cai, 2011). This process can be differentiated using analytical, empirical, and numerical methods. Typically, the

empirical method is employed for the final design, as well as for feasibility and pre-design studies (Mirza Rezky et al., 2021). In 1976, Bieniawski developed the Rock Mass Rating (RMR) classification system (Bieniawski, 1976; Abbas, 2015). This system is widely used in geotechnical engineering to assess the quality of rock masses and is considered the most reliable method for classifying them (Hoek & Brown, 1980). The RMR system is based on five key factors: Uniaxial Compressive Strength of intact rock, Rock Quality Designation (RQD), Discontinuity Spacing, Discontinuity Orientation, and Groundwater Condition (Bieniawski, 1976; Lalhlipua et al., 2019; Hong et al., 2020; Zairemmawii et al., 2021). This method integrates all these criteria to produce a numerical rating score, ranging from 0 to 100, which is determined through field observations and laboratory analysis (Soufi et al., 2018; Muralha & Lamas, 2022). The resulting RMR values influence the stability of rock masses—higher values indicate greater stability.

Kinematic analysis is another method used in geotechnical engineering to assess various forms of slope failure (Verma et al., 2018; Sardana et al., 2019). Its primary objective is to analyze the movement or shifting of rock and soil masses along predefined failure surfaces (Stead & Wolter, 2015). The goal of kinematic analysis is to identify potential failure mechanisms. The Rocscience Dips 7.0 software is commonly used to study different types of slope failures, including planar, toppling, and wedge failures.

For the analysis of slope stability using kinematic analysis and rock mass rating, Romana (1985) developed the Slope Mass Rating (SMR) technique. Higher values indicate a more stable slope, with numerical ratings ranging from 1 to 100 used as a score (Kumar & Pandey, 2021; Sarkar et al., 2012; Romana, 1985; Romana et al., 2015). According to Hong et al. (2020), this approach provides a qualitative evaluation and helps predict slope behavior under different scenarios.

In mountainous areas, rockfall is one of the primary risks associated with rock cuttings for roads, highways, and railways (Dahiya et al., 2024). Brawner and Wyllie developed the Rockfall Hazard Rating System for the Canadian Pacific (Ansari et al., 2013; Siddique et al., 2019). It was later modified by Pierson in 1990 and Santi in

2009 for the Indian rockmass, incorporating significant variables (Pierson et al., 1990; Santi et al., 2009; Sarkar et al., 2016). A rockfall can be triggered by physical, chemical, and biological activities. For example, pore pressure may increase due to precipitation infiltrating cracks and pores in the rock mass, leading to chemical degradation of the rock-forming minerals. Physical factors, such as weathering and erosion, can disintegrate rocks, resulting in smaller fragments (Pinho et al., 2017).

The entire sedimentary column of Mizoram State consists of a repetitive succession of arenaceous and argillaceous rocks, including sandstone, silty-sandstone, siltstone, shale, shaly-sandstone, silty-shale, mudstone, and their admixtures in varying proportions, along with irregular pockets of shell-limestone and intra-formational conglomeratic bands (Karunakaran, 1974; Ganju, 1975; Tiwari, 2014). According to Karunakaran (1974) and Ganju (1975), this succession is categorized into three groups: the Tipam Group of Middle-Upper Pliocene age, the Barail of Oligocene age, and the Surma of Miocene-Lower Pliocene age. The Surma group of Bhuban and the Boka Bil formation comprise the majority of the state's lithology (Singh et al., 2010). The Bhuban Formation is subdivided into Lower, Middle, and Upper Bhuban units based on the ratio of argillaceous to arenaceous components, a key lithological feature (Singh et al., 2010; Kesari, 2011; Tiwari, 2014).

1.2. CLIMATE AND RAINFALL

The climate of Mizoram is moderate, with temperatures ranging from 7°C to 20°C during the winter. In the summertime, temperatures typically range between 17°C and 32°C. Aizawl City and its surrounding areas are directly affected by the South-West Monsoon, which brings heavy rainfall from May to September. The rainfall subsides during the autumn months of October and November, with average temperatures ranging between 19°C and 25°C. Mizoram experiences a humid tropical climate with long summers and short winters, owing to the ample annual rainfall of about 2,540 mm. Heavy and prolonged rainfall is a key factor contributing to landslides, resulting in fatalities and property damage.

1.3. GEOLOGY OF MIZORAM

1.3.1. REGIONAL GEOLOGY

The Surma Basin occupies the northeastern part of India, where the younger Tipam Group rests atop the Surma Group, underlain by deposits of the Barail Group (Karunakaran, 1974; Ganju, 1975). The Miocene-age Surma Series, which includes the Bhuban and Boka Bil Formations, is named after the Surma River (Nandy, 1983; Rahman et al., 2014; Jahan et al., 2017). This stratigraphic sequence is particularly well-developed in the Surma Basin. The Surma Valley and the Sylhet Trough essentially form the core of the Surma Basin. It is bounded to the north by the Shillong Massif and the Barail Range, and to the south by the Tripura Fold Belt (Nandy et al., 1983). To the east, it is bordered by the Barail-Manipur Ridge, and to the west, the basin gradually rises toward the Hinge Zone before merging into the Bengal Foredeep in the southwest (Acharyya, 1997; Devi and Mondal, 2008).

Situated in the northeastern part of the Bengal Basin, the Surma Basin spans more than one million square kilometers and remained largely submerged during the Oligocene and Pliocene periods (Jahan et al., 2017; Nandy et al., 1983). The Dauki Fault, a major regional fault running the length of the northern Surma Valley south of the Shillong Massif, is the most significant tectonic structure in the area. It caused the Archean basement to subside to a depth of approximately 18 km in the Surma Valley (Sarkar and Choudhury, 2015). The formation of the Surma Basin was driven by the interaction of two primary tectonic forces: the uplift of the Shillong Massif to the north and the westward-migrating Indo-Burman Fold Belt on the Burmese Plate (Bijoy et al., 2019; Acharyya, 2008; Islam et al., 2021; Borgohain et al., 2020).

Outcrops of various geological units in the region include the Upper Eocene Kopili Shale at Bagali Bazar Lamakata, the Oligocene Barail deposits at Dauki, the Paleocene Tura Sandstone at Jenam/Renji, and the Eocene Limestone at Takerghat, along with exposures in the broader Sylhet district border zones such as Charagaon, Lalghat, Bhangarghat, and Jafflong (Bhattacharya and Gupta, 2005). However, areas like Tamabil, Jaintiapur, and Jafflong remain underdeveloped (Hossain et al., 2010; Alam et al., 2021). In the sub-latitudinal foothills east of Jaintiapur, forming the northern border of the Surma Basin, the Mio-Plio-Pleistocene sequence—including the Bhuban, Boka Bil, Tipam Sandstones, Girujan Clay, Dupi Tila, and Dihing

formations—dips southward (Nandy et al., 1983; Dasgupta, 1984; Baruah and Pandey, 2019; Borgohain et al., 2020; Gazi et al., 2021).

Geologically young, Mizoram is considered the depocenter of the Surma Basin (Karunakaran, 1974; Ganju, 1975). Geographically, it is located at approximately 23°09'52.35"N latitude and 92°56'15.26"E longitude. About 70% of the exposed rock mass in Mizoram belongs to the Bhuban Formation, part of the Mizoram-Tripura Mio-geosyncline basin (Borgohain and Sarmah, 2022). The lithology is characterized by a Cenozoic sedimentary sequence comprising an intercalated succession of arenaceous and argillaceous sediments, formed as a result of the collision between the Indian and Burmese plates. Sandstone and shale—formed during the Tertiary period—are the most common rocks, representing deposition in a shallow marine environment (Nandy et al., 1983). Most of the rock formations in the region exhibit a north–south trend due to tectonic compression, with older Barail Group rocks predominantly exposed in the eastern part of the state.

The whole sedimentary columns of Mizoram State are composed of a repeating sequence of arenaceous and argillaceous rocks, such as sandstone, silty-sandstone, mudstone, shale, shaly-sandstone, silty-shale, and their admixture in various proportions (Ghosh and Saha, 2014). In addition, there are intra-formational conglomeratic bands and isolated pockets of shell-limestone. This succession is separated into three sequential groups: the Barail; Oligocene, Surma; Miocene-Lower Pliocene, and Tipam Groups; Middle-Upper Pliocene (Singh and Pati, 2014). The majority of the state is included in the Surma Group, which is separated into the Bhuban Formation and the Boka Bil Formation (Sarma and Sharma, 2016). The Bhuban Formation is further divided into Lower, Middle, and Upper Bhuban units according to lithological characteristics of the ratio of argillaceous to arenaceous (Sarma and Sharma, 2014).

Geologically, Mizoram is considered the southern extension of the Surma Basin (Sarkar and Bhattacharya, 2008). The hill ranges form a crucial part of the mobile belt, which is characterized by tightly folded, elongated, asymmetrical north–south trending anticlines that alternate or occur en échelon with large, saucer-shaped synclines displaying a slightly arcuate, westward-convex, sub-meridional alignment (Shrivastava & Chaturvedi, 1979). Most of the hill ranges are composed of older,

compact, and more resistant lithological units, typically exposed within the synclinal troughs. These structures are defined by the broad stratigraphic succession established by Ganju (1975) and Karunakaran (1974).

Mizoram is bordered to the north by Assam and Manipur, to the east by the Chin Hills of Myanmar, to the west by Tripura and the Chittagong Hill Tracts, and to the south by the Arakan Hills of Myanmar. The intensity of faulting increases progressively with the magnitude of folding toward the east. The entire sedimentary sequence comprises sandstone, siltstone, shale, and mudstone. A generalized stratigraphic succession is presented in Table 1.1 (Karunakaran, 1974; Ganju, 1975).

Table 1.1 Generalized Geological Succession in Mizoram (After Karunakaran, 1974; Ganju, 1975)

<i>Age</i>	<i>Group</i>	<i>Sub-Group</i>	<i>Formation</i>	<i>Thickness (in m)</i>	<i>Generalised Lithology</i>	<i>Depositional Environment</i>
<i>Recent Alluvium</i>					Silt, clay & gravel	River deposits
<i>Early Pliocene-Late Miocene</i>	Tipam			+900	Friable sandstone with occasional clay bands	Stream deposits
<i>Miocene to Upper Oligocene</i>	Surma	Boka Bil		+950	Shales with siltstones and sandstones	Shallow marine
		Bhuban	Upper Bhuban	+1100	Arenaceous with sandstones, shales, and siltstones	Shallow marine, near shore to lagoonal
			Middle Bhuban	+3000	Argillaceous with shales, siltstones	Deltaic complex
			Lower Bhuban	+900	Arenaceous with sandstones and silty shales	Shallow marine
<i>Oligocene</i>	Barail			+3000	Shales, siltstones and sandstones	Shallow marine

Data sources	<i>Karynakaran, 1974; Ganju, 1975</i>	<i>Tiwari and Kachhara, 2003; Mandaokar, 2000</i>
--------------	---------------------------------------	---

1.3.2. BARAIL GROUP

The continental margin of the passively rifted western Burma Basin is associated with a significant lithostratigraphic unit of shallow marine origin, known as the Oligocene Barail Group (Rao, 1983; Oinam et al., 2022). This group comprises fine-grained sandstone strata intercalated with silty shales, siltstones, and shales, with a total thickness exceeding 3,000 meters (Das and Ghosh, 2015). The lithology exhibits gradational changes, becoming increasingly arenaceous upward, and is overlain by the Miocene to Upper Oligocene Surma Group (Rao, 1983; Rajkumar et al., 2015; Bharali et al., 2017; Oinam et al., 2022). In several locations, the base of the Barail Group is marked by a thin, coarse, pebbly horizon (Mathur and Evans, 1964). The Barail succession, consisting of alternating shale and sandstone units, is prominently exposed in the eastern part of Mizoram (Borgohain, 2020; Hahnar et al., 2021).

The deposition of this group deposition has been attributed to a major regression event that exposed a significant amount of the Bengal Basin to sedimentary processes (Basu and Roy, 2016). There is evidence of a similar Oligocene lithological sequence at the northern margin of the Sylhet Trough, near the southern part of the Dauki Fault (Johnson and Alam, 1991; Islam et al., 2014). According to Alam (1991), the Barail group depositional habitat can be summarized as a tide-dominated shelf setting, suggesting that tidal activities significantly impacted the sedimentation process (Devi, 2021). This implies that throughout the creation of the Barail layers, the region was subject to regular tidal activity that affected the transit and deposition of sediment (Ganju, 1975; Shijoh et al., 2023).

Over time, the rocks of Barail Group have experienced various tectonic forces that have caused folding, faulting, and other structural deformations. The hills and valleys that can be seen in Northeast India are a result of these geological processes.

It is well known that the Barail Group contains hydrocarbon reserves, especially natural gas.

1.3.3. SURMA GROUP

The Surma Group of Miocene to Upper Oligocene age is divided into Bhuban and Bokabil lithostratigraphic units (Kanukaran, 1974; Ganju, 1975). The Bhuban Formation has been classified into distinct parts within the Surma Group according to its lithological features, physical attributes, and order of superposition. Different depositional environment and sedimentary sequences are represented by the Upper Bhuban Formations (Hiller and Elchi, 1984; Rahman et al., 2014). These sediments were deposited in a range of environments, such as deltaic, fluvial, and lacustrine (lake). The Bhuban Formation deposition was influenced by ongoing tectonic processes related to the Indian Plate's collision and convergence with the Eurasian Plate (Kumar and Mukherjee, 2014). This tectonic activity affected the transport and deposition of material in the region, resulting in the elevation of the Himalayas and other mountain ranges. Table 1.2 lists the Surma basin's geologic sequence.

Table 1.2 Stratigraphic succession of Surma basin (After Hossain et al. 2010)

Age	Group	Formation	Lithology	Depositional Environment
Recent	Alluvium	Alluvium	Sand, silt, clay	Fluvial
Late Pleistocene	Dihing	Dihing	Sandstone, shale	Fluvial
Pliocene-Pleistocene	Dupi Tila	Dupi Tila	Sandstone, shale	Fluvial
Late Miocene-Pliocene	Tipam	Girujan Clay	Clay, sandstone	Fluvial lacustrine
		Tipam Sandstone	Sandstone, Clay	Fluvial
Middle-Late Miocene	Surma	Boka Bil Bhuban	Sandstone, shale, Sandstone, shale	Marine deltaic

Late Eocene- Early Miocene	Barail	Renji Jenam	Sandstone, shale, Shale, Sandstone	Shallow marine deltaic
Late Eocene	Jaintia	Kopili Shale	Shale, minor limestone	Shallow marine deltaic
Early-Middle Eocene		Sylhet Limestone	Limestone	Shallow marine
Paleocene-Early Eocene		Tura Sandstone	Quartz arenites	Shallow marine

The lower Bhuban comprises of arenaceous with sandstones and silty shales extending more than 900 meters thick of shallow marine depositional environment (Karunakaran, 1974; Ganju, 1975). The middle Bhuban differs from the lower bhuban comprising of the argillaceous with shales and siltstones. The sediments were deposited in a deltaic complex and extend more than 3000 meters (Kanukaran, 1974; Ganju, 1975). Over 1100 meters of arenaceous rock, including sandstones, shales, and siltstones, make up the upper Bhuban. Shallow marine, near-shore to lagoonal conditions characterize the depositional environment (Kanukaran, 1974; Ganju, 1975).

The Bokabil lies above the Bhuban, and extend more than 950 meters of shales with siltstones and sandstones lithology. The sediments of Bokabil deposited in a shallow marine environment (Hossain et al. 2010).

1.3.4. TIPAM GROUP

The Tipam Sandstone Formation holds a distinct place in the Assam-Arakan Basin's Tertiary Sequence. This rockmass was deposited as sheet sand in a braided river environment during the Miocene. One important litho-unit of Tertiary deposits that was deposited in the Miocene is the Tipam Sandstone Formation in the Assam-Arakan Basin (Johnson and Alam, 1991). The Upper Assam Shelf, the Arakan-Yoma Fold Belt, the Naga-Patkai Hill ranges, the Dhansiri Valley, and the surrounding areas are all part of the basin, which is a deep stack of river sandstone that has been

deposited almost everywhere (Bharali and Borgohain, 2013). The Tipam Group is composed of two distinct formations: the Girujan Clay Formation and the Tipam Sandstone Formation (Johnson and Alam, 1991). It rises more than 900 meters above the Surmpa group, which is made up of bands of clay and friable sandstone. With minor portions of mudstone and siltstone, the Tipam sandstone formation is characterized by yellowish-brown to reddish-brown coarse-grained sandstone with features including cross-bedding and ripple-laminated sandstone (Bhattacharya and Ghosh, 2013). Johnson and Alam (1991) assert that the presence of cross-bedding and the dynamic quality of the environment is characterized by fluctuating water flow and sediment transport mechanisms, which ripple marks contribute to. It implied that the Tipam group's sediments were deposited in a stream environment. Figure 1.1 displays Mizoram's general geological map.

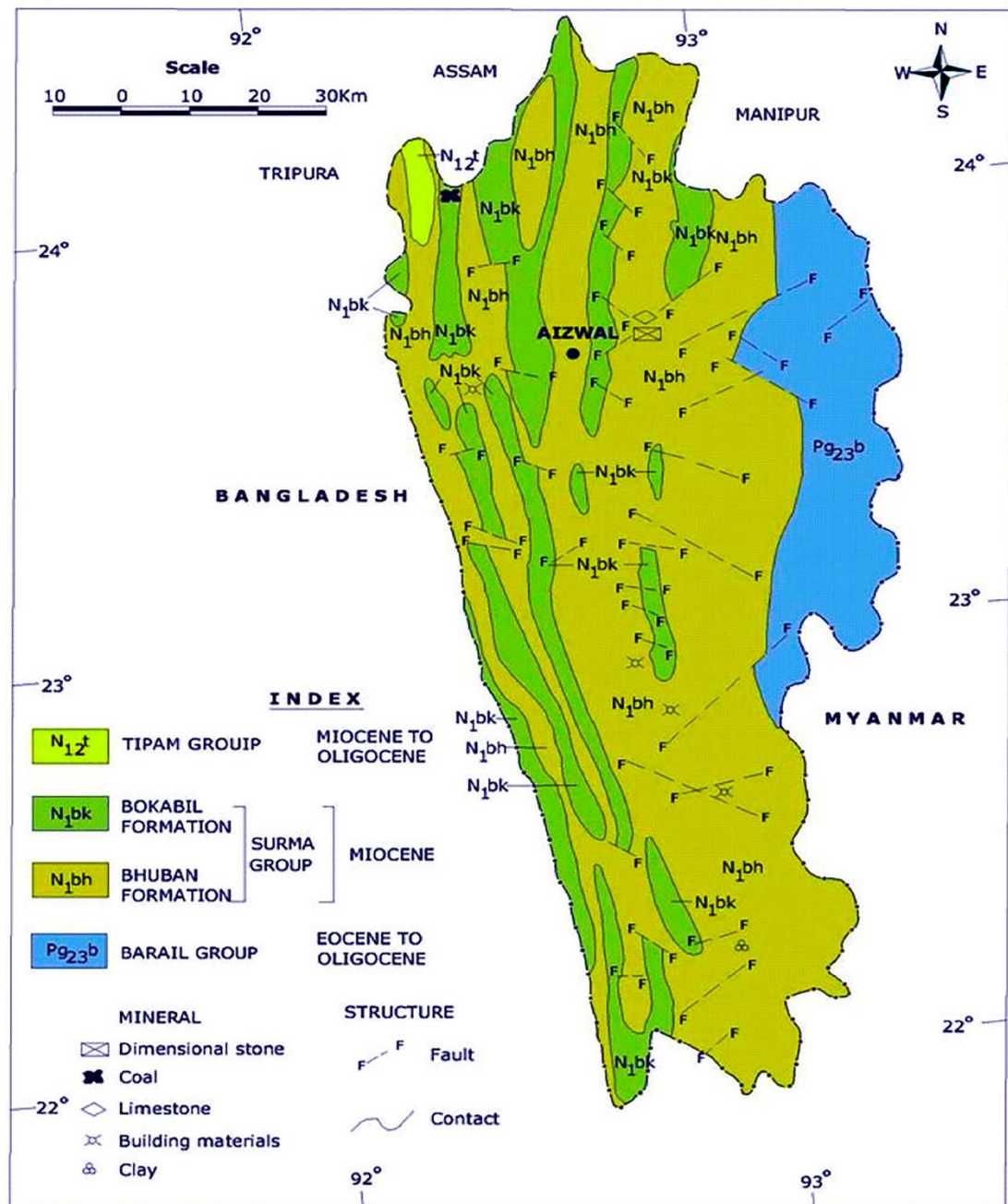


Fig. 1.1 Geological Map of Mizoram (after Kesari, 2011)

1.4. HISTORY OF THE STUDY AREA

The 28.5 km Champhai to Zokhawthar highway was proposed for upgradation from a single-lane state highway to a two-lane national highway standard. This vital roadway traverses several villages, including Zotlang, Mualkawi, Melbuk, Zokhawthar, and parts of Champhai town. Serving as a crucial lifeline for the inhabitants of eastern Mizoram, the road connects to Myanmar and passes through plantation forests, settlements, and areas of regularly farmed jhum land.

Originally classified by the P.W.D. as a state highway with a typical width of about 5 meters, the road was upgraded to a two-lane national highway standard with a total roadway width of 12 meters. The project maintains a maximum gradient of 7.2% along certain stretches, with a ruling gradient of less than 5.0% overall. Improvements included widening, cross-drainage structures, and enhancements to curves and gradients. In most areas, the centerline of the upgraded road remains within the existing Right of Way (RoW), except in a few locations where realignment was necessary. The final projected length of the upgraded road is 26 kilometers (Figure 1.2).

Although the new highway was completed in August 2021, it became inaccessible by November 2021 after multiple landslides occurred along the Champhai to Zokhawthar chainage (Figure 1.3). These landslides were attributed to a heavy thunderstorm that persisted for a week, compounded by several low-magnitude earthquakes during the first week of November 2021.

The region is tectonically active, with clear evidence of local discontinuities and uplifted river terraces. A series of earthquakes followed two moderate earthquakes (Mw 5.1 and Mw 5.5) that occurred on June 21 and 22, 2020, respectively. Subsequent seismic activity in the epicentral region included six earthquakes with magnitudes between 4.0 and 5.0, and numerous smaller events ranging from 3.0 to 3.9. The most severe of these was the Mw 5.5 earthquake on June 22, 2020, with its epicenter near Khawbung "S," approximately 79 kilometers from Champhai.

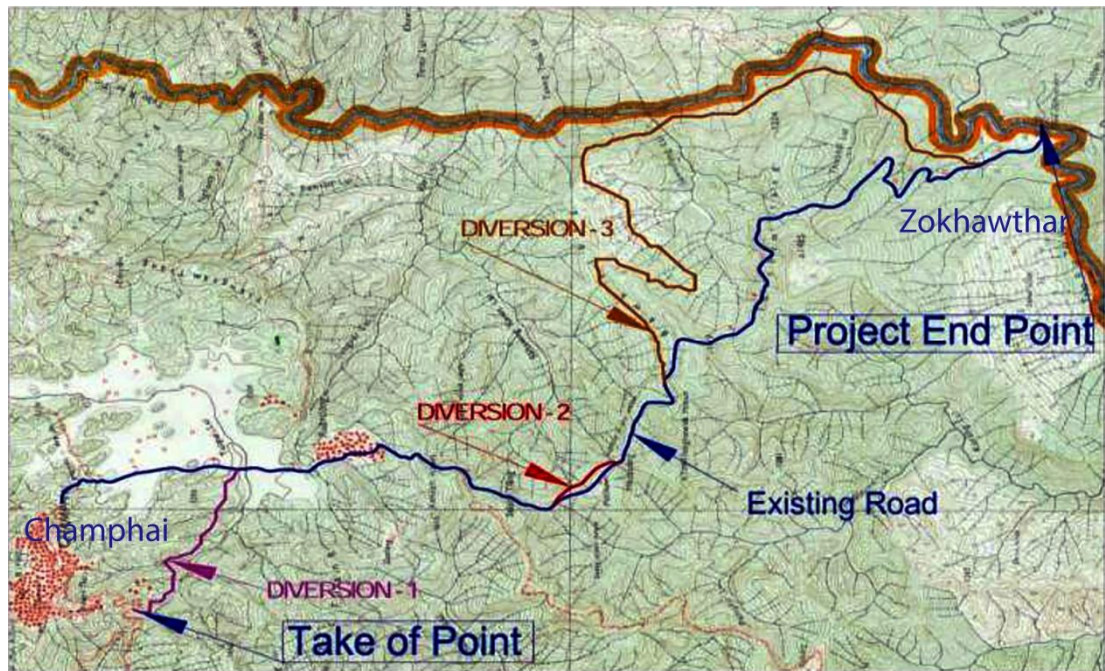


Fig 1.2 Map showing Champhai to Zokhawthar road and realignment (After Public Works Department, Govt. of Mizoram)





Fig. 1.3 Landslides in three different locations (a) Location LS2; (b) Location LS4; (c) Location LS6

1.5. LOCATION AND ACCESSIBILITY OF THE STUDY AREA

Champhai, the district capital of Champhai District, is located in the eastern region of Mizoram (Lalrinawma and Chhakchhuak, 2018). This town lies on the international border between India and Myanmar. The district is bounded by Myanmar to the south and east, Aizawl and Serchhip districts to the west, and the Churachandpur district of Manipur State to the north. Geographically, it spans between latitudes 23°27'22"N and 23°21'55"N, and longitudes 93°19'44"E and 93°23'08"E. Champhai experiences a temperate climate throughout the year, with winter temperatures ranging from 5°C to 12°C and summer temperatures from 15°C to 30°C (Lalnuntluanga and Lalrinchhana, 2020). As the principal trade center in the region, Champhai plays a pivotal role in international commerce, facilitating the import of goods from Myanmar via Zokhawthar.

The new state highway alignment from Champhai to Zokhawthar, passing through Melbuk, was completed in August 2021 with financial support from the World Bank. However, several earthquake tremors and episodes of heavy rainfall during and after the construction period significantly affected the stability of the newly excavated slopes. Multiple large-scale landslides occurred along the highway in October and November 2021. Therefore, comprehensive studies on cut slope instability, along with risk and vulnerability assessments, are urgently required to ensure the safety and sustainability of the current and future Indo–Myanmar trade corridor.

The Tertiary sedimentary Mizoram Fold Belt (MFB) is the easternmost stretch of the Surma basin (Basu and Dutta, 2017). It is separated into the Tipam Group of the late Miocene to Early Pliocene Age, the Surma Group of the Upper Oligocene to Miocene Age, and the Barail Group of the Oligocene Age (Sarma and Sharma, 2015). The longitudinal folds that make up MFB form a long, thin anticline, whereas the synclines that are connected to it are broad and well-developed. Sandstones, shales, and siltstones are found in alternating bands in the Barail group, which includes the lithology from Champhai to Zokhawthar. The litho-units are coarsening upwards, and the sedimentary formations suggest a shallow marine

depositional environment. Many faults, folds, and shear zones evolved in the study region since it is situated in the Indo-Myanmar subduction zone.

The structure is slightly arcuate and convex westward, with the anticline and synclines consisting of a sequence of doubly plunging en-echelon folds. With a NE-SW and NNE-SSW trend, it stretches northward to the Patkai Range and Naga Hills, as well as into the Surma Valley and the western part of the Manipur Hills. The Eocene period and the subsequent formation of the Indo-Burman Orogenic belt are when the Indian plate and Mizoram subduct (Bhaumik and Ghosh, 2012). An upper crustal decollement is produced when the sediments of the basin yield through folding and faulting in a compressive stress environment as a result of the Indian Plate's eastward drift during the Mio-Pliocene (Dutta and Basu, 2015). In the east, near the collision and subduction zones, the deformation was most intense, and the folded bed is exposed to the EW stress field (Bhaumik and Mukhopadhyay, 2013). Figure 1.4 depicts the location of the study area.

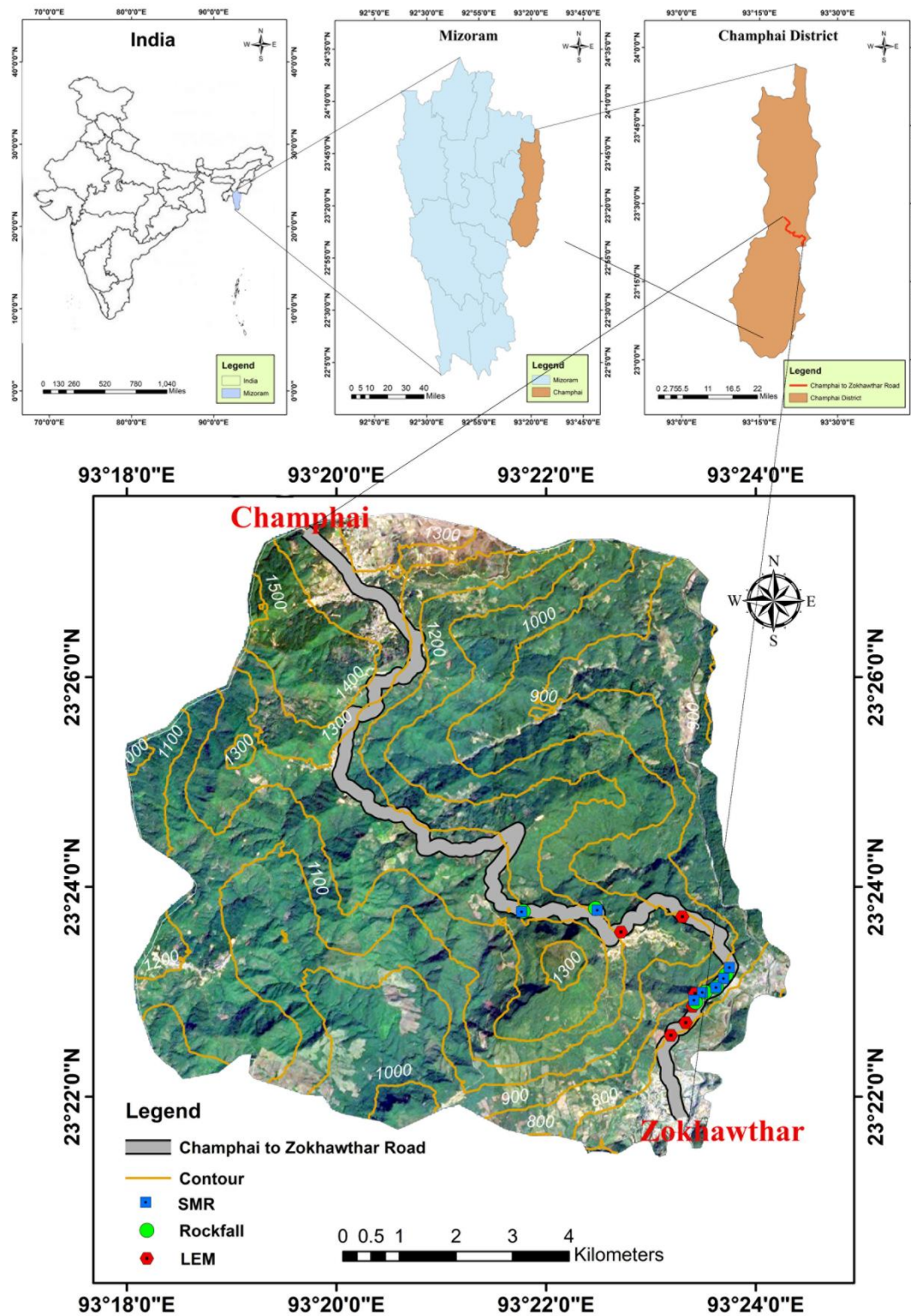


Fig. 1.4 Location Map of the Study area

1.6. SCOPE OF THE RESEARCH

Mizoram Mizoram forms a significant depocenter of the Surma Basin, with sedimentary sequences that date back to the Oligocene to Early Pliocene period (Karunakaran, 1974; Ganju, 1975). The region is characterized by a rugged, hilly terrain situated along the convergent plate boundary between the Indian Plate and the Burmese Plate, an active tectonic zone marked by the presence of numerous faults, thrusts, and folds. These structural features, along with the region's tectonic dynamism, have led to the development of a complex geological setting.

The sedimentary strata in Mizoram are relatively young and geologically immature, often poorly lithified, and composed primarily of interbedded sandstone, shale, and siltstone. Due to their weak cementation, these formations are prone to weathering and disintegration, particularly when exposed to intense environmental conditions. slopes.

The widespread presence of joints, fractures, and local faults further compromises the structural integrity of slopes. These features serve as potential failure planes, facilitating the onset of mass movement processes such as rockfalls, rock slides, debris avalanches, earthflows, and creep. High-angle slopes are particularly vulnerable, as gravitational forces combined with weakened material strength and water infiltration significantly increase the risk of landslides.

In hilly and mountainous regions, landslides are increasingly triggered by anthropogenic activities, often more than by natural causes alone. Human interventions, such as unplanned settlement expansion, road construction, deforestation, slope cutting, and poorly engineered infrastructure, significantly alter the natural balance of slopes. These activities disturb the equilibrium of soil and rock masses, reduce slope stability, and increase the risk of landslides, particularly in areas with pre-existing geological weaknesses. Among these, slope modification for roads and habitation is a major contributor to landslide occurrences. Excavation at the toe of slopes, removal of vegetation, and lack of proper drainage systems can initiate surface erosion, waterlogging, and structural failures, especially during heavy rainfall or seismic events.

To address and mitigate these risks, it is essential to conduct scientific studies of the geotechnical properties of soil and rock. Understanding parameters such as cohesion, shear strength, permeability, porosity, and weathering characteristics enables engineers and planners to assess the stability of slopes and design effective hazard mitigation strategies. Additionally, detailed rock mass characterization, including the analysis of discontinuities, joint spacing, orientation, and rock mass rating systems (e.g., RMR, SMR, GSI), is crucial in identifying vulnerable areas. These assessments allow for the safe planning of infrastructure, reinforcement of unstable zones, and the implementation of early warning systems. Recognizing the role of human activities in landslide initiation and combining it with a rigorous geotechnical understanding of the terrain is vital for sustainable development and disaster risk reduction in hilly regions.

In hilly terrains like Mizoram, road and highway networks are lifelines, essential not only for local connectivity but also for the transport of goods, access to services, and economic development. The Champhai–Zokhawthar State Highway serves as a vital corridor for international trade between India and Myanmar, with strategic importance for both regional commerce and national interests. The highway, particularly the section via Melbuk, was newly constructed and completed in August 2021 under World Bank-funded infrastructure initiatives aimed at enhancing cross-border connectivity.

However, shortly after completion, the region experienced intense rainfall in the mid-year, leading to the occurrence of approximately fifteen massive landslides along the freshly excavated cut slopes of the highway. These landslides disrupted transportation, stranded vehicles, and highlighted the vulnerability of inadequately stabilized slopes, especially when subjected to heavy monsoonal rains. Such slope failures not only pose serious risks to public safety, including injuries and potential fatalities, but also contribute to environmental degradation through the loss of vegetation and soil erosion.

The stability of cut slopes along transportation corridors is a critical geotechnical concern. Unengineered or poorly reinforced slopes are particularly

susceptible to mass wasting processes when disturbed by excavation and exposed to rainfall infiltration. Therefore, a comprehensive geotechnical investigation of the landslide-affected and potentially unstable areas along the highway is essential. This includes analyzing the mechanical properties of soil and rock, slope geometry, drainage patterns, and discontinuities in the rock mass to understand the factors contributing to slope failure.

Mizoram's young sedimentary geology, active tectonic setting, intense rainfall, and structural discontinuities collectively create an environment highly susceptible to various types of slope failures, necessitating detailed hazard assessments and site-specific mitigation strategies. Such investigations will inform the design and implementation of remedial measures, including retaining structures, drainage improvements, slope reinforcement, and early warning systems, ensuring long-term slope stability and the safe, uninterrupted operation of this crucial highway.

1.7. OBJECTIVE OF THE RESEARCH

- 1.** To study the disaster vulnerability and risk assessment of the study area;
- 2.** To determine the geotechnical properties of soil and rock mass characteristics;
- 3.** To determine the cut slope stability analysis using numerical analyses;
- 4.** To suggest mitigation and preventive measures for the study area.

CHAPTER 2

METHODOLOGY

2.1. ATTERBERG LIMIT TEST

Three distinct ranges of moisture content, known as Atterberg limits, are used to categorize the behavior and consistency of fine-grained soils, including silt and clay (Atterberg, 1911). Albert Atterberg, a Swedish soil scientist who developed the idea in the early 1900s, is honored by the namesake of these boundaries. The Atterberg limits are widely used in geotechnical engineering to evaluate soil engineering qualities and anticipate their behaviour under various moisture conditions (Holtz and Kovacs, 1981). As per IS: 2720 (Part 5) - 1985 and ASTM D4318-10, 1994, the Atterberg limit test is done on fine-grained soil to determine the crucial water content, which includes the Liquid Limit and Plastic Limit (BIS, 1985; ASTM, 2010). The Atterberg limit test flowchart is shown in figure 2.1

Understanding the Atterberg limits of soil is crucial in construction and geotechnical engineering, since it determines its suitability for numerous engineering objectives such as foundation design, slope stability analysis, and road construction. Different soil types may exhibit different Atterberg limits, which can have significant ramifications for engineering projects and soil behaviour under various environmental situations.

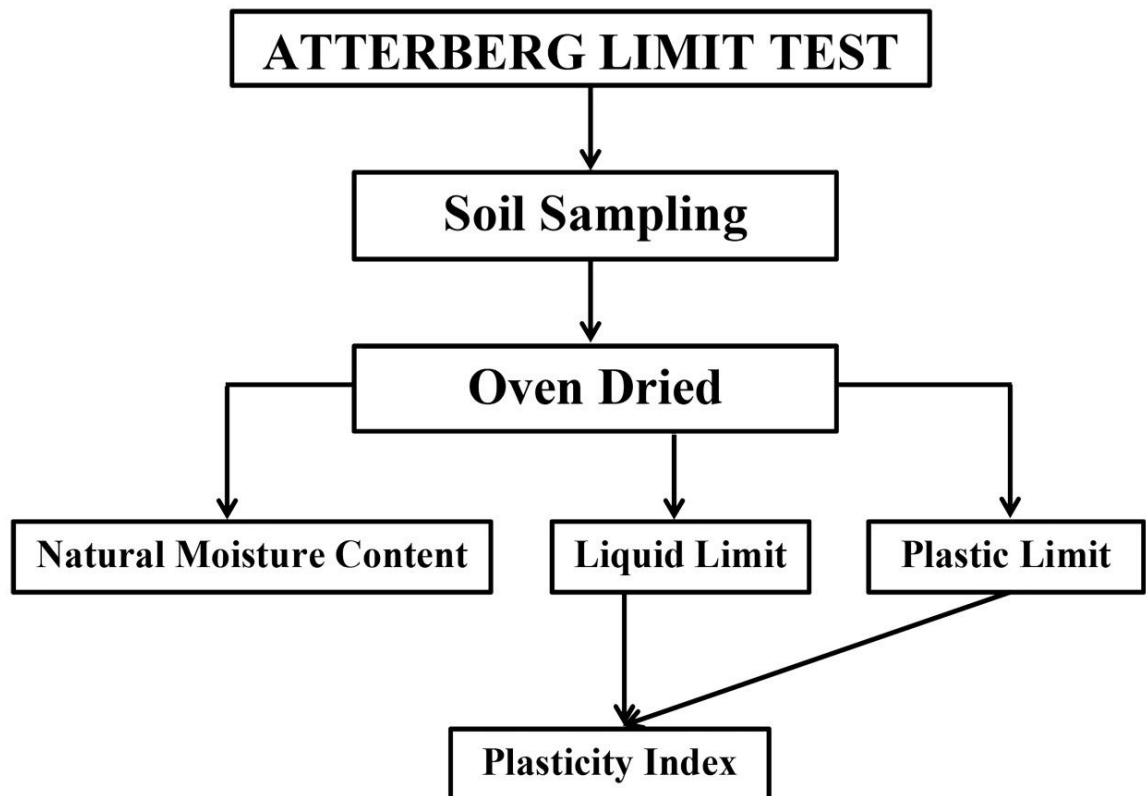


Fig. 2.1 Flowchart of Atterberg Limit Test

2.1.1. Soil Sampling

A representative sampling site that can accurately reflect the soil properties of the area of interest is selected. At a depth of 1.52 meters, about 5 kilograms of an undisturbed soil sample was taken using a core sampler and placed in a sampling bag for laboratory investigation.

2.1.2. Natural Moisture Content (N.M.C.)

The quantity of water in the soil, expressed as a percentage of its weight when completely dry is the natural moisture content.

After cleaning the container, the weight of empty container with the lid is measured and recorded as W1. The appropriate amount of soil samples is taken into the container, crumbled, and then weighed down with a lid and recorded as W2. Following this, it is stored in an oven with the lid off, kept at a constant temperature

of 110 ± 5 °C. The specimen is kept for 24 hours getting dried in the oven. The weight of the oven-dried soil sample with the container is its final mass and recorded as W3.

Calculation

The percent of water content is calculated as follows:

$$W = \{(W2 - W3) / (W3 - W1)\} \times 100 \quad (\text{Equation 2.1})$$

Where,

W = Percentage of moisture content,

W1 = Weight of empty container (in gram).

W2 = Weight of container with wet soil (in gram)

W3 = Weight of container with dry soil (in gram)

Table 2.1 Datasheet for determining Natural Moisture Content (N.M.C.)

Sample No.	Weight of empty container (in g)	Weight of container + wet sample (in g)	Weight of container + Dry sample (in g)	Moisture Content (%)	NMC (%)

2.1.3. Liquid Limit

Liquid limit is one of the most fundamental geotechnical characteristics for identifying different soil types and comprehending how they behave in various moisture conditions. The water content at which soil changes from a plastic to a liquid state is the liquid limit of soil (Atterberg, 1911).

The equipment needed for the determination of liquid limit are:

1. Casagrande apparatus: It is a firm rubber base, a crank, and a metal cup where a soil paste is placed.

2. Oven: A thermostatic-controlled chamber for drying soil. The temperature ranges between 105°C and 110°C.
3. Sieving Machine: A vibrating screen used for classifying soil particles of the same size.
4. Spatula: A metal blade used for mixing soil and water.
5. Mixing Dish: Used to make the paste of soil.
6. Grooving tool: A standard tool used for cutting a groove in a soil-paste.
7. Balance: Precise to within 0.01 grams.
8. Moisture Can: Used to dry soil samples.
9. Container: Containing distilled water to make the paste, mix with the soil.

To determine the liquid limit, collect about 200-gram oven-dried soil samples that pass through a 425 μm sieve. Add distilled water and using a spatula, mix thoroughly to create a paste. Place the thin paste and level using a spatula on the cup of Casagrande Apparatus. Using a grooving tool cut the sample into two halves by making the groove through the center. The Casagrande Apparatus handle is twisted around till the two halves of the soil paste come into contact. Cut the closed portion of the soil sample, and put on the moisture can to determine the moisture content by oven-drying at 105°C to 110°C for 24 hours. Measure the weight of the oven-dried sample. From the obtained moisture content, plot a graph against a number of blows. The moisture content corresponding to 25 blows from the curve is the liquid limit of the soil. By adding the required drops of water, repeat the process with varying water contents to obtain sets of data. Record the number of revolutions or blows ranging between 10 and 40. The datasheet for the determination of liquid limit is given in table 3.

Table 2.2 Datasheet for Liquid Limit

Sample No.	No. of blows	Weight of beaker	Weight of beaker + wet sample (in gram)	Weight of beaker + dry sample (in gram)	Moisture content (%)

2.1.4. Plastic Limit

The plastic limit of soil, which provides details on the consistency and behavior of the soil at varying moisture levels, is a crucial component in geotechnical engineering. The plastic limit is the water content at which soil transitions from a plastic to a semi-solid state (Atterberg, 1911).

The equipment needed for the determination of plastic limit are:

1. Non-absorbent Surface: A flat glass plate of approximately 12 cm in diameter and 10 mm thick with not less than 45 sq. cm.
2. Rod: A measuring stick of approximately 3mm in diameter of 10 cm long.
3. Sieving Machine: A vibrating screen used for classifying soil particles of the same size.
4. Spatula: A metal blade used for mixing soil and water.
5. Mixing Dish: Used to make the paste of soil.
6. Weighing Machine: Precise to within 0.01 grams.
7. Moisture Can: Used to dry soil samples.
8. Container: Containing distilled water to make the paste, mix with the soil.
9. Oven: A thermostatic-controlled chamber for drying soil. The temperature ranges between 105°C and 110°C.

Take about 20 grams of sieved soil into a mixing dish. Gradually add distilled water and mix using a spatula. Mix thoroughly until the soil becomes plastic enough to be easily shaped and molded. Upon applying uniform pressure, hand-roll the plastic soil on a non-absorbent surface into a thread of approximately 3mm in diameter. Continue rolling the soil thread until it crumbles. Collect the crumbled soil

and placed them in a moisture can. Using a weighing machine, measure the weight of moisture can containing the crumbled soil. Then, put the moisture can in the oven of about 105°C to 110°C for 24 hours. Remove the oven-dried soil from the moisture can and weigh it again. The water content of the crumbled soil is determined. The datasheet for the determination of plastic limit is given in table 2.2.

Table 2.3 Datasheet for Plastic Limit

Sample No.	Weight of an empty beaker (in gram)	Weight of beaker + wet sample (in gram)	Weight of beaker + dry sample (in gram)	Moisture content (%)	Plastic limit (wp)

2.1.5. Plasticity Index (P.I.)

The term Plasticity Index (PI) describes the range of moisture content at which a soil exhibits plastic behavior (BIS, 1985). It is a gauge of the soil's malleability. This refers to the distinction between the soil's plastic and liquid limits.

It is given by,

$$P.I. = L.L. - P.L. \quad (\text{Equation 2.2})$$

With an increase in plasticity index, the particle size of soil decreases. Therefore, the plasticity index is a measure of particle fineness. It is possible to develop a relationship between the plasticity index and clay percentage by adjusting the amount of clay in the soil.

2.1.6. Liquidity Index (L.I.)

The liquidity index calculated as follows:-

$$\frac{\text{Natural moisture content of the soil} - \text{Plastic limit of the soil}}{\text{Plasticity Index of the soil}} \quad (\text{Equation 2.3})$$

2.1.7. Consistency Index (C.I.)

The consistency index calculated as follows:-

$$CI = (LL - W) / (LL - PL) \quad (Equation 2.4)$$

where, W is the existing water content, and LL is liquid limit, PL is plastic limit

2.2. PROCTOR COMPACTION TEST

The Proctor compaction test is a laboratory technique used to determine the optimum moisture content at which soil will reach its maximum dry density and become the most compact (Proctor, 1933). This test is crucial in the field of geotechnical engineering to make sure the soil used for building projects, such as roads, embankments, and foundations, has the required compaction qualities to provide stability and support.

The apparatus needed for the determination of proctor compaction test are:

1. Proctor Mould
2. Proctor hammer
3. Moisture can
4. Sieve (4.75 mm)
5. Steel straightedge
6. Oven
7. Digital Weighing Machine

Measure the weight of an empty mould. Take about 2kg of oven-dried soil passes through a 4.75mm sieve. Mix a known amount of soil and water thoroughly. Place the soil in the mould and compact the first layer with 25 blows using a proctor hammer, dropping vertically. Add a second and third layer of soil and repeat the same. After compaction for three layers, trim the excess layer on the top of the mould using a steel straightedge. Measure the weight of the mould containing three compacted layers of soil using the digital weighing machine. Repeat the procedure with an increase in the amount of known water until the weight of the mould and

compacted soil decreases. The datasheet for the proctor compaction test is given in table 2.3.

Table 2.4 Datasheet for Proctor Compaction Test

Sl. No.	Particulars	Unit	Trial		
			1	2	3
1.	Mass of empty mould (M1)	gm	4160	4160	4160
2.	Volume of mould (V)	cc	997.46	997.46	997.46
3.	Mass of mould + Soil Sample (M2)	gm	6100	6180	6160
4.	Mass of wet soil (M)	gm	1940	2020	2000
5.	Wet/ Bulk Density (γ_{wet})	g/cc	1.94	2.03	2.01
6.	Water content (w)	%	8	10	12
7.	Dry density (γ_d)	g/cc	1.80	1.84	1.79

Bulk Density and Dry Density can be calculated using equations

$$\gamma_{wet} = (M2 - M1)/V \quad (Equation 2.5)$$

Where,

γ_{wet} = Bulk Density

M1 = Mass of empty mould

M2 = Mass of mould and soil sample

$$\gamma_d = (100\gamma_{wet})/(100 + w) \quad (Equation 2.6)$$

Where,

γ_d = Dry Density

2.3. DIRECT SHEAR TEST

The Proctor compaction test is a laboratory technique used to determine the optimum moisture content at which soil will reach its maximum dry density and become the most compact (Proctor, 1933). This test is crucial in the field of geotechnical engineering to make sure the soil used for building projects, such as roads, embankments, and foundations, has the required compaction qualities to provide stability and follows:

The apparatus needed for the direct shear test are:

1. A Shear box
2. Gripper disks and porous stones
3. A loading cup
4. Two metallic plates and screws
5. A loading frame and a dial gauge
6. Proving ring and tamper
7. A core cutter, spatula and straightedge
8. Stopwatch
9. Weight plate for applying normal stress

Test Procedure

Place the soil specimen in the shear box overlying the perforated grid plate by filling the shear box. A normal stress (vertical pressure) is applied to the soil sample. Normal stress can be changed to simulate various vertical forces that the soil may encounter in the field. The upper part of the shear box is moved horizontally to progressively apply the shear force to the soil once the normal tension has been applied and stabilized. Sliding along the designated shear plane is caused by this shearing motion. Shear stress and shear displacement can be calculated throughout the test by continually measuring the applied shear force and the horizontal displacement of the upper half of the shear box. The test is repeated on a separate specimen for two times, by applying different normal stress.

The shear strength characteristics of the soil sample are determined using the data collected during the direct shear test. Using the Mohr-Coulomb failure criterion, the cohesion (c) and internal friction angle (ϕ) can be computed by plotting shear stress versus horizontal displacement. The datasheet for the direct shear test is given in table 2.4 and table 2.5.

Table 2.5 Datasheet for Direct Shear Test

Dial Gauge Reading	Dial Gauge Reading in cm	Proving RR Set 1	Proving RR Set 2	Proving RR Set 3	PRR1 *const	PRR2 *const	PRR3 *const	Area corr.	Shear stress 1	Shear stress 2	Shear stress 3

Table 2.6 Datasheet for Cohesion and Angle of Friction

Sl. No.	Normal stress σ (kg/cm ²)	Shear Stress at Failure τ (kg/cm ²)	Cohesion (c) (kg/cm ²)	Angle of Shearing Resistance (Φ)

2.4. SLAKE DURABILITY TEST (SDI)

It is a measure of the rock resistance to disintegration in a slaking fluid as a result of drying and wetting (ASTM, 2020). This slake-durability test examines the resistance of rocks to weathering that contain clay. Putting rock samples in water and watching for swelling or disintegration is the standard elementary procedure. The factors that affect the rock's slaking durability are its porosity and permeability, which regulate pore fluids' entry, retention, and motion inside the rock.

As per IS:10050 – 1981, this test is conducted in a laboratory to determine how resistant a rock and sedimentary materials are to weathering and disintegration brought on by water. As it helps evaluate the long-term stability and endurance of rock materials when they are exposed to climatic conditions, especially those involving wetting and drying cycles, the test is especially significant in the fields of geology and geotechnical engineering.

The apparatus needed for the slake durability test are:

1. Slake durability apparatus
2. Digital balance
3. Oven
4. Water Bath

Procedures

Collect representative rock samples from the field and break it into lumps of 40-60 grams each. Select 10 rock lumps of total weight 400-600 grams. Place the samples in an oven at 105°C until they reach a constant weight. Using a digital balance measure the initial dry weight of the samples as weight A. Transfer the samples into a mesh drum and submerge it into slaking fluid. Rotate the drum at a speed of 20 rpm for 10 minutes. Carefully remove the samples out of the slaking fluid and dry in an oven until it reaches a constant weight at 105°C. Again, measure the weight of oven-dried samples as weight B using a digital balance. Repeat the steps of wetting, rotating, drying, and weighing to obtain weight C. The sub-division of slake-durability scale (IS: 10050-1981) is given in table

The Slake Durability Index (SDI) is calculated by:

$$Id1 = \frac{B-D}{A-D} 100 \quad (Equation 2.7)$$

$$Id2 = \frac{C-D}{A-D} 100 \quad (Equation 2.8)$$

Id1 = Slake Durability Index for First cycle

Id2 = Slake Durability Index for Second cycle

A = Weight of drum plus sample

B = Weight of drum plus retained portion of sample for first cycle

C = Weight of drum plus retained portion of sample for second cycle

D = Weight of drum

Table 2.7 Sub-Division of Slake-Durability Scale (IS:10050 -1981)

Slake Durability Id Percent	Classification
0-25	Very low
Over 25-50	Low
Over 50-75	Medium
Over 75-90	High
Over 90-95	Very High
Over 95-100	Extremely High

2.5. LIMIT EQUILIBRIUM METHOD (LEM)

The Limit Equilibrium Method (LEM) is the fundamental approach in geotechnical engineering to determine slope and structural stability in soil mechanics (Bishop, 1955). It is a simple but commonly used method for determining the equilibrium of a soil mass or structure subjected to external forces, namely resisting forces, i.e., soil shear strength and driving forces; e.g., gravity, applied loads, or water pressure (Fredlund and Rahardjo, 1993). The main goal of this approach is to identify whether the slope or structure is stable or at risk of failure.

Rocscience Software Side 6.0 can perform LEM analysis, with the Ordinary/Fellenius Method, Janbu Method, Bishop Method, and GLE/Morgenstern Price Method being the study areas (Rocscience Inc, 2021). Landslides with translational or rotational movements on different failure surfaces are analyzed using LEM. The purpose of the analysis is to provide the safety factor (Chowdhury, 2009).

The total forces available to prevent collapse along a presumptive plane are compared to the total forces working to cause portions of the slope to slide. The factor of safety (FOS), which can be written as the ratio of these two sums, which can be expressed by;

$$\text{FOS} = \frac{\Sigma \text{Resisting forces}}{\Sigma \text{Driving forces}} \quad (\text{Equation 2.9})$$

Procedures

1. Determine the slope geometry including slope angle, dimension, and other features like water table, lithology, or layer of different soils.
2. Plot the external boundary using slide 6.0.
3. Insert the geotechnical properties such as unit weight, cohesion, angle of friction, and pore pressure (if applicable).
4. For a non-circular surface, the shape and coordinates of the surfaces are defined.
5. Set up the grid, and run the computation.
6. For each method, interpret the model showing a slip circle and factor of safety.

The Limit Equilibrium Method is a basic approach that estimates slope stability conservatively. In practice, it is commonly utilized for preliminary assessments, design, and safety evaluations of slopes, retaining walls, and other geotechnical constructions. However, it has limits, especially in circumstances where the real failure mechanism of the slope is more complex.

2.6. ROCK MASS RATING (RMR) [IS 13365 (Part 2)]:

Rock Mass Rating (RMR) was developed by Z.T. Bieniawski (1973) to analyse tunnel stability and support requirements. The RMR is a quantitative rock mass characterisation system, often known as a rock geomechanical classification system (Bieniawski, 1989; Hoek and Brown, 1997). It is a commonly used geomechanical classification system in civil and mining engineering projects to analyse the engineering quality and stability of rock masses (Bieniawski, 1989; Hoek and Brown, 1997). It consists of five parameters for classifying the properties of rock masses:

The five parameters of Rock Mass Rating System are:

- a) Uniaxial Compressive Strength (UCS) of the Rock
- b) Rock Quality Designation (RQD)
- c) Condition of discontinuities/ Joint condition
- d) Joint spacing
- e) Ground water condition

2.6.1. Uniaxial Compressive Strength (UCS)

It estimate the strength of the entire rock mass, measured in megapascals (Hoek and Brown, 1980; Bieniawski, 1989). The quality of the rock increases with its uniaxial compressive strength. It is applied on intact rock material. When there is no constraining stress, it is the highest axial compressive stress that a rock mass can sustain (Hoek and Brown, 1980; Bieniawski, 1989). The rating for Uniaxial Compressive strength of rockmass is given in table 2.7.

Table 2.8 Ratings for Uniaxial Compressive Strength of Rockmass

Compressive Strength (Mpa)	Point Load Strength (Mpa)	Qualitative Decription	Rating
>250	8	Extremely strong	15
100 to 250	4 to 8	Very Strong	12
50 to 100	2 to 4	Strong	7
25 to 50	1 to 2	Medium	4
5 to 25	Use of UCS is preferred	Weak	2
1 to 5	Use of UCS is preferred	Very Weak	1
<1	Use of UCS is preferred	Extremely Weak	0

2.6.2. Rock Quality Designation (R.Q.D.)

It is a qualitative assessment of the degree of jointing in a rock mass, for the drilled core in lengths of 10 cm or more (Bieniawski, 1989). If coring is not possible, Volumetric Joint Count (J_v) can be used to determine it. Table 2.8 lists the rockmass ratings and RQD classification. Table 2.9 provides the Volumetric Joint Count categorization.

$$R.Q.D. = 115 - 3.3 J_v \text{ (For flat and long blocks)} \quad (\text{Equation 2.10})$$

$$\text{Or, } R.Q.D. = 110 - 2.5 J_v \text{ (For cubic shaped blocks)} \quad (\text{Equation 2.10})$$

Table 2.9 R.Q.D. classification and rating (Bieniawski, 1979)

R.Q.D. (%)	Qualitative description	Rating
90 to 100	Excellent	20
75 to 90	Good	17
50 to 75	Fair	13
25 to 50	Poor	8
<25	Very Poor	3

Table 2.10 Classification of Volumetric Joint Count (J_v)

Degree of Jointing	J_v
Very low	<1
Low	1-3
Moderate	3-10
High	10-30
Very high	30-60
Crushed	>60

2.6.3. Condition of Discontinuities

This parameter assesses the nature of fractures, spacing, and condition of the discontinuities within rock masses. It is divided into four categories, ranging from in-filled and altered discontinuities to fresh and unaffected fractures. It is the measurement of the degree of roughness of the discontinuity surfaces, the length of separation of the discontinuity and the continuity of the joints, weathering of the joint surface, slickenside and infillings or gouge. Table 2.10 is the standard table for Joint separation and its ratings.

Table 2.11 Joint Separation and Rating (Beiniawski, 1979)

Description	Joint Separation (mm)	Rating
Very Rough, un-weathered wall rock tight and discontinuities, no separation	0	30
Rough, Slightly weathered, Wall rock surface separation <1mm	<1	25
Slightly rough, moderately to highly weathered, wall rock surface separation <1mm	<1	20
Slickensides wall rock surface, 1-5mm thick gouge, or 1-5 mm wide continuous discontinuity	1-5	10
Soft gouge of >5mm thick or continuous discontinuity > 5	>5	0

2.6.4. Joint Spacing

The spacing and nature of fractures, joints, and other discontinuities within the rock mass are described by this characteristic. It is divided into five categories, ranging from continuous and close to widely scattered and open. It is a measure taken in perpendicular of a distance between two adjacent discontinuities or between the

joints of the same set. The Classification for Discontinuity Spacing is given in table 2.11.

Table 2.12 Discontinuity Spacing Classification (Bieniawski, 1979)

Spacing (m)	Description	Rating
>2	Very wide	20
0.6 – 2	Wide	15
0.2 – 0.6	Moderate	10
0.06 – 0.2	Close	8
<0.06	Very Close	5

2.6.5. Groundwater Condition

The existence and behaviour of groundwater within the rock mass is assessed. It is classified into five categories, ranging from dry to high water pressures. The groundwater conditions in the field are classified bases of the table 2.12.

Table 2.13 Ground Water Condition and Rating (Bieniawski, 1979)

Inflow per 10 m tunnel length (L/min)	None	<10	10 - 25	25 - 125	>125
Ratio of joint water pressure to major principal stress	0	0 – 0.1	0.1 – 0.2	0.2 – 0.5	>0.5
General Description	Completely dry	Damp	Wet	Dripping	Flowing
Rating	15	10	7	4	0

The RMR system provides a quantitative and qualitative assessment of the geological and geotechnical properties of rock masses, which aids in decision-

making for excavation, tunnelling, slope stability, and other rock engineering applications. This technique can also be used to assess rock-slope stability conditions and crucial sections of the rock mass prone to slope failure. The RMR Classification based on the rock mass characteristics are given in table 2.13.

Table 2.14 R.M.R. Classification on the characteristics of rock mass

A. CLASSIFICATION PARAMETERS AND THEIR RATINGS									
Parameters			Range of values						
1.	Strength of intact rock material	PLI	>10 MPa	4-10 MPa	2-4 MPa	1-2 MPa	For this low range, UCS test is preferred		
		UCS	>250 Mpa	100-250 MPa	50-100 MPa	25-50 MPa	5-25 MPa	1-5 MPa	<1 MPa
	Rating		15	12	7	4	2	1	0
2.	Drill core quality RQD		90%-100%	75%-90%	50%-75%	25%-50%	<25%		
	Rating		20	17	13	8	3		
3.	Spacing of discontinuities		> 2 m	0.6-2 m	200-600 mm	60-200 mm	< 60 mm		
	Rating		20	15	10	8	5		

4.	Condition of discontinuities		Very rough surfaces Not continuous No separation Unweathered wall rock	Slightly rough surfaces Separation < 1 mm Slightly weathered walls	Slightly rough surfaces Separation < 1 mm Highly weathered walls	Slickenside surfaces Or Gouge < 5 mm thick Or Separation 1-5 mm Continuous	Soft gouge > 5 mm thick Or Separation > 5 mm Continuous
			Rating	30	25	20	10
5.	Ground water	Inflow per 10 m tunnel length (l/m)	None	< 10	10-25	25-125	>125
		(Joint water press)/ (Major principal σ)	0	< 0.1	0.1-0.2	0.2-0.5	> 0.5
		General conditions	Completely dry	Damp	Wet	Dripping	Flowing
	Rating		15	10	7	4	0
B. RATING ADJUSTMENT FOR DISCONTINUITY ORIENTATION							
Strike and dip orientations			Very favorable	Favorable	Fair	Unfavorable	Very Unfavorable
Ratings	Tunnels & mines		0	-2	-5	-10	-12
	Foundations		0	-2	-7	-15	-25

	Slopes	0	-5	-25	-50	
C. ROCK MASS DETERMINED FROM TOTAL RATINGS						
Rating	100←81	80←61	60←41	40←21	< 21	
Class Number	I	II	III	IV	V	
Description	Very good rock	Good rock	Fair rock	Poor rock	Very poor rock	
D. MEANING OF ROCK CLASSES						
Class Number	I	II	III	IV	V	
Average Stand-up time	20 yrs for 15 m span	1 year for 10 m span	1 week for 5 m span	10 hrs for 2.5 m span	30 minutes for 1 m span	
Cohesion of rock mass (kPa)	>400	300-400	200-300	100-200	<100	
Friction angle of rock mass(deg)	>45	35-45	25-35	15-25	<15	
E. GUIDELINES FOR CLASSIFICATION OF DISCONTINUITY						
Discontinuity length (persistence)	>1 m	1-3 m	3-10 m	10-20 m	>20 m	
Rating	6	4	2	1	0	
Separation (aperture)	None	<0.1 mm	0.1-1.0 mm	1-5 mm	>5 mm	
Rating	6	5	4	1	0	
Roughness	Very Rough	Rough	Slightly Rough	Smooth	Slickenside	
Rating	6	5	3	1	0	
Infilling(gouge)	None	Hard filing >5 mm	Hard filling <5 mm	Soft filling < 5 mm	Soft filling > 5 mm	

Rating	6	4	2	2	0
Weathering	Unweathered	Slightly weathered	Moderately weathered	Highly weathered	Decomposed
Rating	6	5	3	1	0
F. EFFECT OF DISCONTINUITY STRIKE AND DIP ORIENTATION IN TUNNELLING					
Strike perpendicular to the tunnel axis			Strike parallel to the tunnel axis		
Drive with dip- Dip 45-90°	Drive with dip – Dip 20-45°		Dip 45-90°	Dip 20-45°	
Very favorable	Favorable		Very favorable	Fair	
Drive against dip- Dip 45-90°	Drive against dip- Dip 20-45°		Dip 0-20° Irrespective of strike		
Fair	Unfavorable		Fair		

2.7. GEOLOGICAL STRENGTH INDEX (GSI)

GSI was developed by Dr. Evert Hoek and is particularly useful for predicting the stability of underground excavations, tunnels, and rock slopes (Hoek and Marinos, 2000). The mechanical behavior and quality of rock masses are examined using this geomechanical classification system. It offers a numerical evaluation of the failure propensity and engineering characteristics of a rock mass. Rock condition, discontinuity existence and features, groundwater conditions, and in-situ stress level are only a few of the factors that the GSI system considers when assigning a numerical value to a rock mass (Osgoui and Ulusay, 2010).

Based on visual field study, it is defined by two characteristics: surface condition rating (S.C.R.) and structure rating (S.R.). The roughness, weathering, and infilling ratings determine the SCR, whereas the volumetric joint count—which is provided by an equation—determines the SR (Hoek and Marinos, 2000). The figure 2.2 displays the quantitative GSI chart.

$$SR = -17.5 \ln(J_v) + 79.8 \quad (\text{Equation 2.12})$$

$$SCR = R_r + R_w + R_i \quad (\text{Equation 2.13})$$

(Where J_v = Volumetric Joint Count, R_r = Roughness Rating, R_i = Infilling Rating)

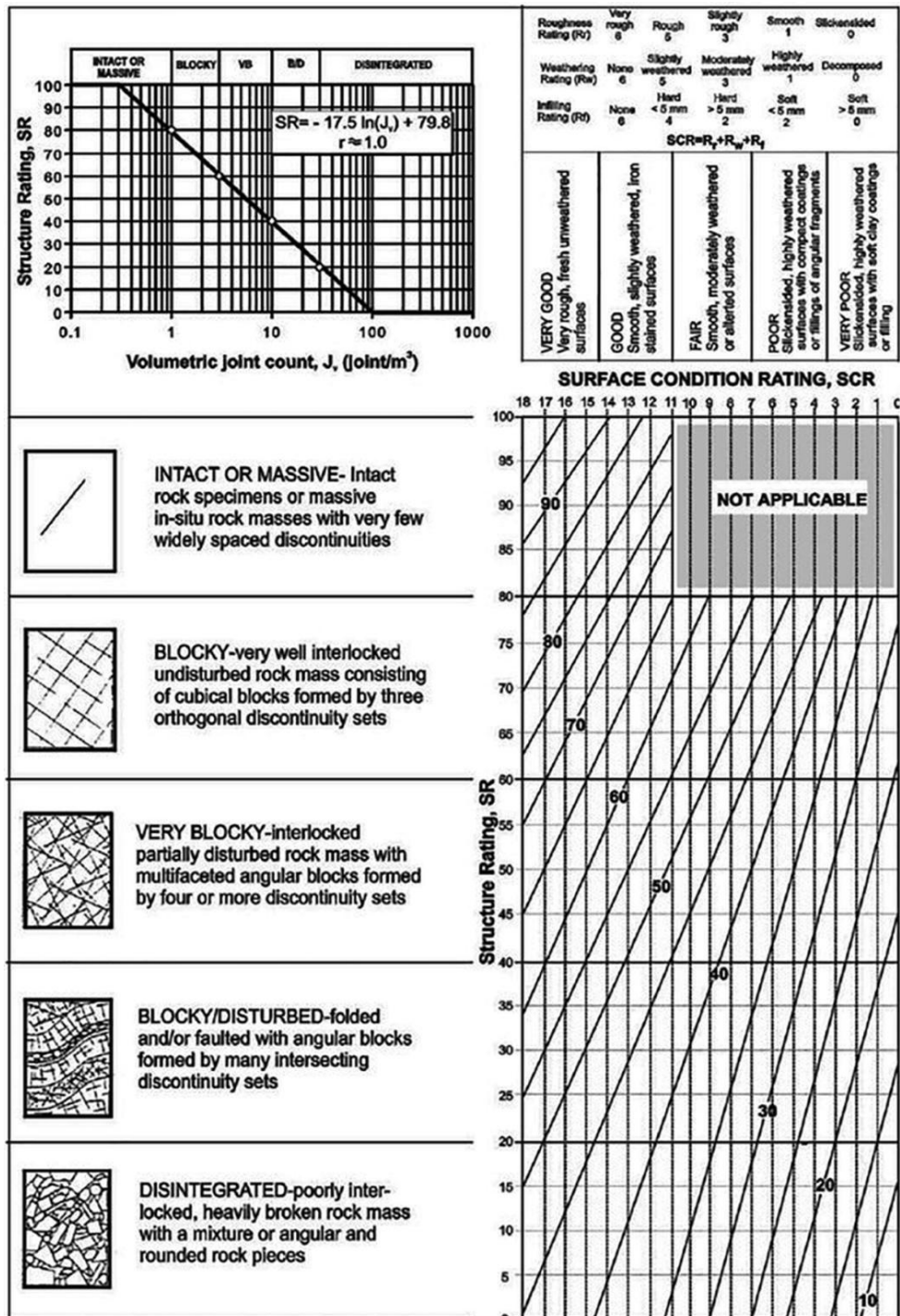


Fig. 2.2 G.S.I. Chart (after Sonmez and Ulusay 1999)

2.8. KINEMATIC ANALYSIS

Kinematic analysis is used to evaluate the safety and stability of slopes under different conditions and to identify possible failure mechanisms (Duncan, 1996; Bishop, 1955). This method of geotechnical engineering addresses slopes that are either man-made or natural. It entails determining possible causes of slope collapse as well as examining the movement of rock masses and soil along preset failure surfaces.

Rocscience software Dips 7.0 describes how blocks or boulders move along geological structures or slip out from the slope's face. For various kinds of slope failures to hold, stereographic projection in kinematic analysis must satisfy planar sliding, wedge sliding, and toppling.

Planar failure: A planar failure happens when the discontinuity's dip angle is smaller than the slope face's angle. At a distance of $\pm 20^\circ$ from the siding surface, the sliding plane needs to be parallel or nearly parallel. This means that the plunge needs to be bigger than the friction angle of the slope and lower than the slope face. The sliding surface's upper end either closes in a tension break or crosses the upper slope.

Toppling failure: It occurs when the discontinuity plane dips into the slope within 10° of a high angle ($> 70^\circ$). The angle of the slope face should be smaller than the dip angle of discontinuity.

Wedge failure: Wedge failure happens when two or more discontinuities meet. The intersecting line of the plunge should be more than the angle of friction between the two side planes and less than the dip angle of the slope face. From an upright position to the line of intersection, the slope face's inclination is measured.

2.8.1. Slope Geometry and Failure Surfaces

Knowing the geometry of the slope under study is the first step in performing kinematic analysis. Among other crucial characteristics, this entails figuring out its angle and discontinuities (such joints, faults, or bedding planes). Additionally,

depending on the characteristics of specific hillslopes, it explains possible surface failures such as circular, ridge-shaped, and flat varieties.

2.8.2. Block Analysis

Kinematics study often involves subdividing the slope into wedges or blocks, which are characterized by discontinuities and possible failure surfaces. Each block is then evaluated for potential movement and instability.

2.8.3. Discontinuity Characterization

The presence and orientation of fractures in the slope materials (e.g. bedding planes) are very important. The orientation of these discontinuities can significantly affect the stability of a slope, thus they must be defined in terms of their dip, dip direction, and spacing (Duncan, 1996).

2.8.4. Block Movement Assessment

The movement of each block is assessed through the relative motion of the blocks along discontinuities and via designated failure surfaces. Whether any blocks are prone to sliding, toppling, or other forms of failure is what this primarily aims at identifying.

2.8.5. Risk Assessment and Mitigation Measures

Kinematic analysis results aid in evaluating the risk associated with slope failure when various scenarios such as heavy rainfall, seismic activity, or changes in loadings occur (Duncan and Wright, 2005; Saraswat and Choudhary, 2018). Recommendations on stabilization measures can be made based on this research. These may entail the addition of structures for support like retaining walls or rock bolts, changing the geometry of the slope, or introduction of drainage techniques.

Kinematic analysis is a useful technique in geotechnical engineering for assessing the stability of different slopes, such as cliffs, excavation sites, and embankments. This helps with the construction of safe and stable slopes by revealing what is likely to cause failures. Numerical modeling methods and contemporary

geotechnical software are frequently employed in complex slope geometries that call for in-depth kinematic analyses used.

2.9. SLOPE MASS RATING (S.M.R.)

This classification system for rock slopes is used for both analyzing the stability of rock slopes and designing and supporting them (Romana, 1985). In the 1980s, Romana and Antonini invented the SMR method for evaluating the quality and condition of rock masses, especially in geotechnical engineering contexts (Antonini and Romana, 1992). Like the Geological Strength Index (GSI) or Rock Mass Rating (RMR) approach, it measures rock mass properties (Romana, 1994; Bieniawski, 1989).

Slope Mass Rating determines the various classes of slopes and their susceptibility to instability (Romana, 1985). It is used to assess the stability of rock slopes (Hoek and Bray, 1981). It is predicated on a thorough examination of the field, which involves gathering information about the orientation of discontinuities with respect to the slope and the technique used to excavate the cut-slope (Romana, 1994). Kinematic analysis must be performed to identify the slope's probable mode of collapse in order to calculate SMR. Using the formula, the adjustment factors (F1, F2, and F3) were computed by deducting them from the RMRB. The table 2.15 shows the slope mass rating adjustment factor following M. Romana in 1985.

$$SMR = RMR_B + F1.F2.F3 + F4 \quad (\text{Equation 2.14})$$

where, the adjustments factors F1,F2,F3 are based on the potential mode of failure, from the kinematic analysis, and F4 depends on the mode of excavation of the slope.

α_j – dip direction of the discontinuity; α_j – dip direction of the slope; α_i –dip direction of intersection of two lines of discontinuities; β_j – dip of discontinuity; β_i – angle of plunge of intersection line of two sets of discontinuities; β_s – dip of the slope

Table 2.15 Slope Mass Rating Adjustment Factor

A. ADJUSTMENT FACTOR FOR F ₁ , F ₂ , F ₃						
Case of slope Failure		Very Favourable	Favourable	Fair	Unfavourable	Very Unfavourable
P	($\alpha_j - \alpha_s$)	>30°	30 ° – 40°	20° – 10°	10°- 5°	<5°
T	($\alpha_j - \alpha_s - 180$)					
W	($\alpha_i - \alpha_s$)					
P/W/T	F ₁	0.15	0.40	0.70	0.85	1
P	β_j	<20°	20° – 30°	30° – 35°	35° – 45°	>45°
W	β_i					
P/W	F ₂	0.15	0.40	0.70	0.85	1
T	F ₂	1	1	1	1	1
P	($\beta_j - \beta_s$)	>10°	10° – 0°	0°	0° – (-10°)	<-10°
W	($\beta_i - \beta_s$)					
T	($\beta_j + \beta_s$)	<110°	110° – 120°	>120°	-	-
P/T/W	F ₃	0	-6	-25	-50	-60
B. SMR ADJUSTMENT FACTOR FOR F ₄						
Method of Excavation (F ₄)			F ₄ Value			
Natural Slope			15			
Pre – Splitting			10			
Smooth Blasting			8			
Nortmal Blasting Or Mechanical excavation			0			
Poor Blasting			-8			
C. SMR RATINGS						

Class No.	V	IV	III	II	I
SMR Value	0 -20	21 – 40	41 – 60	61 – 80	81 – 100
Rock Mass Description	Very Bad	Bad	Normal	Good	Very Good
Stability	Completely Unstable	Partially Stable	Stable	Stable	Completely stable
Failures	Big Planar or Circular	Planer or Big Wedges	Planner along with some joint and many Wedges	Some Block Failure	No Failure
Probability of Failure	0.9	0.6	0.4	0.2	0

All the parameters are rated against their relevant scale to determine their SMR value and all scores are summed up at the end. More stable and favorable conditions on rock slopes would therefore be indicated by higher values of SMR while smaller figures imply less stability. It assists in making well-informed decisions on slope management, excavation methods, and support measures, especially in mining and civil engineering projects where the stability of rock slopes is essential to both project success and worker safety.

2.10. ROCKFALL HAZARD RATING SYSTEM

Rockfalls highways, and railroads built in rock in steep areas are also at risk from rockfalls. Using the Rocfall program, the Colorado Rockfall Hazard Rating System (based on Russell, 2005) models the trajectory and endpoint, estimates the velocity and maximum impact energy, and conducts the study. The number of fatalities from rockfalls is about equivalent to the total number of fatalities from rock slope instability, despite the fact that rockfalls do not pose the same economic danger

as larger failures that might shut down important traffic routes for days (Brunner and Varnes, 2006). Usually, a biological or climatic event that modifies the forces exerted on a rock causes a rockfall. These phenomena could include chemical weathering or degradation of the rock, erosion of the surrounding material during heavy downpours, freeze-thaw cycles in cold climates, growth of roots or leverage from roots moving in strong winds, or increases in pore pressure caused by rainfall infiltration (Gonzalez and Dussan, 2011; Fookes, 1997). The possibility of a rockfall being automatically started in a setting where ongoing is probably one or two orders of magnitude larger than the previously mentioned climatic and biological beginning events (Hung and Evans, 1988; Varnes, 1978).

Rockfall hazard analysis is a systematic method for assessing the risk and the potential consequences of rockfall events in a given area. Rockfalls are natural rock-slope movements in mountainous terrains and cliffs with a rapid free fall of large rock pieces. These events threaten lives, transportation corridors, and infrastructure. A rockfall hazard analysis helps in understanding potential hazards and implementing appropriate mitigation measures. The Rockfall hazard rating system for India is given in the table.

Table 2.16 Rockfall Hazard Rating System of India

Category		3points	9points	27 points	81 points
Slope	Slope height	7.5 m	15 m	23 m	30 m
	Average Slope Angle Score	A	B	C	D
	Vegetation	Fully Vegetated	Patchy Vegetated	Isolated Plants	None
	Lunching Features	None Smooth Slope	Minor (<0.6m) Surface Variation	Many (0.6-1.8m) Surface Variation	Major (>1-8m) Surface Variation
	Ditch Catchment	Good Catchment	Moderate catchment	Limited catchment	No catchment
te	Annual Precipitation	254 mm	508 mm	762 mm	1016 mm

	Annual Freeze/ Thaw Cycle		1 to 5	6 to 10	11 to 15	>16
	Seepage/ water		Dry	Damp/ Wet	Dripping	Running Water
	Slope Aspect		W	N, S, NW, SW	SE, NE	E
Geology	Sedimentary Rock	Degree of undercutting	0 to 0.3 m	0.3 to 0.6m	0.6 to 1.2m	>1.2m
		Slake Durability Index	95 to 100 %	60 to 95 %	30 to 60 %	<30 %
		Degree of interbedding	1 to 2 weak interbed, <15 cm	1 to 2 weak interbed, >15 cm	>2 weak interbed, <15 cm	>2 weak interbed, >15 cm
	Crystalline Rock	Rock Character	Homogeneous/ Massive	Small Fault/ Strong Veins	Schist Shear Zones <15 cm	Weak pematite's/ micas/ shear zones >15 cm
		Degree of overhang	0 to 0.3m	0.3 to 0.6m	0.6 to 1.2m	>1.2m
		Weathering Grade	Fresh	Surface Staining	Slightly Altered/ Softened	Core Stone
	Discontinuities	Block Size/ Volume	0.3m/2.3m ³	0.6m/4.6m ³	0.9m/6.9m ³	1.2m/9.2m ³
		Block Shape	Tabular	Blocky	Blocky to angular	Rounded and Smooth
		Number of sets	1	1 plus Random	2	>2
		Persistence / Orientation	<3m and Dip into slope	>3m and dips into slope	<3 meter and day light out of the slope	>3m and Day light out of the slope
		Apertures	Closed	0.1 to 1 mm	1 to 5 mm	>5mm
		Weathering Condition	Grade I & II	Grade III	Grade IV	Grade V & IV
		Friction	Rough	Undulating	Planner	Slickensided
		Infilling material	Heal infilling	Coarse Grain Fault Gouge	Fine Grain Fault Gouge	Clay Infilling

Traffic	Percentage Decision Sight Distance (DSD)	100%	80%	60%	40%
	Average Vehicle Risk (AVR)	25%	50%	75%	100%
	Road width including Pavement Shoulder (m)	13.2m	10.8m	8.4 m	6m
	No. of accident	0 to 2	3 to 5	6 to 8	9 and over
Rock History/ Frequency		0 to 3 per year	4 to 7 per year	8 to 12 per year	>12peryear

Geologists, engineers, and specialists in risk assessment work in interdisciplinary teams to analyse the hazards associated with rockfalls. The objective is to establish a thorough knowledge of the rockfall danger and to design mitigation plans for the related hazards. Establishing a monitoring program to keep tabs on any modifications to the environmental and geological factors could affect the risk of rockfall. If a rockfall occurs, create an emergency response plan to control and lessen its effects.

2.11. ANALYSIS OF RAINFALL

The summer-monsoon season in Mizoram typically begins in April and continues until late October, with the peak rainfall occurring from May to September. During this extended monsoonal period, the region receives approximately 90% of its annual rainfall, making it one of the wettest periods of the year. This intense and prolonged precipitation has a direct impact on slope stability, particularly in Mizoram's rugged and steep terrain.

Rainfall is widely recognized as one of the primary triggers of landslides in this region. When rainfall intensity and duration increase, infiltration into the soil and underlying rock formations also intensifies. This process leads to increased pore water pressure within the soil, which, in turn, reduces the effective stress and shear strength of slope materials. The loss of shear strength—especially during the peak monsoon months—can lead to the initiation of slope failures and landslides.

Additionally, the percolation of water through soil layers and into existing joints and fractures in the rock mass contributes to mechanical weakening. These structural weaknesses, already vulnerable due to the region's geological conditions, become more susceptible to failure when saturated. The build-up of pore pressure in slopes reduces frictional resistance, making it easier for soil or rock masses to slide.

A comparison between historical rainfall records and landslide event data in Mizoram clearly shows a strong correlation between high rainfall periods and increased landslide frequency. Almost all documented major landslides in the region have occurred during or immediately after heavy monsoon rains, underscoring the critical role of precipitation in triggering slope failures.

The summer-monsoon rains act as a dominant geomorphic agent, both through direct physical processes (like erosion and saturation) and indirect mechanisms (such as increasing pore water pressure and weakening structural integrity). Therefore, rainfall-induced slope instability should be a central consideration in hazard assessment, slope management, and land-use planning in Mizoram.

CHAPTER 3

LITERATURE REVIEW

Landslides studies in different parts of the world in relation to the present study are summarized:

Abbas Taheri and Kazuo Tani (2009) introduced the Slope Stability Rating (SSR) classification system, designed to assess the stability of heavily jointed rock slopes. This system builds upon the modified Geological Strength Index (GSI) and incorporates five additional parameters: uniaxial compressive strength (UCS), rock type, slope excavation method, groundwater conditions, and seismic forces. The SSR is calculated by summing the ratings of these parameters, providing an overall stability assessment for the rock mass.

Abdullah et al. (2018) conducted research on interbedded calcareous sandstone and siltstone with suitable topography in the Karang Sambung district of Central Java, Indonesia, where a small local quarry was present. They analyzed the slope using empirical, kinematic, limit equilibrium, and finite element methods. Based on their findings, the slope in the study area poses a high risk of wedge failure.

Ahmad et al. (2013) used petrographic investigations, XRD, and geomechanical analyses to examine the physical and engineering behavior of basaltic soils and slope stability along SH-72 in Maharashtra. They modeled soil stability using numerical software based on the Limit Equilibrium Method (LEM).

Amir et al. (2021) conducted a slope stability analysis using four distinct Limit Equilibrium Methods—Bishop, Spencer, Janbu, and Morgenstern-Price—to evaluate the impact of a weak layer on slope stability in the context of Newmark analysis. They found that seismic waves have the strongest effect on slope stability when the slope contains an inclined weak layer, whereas the potential failure surface area is greatest when a horizontal weak layer exists at the base of the slope. All four

Limit Equilibrium Methods estimated the maximum effect of seismic waves while maintaining a minimum safety factor.

Ansari et al. (2021) investigated the geotechnical characteristics and instability of slopes composed of in-situ saprolitic soils, particularly phyllite-derived soils, along National Highway-7 in Uttarakhand, India. The study analyzed the physical, microstructural, and geotechnical properties of these soils and their influence on slope instability. Four locations along the highway were assessed through field surveys and laboratory tests to gather geotechnical, chemical, and microstructural data. Stability analyses were conducted using multiple methods, identifying locations 2 and 4 as unstable, while locations 1 and 3 were found to be stable. The results demonstrated that Finite Difference Method (FDM) analysis closely aligned with ground observations, providing valuable insights into soil composition and behavior. This research has implications for future evaluations of similar soils and their applications in construction.

Ansari et al. (2020) analyzed slope stability on road-cut slopes at Devprayag in the Lesser Himalaya, India. The vulnerable slopes were numerically simulated under both dry and saturated conditions using the Limit Equilibrium Method (LEM) and Finite Element Method (FEM). The findings revealed that the area is in a critical state and particularly susceptible to failure during the rainy season due to water percolation through rock fractures.

Ansari et al. (2013) introduced the Rockfall Hazard Rating System for India (RHRSI), a modified version of the technique originally developed by Pierson et al. (1990) and Santi et al. (2009). The revised methodology included new factors while excluding those irrelevant to the Indian subcontinent. They proposed five evaluation categories: slope conditions, climatic conditions, geological conditions, traffic conditions, and rockfall history. Additionally, they recommended incorporating the Slake Durability Index (SDI) for assessing sedimentary rocks within the RHRSI framework.

Azeze (2020) conducted a study in the Gundwin Town area of northeastern Ethiopia, investigating the causes, failure mechanisms, landslide distribution,

geotechnical conditions, slope stability, and factor of safety calculations. This region experiences high landslip activity. The study revealed that, in addition to the type of soil, other factors such as land use and groundwater significantly influence slope failure. The soil samples analyzed included both disturbed and undisturbed materials from the specified slope. Groundwater depth was assessed using parameters such as Atterberg limits (liquid and plastic limits), natural moisture content, unit weight, specific gravity, and shear strength characteristics. Key contributors to slope failure identified in the study include slope angle, slope geometry and modification, land use, groundwater conditions, soil type, and rainfall. The shear-normal force assumption was used to plot safety factor versus lambda graphs, enabling comparison of safety coefficients.

Azeze (2020) investigated slope failure in the Goncha Siso Eneses area of northwestern Ethiopia. This research confirmed that soil properties play a critical role in slope instability. The soils from four selected failed slope sections exhibited similar characteristics. For three of these slope sections, the minimum factor of safety and critical slip surfaces were calculated based on varying parameters, including cohesion, internal friction angle, and plasticity index. The slope stability analysis was conducted using this input data. The study found that rainfall is a major triggering factor at the site. Concave slope geometries, particularly in the Angot and Inegode areas, contributed to precipitation ponding and increased groundwater infiltration, further confirming groundwater's significant impact on slope stability.

Beyabanaki (2021) examined the effect of weak layers on slope stability under seismic loading using four Limit Equilibrium Methods—Bishop, Janbu, Spencer, and Morgenstern-Price. The study addressed a gap in research regarding how weak layers influence slope failure during seismic events, aiming to guide geotechnical, civil, and mining engineers in selecting optimal methods for assessing earthquake-induced landslides in slopes with weak strata. Four scenarios with varying weak layer orientations and locations were simulated using SLIDE version 9.008. Results showed that seismic forces most severely affect slope stability when the weak layer is inclined. Furthermore, the largest potential failure surface area was observed when a horizontal weak layer was located near the base of the slope. The

study recommends using analytical methods that identify the lowest safety factor and the largest potential failure surface, depending on the orientation and position of the weak layer within the slope.

Buyuksagis and Goktan (2006) examined various types of Schmidt hammers in terms of accurately estimating rock Uniaxial Compressive Strength (UCS). They determined that the N-type hammer appeared to be a more effective tool for estimating rock strength within the approximate UCS range of 20-290MPa.

Carvajal et al. (2011) used unmanned aerial vehicles (UAV) to survey landslides along road embankments. They concluded that there was a total inaccuracy of up to 0.12 m in geometric characterization of landslides in road embankments. Both obtained products, DEM and ortho-photos, can be utilized as input data for some of the more commonly used methods and LEM. However, the concept does not applicable to climatic conditions, specifically wind speeds of up to 5m/s.

Epada et al. (2012) investigated the triggering events and mechanisms of a landslide that occurred in Kekem, Western Cameroon, in 2007. Geophysical and geotechnical surveys were conducted to better understand the triggered processes and mechanism of the landslide. The geoelectric analysis indicated clayey sand-filled fracture zones as well as a geographical distribution of argillaceous elements. Penetrometer surveys revealed the existence of these fractures. The mechanical and mineralogical properties of the soil, as well as the angle of internal friction, influence stability. This study demonstrates that electrical soundings combined with geological surveys are effective instruments for characterisation of landslips.

Gougazeh and Al-Shabatat (2013) evaluated the Tannur dam, located 150 km south of Amman and part of the Southern Ghors project for water supply and irrigation in the Jordan Valley. The study looked into the physical and engineering qualities of surface soil samples, as well as alluvium and landslide materials at the dam site and reservoir area, and how these affected the dam abutments' stability. X-ray diffraction (XRD) and particle size distribution (PSD) were used to determine the mineral composition of the samples collected at the site. The results of the geological

and engineering investigations have supplied significant information regarding the physical, engineering, and geotechnical features of the soil, alluvium, and land-slide material at the dam site, which influence the stability. The Atterberg limits, grain size characteristics, and mineralogical composition show that both alluvation and soils at the dam site are very comparable, while there are some composition variances that explain the plasticity difference. Soil stabilizing measures are advised to mitigate the effects of subsurface swelling of the expansive clays in the upper part of the left abutment at the Dam site.

Guillard-Gonclaves et al. (2016) conducted research on the risk assessment of buildings' physical vulnerability to landslides. The risk analysis is used to estimate the risk of landslides. The study area is located in the province of Loures, a municipality in southern Spain. The questionnaire was completed by 52 professionals who participated in the study. The buildings' susceptibility was examined using a bivariate statistical technique. The data showed that one structure was more vulnerable than the others. The vulnerability of the study area was more difficult to quantify than that of higher magnitude landslides. The analysis of the vulnerability for the buildings of the Loures municipality was carried out using a multivariate method.

Ganesh et al. (2017) conducted geophysical prospecting in a specific location along the Mettupalayam-Coonoor Highway, Nilgiris District, Tamil Nadu, India. The geophysical survey data analysis clearly demonstrates the thickness and depth of the top soil. The electrical resistivity study is carried out to characterize and quantify the thickness and depth of the bottom soil. The depth and thickness of the soil, as well as the soil depth, are also investigated.

Gao (2017) investigated soil slope stability, a significant issue in geological contexts prone to landslides and debris flow. In this study, a new global optimization algorithm, the enhanced black hole algorithm, was proposed and merged with the Spencer and Morgenstern-Price methods to create a novel approach for determining the critical slip surface of soil slopes. In terms of locating crucial slip surfaces, the revised black hole algorithm outperformed prior research and the black hole method.

The novel method was validated using numerical soil slope examples and a real-world application in a highway landslide, with encouraging results. The improved black hole algorithm offers a practical and efficient solution for locating critical slip surfaces in soil slopes, with simplified parameter tuning and better accuracy compared to existing methods.

Gupta and Ahmed (2007) investigated a landslide caused by rain at the Surabhi Resort in Missouri. They gathered geotechnical soil data such as moisture content, grain size analysis, and Atterberg's limit, as well as direct shear and point load tests. They also classified the rock mass near the landslide using RMR, Q-system, and GSI categories.

Gupta and Ahmed (2007) researched a landslide caused by rains at the Surabhi Resort in Missouri. They collected geotechnical soil metrics such as moisture content, grain size analysis, and Atterberg's limit, as well as tests like direct shear and point load testing. They also classified the rock mass surrounding the landslide using RMR, Q-system, and GSI classifications.

Janak and Indra (2021) investigated a road cut-slope at Jiling, Nuwakot district, along the Galchi-Trishuti-Mailung-Syaprubeshi-Rasuwigadi route. They discovered that the Jiling District was a sensitive area for slope instability. The results of computer simulations revealed that the various parameters influence the stability of the cut slope. Following the application of the ground anchor, the Factor of Safety (FOS) increased from 0.809 to 1.52.

Hang et al. (2021) investigated the slope stability of Tianmogou, Southeast Tibet. The 3D model was analyzed using a computer-aided design section for numerical analysis of the limit equilibrium method (LEM) and the strength reduction method (SRM). The LEM and SRM are used in the slope stability analysis to provide a more accurate representation of slope stability. According to their findings, the slope has continual displacement variation, and there is still a possibility of landslide disaster due to the continuing influence of authorized rainfall.

He et al. (2012) investigated the rockburst behavior of oriented sandstone with a modified triaxial rock testing device. High-speed cameras capture fracture progression and rock fragment ejection, while scanning electron microscope (SEM) photography reveals microscopic details of the fragments. The results reveal that the mass and velocity of fragments are critical criteria for detecting energy-transferring processes in rockburst testing. The study found that bedding orientation influences rockburst behavior, with rock strength controlling perpendicular orientations and structural stability controlling parallel orientations. Laboratory investigations on sandstone demonstrate the importance of bedding orientation in determining rockburst proneness. Future studies should look into various orientations to better understand their impact on rock burst occurrence.

Hussin et al. (2022) investigated the stability and probable failure of three rock mass categorization methods (Rock Mass Rating (RMR) and Slope Mass Rating) in an abandoned limestone quarry in Perak, Malaysia, for future urban development. Rockfall analysis was used to examine the trajectory of the rock block, and slope kinematic analysis was used to assess the potential cause of failure. Rockfall scenarios were simulated using input data on rock material qualities to assess the site's safety. The findings of this study revealed that the rehabilitation process of abandoned quarry sites necessitates comprehensive geology inputs. The RMR system was used to assess the quality of rock bodies, and the results showed that they ranged from class I (extremely stable) to IV. Furthermore, the rockfall analysis with different rock block sizes proved the effectiveness of gravel-sized rock blocks. The simulation results further demonstrated that the size of the rock block has no effect on the trajectory distance if the fall occurs.

Ip et al. (2020) investigated slope stability in Singapore, where residual soils are often unsaturated due to a deep groundwater table. Ordinary Kriging was used to create spatial distribution maps for three soil properties: effective cohesion, effective friction angle, and saturated permeability. They used this method to estimate soil parameters. Pore-water pressure distribution obtained from the TRIGRS model was used in Scoops 3D to analyze slope stability in the small zonation.

Janak and Indra (2021) investigated cut-slope stability conditions for geological and geotechnical features along the National Highway-7 (NH-7), Uttarakhand, India. They used a deterministic and probabilistic approach to establish the limit equilibrium slope stability. The study's reliability was assessed using finite element properties as well as the mineral composition of the slope materials (debris).

Janevski and Jovanovski (2021) investigated the slope stability method utilizing classic limit equilibrium methods to assess the possibility of circular and non-circular failures, as well as the relatively recent empirical methodology Q-slope. Barton and Bar devised the Q-slope approach (2015, 2017). The fundamental advantage of Q-slope is that the estimation is valid for long-term stable angles without reinforcement. They discovered that both LEM and Q-Slope apply to terrains formed from weathered and tectonically disturbed schist. They believe that combining several instruments and approaches, particularly under highly changeable rock mass circumstances, can produce the most dependable findings.

Kainthola et al. researched slope failures along hill cut roads, which are a big irritant for commuters and highway planners since they can pose a serious hazard. The paper examines the distinct element (DEM) numerical simulation of a 60-meter-high, basaltic and lateritic road cut hill slope in Mahabaleshwar, India, utilizing a DEM technique to determine the factor of safety as well as insights into the likely deformational mechanism for the three scenarios. The three situations were analyzed using the DEM numerical mode, which employs a discrete element analysis (DEA) technique. The DEA numerical mode has also been used to model the seismic response of an open-cast mine. The study's findings have also been compared to existing literature.

Kesimal et al. (2008) investigated the effect of blast-induced acceleration on slope stability at a limestone quarry in Arakli-Tasonu, where a planar shear failure was observed. The study challenge focuses on understanding the failure's triggering mechanism as well as the impact of uncontrolled blasting on slope stability. The process consists of field measurements, laboratory assessments, and limit equilibrium analysis. The results reveal that blast-induced acceleration has a considerable effect

on slope stability, with safety factors falling below the minimal threshold in the presence of water-filled tension cracks. The implications indicate that managing blast design parameters is critical for avoiding slope instability.

Kumar et al. (2017) investigated the major risk of landslides in mountainous terrains, specifically the rock slopes of Amiya, Nainital, Uttarakhand, India. The study problem is to examine the stability of these slopes using geotechnical engineering approaches to avoid possible tragedies. The study's goal is to quantify the global factor of safety (FOS) and compare the conventional Limit Equilibrium Model to sophisticated Numerical Models based on the Mohr-Coulomb failure criterion. The process entails determining rock-mass properties from field samples and employing a variety of stability analysis procedures. The results demonstrate that the slope is stable under normal conditions but may collapse with certain movements and shocks.

Kundu et al. (2018) conducted research on soil slope stability along National Highway-05 at Luhri, Himachal Pradesh, India, which is prone to frequent landslides. The study assessed slope stability under static conditions using both probabilistic and deterministic methodologies, specifically the limit equilibrium method (LEM) and the finite element method (FEM). Both approaches identified vulnerable zones in the research area and determined that the slope is critically stable. A solution involving slope geometry adjustment was developed to improve stability and defend against external variables such as rainfall and earthquakes. The research area's vulnerability to slope failures was related to a variety of anthropogenic activities and natural processes, necessitating the development of corrective measures. The findings indicate that altering the slope shape via benching could effectively boost stability, as shown by LEM and FEM calculations.

Laldinpuia (2019) conducted a cut slope stability analysis of the Rangvamaul Landslide along Aizawl Airport Road in Northeast India. He classified the landslide as debris slide, earth slide, or translational type. According to the deterministic analyses (LEM), the factor of safety is less than unity. Mitigation and protection measures are also recommended.

Laldinpuia (2019) conducted a geological investigation and monitoring of the Ramhlun Sports Complex landslide in Aizawl, Mizoram. He calculated the Atterberg limit, California Bearing Ratio (CBR), Optimal Moisture Content, and Maximum Dry Density (MDD) for each soil sample. Erosion is moving quickly due to the high moisture content and poor CBR and MDD values. Based on the assessment, he decided that the region is unsuitable and unsafe for settlement and building.

Laldinpuia (2018) evaluated the safety factor of the Rangvamlal landslide along the Aizawl airport route using the LEM method. He used Slide 6.0 software to examine the Mohr-Coulomb criterion using multiple approaches, including Ordinary/Fellenius, Bishop simplified, Janbu simplified, Spencer, US Corps of Engineer, and GLE/Morgenstern Price. He also designed and recommended mitigation strategies.

Laldinpuia et al. (2013) investigated Laipuitlang Rockslide in Aizawl, Mizoram. They found that the slide began in the silty-sandstone bedding, which was very worn and steep, and where the road had been carved unsafely. Furthermore, a large permanent structure was built on top. Weathered joint bedding, steep slope, heavy rainfall, water seepage, dangerous rock bed cutting, and overweight building design were all contributing factors to the rockslide, according to field observations.

Laldinpuia (2013) conducted a geological examination of the slumping areas in Saiha town, Southern Mizoram, India. The slumping could be caused by significant precipitation percolation into thick regolith, resulting in pore pressure and reduced soil resistance. The slumping rate rises during the monsoon and falls throughout the other seasons. He also advised mitigating measures such as not constructing RCC buildings in the area and constructing an appropriate drainage system, breast wall, retaining wall, toe wall, and check dam.

Lalhlimpaia et al. (2019) investigated a road-cutting portion along Ngaizel in Aizawl, Mizoram. The Rock Mass Rating rating of 15 out of 100 places the area in category V, indicating that the rock mass is very poor. The main causes of rockfalls include slope angle, geomechanical parameters of rock mass, and anthropogenic activity.

Li et al. (2023) seek to evaluate the impacts of borehole size, roughness, and installation water pressure on the pull load capacity of inflatable rock bolts put in a hard rock mass. The test findings revealed that the load capacity was higher in boreholes near the bolt's initial profile diameter or completely unfolded diameter. In small boreholes, the shoulders of the bolt tongue are compressed tightly, increasing the bolt's load capability. Percussively drilled boreholes have an additional friction angle of around 5.83° , according to back calculations. The experiments revealed that the draw load capacity improves as the installation water pressure increases within the evaluated pressure range. The frictional scratches on the bolts' surfaces indicate that an inflatable bolt is secured in the borehole in three zones along its perimeter: two tongue shoulders and an area opposite the tongue.

Monteiro et al. (2017) investigated effective shear strength values determined by the triaxial test on re-molded sand soil specimens with 50mm and 38mm diameters. They found that using a specimen with a diameter of 38 mm was not recommended.

Niethammer et al. (2008) successfully used unmanned aerial vehicles (UAV) to create high-resolution digital surface models of landslides in the Super-Sauze landslide (Southern France).

Park et al. (2015) present a grid-based probabilistic kinematic analysis method for determining the stability of rock slopes in a geographic information system (GIS). A probabilistic analysis module was created and applied on a cell-by-cell basis to forecast instability in spatially distributed slopes utilizing a GIS environment. Because a probability analysis may be done in a GIS-based context, the proposed approach is a significant tool for overcoming past study restrictions. To test the practicality of our technique, we used steep rock cut slopes in the mountainous area of Baehuryeong, Chuncheon.

Qain et al. (2019) investigate soil slope stability utilizing finite element upper bound (UB) and lower bound (LB) limit analysis (LA) methods on inhomogeneous soil slopes using the Mohr-Coulomb parameters. The goal is to create stability charts for inhomogeneous un-drained soil slope stability and use an artificial neural network

(ANN) to provide reliable stability ratings. The process entails assessing slopes with various parameters and comparing the findings from LA methods to conventional methods. The findings indicate that N_{2ci} increases with specific parameters, and that the ANN technique delivers more convenient and accurate stability forecasts. The study indicates that N_{2ci} values obtained using LA methods are more dependable than those obtained using conventional approaches, and that the ANN training package is an effective tool for slope stability design. The findings can help improve slope stability assessments in geotechnical engineering projects.

Rakshit et al. (2018) investigated the geodynamic evolutionary mechanisms along the Indo-Burmese Ranges (IBR), which serve as the border between the inflexible Burmese Plate and the north-eastward sliding, obliquely sloping Mizoram fold belt. The neotectonic characteristics are linked to the lineament distribution. Lineament research and morphologic fingerprints revealed indicators of active tectonic deformation from the early Pleistocene to the present. The antecedent rivers' lineaments include signs of varied stress components. The results of morphology and lineamental signatures were connected for the river offset lines. The model predicts syntectonic uplift in the study area, as well as evolving IBR during Late Oligocenous thrusting events. This research can indicate probable petroleum migration routes via minute fissures generated during active deformation in the region.

Rao (2020) investigates the mechanical behavior of rocks, rockmass, and crystalline rocks under different loading and unloading situations in order to better understand their strength and deformation properties for civil engineering design. The study challenge entails characterizing rocks, isotropic, anisotropic, and weathered rocks, as well as rockmass, under various stress conditions in order to develop prediction models and solutions for real-world scenarios. The process entails physical modeling of jointed rockmass under various stress states, large-scale testing of rock joints, and the development of analytical solutions for measuring wellbore stability. The findings highlight the crucial role of intermediate primary stress in strength and deformation, present new polyaxial failure criteria, and shed light on brittle fracture propagation and interlocking mechanisms in crystalline rocks. The research findings have significance for the creation of novel models and solutions for

engineering design, as well as a better knowledge of the behavior of rocks and rockmass under varied stress circumstances.

Sardana et al. (2019) investigated road cut slopes along NH-44A from Aizawl to Lengpui Airport in Mizoram, Northeast India. This study used rockmass characterisation to determine the susceptibility of rock slopes along the NH-44A route to landslides. Rock Mass Rating (RMR), geological strength index (GSI), kinematic analysis, and various slope mass rating methodologies have all been used to forecast the stability class of different road-cut slopes. The results demonstrate that the probable failure modes (planar, wedge, and topple) were discovered in the wedge failure for two slopes (L-1 and L-3), in addition to wedge failure. Toppling was the observed failure mode during wedge failure. Kinematic analyses support the reported failure modes during wedge collapse. The slopes of the Aizawl-Lengpui Airport Highway were evaluated for their stability class.

Shama et al. (2017) investigated the geotechnical properties of unconsolidated basaltic soils in the Malshej Ghat region of Maharashtra, India, as a result of recurrent road cut hill slope (RCHS) failures along National Highway-222. The research problem is the considerable diversity in geotechnical qualities of these soils, which causes slope instability and risks for humans. The goal is to assess the geotechnical qualities of these soils using laboratory testing and analysis. The approach includes collecting soil samples from five points along the RCHS, carrying out tests such as moisture content, grain size analysis, Atterberg limits, and strength testing, and applying ASTM standards for analysis. The results demonstrate significant heterogeneity in characteristics, necessitating a location-specific approach to slope stability research. The ramifications include the need for precise geotechnical characterisation for infrastructure projects in mountainous areas.

Sharma et al. (2011) conducted a study to predict the impact strength index (ISI), sonic damping index (SDI), and P-wave velocity of various rocks using empirical models. This study's findings indicate that the Schmidt hammer rebound number can be used to predict ISI, SDI, and P wave velocity. The study also suggests

that P-wave velocity has an exponential relationship with Schmidt rebound number, while ISI and SDI can be connected with Schmidt damping number.

Siddique et al. (2015) investigated landslides along National Highway-58 (NH-58) in the Himalayan terrain to identify safe zones, areas affected by geo-hazards, the current and future vulnerability to landslides, and to characterize the rock mass along NH 58 near Laxman Jhula between Jonk and Rishikesh. In the Garhwal Himalayas region, stability investigations were carried out on 50 road cut slopes utilizing rock mass rating (RMR) and geological strength index (GSI) classification methods. Rock mass data were recorded for slope stability analysis using Bieniawski's (1979) RMR and Romana et al.'s (2012a) SMR geomechanics classification. The LSS values show a strong association between the slopes under consideration and the SMR data. The kinematic analysis based on Markland's test was carried out utilizing the internal friction angle of rock, relative orientation of slopes, and discontinuities, which were measured two to three times in order to discover any possible structurally controlled collapse at the sites under consideration.

Singh et al. (2013) evaluated road-cut slopes along NH-109 using both traditional LEM and numerical FEM approaches.

Singh (2009) conducted a geotechnical assessment of Holangi-Naharlagun Road in Itanagar, Arunachal Pradesh. He discovered that high rainfall, the unconsolidated nature of sediments and joint planes, weak lithology, and human activity all contribute to roadside landslides. He also advised appropriate mitigating actions.

Sissakian et al. (2021) examined the route that passes the Haibat Sultan Mountain in northern Iraq. They've divided the study area into four sections: A, B, C, and D. According to the investigation, Sections A-B and B-C experienced landslides caused by large rocks and soil failure inside the residual soil and/or severely worn claystone beds. Section C-D experienced mass wasting and wedge failure as a result of the presence of soft, well-bedded, and densely joined clay beds. They have advised four corrective actions.

Smith (2015) investigates the role of stress-induced structural deformations in determining rock slope stability. This research discusses how slope-parallel compressive stress affects rock slope stability. The kinematics of rock slope instability were investigated using a stereo-net as a graphical tool to show the possibility for structural slope instability in the rock mass.

Solanki et al. (2019) researched a catastrophic landslide that happened near Khotila village in Dharchula, Nepal, on October 4, 2016. The slope has been modeled with finite-element analysis. The examination of daily rainfall data for the landslide indicates a soft soil with compressive strength. The finite element analysis has been performed, which indicates a weak soil overlying the rockmass, confirming the soil as soft soil. Finite element modeling indicates low tensile strength. The slope has been discovered to be unstable during the rainy season, and the risk caused by this landslide must be assessed in order to lessen the risk.

Thiebes et al. (2013) used the physically based CHASM model to evaluate the stability of a reactivated landslide in the Swabian Alb and integrated it into a prototype early warning system. The system uses automated model runs based on hydrological monitoring and rainfall forecasts, with notifications provided to specialists for decision-making. The results indicate possible instability with low Factor of Safety values, emphasizing the importance of high-quality data on mechanical characteristics and pore water pressure regimes. The study highlights the potential of CHASM for landslide early warning by implementing international geospatial standards for system interoperability. The paper indicates that CHASM can increase the reliability of landslide early warning systems and recommends that future research focus on incorporating slope stability models to improve warning accuracy.

Tsuchida et al. (2019) describe the findings of their analysis of the 2014 Hiroshima landslide tragedy, as well as the process of slope failures that caused several debris flows. A field assessment of the mountain stream where large-scale damage occurred was conducted, and the features of debris flows that caused significant damage were explored. It was discovered that the actual damage caused

by debris flows was substantially worse than projected at 11 of the 18 mountain streams in the Midorii and Yagi districts, where the heaviest damage occurred. Furthermore, the actual volumes of flowing mass in the mountain streams were significantly lower than those projected for the other mountain streams. The field survey determined the volume of the unstable mass of soil, thus the specific restricted regions and zones in the downstream areas were defined accordingly. Damage to structures and human lives occurred far beyond the designated boundaries.

Xu (2011) addressed the critical necessity to assess debris slope stability with a three-dimensional finite element contact approach based on maximum shear stress theory. The study focuses on the Guanjia debris slope in Zhejiang, China, which developed fissures and collapsed after rainfall. Several slope stability analysis methods were used, including traditional limit equilibrium and finite element approaches. The results suggest that the proposed method, which takes into account the spatial influence of the debris slope, delivers more reasonable and trustworthy results than existing methods. The safety factors calculated suggest a critical failure state for the slope. More study is needed to evaluate the proposed approach for other types of slopes. This study emphasizes the need of using an acceptable method for slope stability analysis and offers useful insights for assessing and regulating debris slope stability.

Yalcin (2011) investigated and evaluated the geotechnical properties of landslide locations and their immediate surroundings, comparing them to those of non-landslide areas. The findings indicated that shear strength can be a significant influence in the incidence of landslips in Trabzon province during rainstorms.

According to Yang et al. (2023), landslides are major mountain dangers that result from earthquake-triggered landslide models. They suggest a spatially heterogeneous sampling technique based on local ratios of landslide to non-landslide region. They created a new approach based on a random forest model with the same hyper-parameters as the previous one. The performance of the novel technique was assessed by comparing it to two random forest models. The results show that the

proposed strategy outperforms the existing approach for identifying high landslide threats.

Yilmaz et al. (2008) investigated and published a method for converting RocFall program results to a hazard map in ArcGIS with FallGIS computer code. This study was carried out in Sebinkarahisar, Turkey.

Zairemmawii et al. (2021) investigated rockfall on the state highway in the southern neighborhood of Aizawl, Mizoram. Kinematic analysis was used with the Rocscience software Dips 6.0 to examine the rockfall's behavior. The observed potential modes of collapse for slopes are toppling, planar, and wedge.

CHAPTER 4

RESULTS AND DISCUSSIONS

This chapter presents the findings gathered from multiple field research and laboratory observations. The data show information about the distinctive characteristics and conditions of the studied area.

4.1. FIELD OBSERVATIONS

The study area lies between 23°27'22"N to 23°21'55"N latitudes and 93°19'44"E to 93°23'08"E longitudes. Field photographs depict the observed field condition for all the study slopes. Field studies were conducted in the research area to identify the failed slopes and vulnerable instability variables, including topography, geology, vegetation, drainage patterns, and landslide evidence, by conducting detailed visual surveys of the locations. Rock and soil samples were taken from the field and tested in a laboratory. Field photographs are displayed in figure 4.1 to 4.7.

Six massive landslides are analyzed using the limit equilibrium method (LEM), and each location is named LS1, LS2, LS3, LS4, LS5, and LS6. With a reasonably thick overburden, composed of loose soil at the upslope, a debris slide of dimension 100 meters in width and 62.2 meters in length was observed in location LS1. A landslide of dimension 189 meters in width and 69.57 meters in length was observed at LS2. It is an active debris slide caused by the collapse of the cut slope, in which loose soil slides rapidly down the hillside. In location LS3, a debris slide of thick overburden material occurred due to the destabilization of the slope in the process of road excavation for road construction. The landslide stretched about 142 meters in width and 101.5 meters in length. In LS4, a debris slide of loose, younger material measuring 145.9 meters in length and 95 meters in width is observed. In LS5, a debris slide measuring 145 meters in width and 62 meters in height occurred.

The landslide in LS6 measures 112 meters in width and 54.7 meters in height. A thick overburden composed of colluvium failure in a segmented manner.

For rock mass characterization, vulnerability analysis, and slope stability analyses, seven slopes from different locations are selected. The seven slopes are named as S1, S2, S3, S4, S5, S6, and S7. Different methodologies, which include Rock Mass Ratings (RMR), Kinematic Analysis, and Slope Mass Ratings, are used.

Table 4.1 Sampling sites and slopes under investigation for rock mass characterization

Site	Location
S1	23°23'45.75"N; 93°21'46.00"E
S2	23°23'46.67"N; 93°22'29.33"E
S3	23°23'13.90"N; 93°23'44.93"E
S4	23°23'7.59"N; 93°23'41.62"E
S5	23°23'2.45"N; 93°23'37.28"E
S6	23°22'59.64"N; 93°23'29.44"E
S7	23°22'55.22"N; 93°23'24.67"E

For Rockfall Hazard Rating, six slopes (R1, R2, R3, R4, R5, and R6) are analyzed. A rocsience software Rocfall 4.0 is used for analyzing the bounce height, run-out distance, kinetic energy and translational energy of detached rocks.

The detailed investigations and analyses for each location are discussed sub-heading 4.2 to 4.12. Some of the field photographs are displayed in figures 4.1 to 4.7.



Fig. 4.1 Collapsed Road and Landslides (*The road collapsed and was inaccessible due to landslide.*
Dotted lines represent the road which was collapsed)

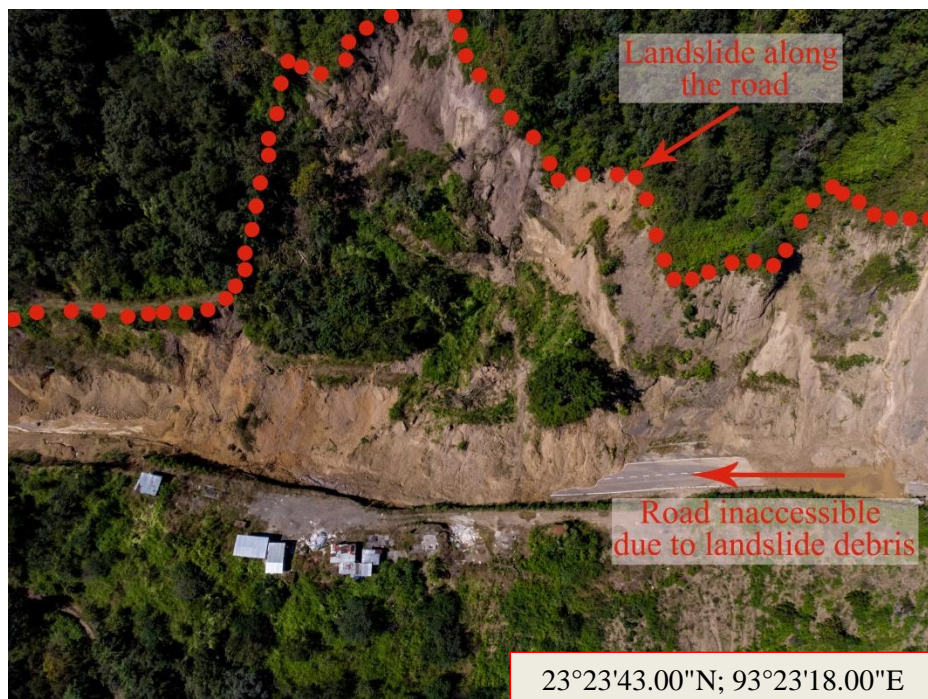


Fig. 4.2 Landslide along the road, which made the road inaccessible



Fig. 4.3 Road and retaining wall collapsed



Fig. 4.4 Slope Failure (*The slope collapsed due to the failure of the joints. Boulders that fell from the slope completely blocked the road*)



Fig. 4.5 Collapsed Retaining Wall (*Due to the collapse of the retaining wall, cracks developed on the road*)



Fig. 4.6 Bedding Plane Failure



Fig. 4.7 Road subsidence (*caused by a landslide at the downhill*)

4.2. DETERMINATION OF ATTERBERG LIMIT

The fundamental metric for comprehending how soils respond to changes in moisture content is the Atterberg limits. As per IS: 2720 (Part 5)-1985, the Atterberg limits test was performed on a fine-grained soil.

4.2.1. *Natural Moisture Content (NMC)*

The geotechnical characteristics of soil including compaction, strength, and stiffness, can be affected by variations in NMC. From laboratory investigation, sample no. LS5 has the highest moisture content, constituting 33.56% of the total weight of the soil, which is one-third of the total weight. Conversely, sample no. LS2 has the lowest NMC of 17.98%, which is relatively less than the other samples. The detailed calculations for the natural moisture content (NMC) for six locations are given in Table 4.1.

Table 4.2 Calculations for Natural Moisture Content (NMC)

Sample No.	Weight of empty container (W1)	Weight of container + wet sample (W2)	Weight of container + dry sample (W3)	Moisture Content	NMC (%)
LS1	38.98	47.09	46.51	7.70252324	22.01
	33.77	48.06	43.49	47.01646091	
	30.77	40.6	39.6	11.32502831	
LS2	32.79	41.89	40.65	15.77608142	17.98
	33.96	49.87	47.02	21.82235835	
	33.01	40.63	39.56	16.33587786	
LS3	26.2	40.25	37.46	24.77797513	25.50
	28.92	41.86	39.04	27.86561265	
	26.34	40.92	38.11	23.87425658	
LS4	31.59	38.75	37.27	26.05633803	19.28
	31.98	40.84	39.68	15.06493506	
	33.15	39.3	38.42	16.69829222	

LS5	39.33	47.12	45.41	28.125	33.56
	33.77	48.06	43.49	47.01646091	
	30.77	40.6	38.6	25.54278416	
LS6	35.02	46.51	44.8	17.48466258	31.31
	35.32	43.69	41.44	36.76470588	
	34.93	43.13	40.8	39.69335605	

4.2.2. Liquid limit

Liquid limit is the lowest water content at which soil maintains its liquid state yet has a small shearing force against flow. To determine the liquid limit, 200 grams of oven-dried soil are extracted and run through a 425 μm sieve. One tool for evaluating the liquid limit test is the Casagrande apparatus. A mixture of soil and water, which forms a thin soil-paste, is placed on the Casagrande apparatus. It is cut into two halves using a spatula to form a groove. The number of blows required for the soil to seal a groove of a specific length is used to record the findings. The liquid limit for each sample is given in table 4.1 and the graphs for each sample (LS1, LS2, S3, LS4, LS5, and LS6) are displayed in figure 4.8 to 4.13.

Table 4.3 Calculations of liquid limit for each soil sample

Sample No	No. of Blows	Moisture Content	Liquid Limit
LS1	21	32.34	20.32
	28	28.85	
	37	23.73	
	38	22.45	
LS2	23	20.75	20.29
	28	19.44	
	36	18.78	
	39	17.22	

LS3	22	34.55	34.01
	29	33.29	
	37	32.05	
	38	31.54	
LS4	23	21.51	21.06
	32	19.25	
	36	17.89	
	38	16.26	
LS5	22	44.52	43.68
	27	43.25	
	31	41.78	
	33	41.01	
LS6	21	41.55	41.07
	25	40.96	
	36	40.01	
	39	39.78	

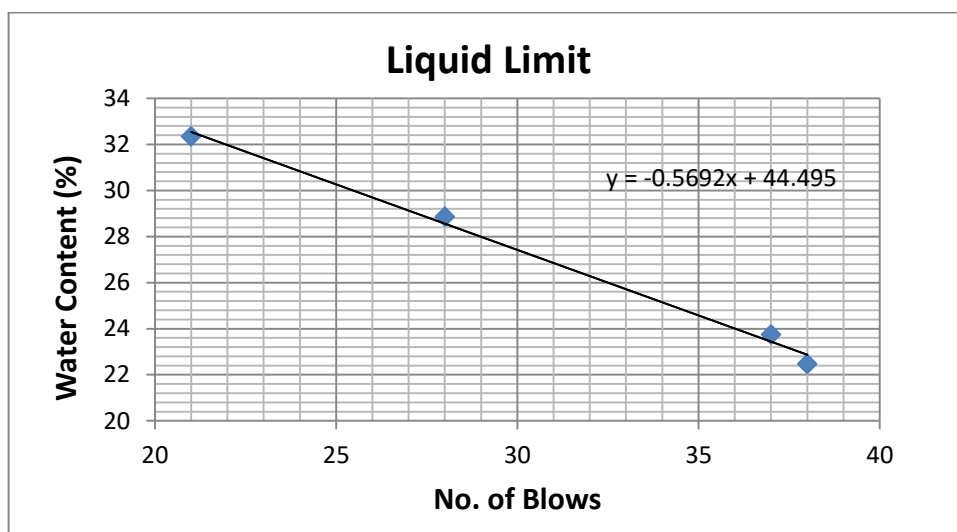


Fig. 4.8 Liquid Limit of LS1

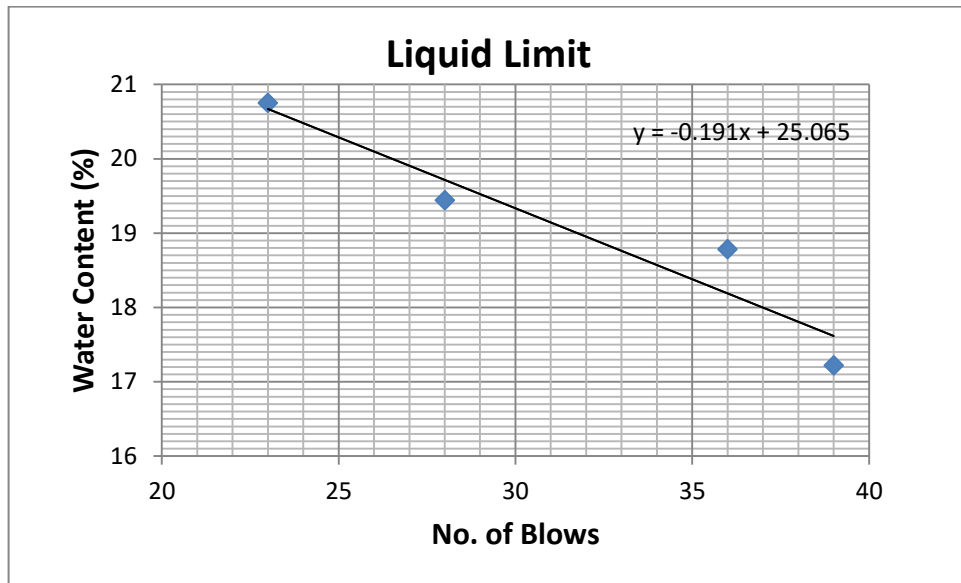


Fig. 4.9 Liquid Limit of LS2

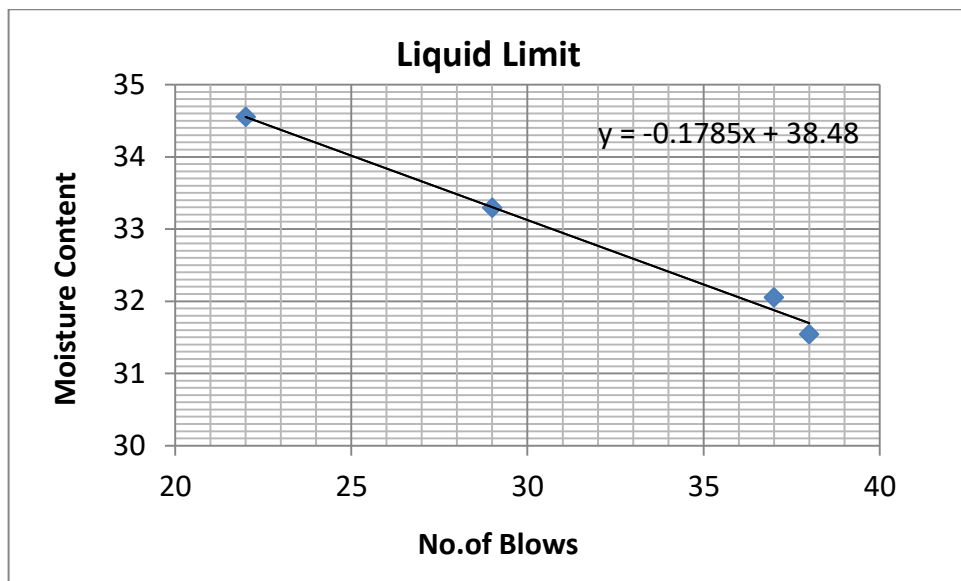


Fig. 4.10 Liquid Limit of LS3

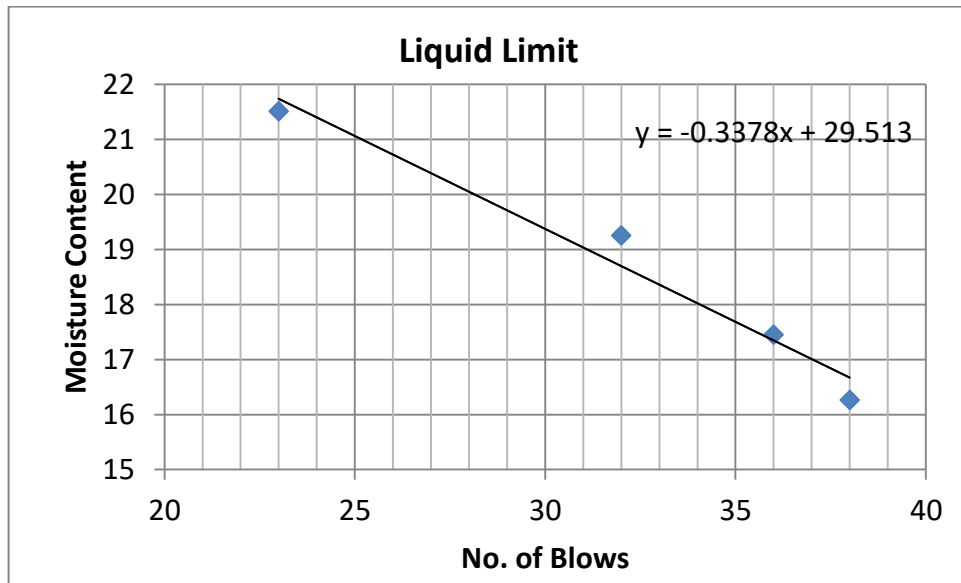


Fig. 4.11 Liquid Limit of LS4

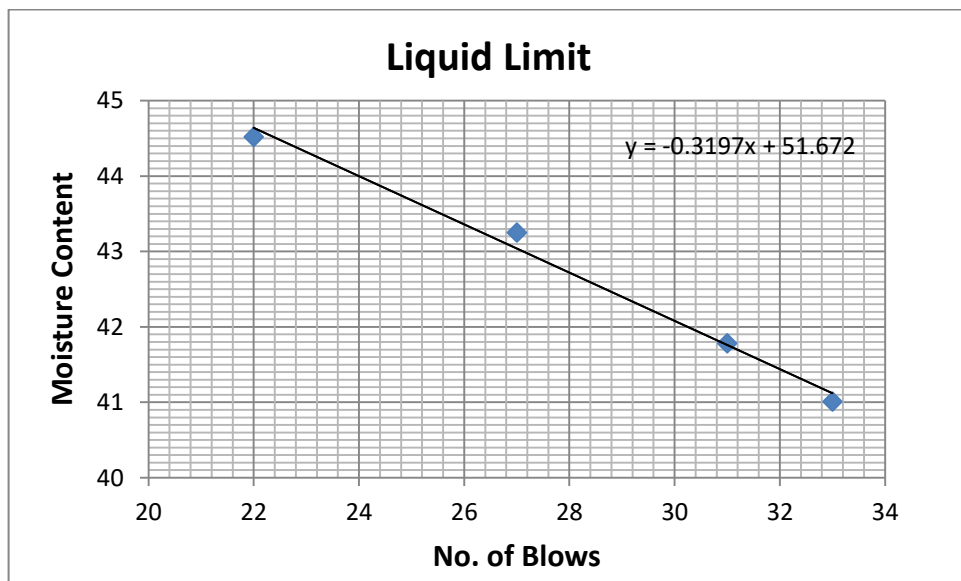


Fig. 4.12 Liquid Limit of LS5

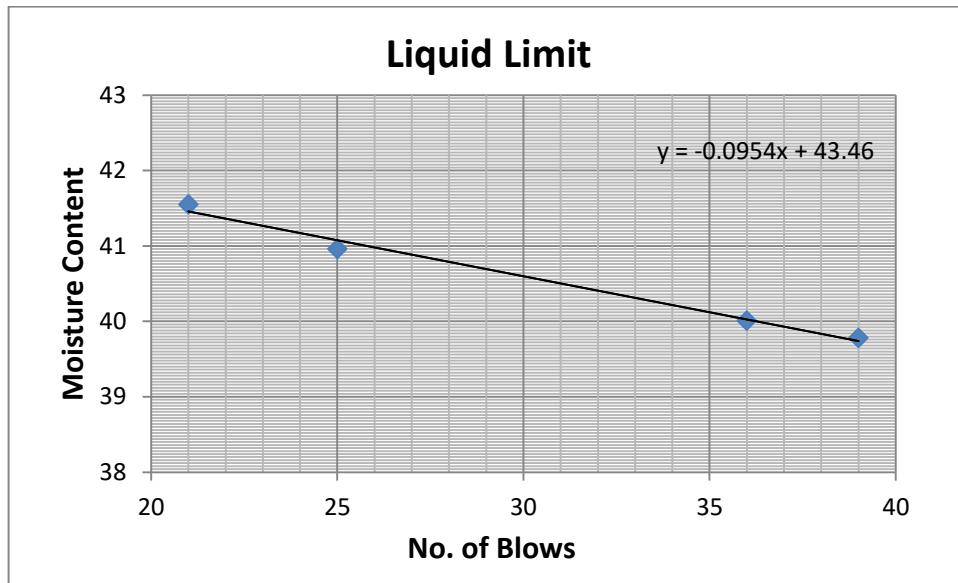


Fig. 4.13 Liquid Limit of LS6

4.2.3. Plastic limit

The Indian Standard IS: 2720 (Part 5)-1985 is followed for performing the Plastic Limit test. The prepared sample is rolled on the glass plate into a thin thread about 3 mm in diameter before it crumbles. Once the soil thread crumbles, it is then collected into a container. The weight of the soil moisture is measured. The plastic limit ranges from 17.70 (LS2) to 31.89 (LS5). The plastic limit for different location is given in table 4.2.

Table 4.4 Results of plastic limits for each soil sample

Sample No.	Weight of container with Lid, W1 (in gram)	Weight of container with Lid + wet of soil, W2 (in gram)	Weight of container with Lid + dry of soil, W3 (in gram)	Weight of dry soil	Weight of water in the soil	Moisture content, w (%)	Plastic Limit
LS1	5.38	7.00	6.73	1.35	0.27	20.00	19.66
	4.71	6.37	6.09	1.38	0.28	20.29	
	4.59	6.59	6.27	1.68	0.32	19.04	
	4.27	6.74	6.34	2.07	0.4	19.32	
LS2	26.48	29.68	29.18	2.70	0.50	18.51	17.62

	26.65	29.45	29.03	2.38	0.42	17.64	
	26.68	32.07	31.29	4.61	0.78	16.92	
	25.89	32.03	31.12	5.23	0.91	17.39	
LS3	26.41	31.83	30.88	4.47	0.95	21.25	22.22
	26.13	29.73	29.04	2.91	0.69	23.71	
	26.39	31.04	30.19	3.80	0.85	22.36	
	26.44	30.78	30.01	3.57	0.77	21.56	
LS4	26.65	33.03	32.01	5.36	1.02	19.03	18.65
	26.40	32.16	31.26	4.86	0.90	18.51	
	26.60	31.86	30.86	4.26	0.82	19.24	
	26.01	31.94	31.01	5	0.93	18.6	
LS5	26.01	28.37	27.81	1.80	0.56	31.11	31.84
	26.46	28.64	28.08	1.62	0.56	34.56	
	26.09	27.91	27.49	1.40	0.42	30.00	
	26.25	28.91	28.27	2.02	0.64	31.68	
LS6	5.26	6.45	6.38	1.12	0.07	36.25	27.83
	4.54	6.14	5.71	1.17	0.43	36.75	
	4.61	6.37	5.88	1.27	0.49	38.58	
	4.57	6.15	5.81	1.24	0.34	27.41	

4.2.4. Plasticity Index

The Plasticity Index determines the ability of fine-grained soils to undergo deformation without cracking. Soil with a higher plasticity index has a greater potential for changing its volume. The plasticity index is given in table 4.3.

Table 4.5 Plasticity index for different location

Sample No.	Plasticity Index	Classification
LS1	9.54	Medium plastic

LS2	2.67	Slightly Plastic
LS3	11.79	Medium plastic
LS4	2.41	Slightly plastic
LS5	11.84	Medium Plastic
LS6	13.24	Medium Plastic

4.2.5. *Liquidity Index (L.I.) and Consistency Index (C.I.)*

The liquidity index indicates the consistency of cohesive soil in its natural condition relative to other states. Alternately, the firmness of soil is determined by its consistency index. According to the standard classification provided by Coduto (1999) and updated after Sower (1979), the soil is classified as medium stiff to stiff based on the obtained values of the fluidity index and consistency index. Table 4.5 provides the obtained value for each sample.

Table 4.6 Liquidity Index and Consistency Index and their classification

Sample No	Liquidity Index	Classification	Consistency Index	Classification
LS1	0.23	Stiff	0.77	Stiff
LS2	0.13	Stiff	0.87	Stiff
LS3	0.27	Medium Stiff	0.72	Medium Stiff
LS4	0.26	Stiff	0.73	Stiff
LS5	0.14	Stiff	0.85	Stiff
LS6	0.26	Medium Stiff	0.7	Medium Stiff

4.3. ANALYSIS USING PROCTOR COMPACTION

Proctor Compaction Test is a widely used method for assessing the ideal moisture content and maximum dry density of soil. These parameters are fundamental in construction, slope development and civil engineering. By conducting compaction test, the amount of moisture content and density of the soil for the required compactness can be determined. The value of dry density for each prepared sample as per IS: 2720 Part VII-1980 is given in table 4.4 to 4.9 and the graphs of the compaction curve (moisture content vs. density) for each location is given in figure 4.14 to 4.20.

Table 4.7 Standard Proctor Test for LS1

Sl. No.	Particulars	Unit	Trial		
			1	2	3
1.	Mass of empty mould (M1)	gm	4160	4160	4160
2.	Volume of mould (V)	cc	997.46	997.46	997.46
3.	Mass of mould + Soil Sample (M2)	gm	6100	6180	6160
4.	Mass of wet soil (M)	gm	1940	2020	2000
5.	Wet/ Bulk Density (γ_{wet})	g/cc	1.94	2.03	2.01
6.	Water content (w)	%	8	10	12
7.	Dry density (γ_d)	g/cc	1.80	1.84	1.79

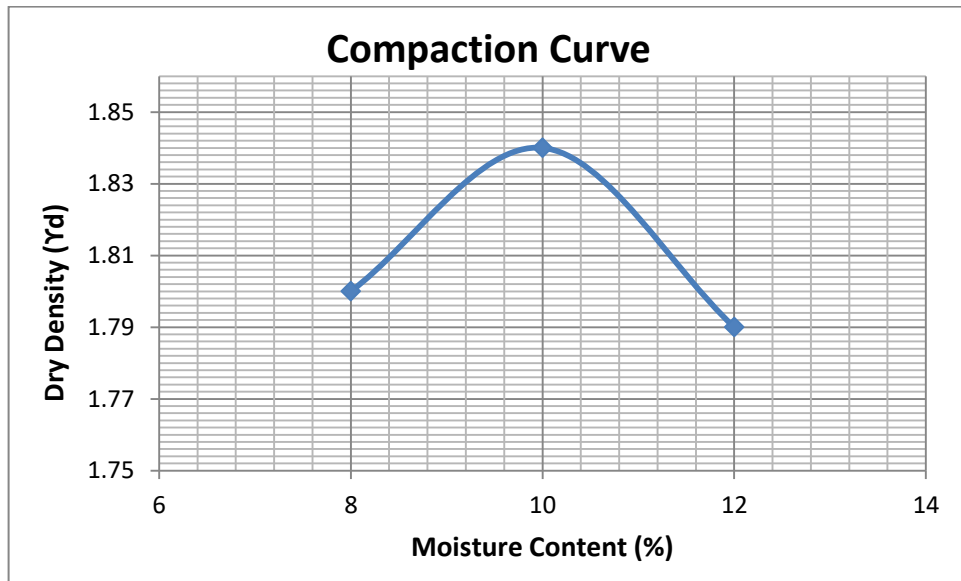


Fig. 4.14 Moisture Content Vs. Dry Density for LS1

Table 4.8 Standard Proctor Test for LS2

Sl. No.	Particulars	Unit	Trial		
			1	2	3
1.	Mass of empty mould (M1)	gm	4160	4160	4160
2.	Volume of mould (V)	cc	997.46	997.46	997.46
3.	Mass of mould + Soil Sample (M2)	gm	6120	6180	6180
4.	Mass of wet soil (M)	gm	1960	2020	2020
5.	Wet/ Bulk Density (γ_{wet})	g/cc	1.9	2.03	2.03
6.	Water content (w)	%	8	10	12
7.	Dry density (γ_d)	g/cc	1.82	1.84	1.81

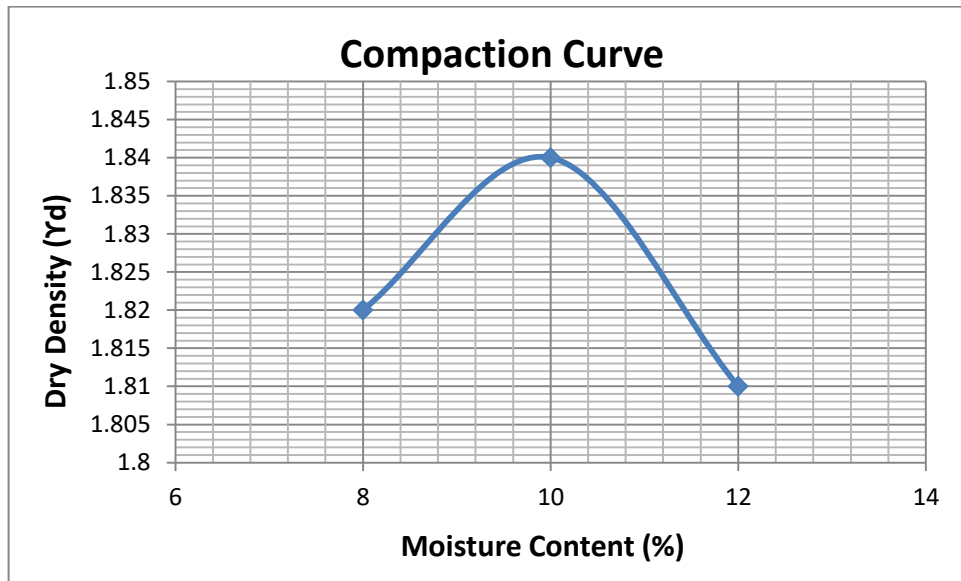


Fig. 4.15 Moisture Content Vs. Dry Density for LS2

Table 4.9 Standard Proctor Test for LS3

Sl. No.	Particulars	Unit	Trial		
			1	2	3
1.	Mass of empty mould (M1)	gm	4160	4160	4160
2.	Volume of mould (V)	cc	997.46	997.46	997.46
3.	Mass of mould + Soil Sample (M2)	gm	5960	6140	6120
4.	Mass of wet soil (M)	gm	1800	1980	1960
5.	Wet/ Bulk Density (γ_{wet})	g/cc	1.80	1.99	1.96
6.	Water content (w)	%	10	12	14
7.	Dry density (γ_d)	g/cc	1.64	1.77	1.72

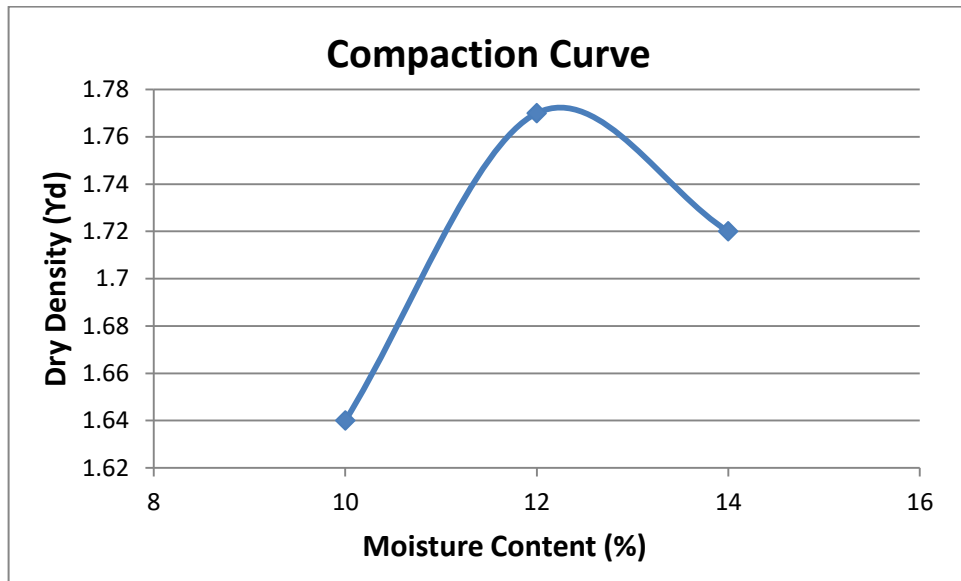


Fig. 4.16 Moisture Content Vs. Dry Density for LS3

Table 4.10 Standard Proctor Test for LS4

Sl. No.	Particulars	Unit	Trial		
			1	2	3
1.	Mass of empty mould (M1)	gm	4160	4160	4160
2.	Volume of mould (V)	cc	997.46	997.46	997.46
3.	Mass of mould + Soil Sample (M2)	gm	6140	6220	6200
4.	Mass of wet soil (M)	gm	1980	2060	2040
5.	Wet/ Bulk Density (Y _{wet})	g/cc	1.99	2.07	2.05
6.	Water content (w)	%	8	10	12
7.	Dry density (Y _d)	g/cc	1.84	1.88	1.83

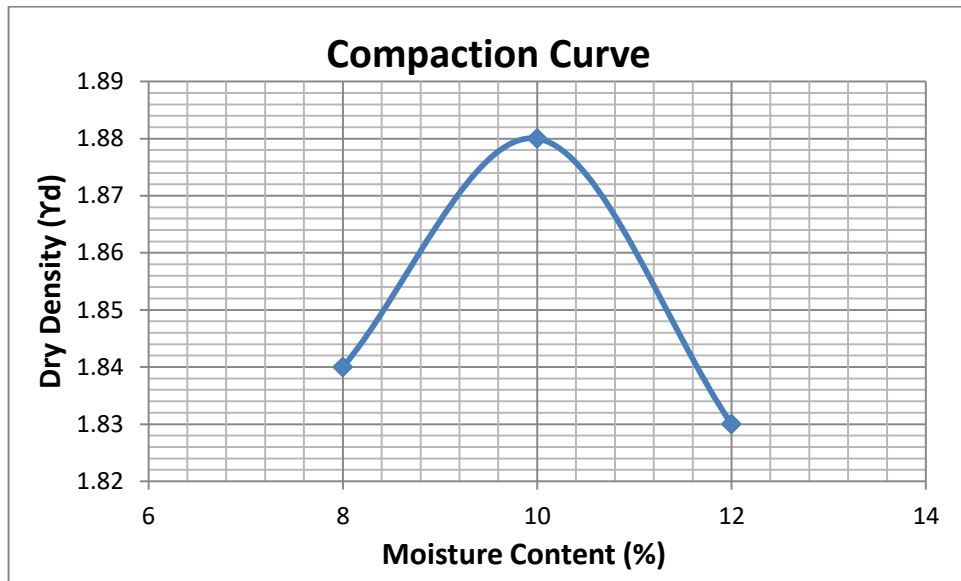


Fig. 4.17 Moisture Content Vs. Dry Density for LS4

Table 4.11 Standard Proctor Test for LS5

Sl. No.	Particulars	Unit	Trial		
			1	2	3
1.	Mass of empty mould (M1)	gm	4160	4160	4160
2.	Volume of mould (V)	cc	997.46	997.46	997.46
3.	Mass of mould + Soil Sample (M2)	gm	5960	6020	5980
4.	Mass of wet soil (M)	gm	1800	1860	1820
5.	Wet/ Bulk Density (γ_{wet})	g/cc	1.80	1.86	1.82
6.	Water content (w)	%	18	20	22
7.	Dry density (γ_d)	g/cc	1.53	1.55	1.50

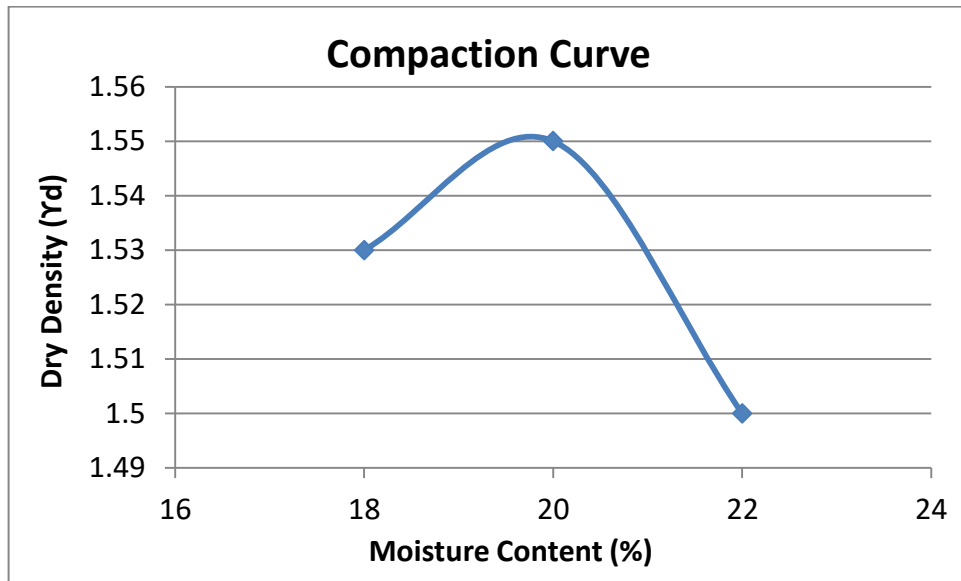


Fig. 4.18 Moisture Content Vs. Dry Density for LS5

Table 4.12 Standard Proctor Test for LS6

Sl. No.	Particulars	Unit	Trial		
			1	2	3
1.	Mass of empty mould (M1)	gm	4160	4160	4160
2.	Volume of mould (V)	cc	997.46	997.46	997.46
3.	Mass of mould + Soil Sample (M2)	gm	5780	5920	5960
4.	Mass of wet soil (M)	gm	1620	1760	1800
5.	Wet/ Bulk Density (Y _{wet})	g/cc	1.62	1.76	1.80
6.	Water content (w)	%	18	20	22
7.	Dry density (Y _d)	g/cc	1.38	1.47	1.39

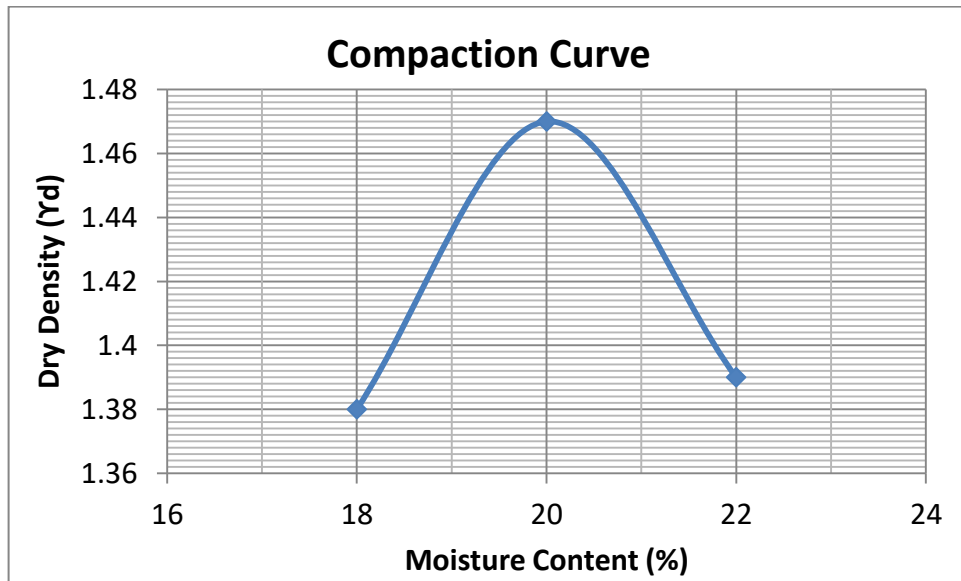


Fig. 4.19 Moisture Content Vs. Dry Density for LS6

4.4. DIRECT SHEAR TEST

The direct shear test was performed as per IS: 2720 (Part 13)-1986 to ascertain the shear properties of soil, namely cohesion (c) and angle of friction (Φ). It offers important information on the mechanical characteristics of soil. Interlocking action and sliding and rolling friction are the causes of the friction between sand particles. A direct shear test was performed for six samples, each sample representing different locations. The cohesion (c) ranges between 0.145 and 0.27, and the angle of friction ranges between 7.26° and 40.29° . The results of direct shear tests are given in table 4.10, and figure 4.21 to 4.26 show the graphs representing Normal Stress versus Shear Stress.

Table 4.13 Direct shear test value for each location

Sl. No.	Normal stress σ (kg/cm ²)	Shear Stress at Failure τ (kg/cm ²)	Cohesion (c) (kg/cm ²)	Angle of Shearing Resistance (Φ)
LS1	0.5	0.439	0.216	21.86°

	1	0.574		
	1.5	0.840		
LS2	0.5	0.386	0.163	22.04°
	1	0.533		
	1.5	0.788		
LS3	0.5	0.263	0.392	9.99°
	1	0.420		
	1.5	0.893		
LS4	0.5	0.293	0.145	17.84°
	1	0.495		
	1.5	0.615		
LS5	0.5	0.686	0.27	40.29°
	1	1.151		
	1.5	1.534		
LS6	0.5	0.248	0.168	7.26°
	1	0.263		
	1.5	0.375		

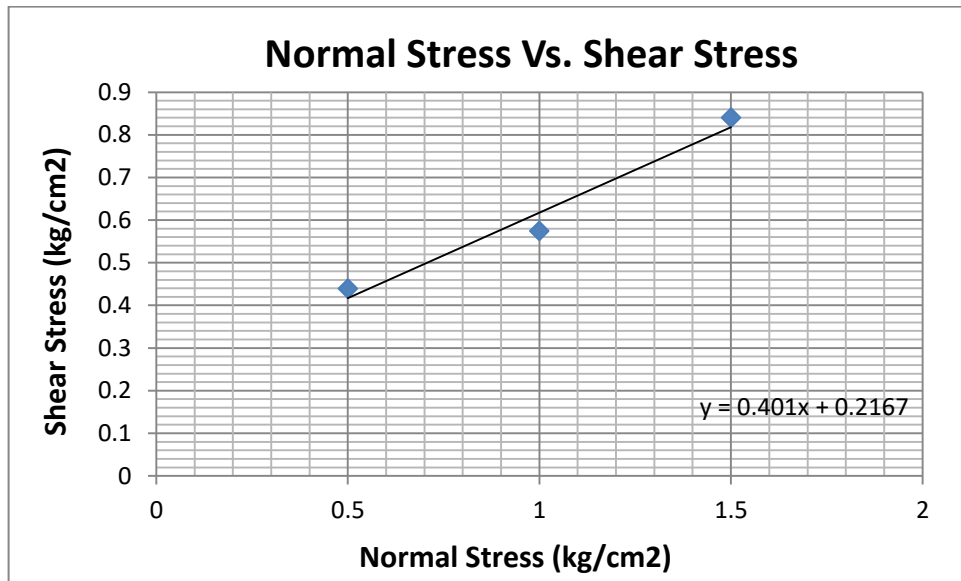


Fig. 4.20 Shear Stress at Failure for LS1

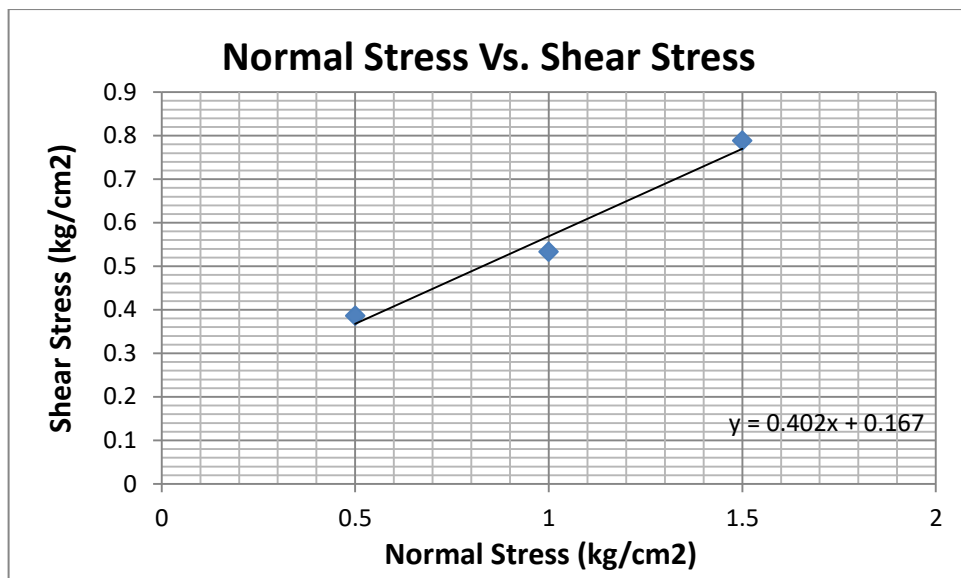


Fig. 4.21 Shear Stress at Failure for LS2

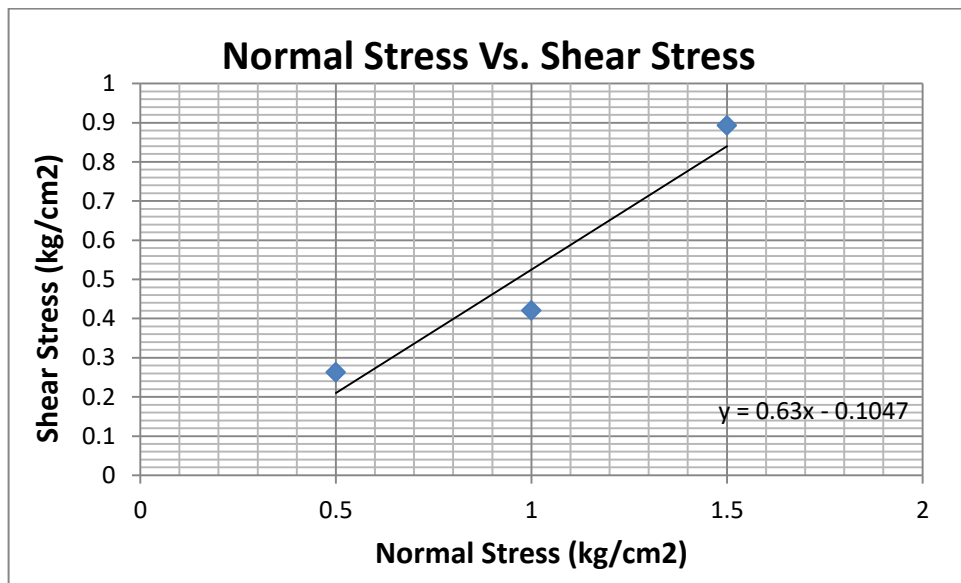


Fig. 4.22 Shear Stress at Failure for LS3

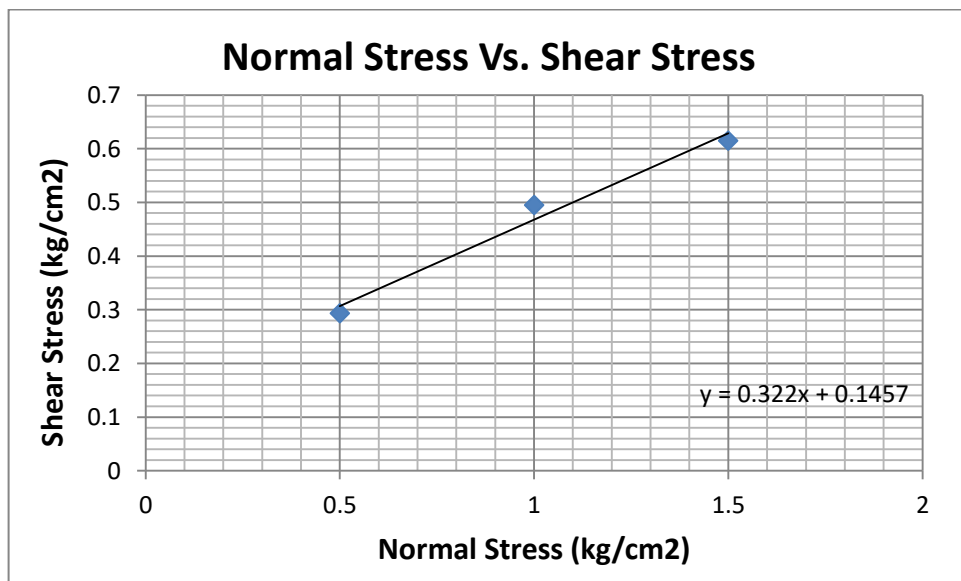


Fig. 4.23 Shear Stress at Failure for LS4

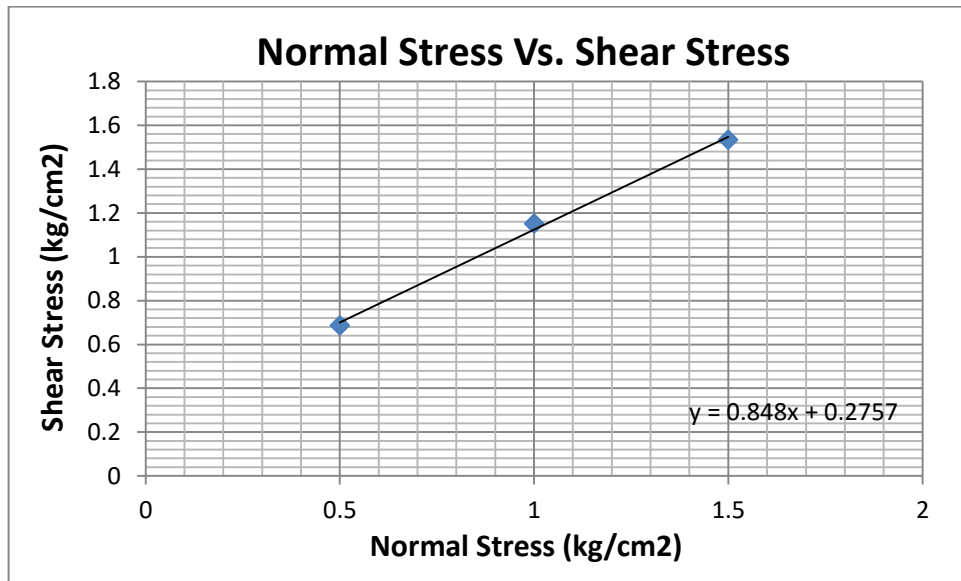


Fig. 4.25 Shear Stress at Failure for LS5

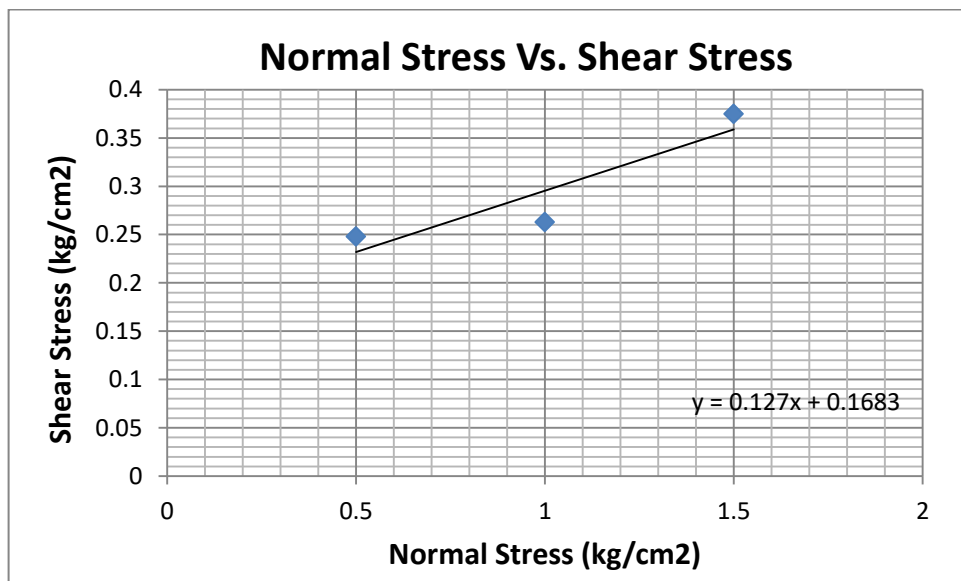


Fig. 4.25 Shear Stress at Failure for LS6

4.5. ANALYSIS OF SLOPE STABILITY USING LIMIT EQUILIBRIUM METHOD (LEM)

Slope stability analyses for selected sites, i.e., LS1, LS2, LS3, LS4, LS5, and LS6 were done using a Limit Equilibrium Method, as shown in figure 4.27 to 4.50. Different techniques, including the GLE/Morgenstern-Price, Janbu Simplified, Bishop Simplified, and Ordinary/Fellenius approaches, were applied using the Rocscience program Slide 6.0. Using the Mohr-Coulomb criterion, a factor of safety is determined numerically.

The angle of friction and the cohesion of a soil obtained by the direct shear test, and dry unit weight obtained by standard proctor test are utilized in the LEM for analyzing slope stability, which is shown in table. The factor of safety obtained by different methods for each sites are given in table 4.11.

Table 4.14 Input Parameters of soil properties for different study sites

Location	Unit Weight (kN/m ³)	Strength type	Cohesion (kg/cm ²)	Friction Angle (Φ)	Water Surface	Ru value
LS1	19.79	Mohr-Coulomb	0.216	21.86°	None	0
LS2	17.02	Mohr-Coulomb	0.163	22.04°	None	0
LS3	19.2	Mohr-Coulomb	0.392	9.99°	None	0
LS4	18.05	Mohr-Coulomb	0.145	17.84°	None	0
LS5	15.205	Mohr-Coulomb	0.27	40.29°	None	0
LS6	16.08	Mohr-Coulomb	0.168	7.26°	None	0

4.5.1. LS1 (23°23'34.22"N; 93°22'42.90"E)

Melbuk village is located on the crown of LS1 and the road connecting Zokhawthar runs through the town. It is an active debris slide due to large-scale cut slope failure, with a relatively thick overburden, mainly loose soil, present at the upslope. The unchannelized water penetrating the thick overburden reduced the cohesiveness of the soil. Gabion walls were constructed at the base of the landslide with no slope-easing techniques used. It destroyed the road and parts of the gabion walls causing the asphalt to pop up. The affected area stretched about 100 meters in width and 62.2 meters in length. The average factor of safety for different methods is 0.827. Figure 4.27 (a) and (b) display the field photograph and figures 4.28, 4.29, 4.30, and 4.31 display LEM analyses using different methods.





Fig. 4.26 Field photograph of LS1

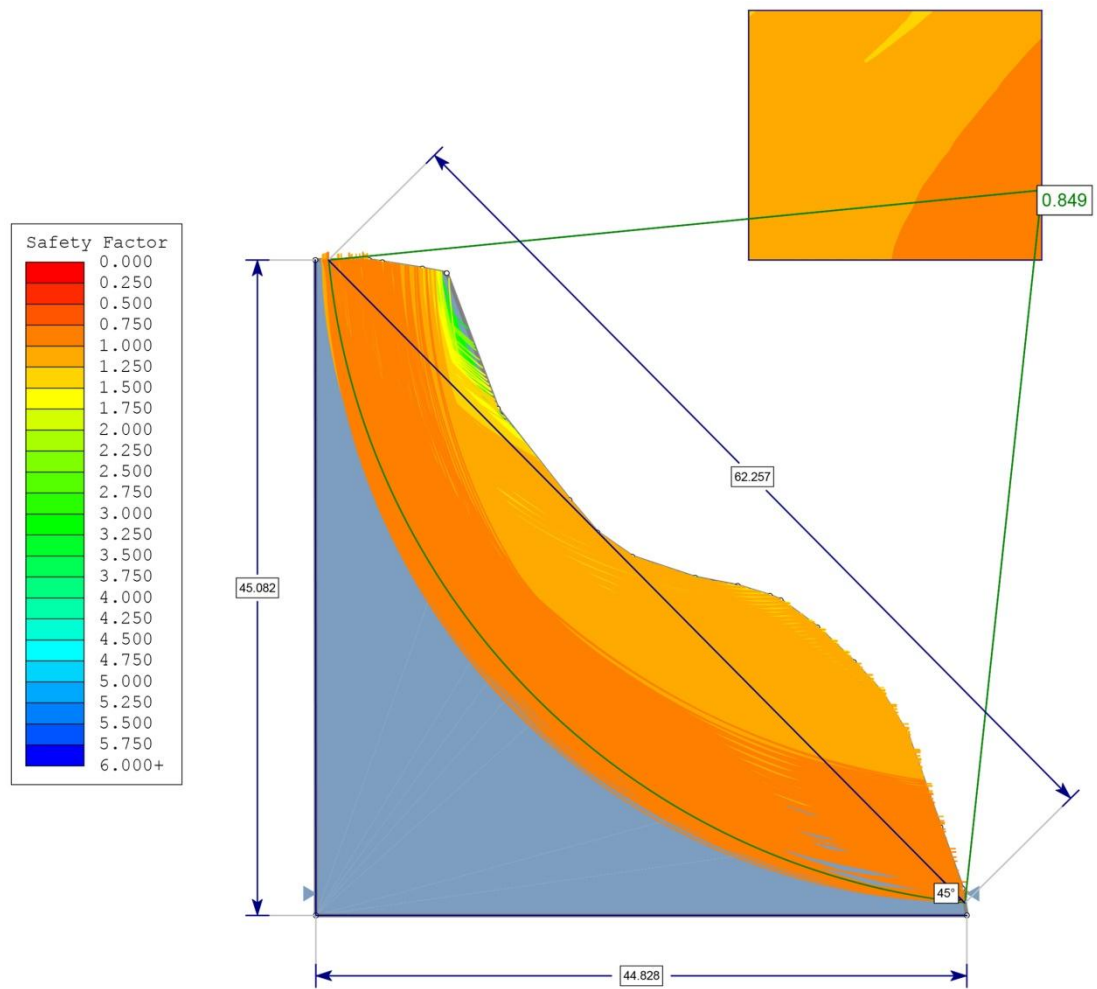


Fig. 4.27 GLE/ Morgenstern-Price method of LEM Analysis for LS1

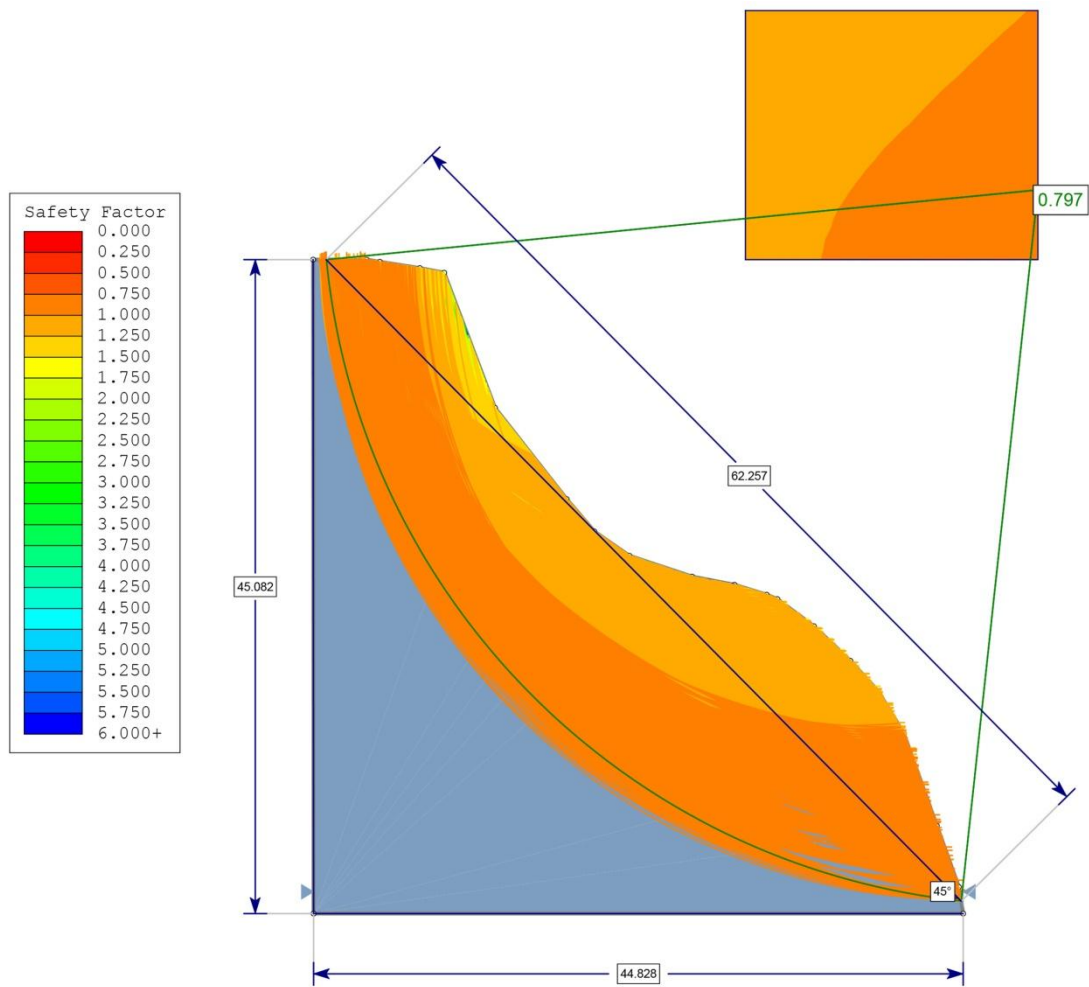


Fig. 4.28 Janbu Simplified method of LEM Analysis for LS1

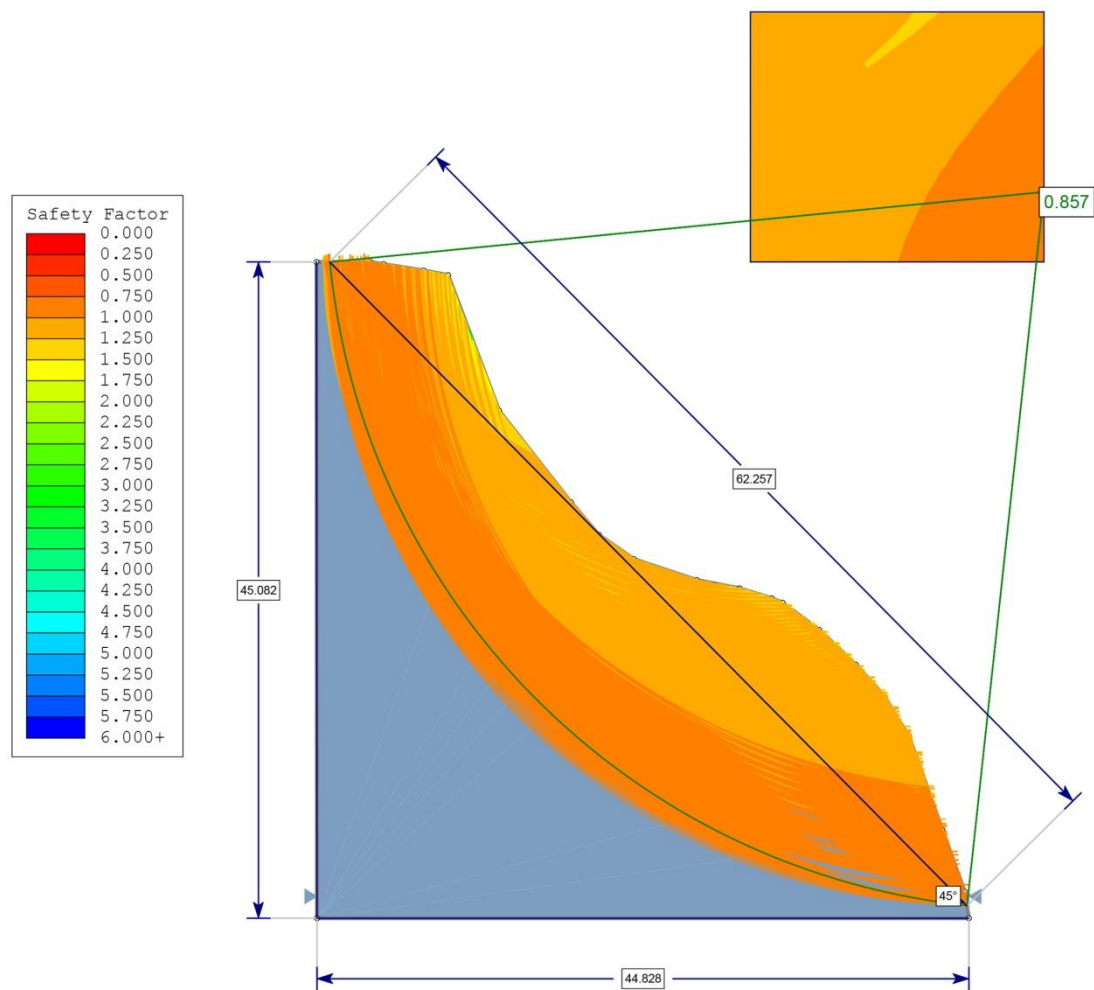


Fig. 4.29 Bishop Simplified of LEM Analysis for LS1

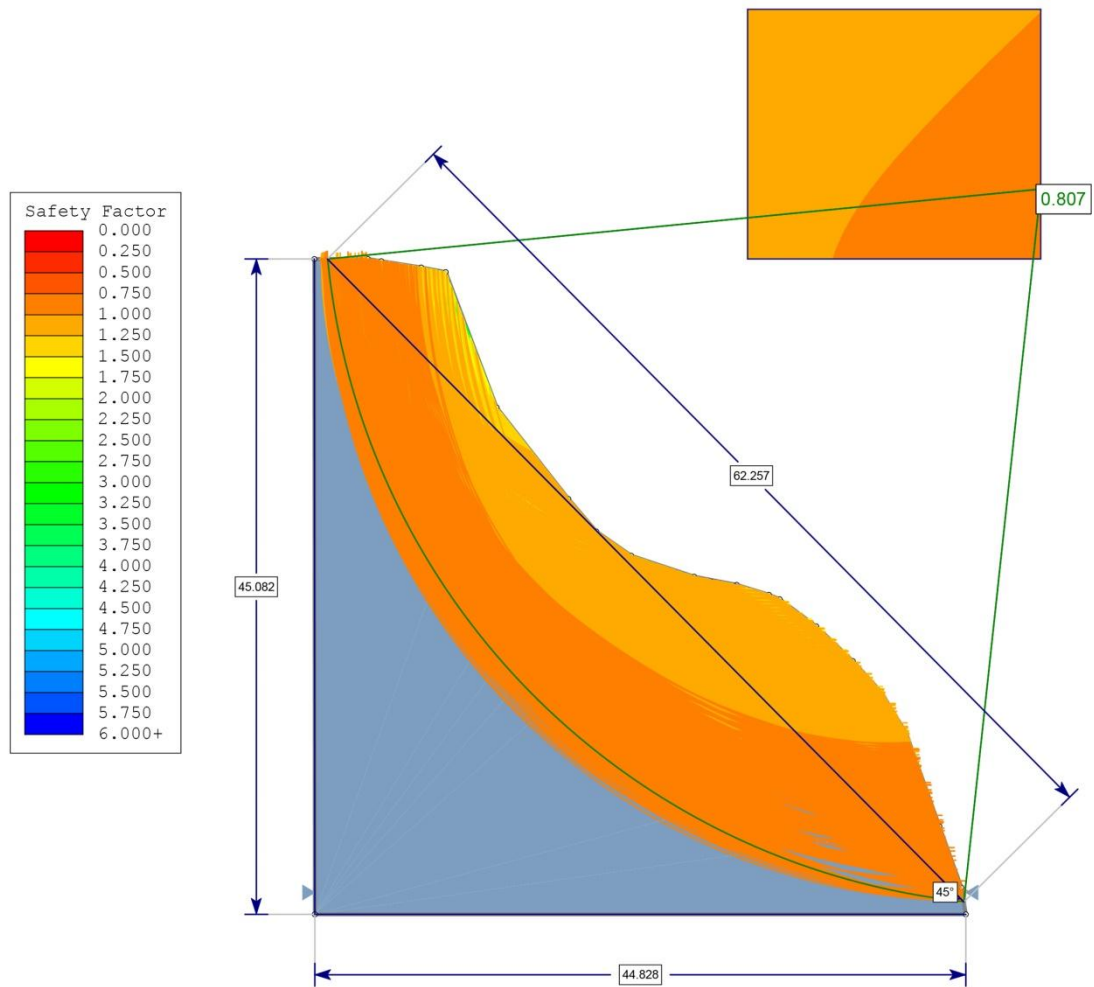


Fig. 4.30 Ordinary/ Fellenius method of LEM Analysis for LS1

4.5.2. LS2 (23°23'43.00"N; 93°23'18.00"E)

Zokhawthar Road via Melbuk is located on the uphill of LS2. It is an active debris slide due to cut-slope failure, where unconsolidated earth material moves rapidly down the slope. A gabion walls at the toe were damaged by landslide debris. The unchannelized widespread flow of water including surface runoff and those penetrating the ground contributes as one of the triggering factors for LS2 slope failure. The sliding area stretched about 189 meters in width and 69.57 meters in length. The average factor of safety for different methods is 0.719. Figures 4.32 (a) (b) and (c) display the field photographs and figures 4.33, 4.34, 4.35, and 4.36 display LEM analyses using different methods.





Fig. 4.31 Field Photographs of LS2

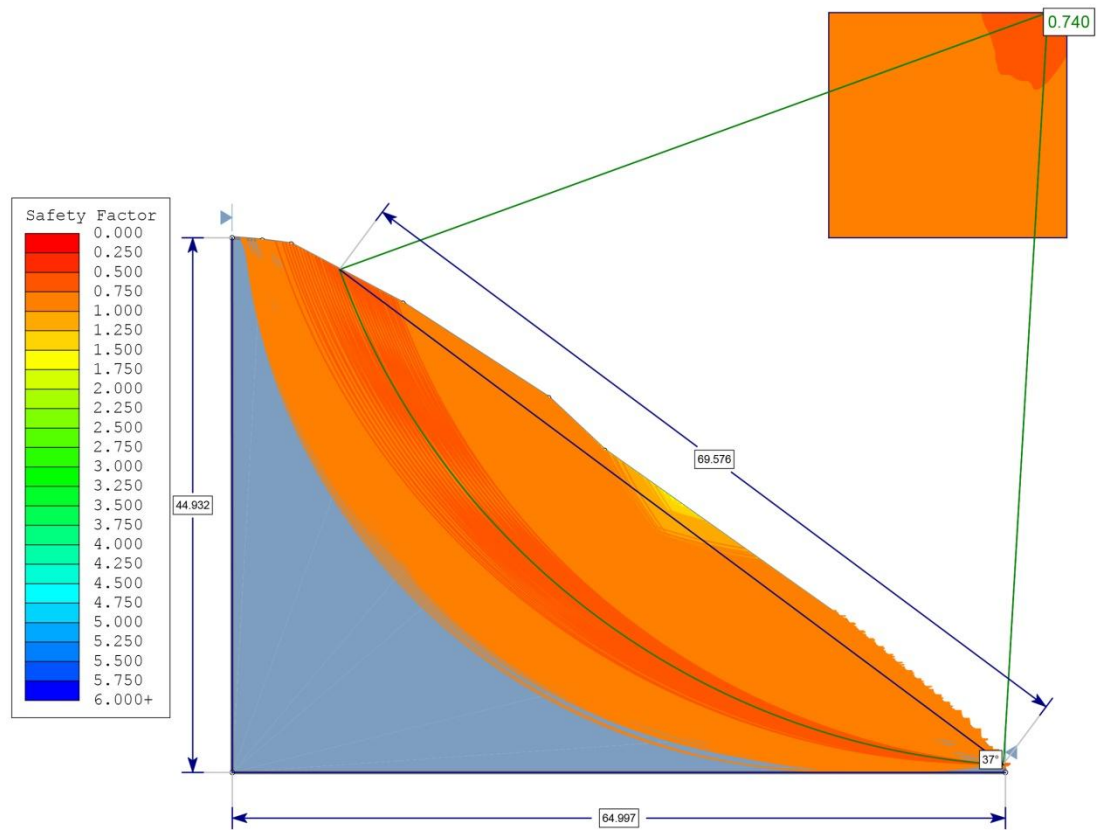


Fig. 4.32 GLE/ Morgenstern-Price method of LEM Analysis for LS2

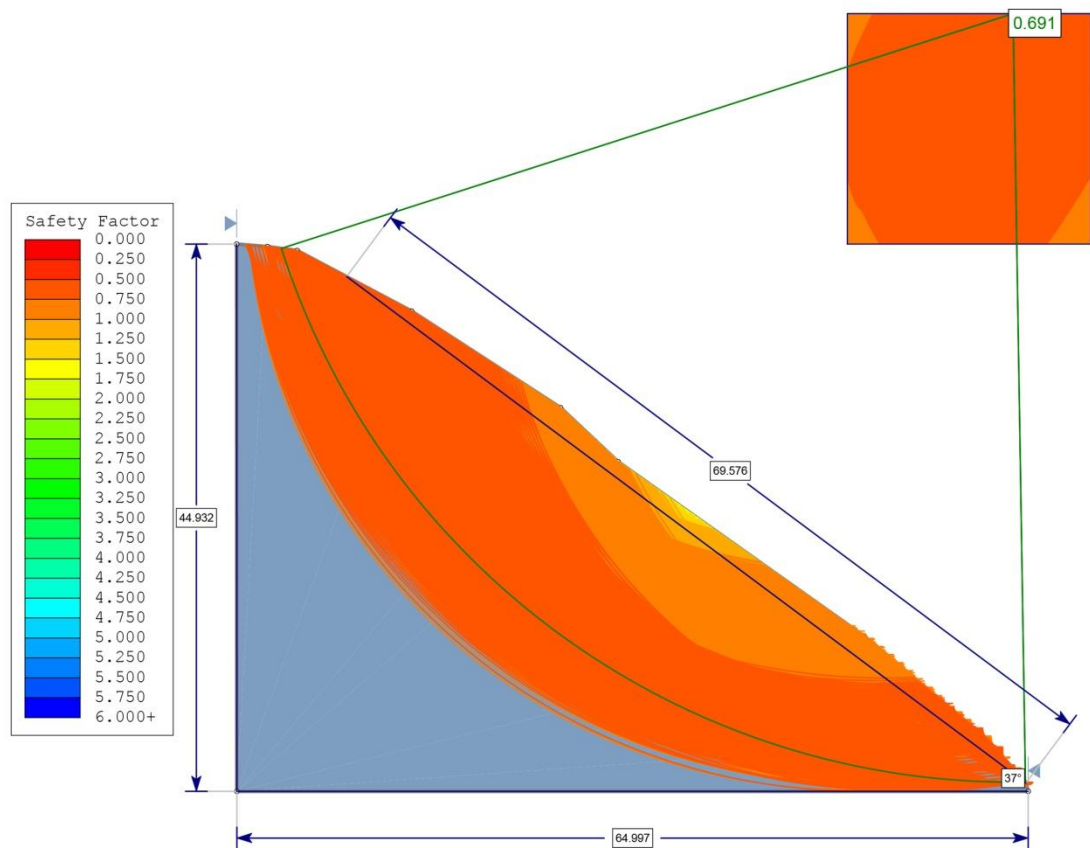


Fig. 4.33 Janbu Simplified method of LEM Analysis for LS2

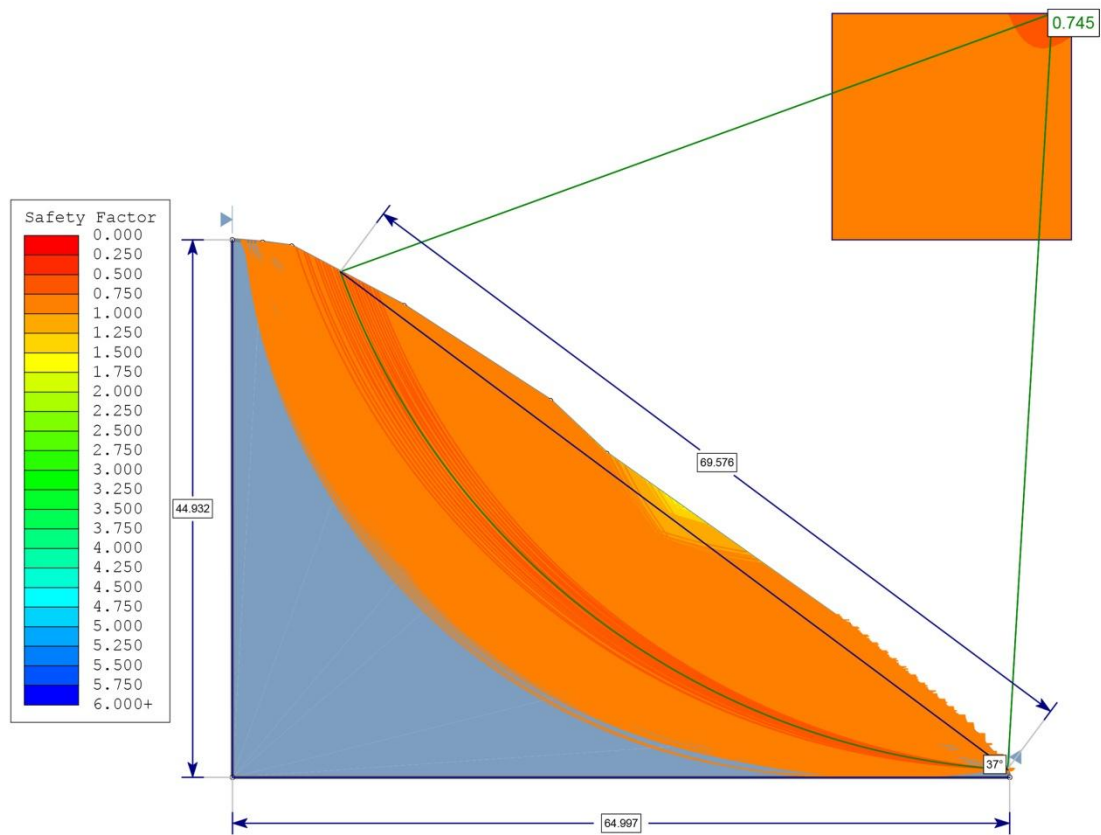


Fig. 4.34 Bishop Simplified Method of LEM Analysis for LS2

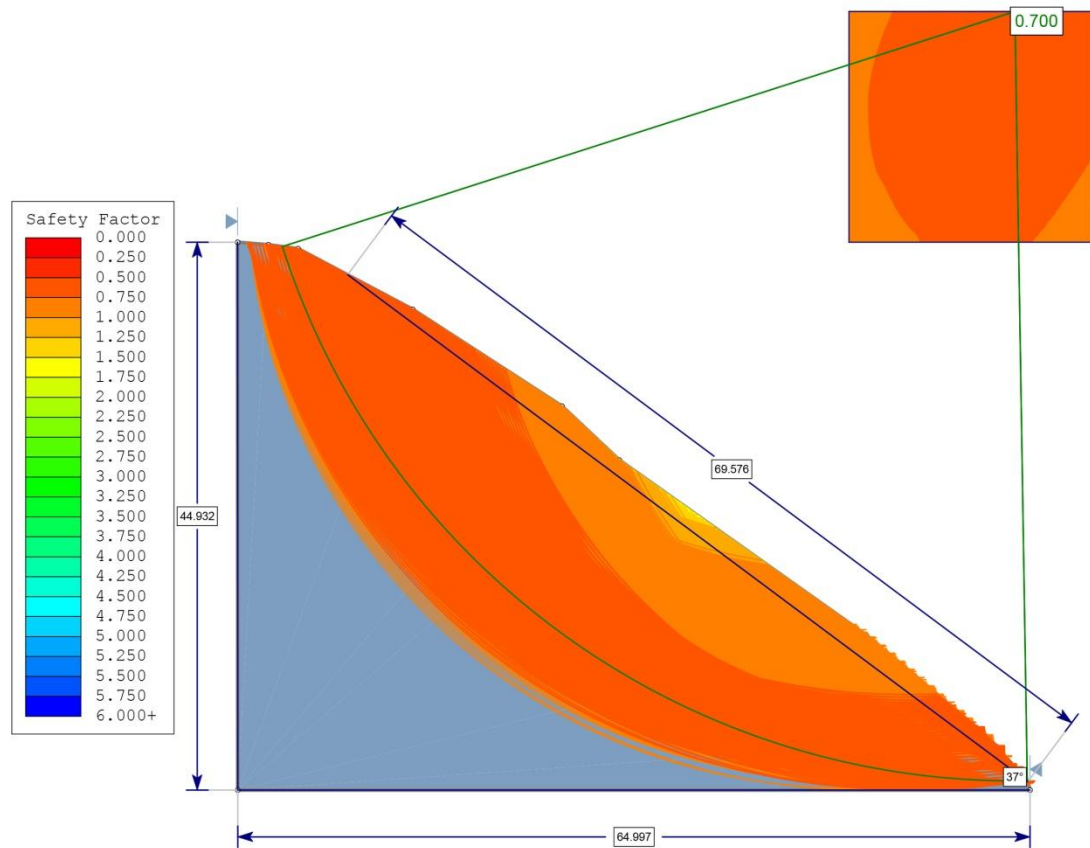


Fig. 4.35 Ordinary/ Fellenius Method of LEM Analysis for LS2

4.5.3. LS3 (23°22'59.01"N; 93°23'25.37"E)

A debris slide is observed at LS3 of 142 meters in width and 101.5 meters in length. A dam-like structure for the road was constructed in a depression where a small stream is flowing. Geotextile materials were used on both sides of the wall. A wide slope cutting for road construction has made it vulnerable to failure. A wide slope cutting for road construction has made it vulnerable to failure. The average factor of safety obtained from different methods is 0.674. Figure 4.37 display the field photograph and figures 4.38, 4.39, 4.40, and 4.41 display LEM analyses using different methods.



Fig. 4.36 Field photograph of failed slope in LS3

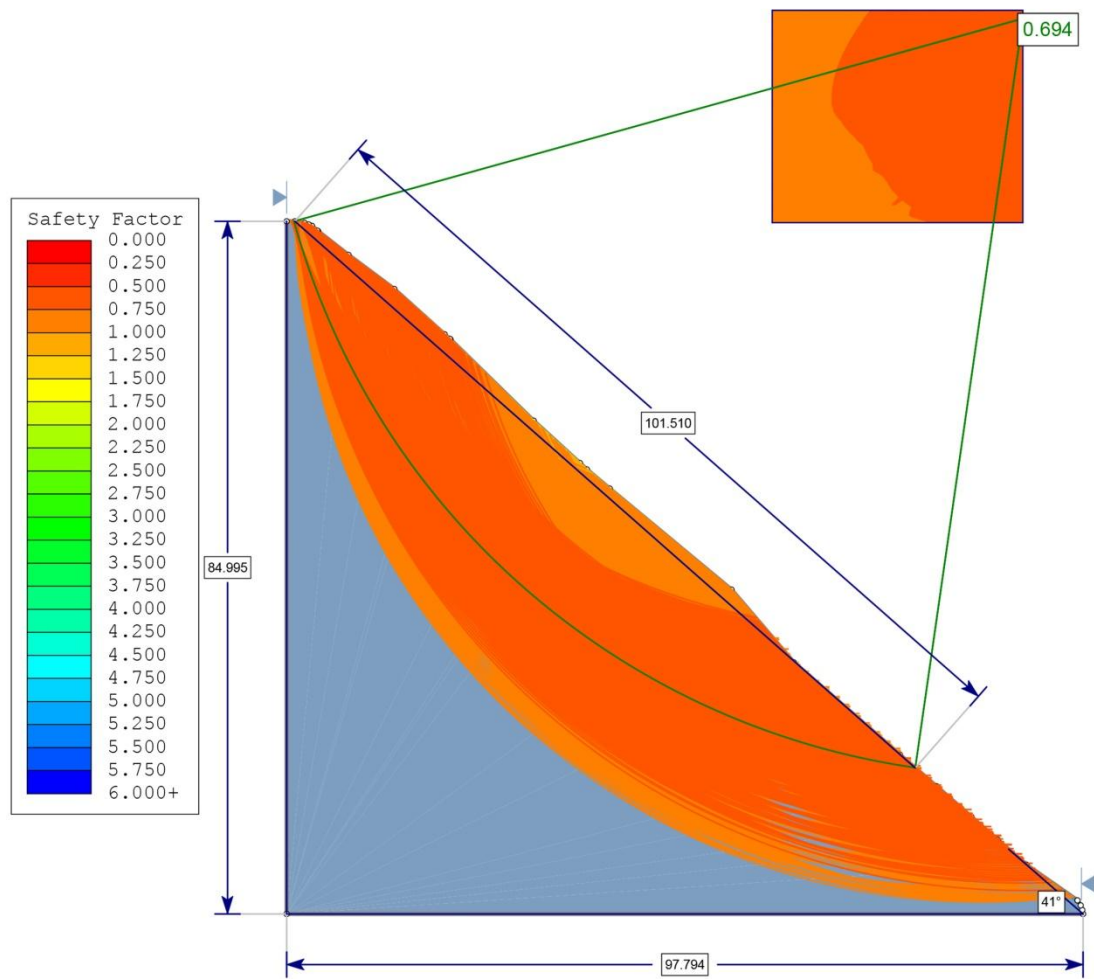


Fig. 4.37 GLE/ Morgenstern-Price Method of LEM Analysis for LS3

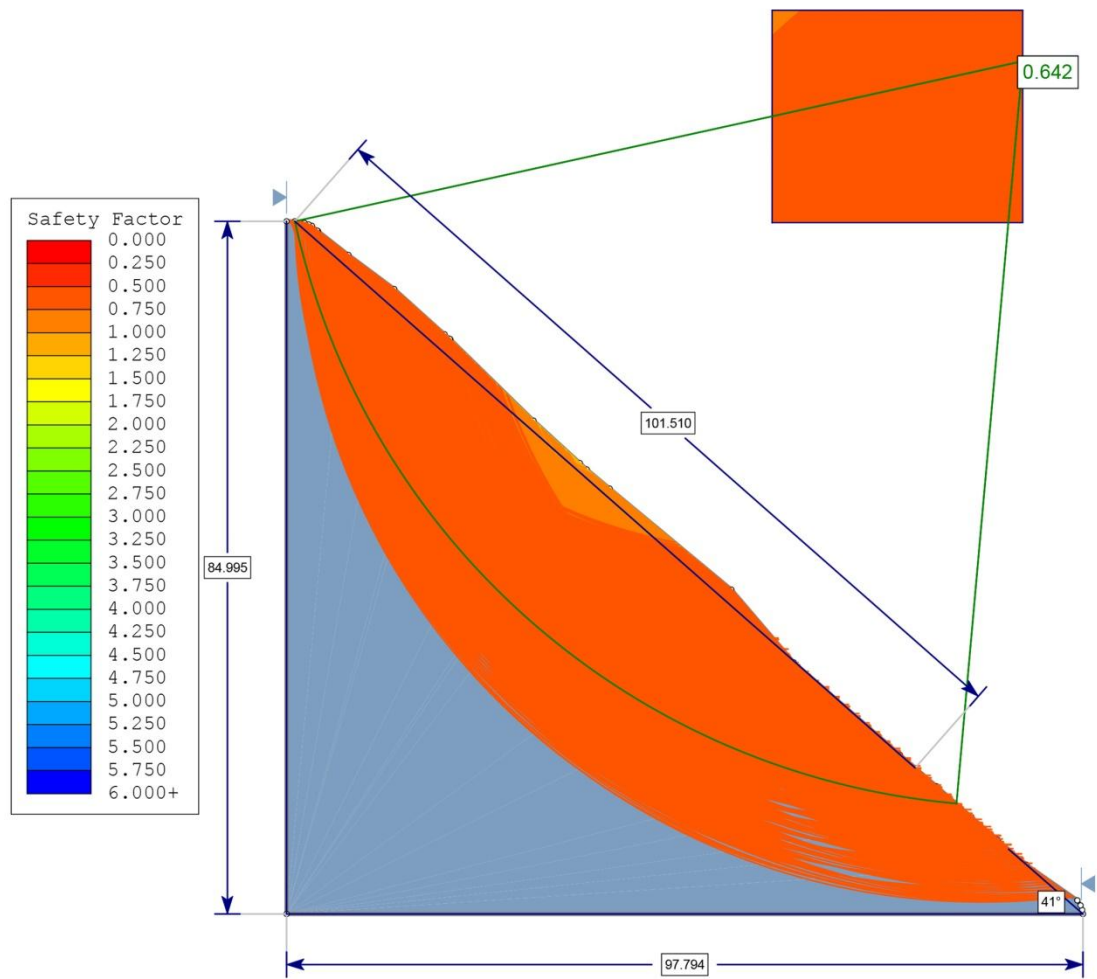


Fig. 4.38 Janbu Simplified Method of LEM Analysis for LS3

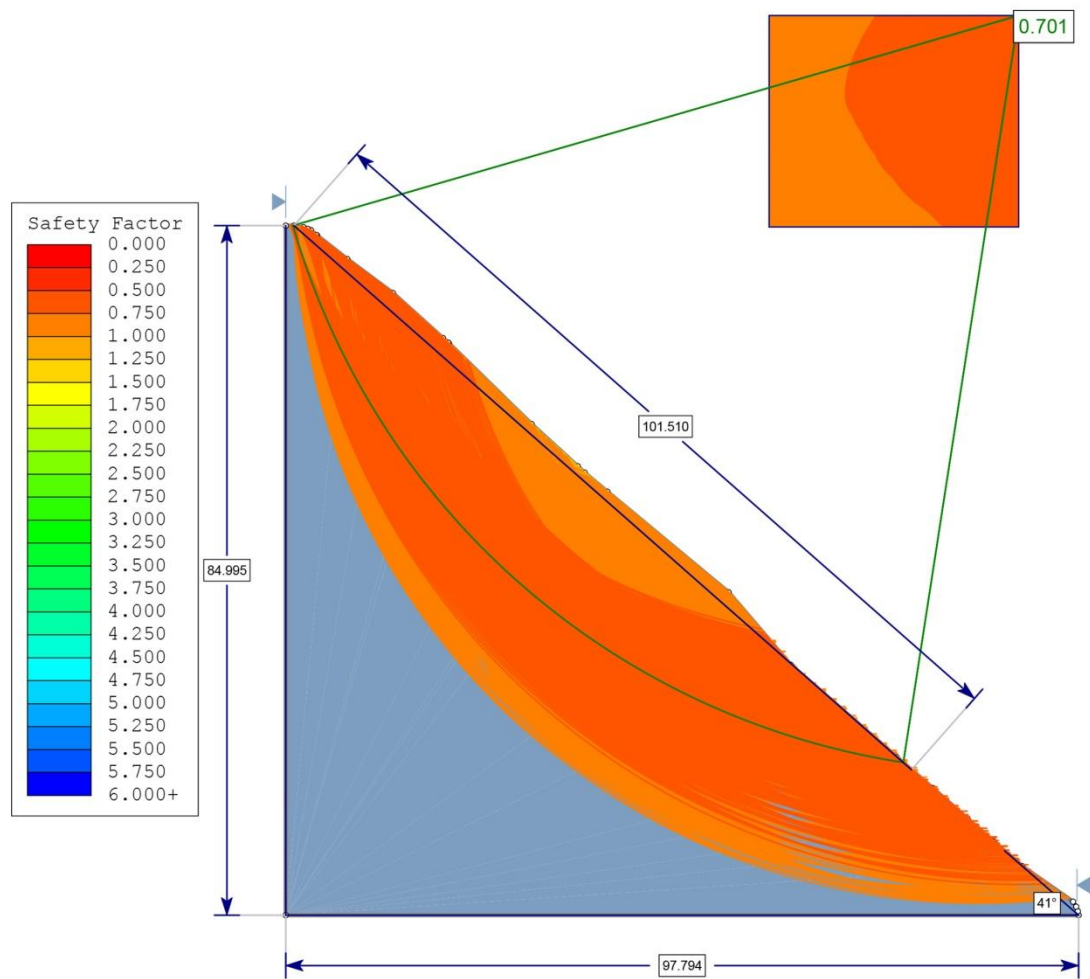


Fig. 4.39 Bishop Simplified Method of LEM Analysis for LS3

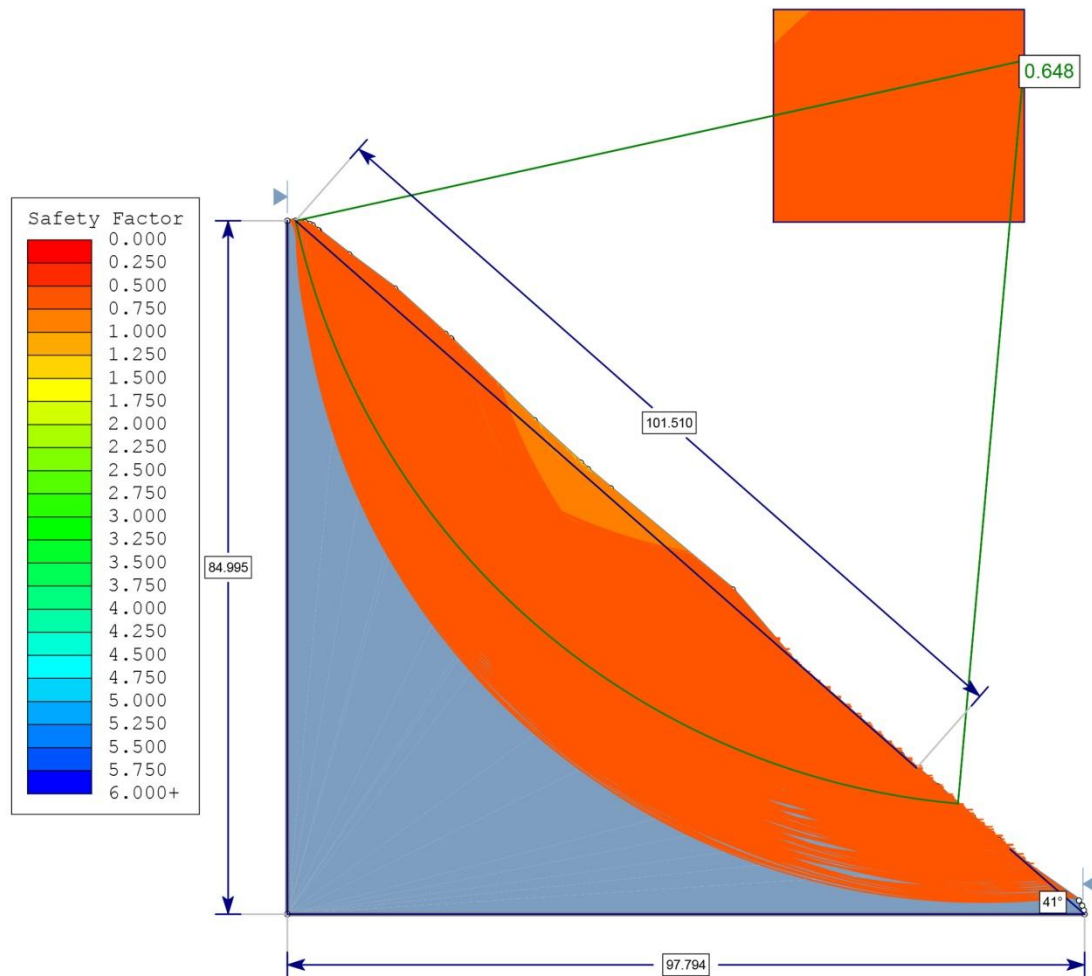


Fig. 4.40 Ordinary/ Fellenius Method of LEM Analysis for LS3

4.5.4. LS4 (23°22'51.72"N; 93°23'23.96"E)

A debris slide of 145.9 meters length and 95 meters width of loose, younger material is observed at LS4. A culvert is constructed along a small stream. Fragile lithology and toe-cutting of the slope for road construction destabilized the hill, which caused landslides. Both sides of the slopes failed, and the culvert has been obstructed by this waste, resulting in water-laden debris to erosion. Part of the culvert along the road has been damaged and was overburdened by debris. The average factor of safety obtained from different methods is 0.58. Figure 4.42 display the field photograph and figures 4.43, 4.44, 4.45, and 4.46 display LEM analyses using different methods.

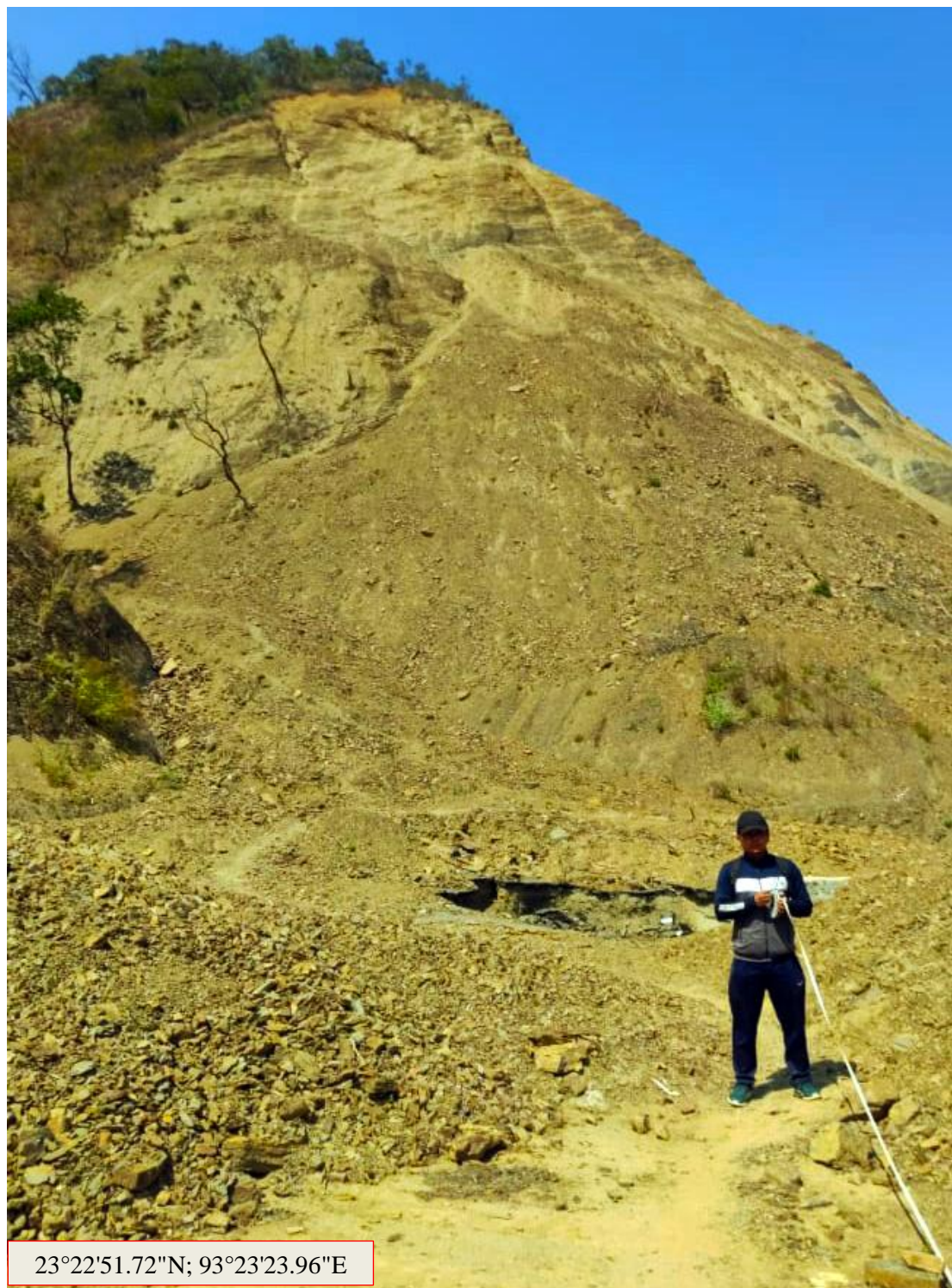


Fig. 4.41 Field photograph of LS4

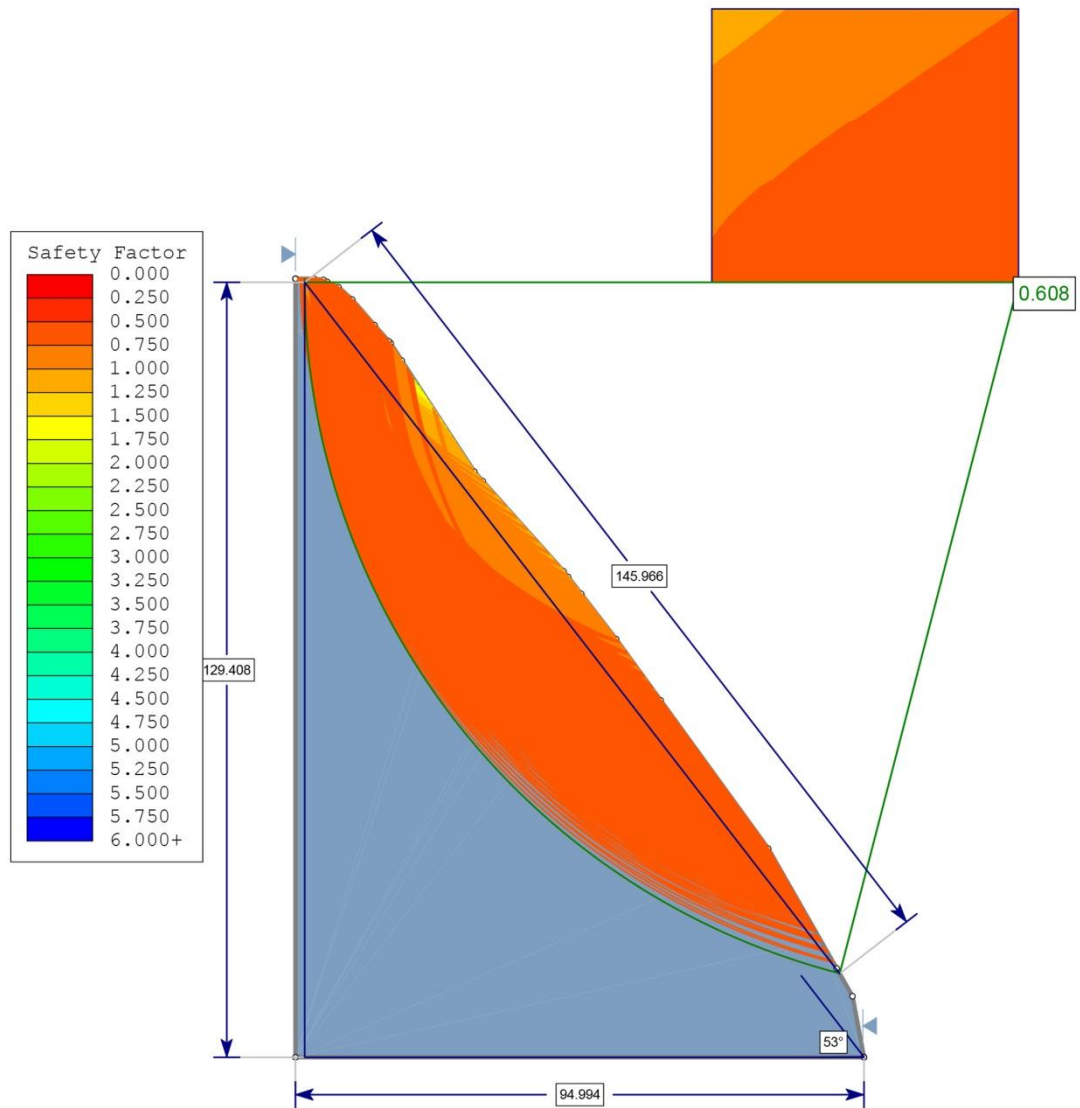


Fig. 4.42 GLE/ Morgenstern-Price Method of LEM Analysis for LS4

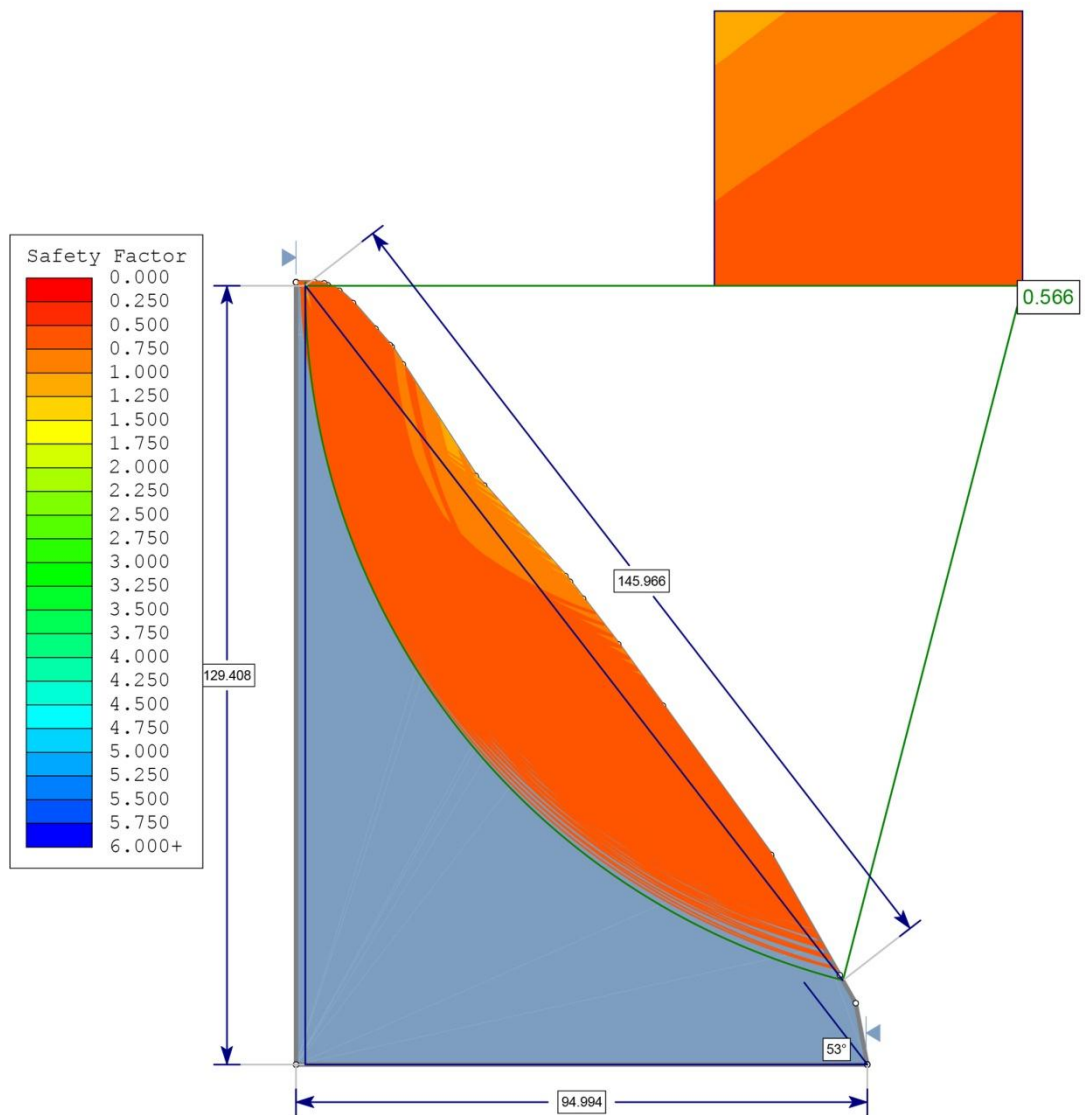


Fig. 4.43 Janbu Simplified Method of LEM Analysis for LS4

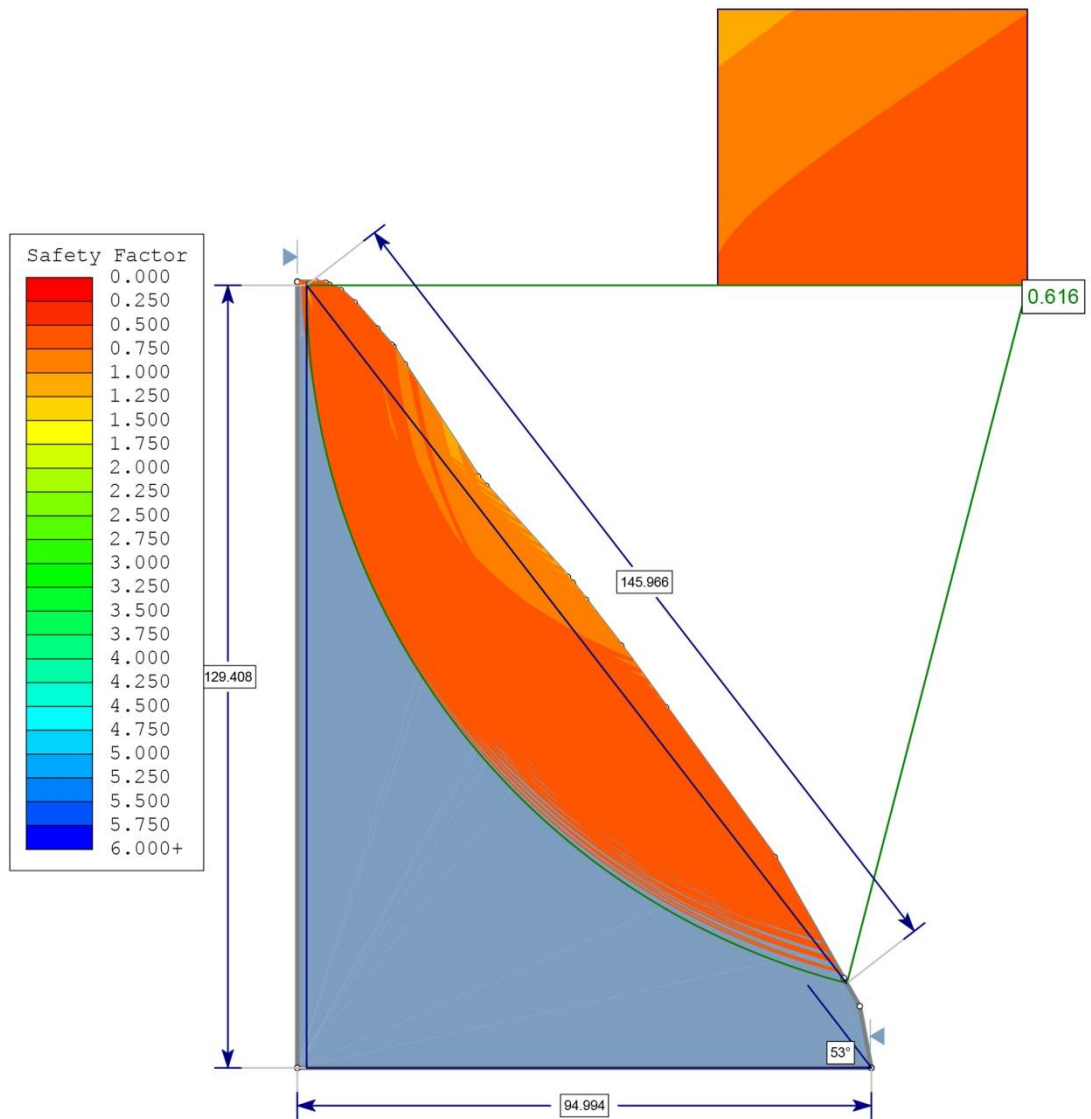


Fig. 4.44 Bishop Simplified Method of LEM Analysis for LS4

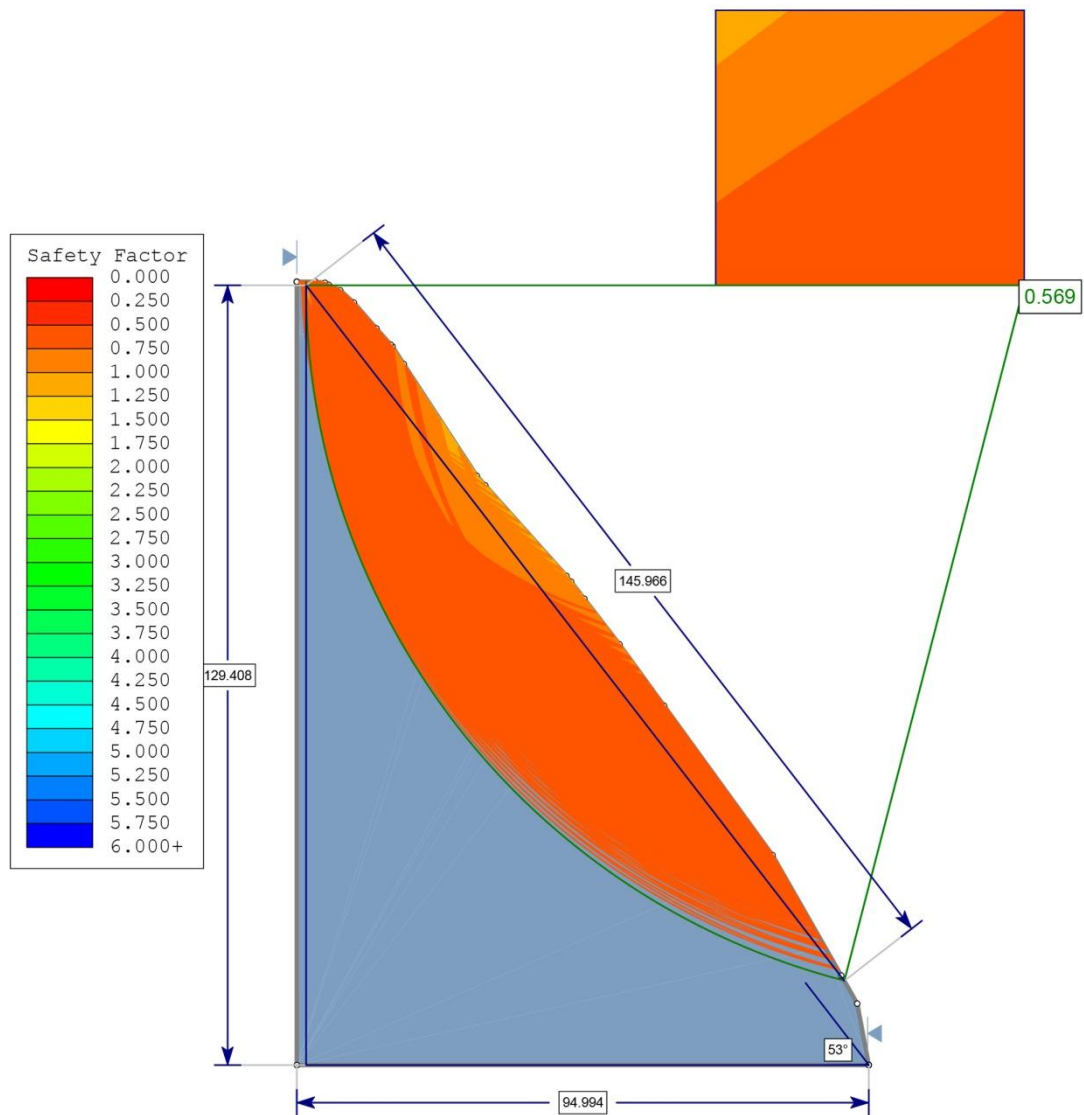


Fig. 4.45 Ordinary/ Fellenius Method of LEM Analysis for LS4

4.5.5. LS5 (23°22'42.34"N; 93°23'20.02"E)

In location LS5, the road for highway was constructed by cutting a hill at the lower portion of the mid slope. It has been observed that the uphill side has weak bedrock with comparatively thick overburden. In monsoon, rainwater acts as a lubricant by passing through the ground as eroding the surface. A debris slide of dimension 145 meters width and 62 meters height occurred, and the asphalt used for surfacing the road popped out. The average factor of safety obtained from different

methods is 0.82. Figure 4.52 display the field photograph and figures 4.53, 4.54, 4.55, and 4.56 display LEM analyses using different methods.



Fig. 4.46 Field Photographs of LS5

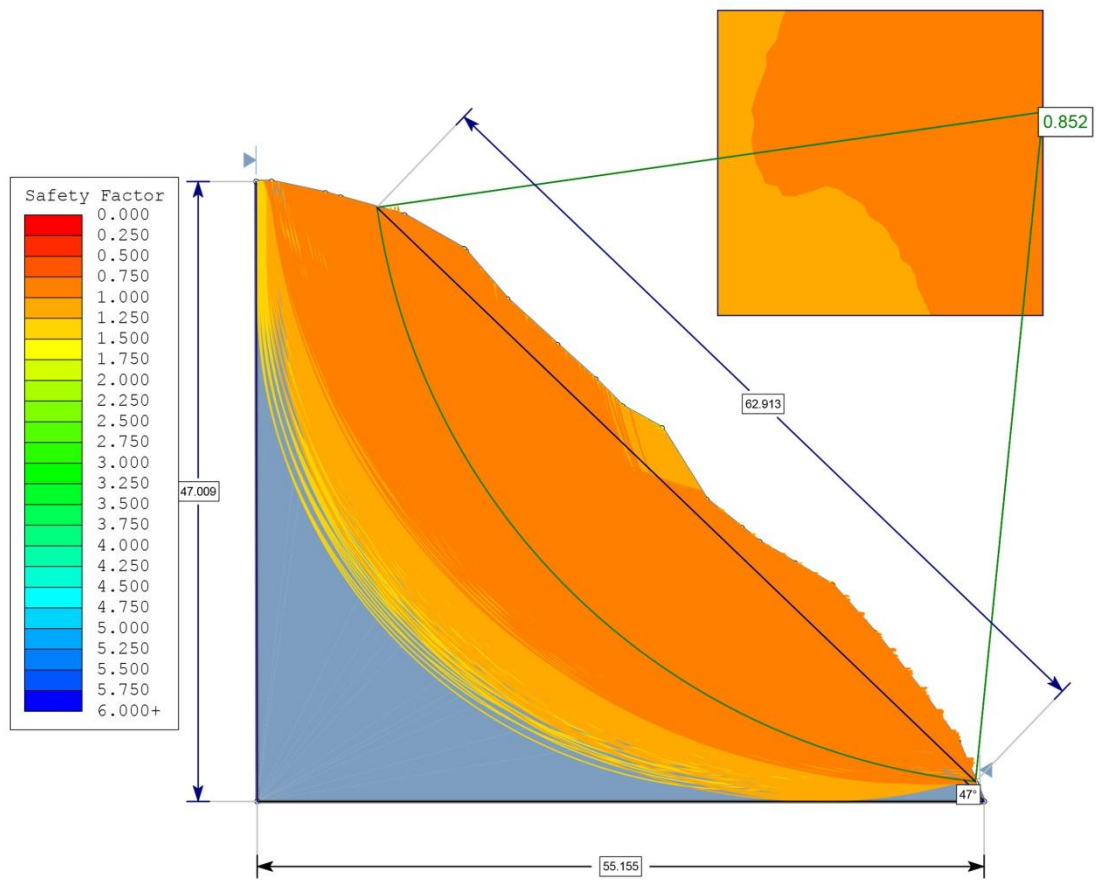


Fig. 4.47 GLE/ Morgenstern-Price Method of LEM Analysis for LS5

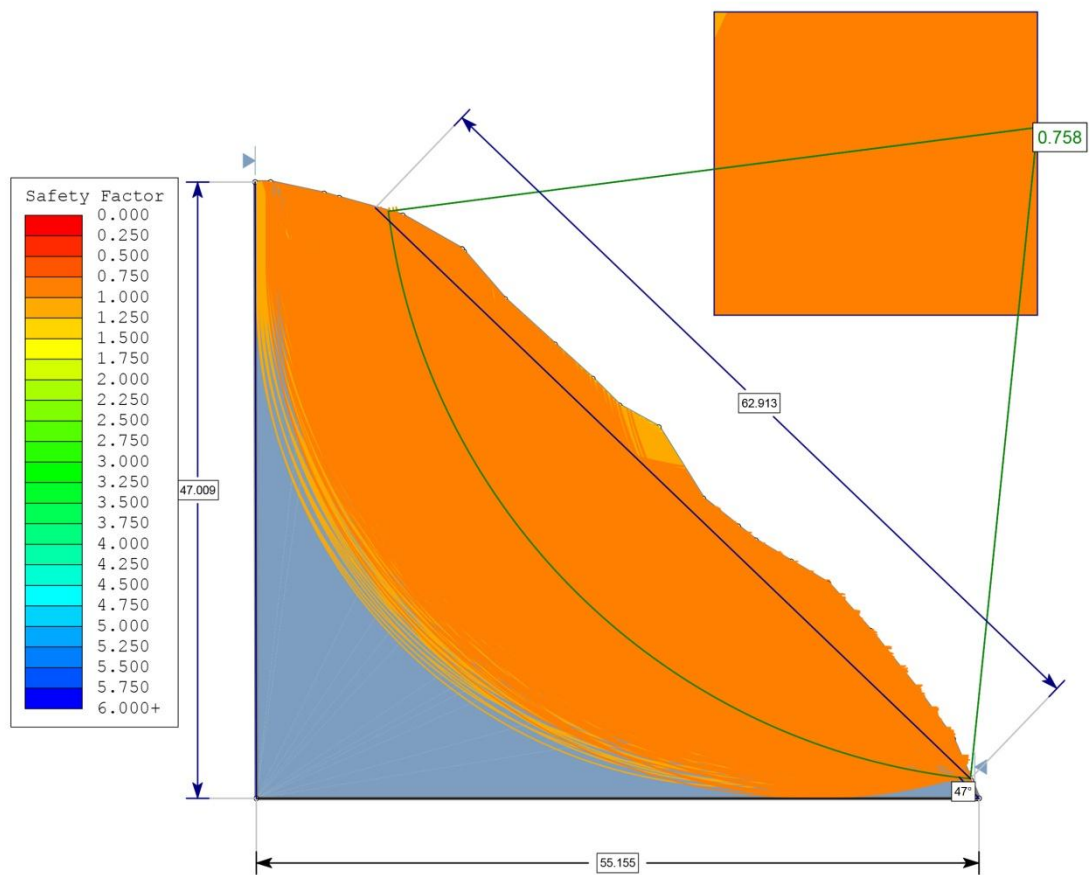


Fig. 4.48 Janbu Simplified Method of LEM Analysis for LS5

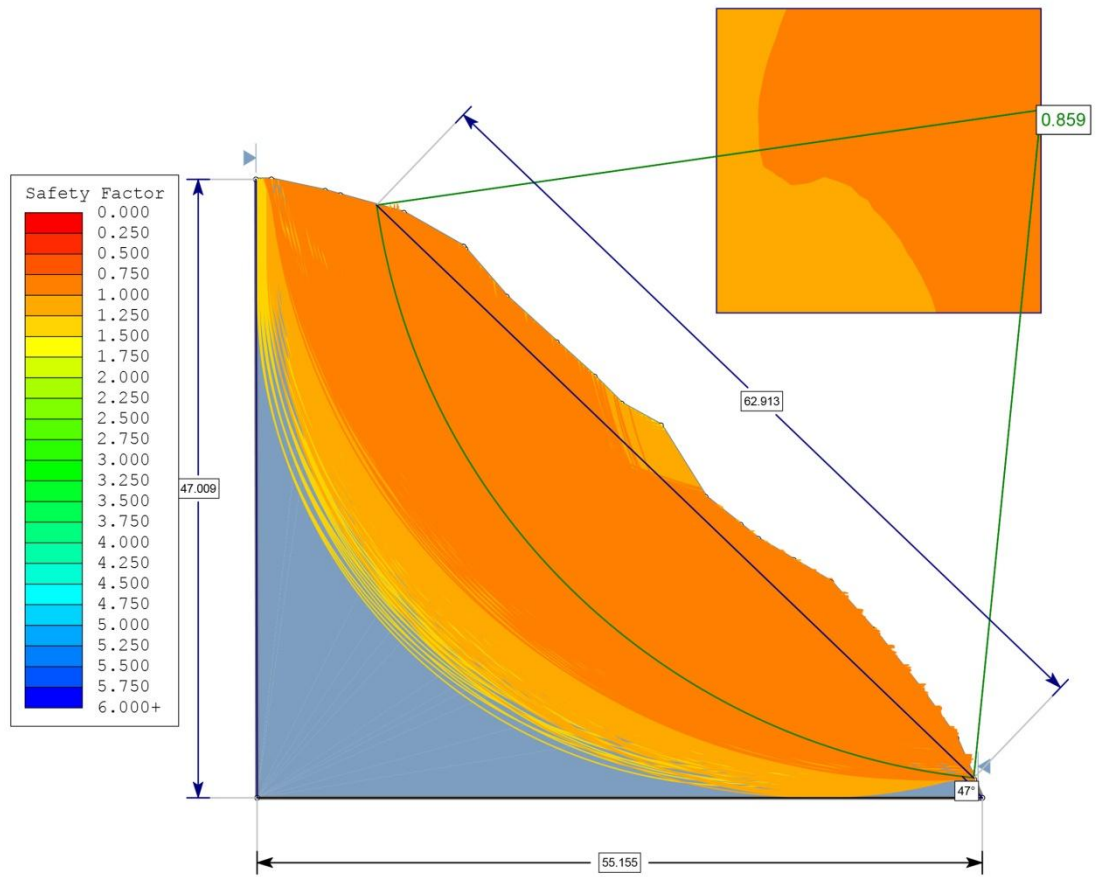


Fig. 4.49 Bishop Simplified Method of LEM Analysis for LS5

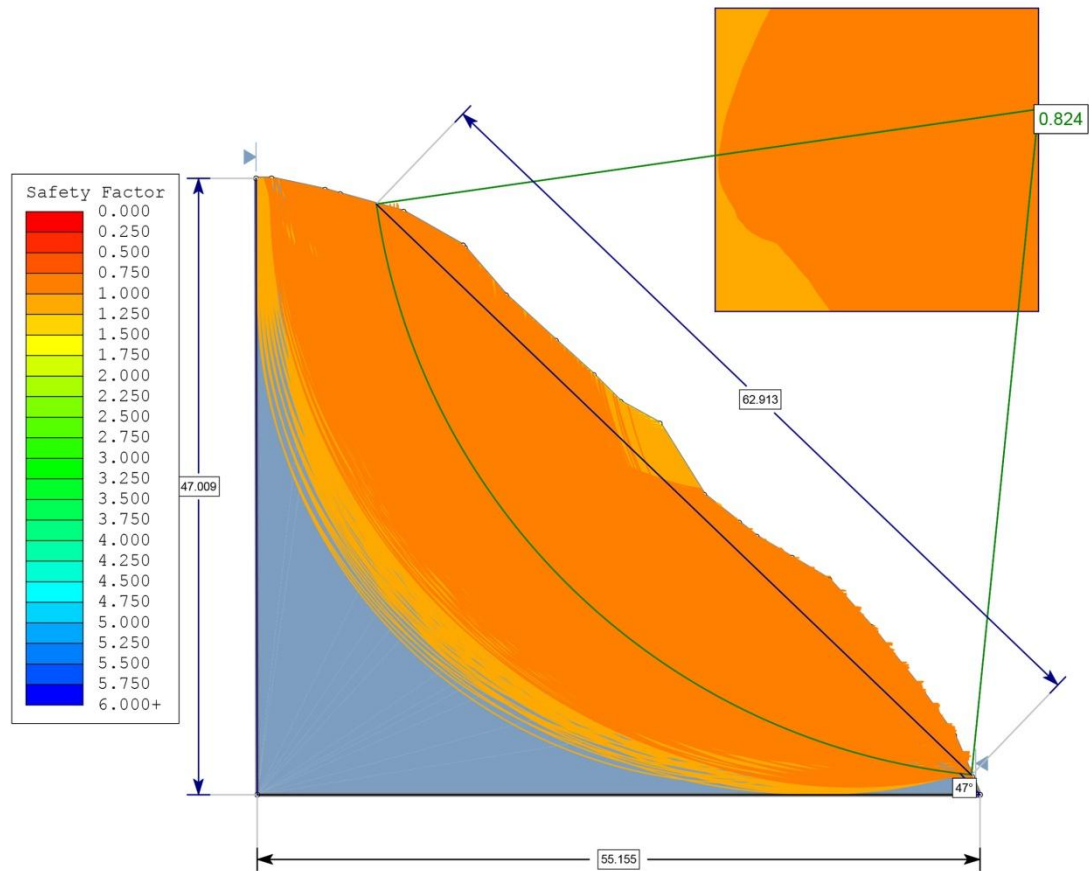


Fig. 4.50 Ordinary/ Fellenius Method of LEM Analysis for LS5

4.5.6. LS6 (23°22'35.15"N; 93°23'11.49"E)

The construction of road for highway has been extended in the slope LS6. An overburden of thick colluvium covered the crown portion of the hill. A toe cutting at the mid-slope for the road destabilized the slope. It is a retrogressive landslide where sliding occur in a segmented failure manner. The dimension of LS6 is 112 meter width and 54.7 meter height. The average factor of safety obtained from different methods is 0.59. Figure 4.57 display the field photograph and figures 4.58, 4.59, 4.605, and 4.61 display LEM analyses using different methods.

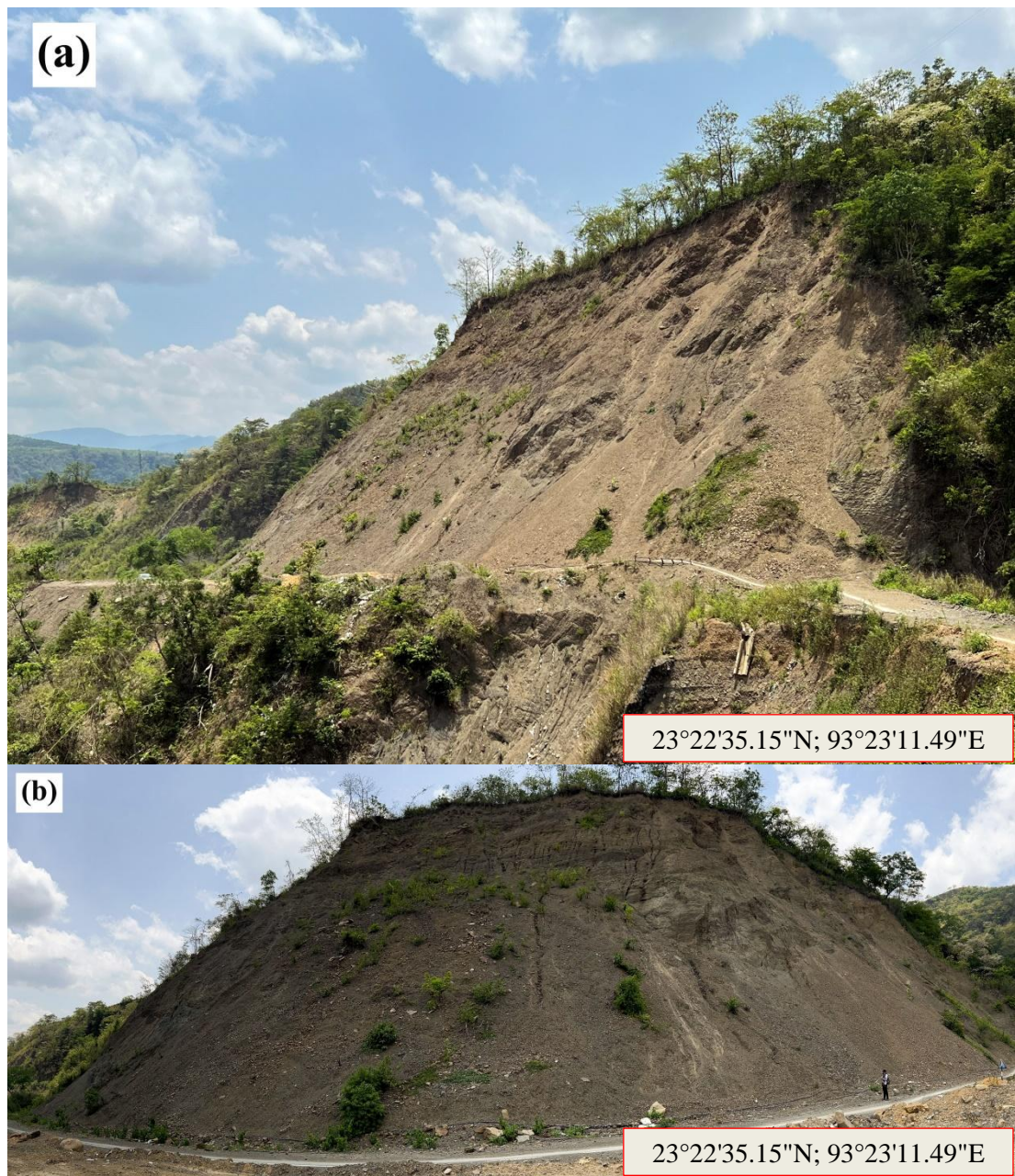


Fig. 4.51 Field Photographs of LS6 (a) Side view of LS6 (b) Panoramic view of LS6

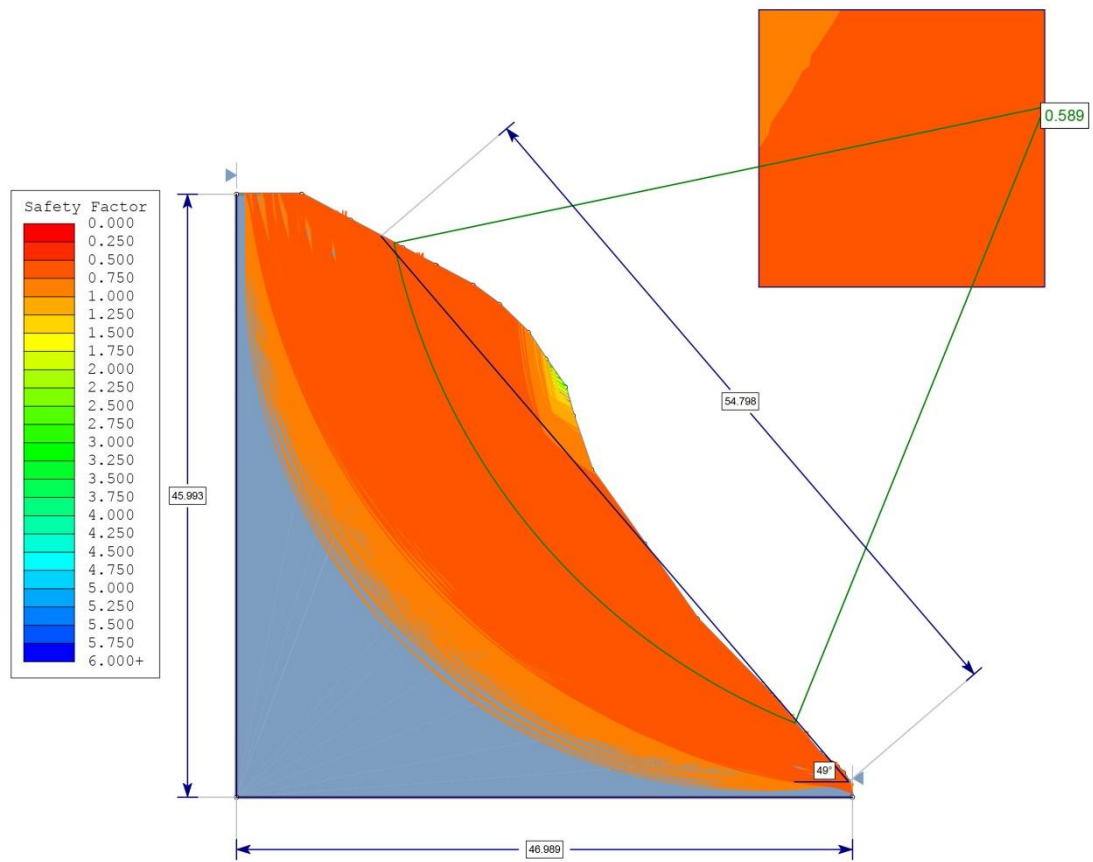


Fig. 4.52 GLE/ Morgenstern-Price Method of LEM Analysis for LS6

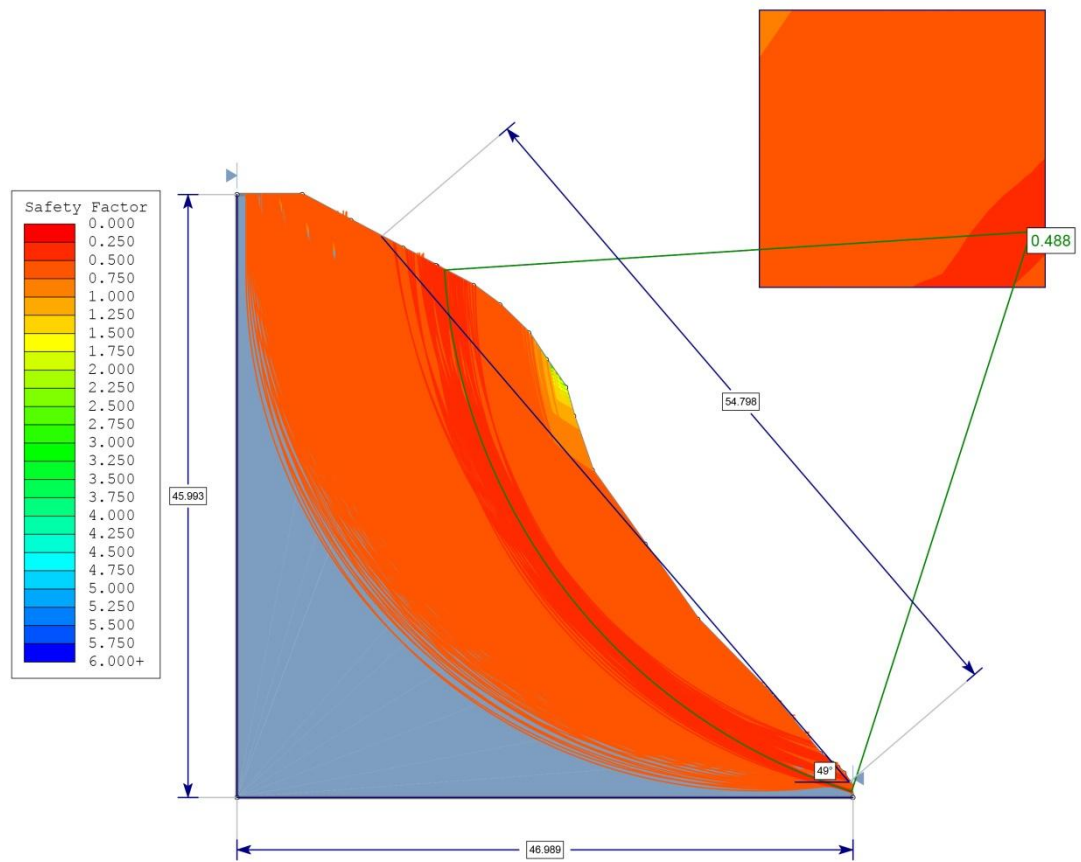


Fig. 4.53 Janbu Simplified Method of LEM Analysis for LS6

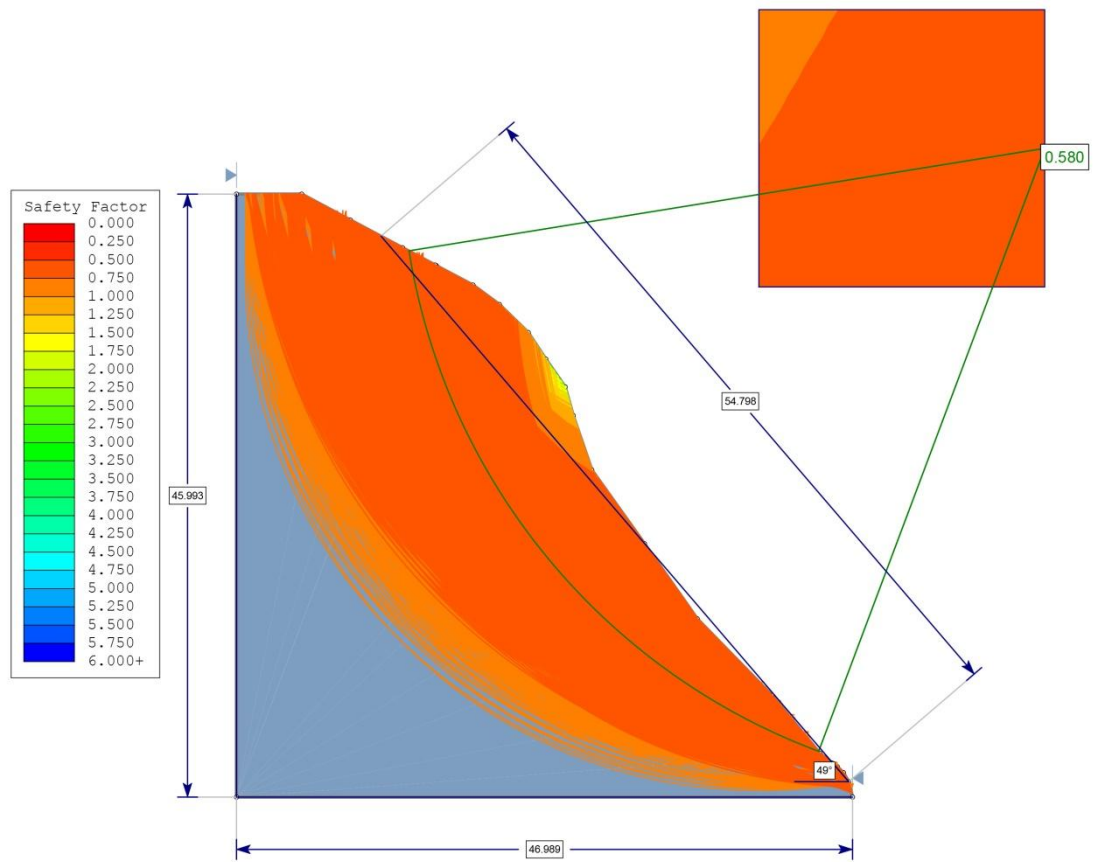


Fig. 4.54 Bishop Simplified Method of LEM Analysis for LS6

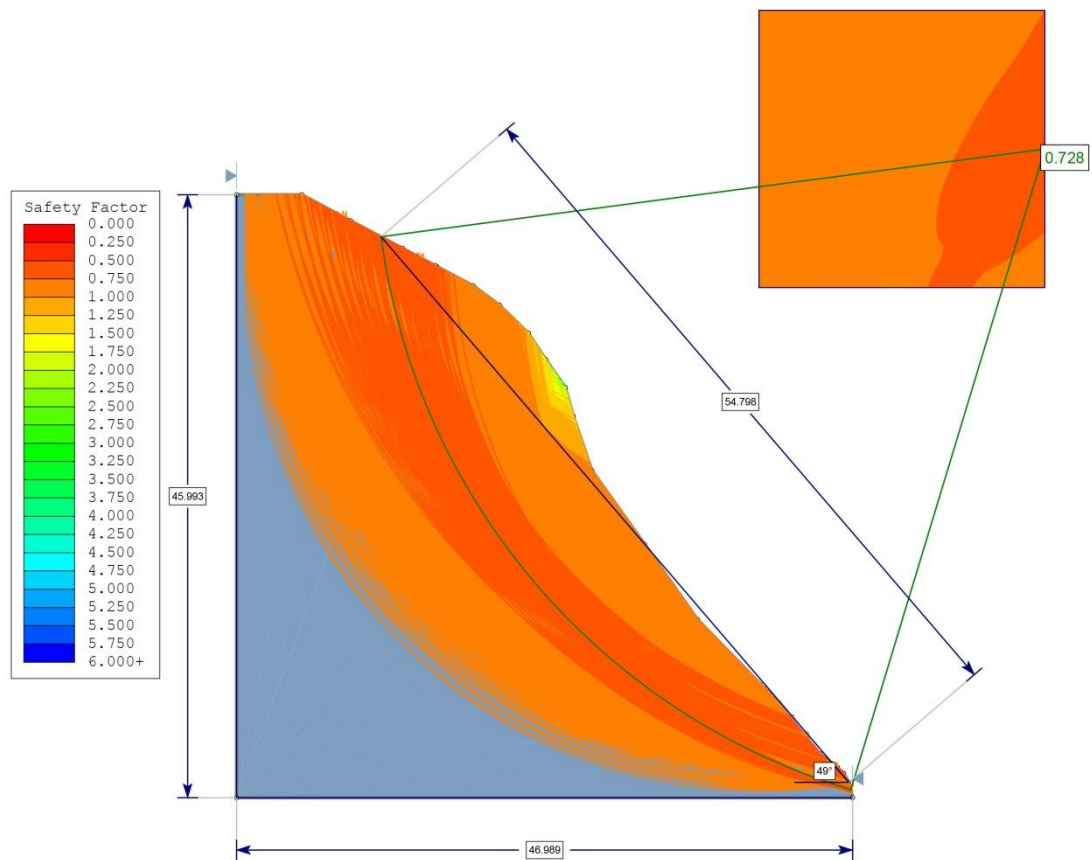


Fig. 4.55 Ordinary/ Fellenius Method of LEM Analysis for LS6

According to the results of the Ordinary/Fellenius, Janbu Simplified, Bishop Simplified, and Limit Equilibrium Method for GLE/Morgenstern-Price slope stability analysis, each slope (LS1, LS2, LS3, LS4, LS5, and LS6) has a factor of safety that is less than unity, or below 1, indicating that it is unstable and highly prone to slope failure when the stress is below the allowable limit. Table 4.14 provides a summary of the factor of safety for each slope that was examined using various LEM techniques. The overall factor of safety for each approach is displayed in Figure 4.62.

Table 4.15 Factor of Safety for each study site

Method	LS1	LS2	LS3	LS4	LS5	LS6
GLE/ Morgenstern-Price	0.849	0.74	0.694	0.608	0.852	0.589
Janbu Simplified	0.797	0.691	0.642	0.566	0.758	0.488
Bishop Simplified	0.857	0.745	0.701	0.616	0.859	0.58
Ordinary/ Fellenius	0.807	0.7	0.648	0.569	0.824	0.728

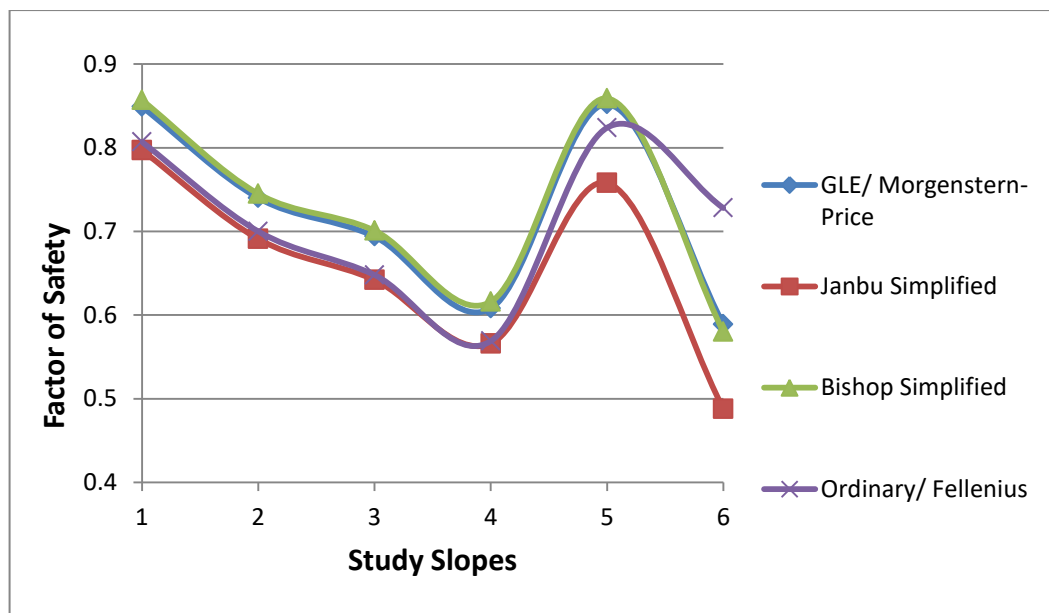


Fig. 4.56 LEM Analyses using different methods

4.6. SLAKE DURABILITY TEST

The purpose of slake durability test is to determine how resistant a rock is to deterioration and disintegration after being repeatedly wet and dried in a slaking fluid, often water. The slake durability index for each cycle is shown in table 4.15.

Table 4.16 Slake Durability Index for each cycle

Sample No.	Rock Type	SDI (%) In each cycle				ID ₂	Durability
		1	2	3	4		
S1	Sandstone	96.46	93.55	91.22	90.63	93.55	Very High
S2	Siltstone	92.84	89.65	88.56	84.23	89.65	High
S3	Siltstone	88.45	85.71	80.81	79.12	85.71	High
S4	Sandstone	97.65	94.05	93.44	91.74	94.05	Very High
S5	Sandstone	98.12	92.62	91.83	89.24	92.12	Very High
S6	Sandstone	95.00	92.31	87.42	87.31	92.31	Very High
S7	Sandstone	94.12	92.80	90.64	89.50	92.80	Very High

4.7. ROCK MASS RATING (R.M.R.) METHOD

Seven road cut-slopes were investigated and analyzed using Rock Mass Rating method. The Rock Mass Rating (RMR) proposed by Bieniawski (1976) was used for the geo-mechanical classification of rock, which comprises six basic parameters, i.e., uniaxial compressive strength (UCS) of intact rock, Rock Quality Designation (RQD), Spacing of discontinuities, Condition of discontinuities, Orientation of discontinuities, and Groundwater condition. These parameters were used to characterize the rock mass by assigning the RMR value and its classes to the cut slope under investigation. Table 4.16 lists the ratings for each parameter, and Table 4.17 lists the RMR categorization for each slope.

Table 4.17 Rock Mass Rating for different locations

Location No.	U.C.S.	R.Q.D.	S.D.	D.L.	Separation (Aperture)	Roughness	Infilling (Gouge)	Weathering	G.W.
S1	62.04 Mpa	71%	0.34m	4.3m	1-5mm	Slightly Rough	None	Slightly weathered	Dry
Rating	7	13	10	2	1	3	6	5	15
S2	70.84 Mpa	69%	0.41m	3.9m	1-5mm	Rough	None	Slightly Weathered	Dry
Rating	7	13	10	2	1	5	6	5	15
S3	66.91 Mpa	65%	0.59m	4.6m	1-5mm	Slightly Rough	None	Slightly Weathered	Dry
Rating	7	13	10	2	1	3	6	5	15
S4	46.13 Mpa	43%	0.57m	5.4m	0.1-1.0mm	Rough	Hard filling <5mm	Moderately Weathered	Dry
Rating	4	8	10	2	4	5	2	3	15
S5	47.32 Mpa	48%	0.33m	2.21m	0.1-1.0mm	Rough	None	Moderately Weathered	Dry
Rating	4	8	10	4	4	5	5	3	15
S6	44.16 Mpa	39%	0.42m	2.98m	1-5mm	Rough	Hard filling <5mm	Slightly weathered	Dry
Rating	4	8	10	4	1	5	2	5	15
S7	62.37	54%	0.80m	4.96m	0.1-1.0mm	Slightly	None	Slightly	Dry

	Mpa					Rough		weathered	
Rating	7	13	15	2	4	3	5	5	15

Table 4.18 RMR Classification for different selected slopes

Location No.	Dip & Strike Orientation	R.M.R. Value	Class No.	Description	A.S.U.T.	Cohesion	Friction Angle
S1	Favorable	57	III	Fair Rock	1 week for 5 m span	200-300	25-35
Rating	-5						
S2	Favorable	59	III	Fair Rock	1 week for 5 m span	200-300	25-35
Rating	-5						
S3	Favorable	57	III	Fair Rock	1 week for 5 m span	200-300	25-35
Rating	-5						
S4	Fair	28	IV	Poor Rock	10 hours for 2.5 m span	100-200	15-25
Rating	-25						
S5	Fair	33	IV	Poor Rock	10 hours for 2.5 m span	100-200	15-25
Rating	-25						
S6	Fair	29	IV	Poor Rock	10 hours for 2.5 m span	100-200	15-25
Rating	-25						
S7	Fair	44	III	Fair Rock	1 week for 5 m span	200-300	25-35
Rating	-25						

4.8. DETERMINATION OF GEOLOGICAL STRENGTH INDEX (G.S.I.)

The GSI classification modified by Somnez & Ulusay (1999) was used to produce a more numerical, quantitative assessment of rock mass. Surface condition

rating (SCR) was determined using volumetric joint count. Structural rating (SR) was determined based on surface roughness (Rr), weathering (Rw), and infilling (Rf). In Figure 2.2, the rating of SR and SCR is plotted to generate a GSI number. Table 4.18 shows the detailed rating for each study site, and figure 4.63 displays the GSI value.

Table 4.19 GSI Rating based on Structural Rating and Surface Condition Rating

Spot No	Structural Rating (SR) = -17.5 $\ln(J_v)$ + 79.8	Surface Condition Rating (SCR)			Total SCR Rating	GSI value from graph (SR Vs. SCR)
		Roughness Rating (Rr)	Weathering Rating (Rw)	Infilling Rating (Rf)		
S1	$J_v=13.3$	Slightly Rough	Slightly weathered	None	13	46
Rating	34.5	3	5	6		
S2	$J_v=13.9$	Rough	Slightly weathered	None	16	54
Rating	33.7	5	5	6		
S3	$J_v=15.1$	Slightly Rough	Slightly weathered	None	14	48
Rating	32.2	3	5	6		
S4	$J_v=21.8$	Rough	Moderately weathered	Hard filling <5mm	12	43
Rating	25.8	5	3	4		
S5	$J_v=20.3$	Rough	Moderately Weathered	None	14	46
Rating	27.1	5	3	6		
S6	$J_v=23.03$	Rough	Slightly weathered	Hard filling <5mm	12	42

Rating	24.9	5	3	4		
S7	Jv=18.4	Slightly Rough	Slightly weathered	None	12	44
Rating	28.8	3	3	6		

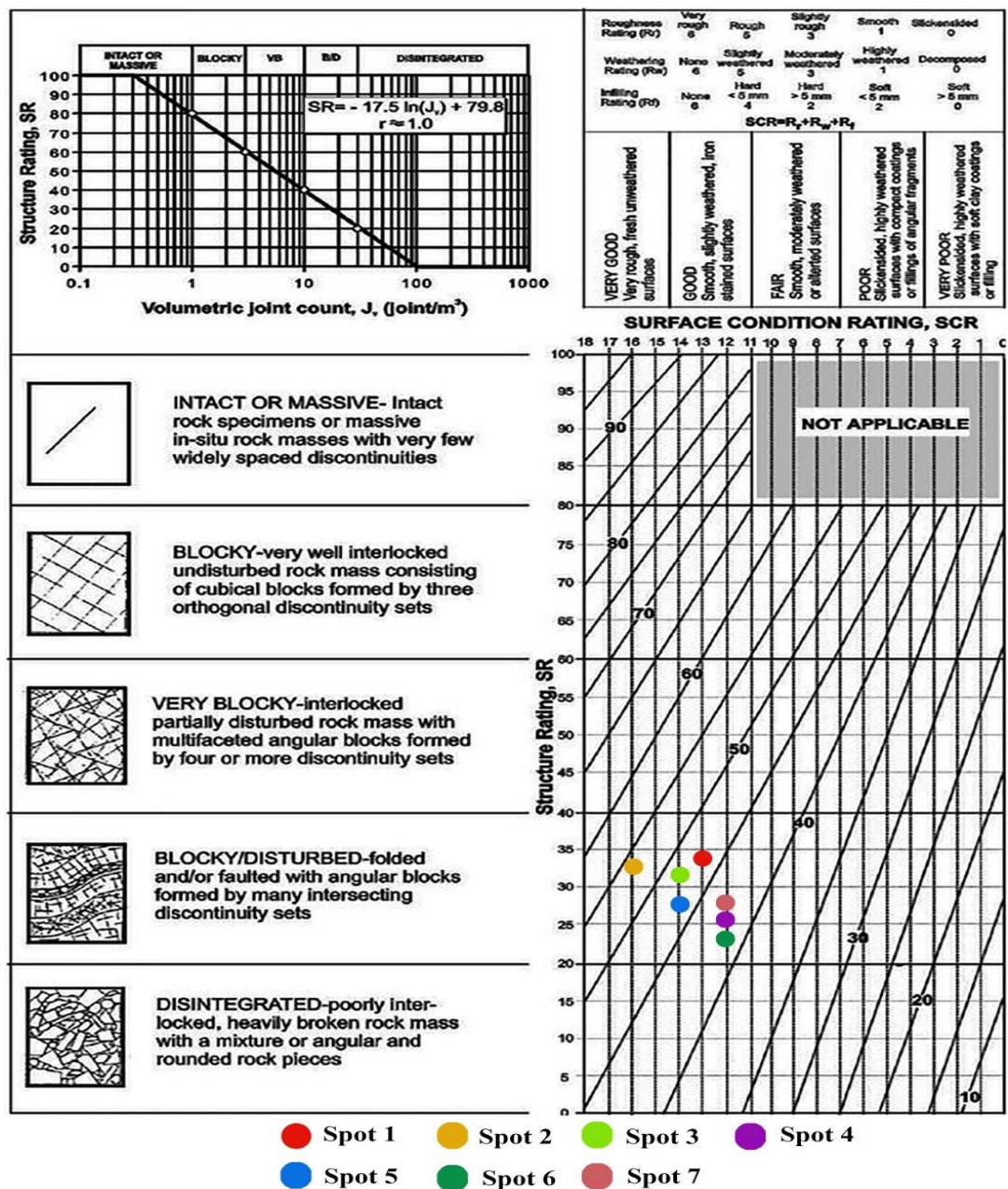


Fig. 4.57 G.S.I. Rating for each study sites

4.9. KINEMATIC ANALYSIS

To study disaster vulnerability and risk assessment, Rocscience software Dips 7.0 was used for Kinematic Analysis. The primary factor that significantly controls the stability of the rock mass is the orientation of discontinuities. The Kinematic Analysis used a stereographic projection (figure 4.53 to 4.59), where a three-dimensional space is represented in two dimensions. It evaluates the potential mode of slope failure, as shown in table 4.19.

Table 4.20 Rock attitudes for kinematic analysis

Location	Slope		Bedding Plane		Joint (J1)		Joint (J2)		Possible Failure
	Dip Amount	Dip Direction	Dip Amount	Dip Direction	Dip Amount	Dip Direction	Dip Amount	Dip Direction	
S1	76°	N169	35°	N45	41°	N356	39°	N269	Direct Toppling (33.33%)
S2	79°	N142	29°	N203	38°	N2158	21°	N346	Direct Toppling (33.33%)
S3	81°	N193	21°	N346	66°	N218	62°	N122	Wedge (33.33%)
S4	69°	N87	23°	N335	69°	N157	55°	N298	Direct Toppling (33.33)
S5	81°	N94	39°	N63	55°	N132	63°	N197	Wedge (66.67%)
S6	69°	N118	62°	N108	45°	N83	75°	N140	Wedge (66.67%)
S7	78°	N102	31°	N246	44°	N72	67°	N125	Wedge (33.33%)

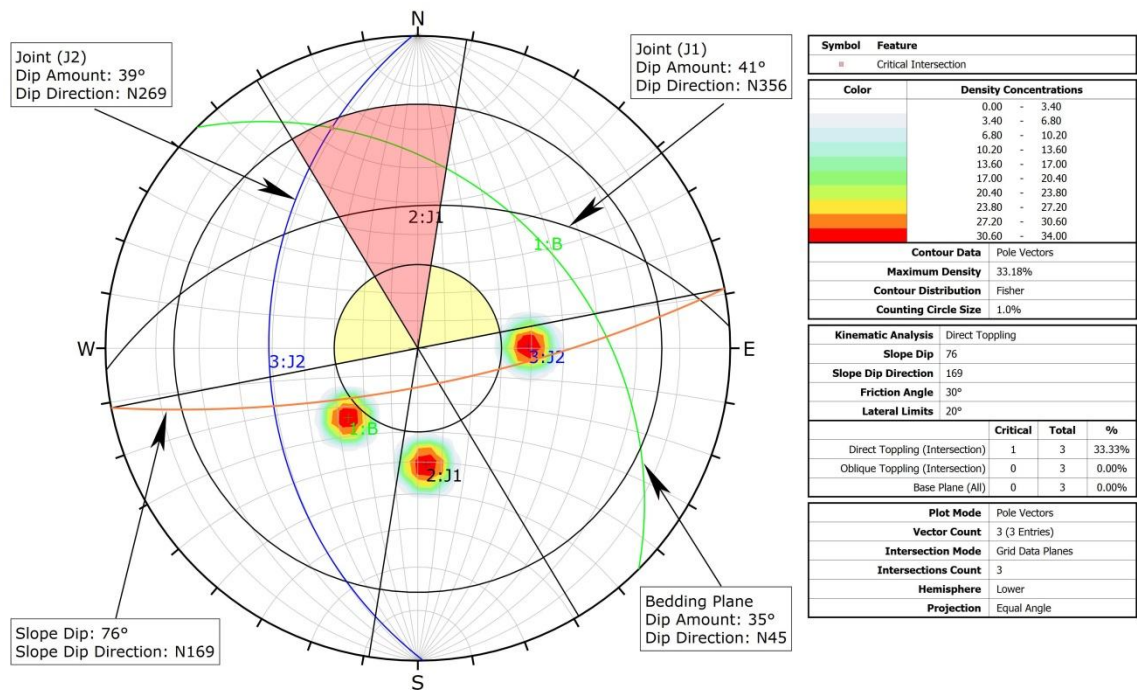


Fig. 4.58 Stereographic Projection showing the potential for direct toppling failure at S1

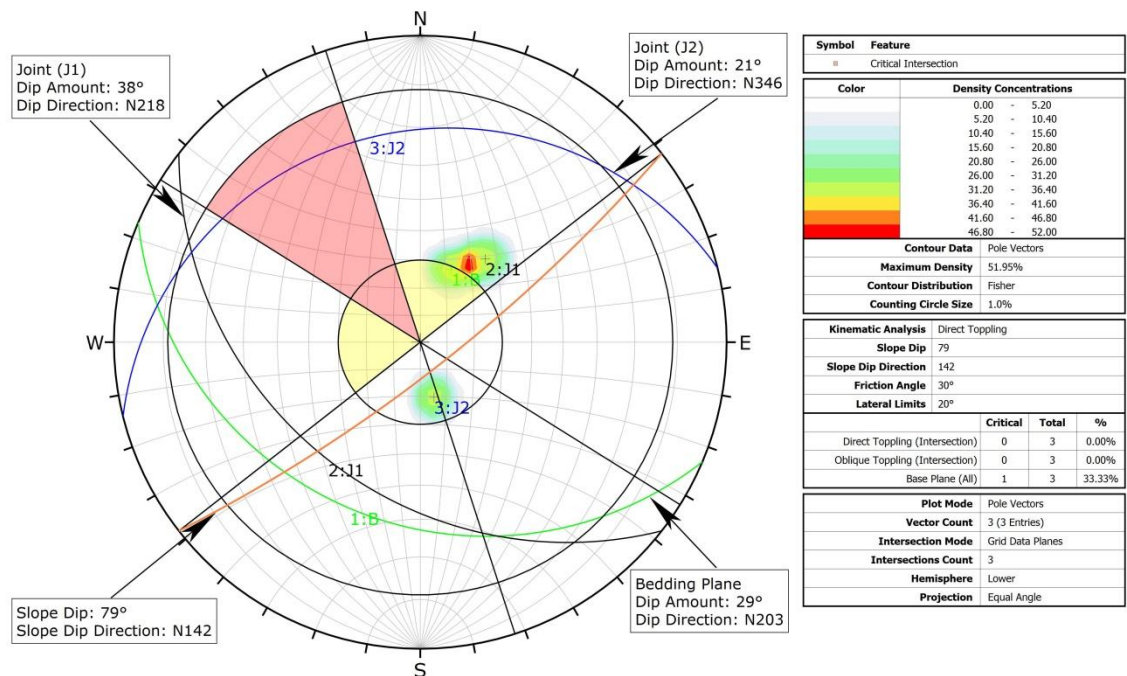


Fig. 4.59 Stereographic Projection showing the potential for direct toppling failure at S2

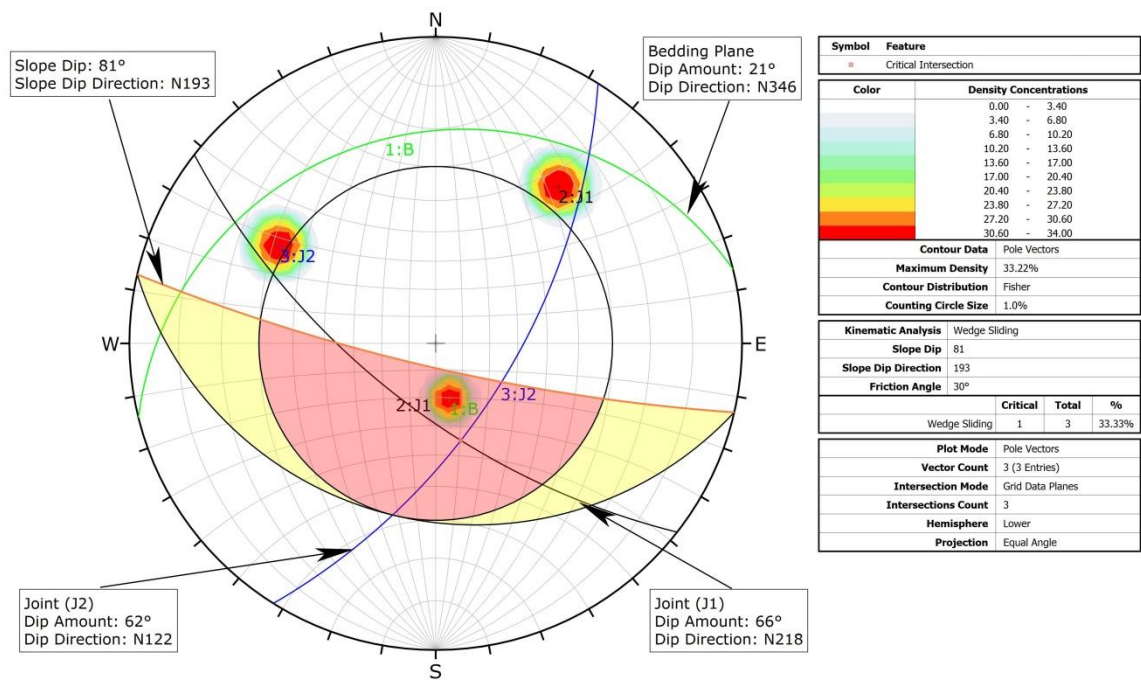


Fig. 4.60 Stereographic Projection showing the potential for wedge failure at S3

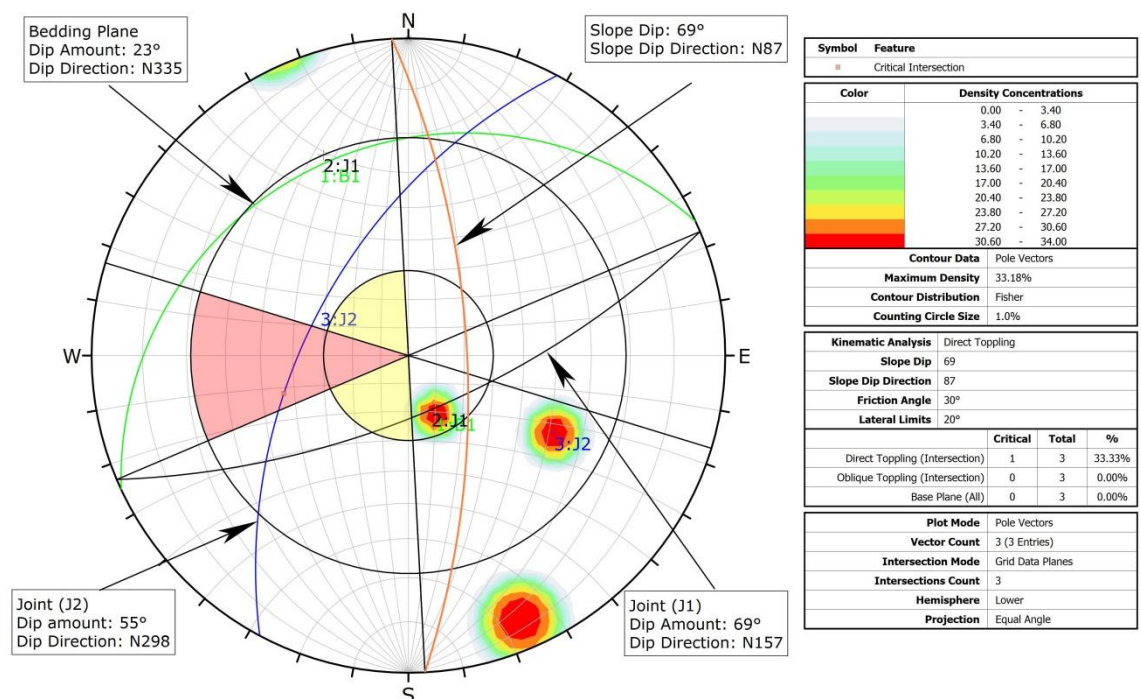


Fig. 4.61 Stereographic Projection showing the potential for direct toppling failure at S4

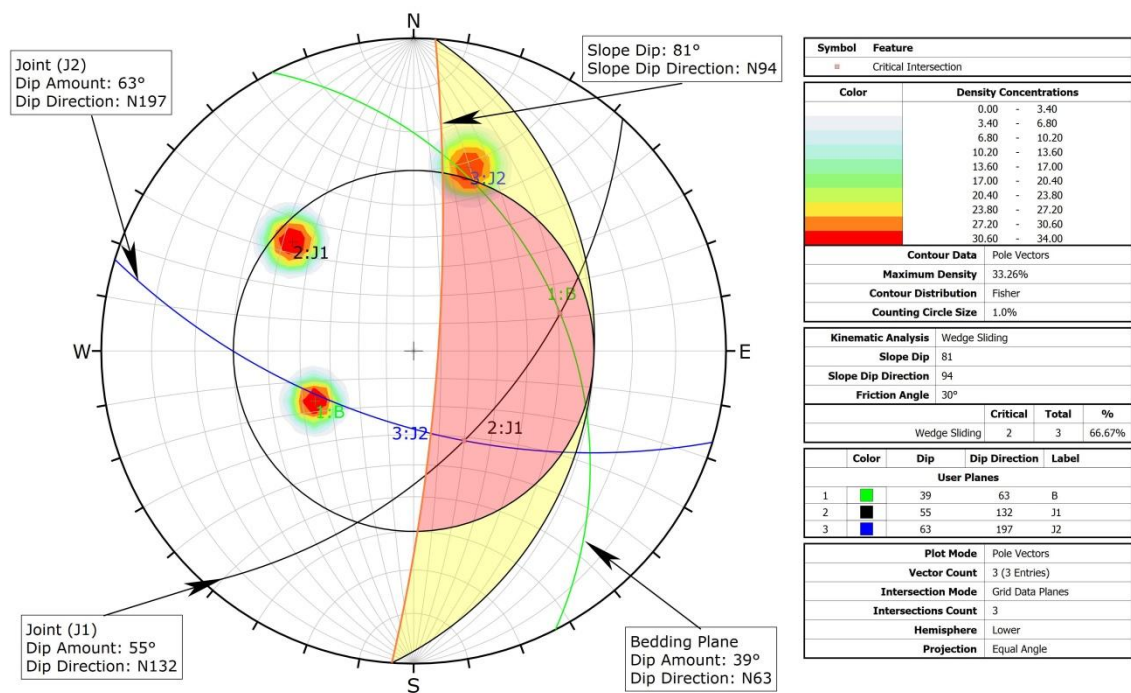


Fig. 4.62 Stereographic Projection showing the potential for wedge failure at S5

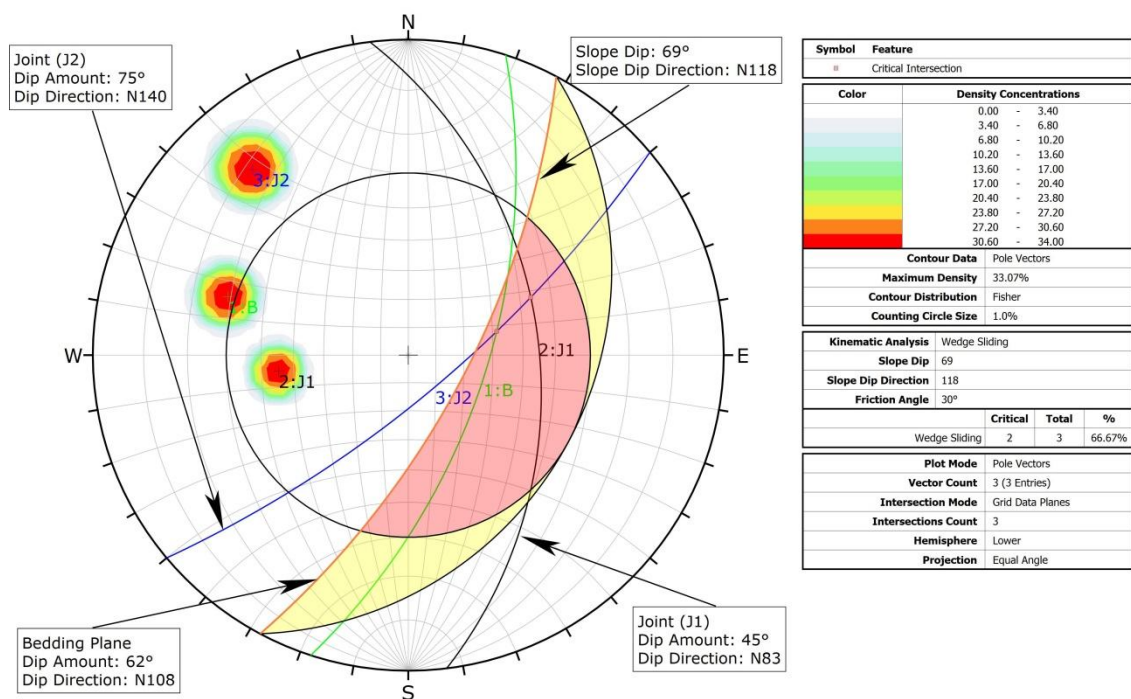


Fig. 4.63 Stereographic Projection showing the potential for wedge failure at S6

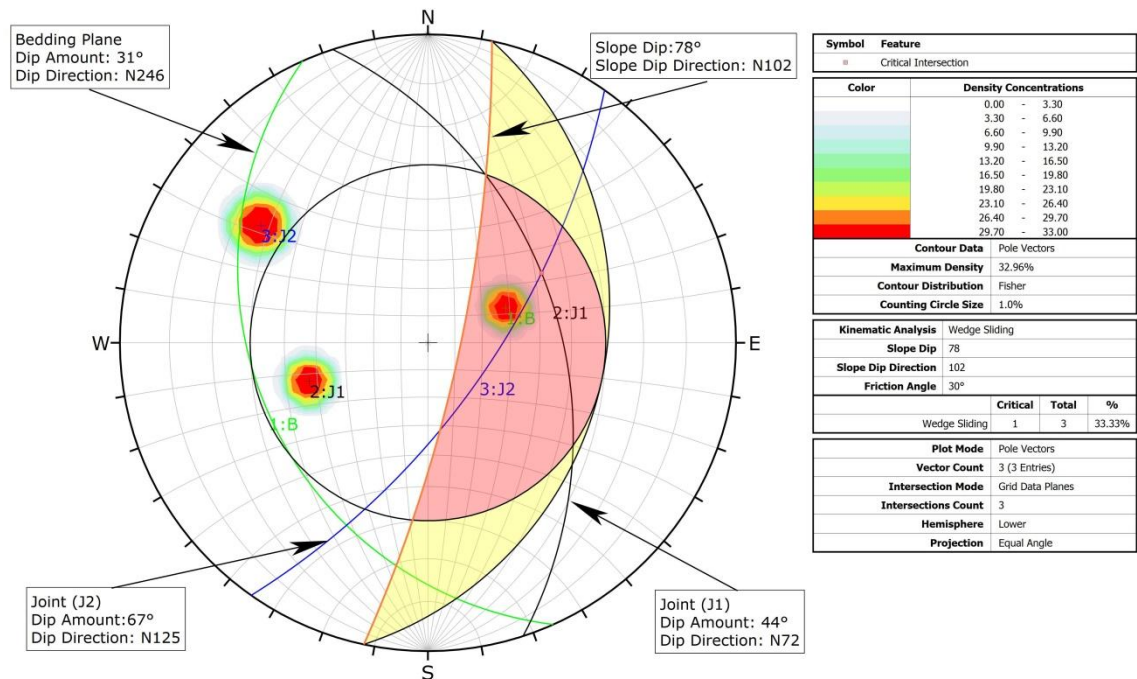


Fig. 4.64 Stereographic Projection showing the potential for wedge failure at S7

4.10. DETERMINATION OF SLOPE MASS RATING (S.M.R.)

Slope Mass Rating for different locations was calculated by reducing the value of basic rock mass rating (RMRb) by subtracting the three adjustment factors, i.e., F1, F2, and F3, based on their geometric relationship of the slope and discontinuities, and adding one adjustment factor F4, where F4 is the method of excavation used. The detailed rating for each slope is given in table 4.20.

Table 4.21 Slope Mass Rating for each location

Location No.	RMR	Joint	F1	F2	F3	F4	SMR	Class	Rock Mass Description	Stability	Probability Failure
S1	57	J1	1	1	-6	0	51	III	Normal	Partially Stable	0.4
		J2	1	1	-6	0	51	III	Normal	Partially Stable	0.4

		J3	1	1	-6	0	51	III	Normal	Partially Stable	0.4
S2	59	J1	1	1	-6	0	53	III	Normal	Partially Stable	0.4
		J2	1	1	-6	0	53	III	Normal	Partially Stable	0.4
		J3	1	1	-6	0	53	III	Normal	Partially Stable	0.4
S3	57	J1	0.15	1	-60	0	48	III	Normal	Partially Stable	0.4
		J2	0.15	1	-60	0	48	III	Normal	Partially Stable	0.4
		J3	0.15	1	-60	0	48	III	Normal	Partially Stable	0.4
S4	28	J1	1	1	0	0	28	IV	Bad	Unstable	0.6
		J3	1	1	0	0	28	IV	Bad	Unstable	0.6
		J3	1	1	0	0	28	IV	Bad	Unstable	0.6
S5	33	J1	1	1	-6	0	27	IV	Bad	Unstable	0.6
		J2	1	1	-6	0	27	IV	Bad	Unstable	0.6
		J3	1	1	-6	0	27	IV	Bad	Unstable	0.6
S6	29	J1	0.15	1	-60	0	20	V	Very Bad	Completely Unstable	0.6
		J2	0.15	1	-60	0	20	V	Very Bad	Completely Unstable	0.6
		J3	0.15	1	-60	0	20	V	Very Bad	Completely	0.6

										Unstable	
S7	44	J1	1	1	-25	0	19	V	Very Bad	Completely Unstable	0.9
		J2	1	1	-25	0	19	V	Very Bad	Completely Unstable	0.9
		J3	1	1	-25	0	19	V	Very Bad	Completely Unstable	0.9

4.11. ROCKFALL HAZARD RATING

For the determination of the cut slope, different 6 slopes were analyzed using the Rockfall Hazard Rating System for Indian Rockmass. Each slope height were measured using Leica DISTO S910, whereas the road width was measured using a measuring tape. The slope angle for different locations were measured using Burnton Compass, and the average slope angle lies between 48° and 86°. The ditch length for each location is narrow, and four sites are assigned ratings less than 30 percent. No seepage was observed during field investigation, and considered as dry. The result of the slake durability index performed in a laboratory lies between 60 to 95 percent. The final hazard ratings for each slope are obtained by the algebraic sum of the scores for each criterion, which determines the risk of rockfall. The slope with the highest total scores is identified as the most vulnerable and prioritized for further action. The detailed scoring of Rockfall Hazard Rating System for Slope, Climate, Geology (Sedimentary Rock), Traffic, and Rock History/ Frequency is given in table 4.21, 4.22, 4.23, 4.24 and 4.25, respectively. The Cumulative Score for Rockfall Hazard Rating System of each slope is given table 4.26.

Table 4.22 Detailed Scoring of Rockfall Hazard Rating System for Slope

		R1	R2	R3	R4	R5	R6
SLOPE	Slope Height	9.32 m	9.97	64.1m	19.45m	37.6	15.08 m
	<i>Score</i>	4	4	81	17.27	81	4
	Avg. Slope Angle	80	79	64	72	69	58
	<i>Score</i>	9	9	9	9	9	9
	Launching Features	Minor	Minor	Minor	Many	Minor	Minor
	<i>Score</i>	9	9	9	9	27	27
	Ditch Catchment	No catchment	Limited catchment	No catchment	Limited catchment	No catchment	No catchment
	<i>Score</i>	81	27	81	27	81	81
	Vegetation	Isolated plant	Isolated plant	Isolated plant	Isolated plant	Isolated plant	Isolated plant
	<i>Score</i>	27	27	27	27	27	27

Table 4.23 Detailed Scoring of Rockfall Hazard Rating System for Climate

CLIMATE		R1	R2	R3	R4	R5	R6
	Annual Precipitation	1518	1518	1518	1518	1518	1518
	<i>Score</i>	81	81	81	81	81	81
	Seepage/Water	Dry	Dry	Dry	Dry	Dry	Wet/Damp
	<i>Score</i>	3	3	3	3	3	3

	Annual Freeze/ thaw cycles	-	-	-	-	-	-
	Slope Aspect	SW	SW	SE	SE	SE	SE
	<i>Score</i>	9	9	27	27	27	27

Table 4.24 Detailed Scoring of Rockfall Hazard Rating System for Geology (Sedimentary Rock)

GEOLOGY		R1	R2	R3	R4	R5	R6
	Degree of Undercutting	0.3 to 0.6 m	0.3 to 0.6 m	0 to 0.3 m	0 to 0.3m	0 to 0.3m	0 to 0.3m
	<i>Score</i>	9	9	3	3	3	3
	S.D.I.	60 to 95%	60 to 95 %	95 to 100 %	60 to 95%	60 to 95%	60 to 95 %
	<i>Score</i>	9	9	3	9	9	9
	Degree of Interbedding	1 to 2 weak interbed, <15 cm	1 to 2 weak interbed, <15 cm	> 2 weak interbed, <15 cm	1 to 2 weak interbed, <15 cm	> 2 weak interbed, <15 cm	> 2 weak interbed, <15 cm
	<i>Score</i>	3	3	27	3	27	27
	Discontinuities						
	Block size/ Volume	0.29m	0.34m	1.12m	1.18m	0.95m	0.24m
	<i>Score</i>	3	3	27	27	9	3
	Block Shape	Blocky	Tabular	Blocky to Angular	Blocky	Blocky to Angular	Tabular
	<i>Score</i>	9	3	27	9	27	3

	Number of Sets	2	1 plus random	2	2	2	1 plus random
	<i>Score</i>	27	9	27	27	27	9
	Persistence/ Orientation	<3m and dips into slope	<3m and dips into slope	<3m and dips into slope	<3m and dips into slope	<3m and dips into slope	<3m and dips into slope
	<i>Score</i>	3	3	3	3	3	3
	Aperture	0.1 to 1 mm	0.1 to 1 mm	0.1 to 1 mm	0.1 to 1 mm	1 to 5 mm	0.1 to 1 mm
	<i>Score</i>	9	9	9	9	27	27
	Weathering Condition	Grade 1&2	Grade 1&2	Grade III	Grade 1&2	Grade III	Grade III
	<i>Score</i>	3	3	9	3	9	9
	Friction	Rough	Rough	Planar	Rough	Planar	Planar
	<i>Score</i>	3	3	27	3	27	27
	Infilling Material	Heal infilling	Heal infilling	Heal infilling	Heal infilling	Heal infilling	Heal infilling
	<i>Score</i>	3	3	3	3	3	3

Table 4.25 Detailed Scoring of Rockfall Hazard Rating System for Traffic

TRAFFIC		R1	R2	R3	R4	R5	R6
	Sight Distance	90%	85%	80 %	80%	75%	80%
	<i>Score</i>	5	6	9	9	11	9
	Avg. Vehicle Risk	5%	7.5%	55.9%	9.9%	60.42%	35.3%
	<i>Score</i>	3	3	11.6	3	14.22	4

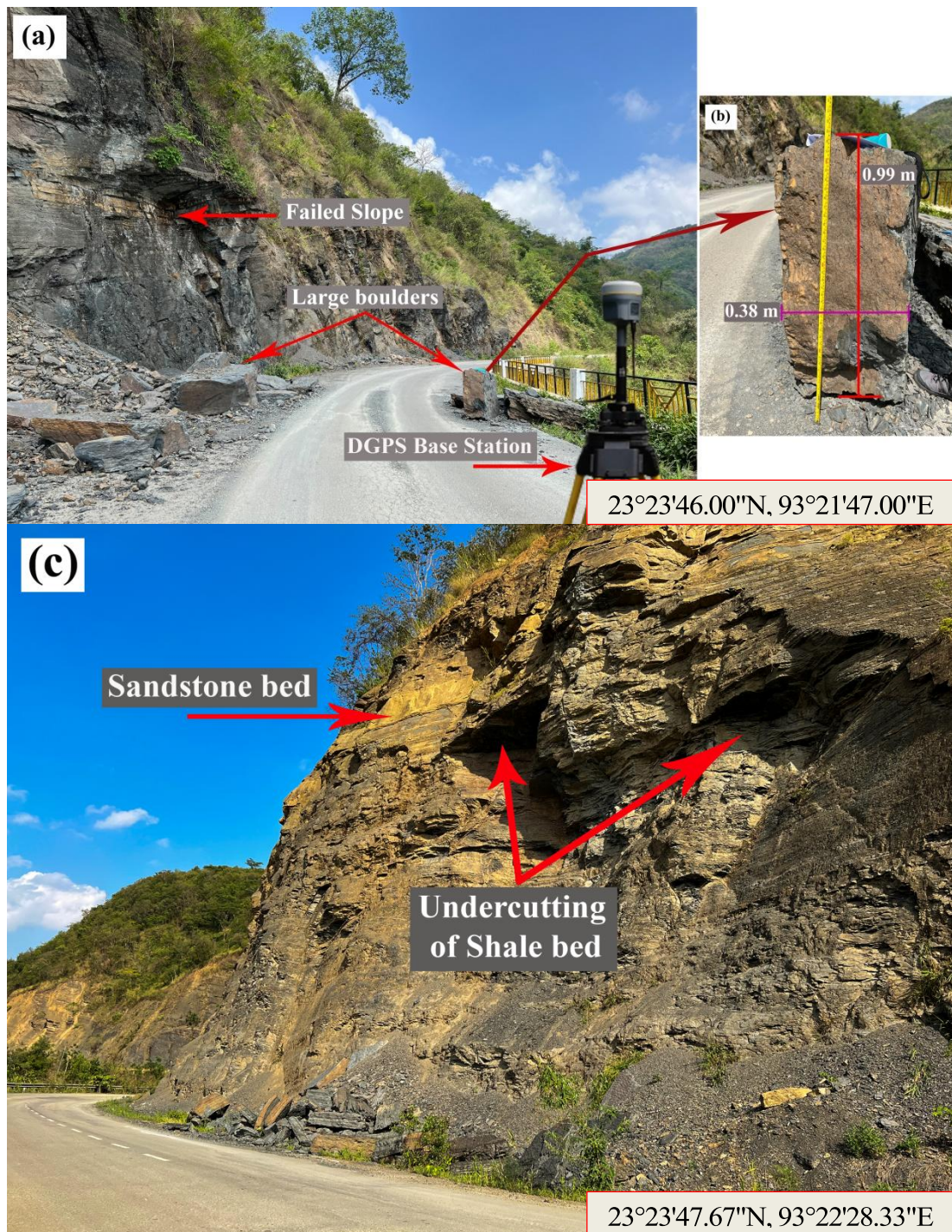
	Road Width	7.62 m	7.92 m	7.65 m	7.65 m	7.65 m	7.65 m
	<i>Score</i>	38.58	33.63	38.05	38.05	38.05	38.05
	No. of Accident	0 to 2	0 to 2	0 to 2	0 to 2	0 to 2	0 to 2
	<i>Score</i>	3	3	3	3	3	3

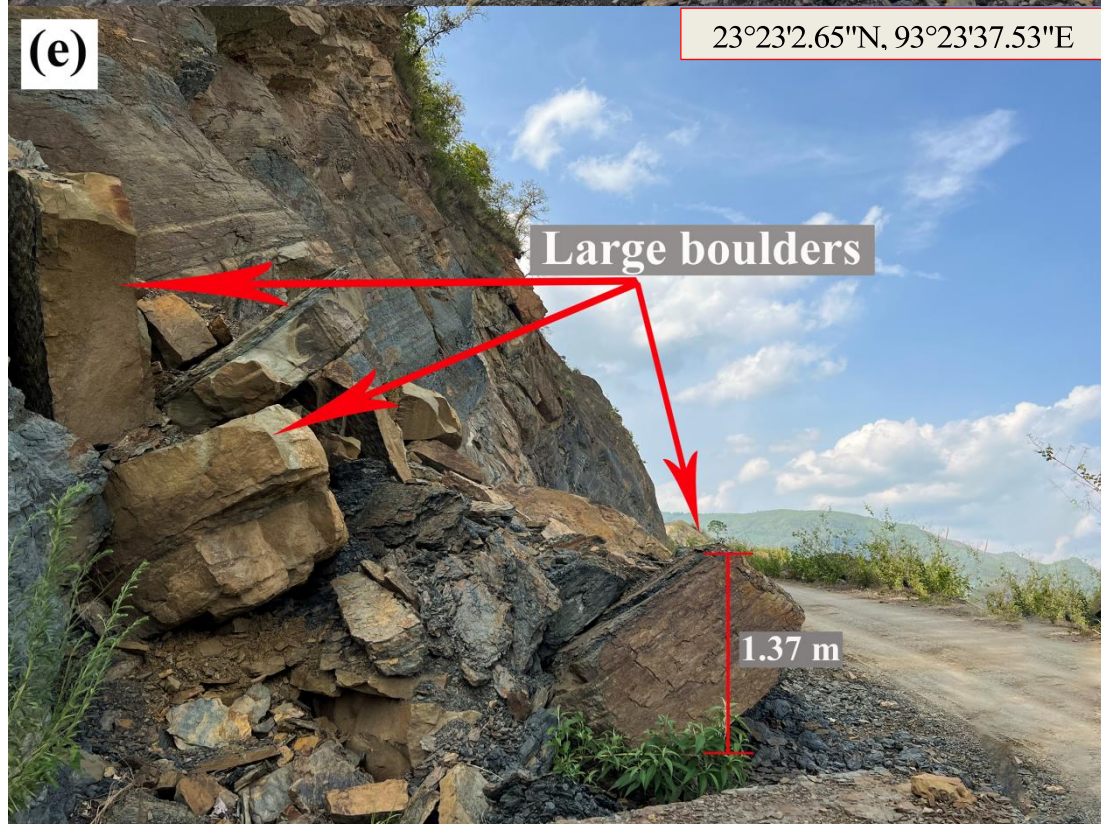
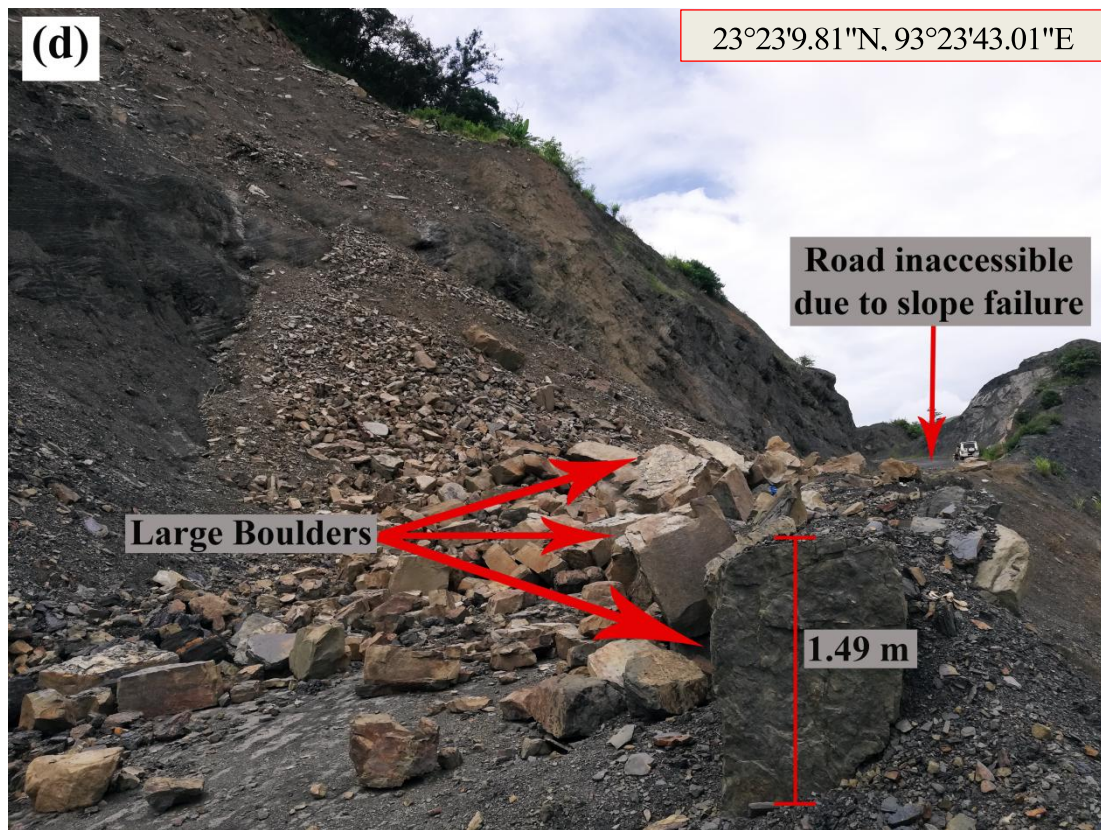
Table 4.26 Detailed Scoring of Rockfall Hazard Rating System for Rock History/ Frequency

Rock History/ Frequency	R1	R2	R3	R4	R5	R6
	0 to 3 per year	0 to 3 per year	8 to 12 per year	3 to 5 per year	8 to 12 per year	8 to 12 per year
	3	3	27	9	27	27

Table 4.27 Cumulative Score for Rockfall Hazard Rating System

Cumulative Score						
Site	Location	Slope	Climate	Geology	Traffic	Total Score
R1	23°23'46.00"N, 93°21'47.00"E	130	93	81	52	356
R2	23°23'47.67"N, 93°22'28.33"E	76	93	57	48	274
R3	23°23'9.81"N, 93°23'43.01"E	207	111	165	88	571
R4	23°23'2.65"N, 93°23'37.53"E	89	111	99	62	361
R5	23°22'59.85"N; 93°23'31.10"E	225	111	171	93	600
R6	23°22'53.98"N; 93°23'25.58"E	148	111	123	81	463





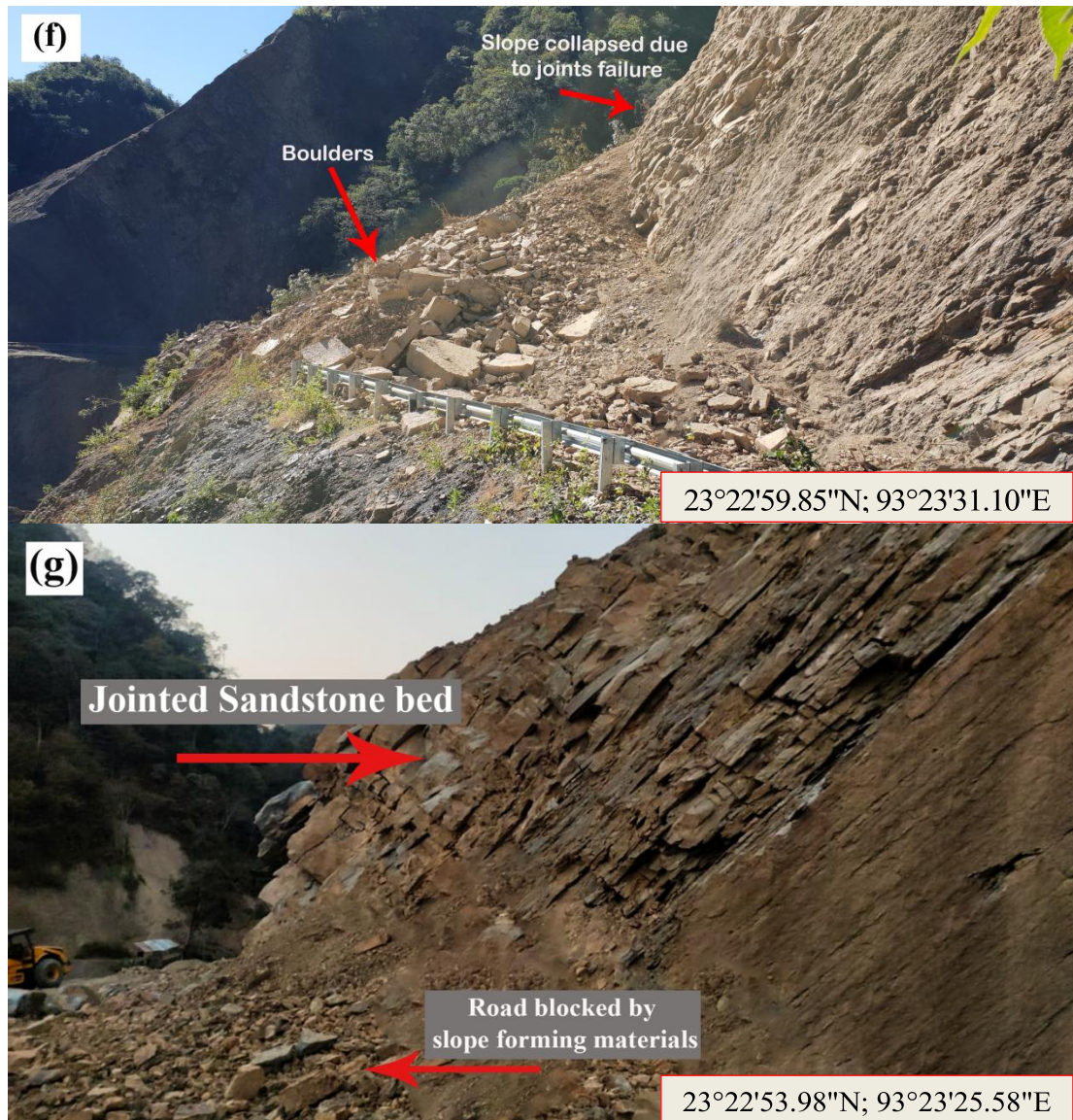


Fig. 4.65 Field Photographs; (a) Location R1 (b) Detached rock at R1 (c) Location R2 (d) Location R3 (e) Location R4 (f) Location R5 (g) Location R6

4.11.1. Numerical Simulation

The Rocscience Software Rocfall 4.0 software is used to generate a two-dimensional slope geometry trace. The bedrock wherein the slopes were developed is mainly sandstone and siltstone, and the geometries were created to accurately depict the road cut-slopes. Simulations were done for detached rock trajectories on a slope considering free of any obstacle to align with the field conditions. The average weights of falling boulders were approximately deduced to vary from 15 to 500 kg;

this is based on multiple measurements of rock blocks from the field. In order to generate the trajectories for detached rocks, point seeders were in the slopes at multiple locations to ensure maximum vulnerability depending on the height of the slopes.

This research examines the maximum bounce height, run-out distance, total kinetic energy, and translational energy. Table 4.27 displays the parameters for the coefficient of restitution that the Rocfall 4.0 software utilized. Figure 4.60 to 4.65 display the simulation of rockfall trajectories.

Table 4.28 Coefficient of Restitution for surface type

Surface Type	Normal Restitution (Rn)		Tangential Restitution (Rt)	
	Mean	Standard Deviation	Mean	Standard Deviation
Rock Surface (Sandstone)	0.520	0.040	0.990	0.990
Asphalt	0.390	0.040	0.890	0.130
Rock Talus	0.350	0.040	0.850	0.040

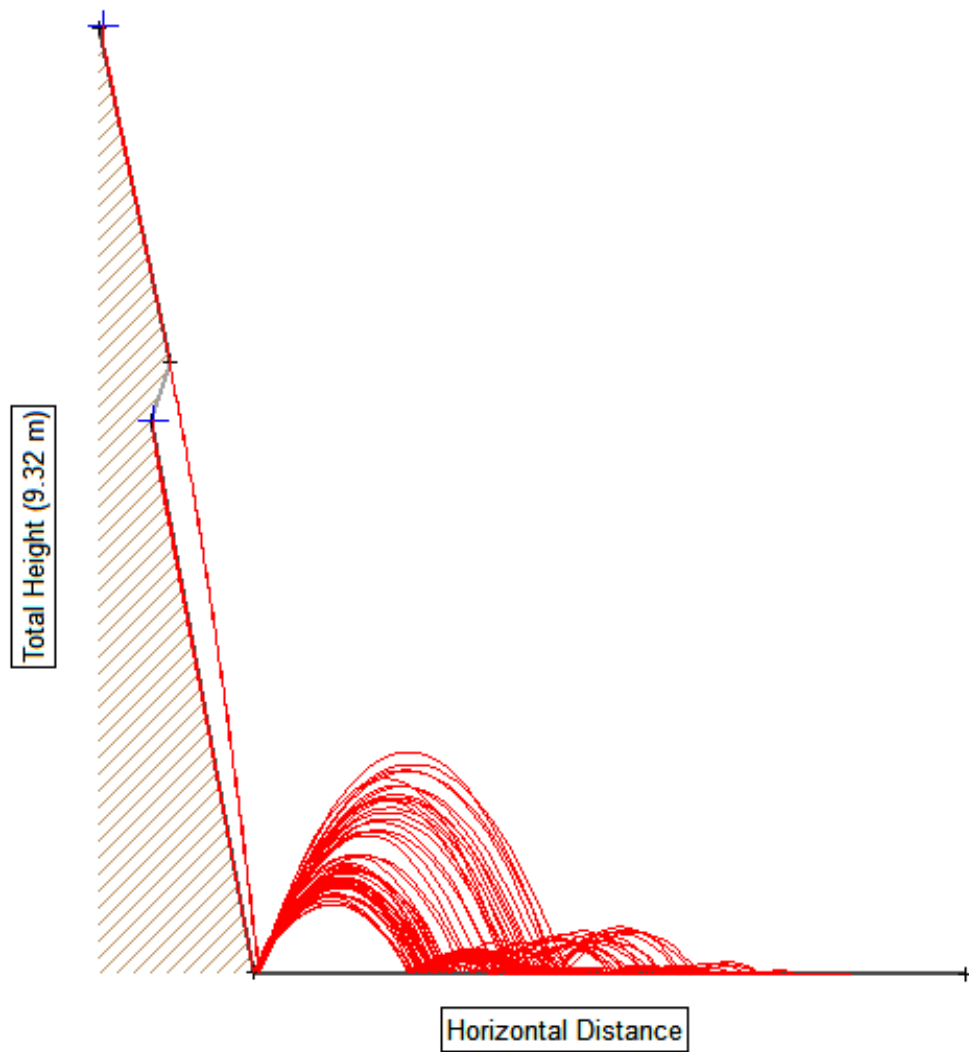


Fig. 4.66 Simulation of Rockfall trajectories detached from R1

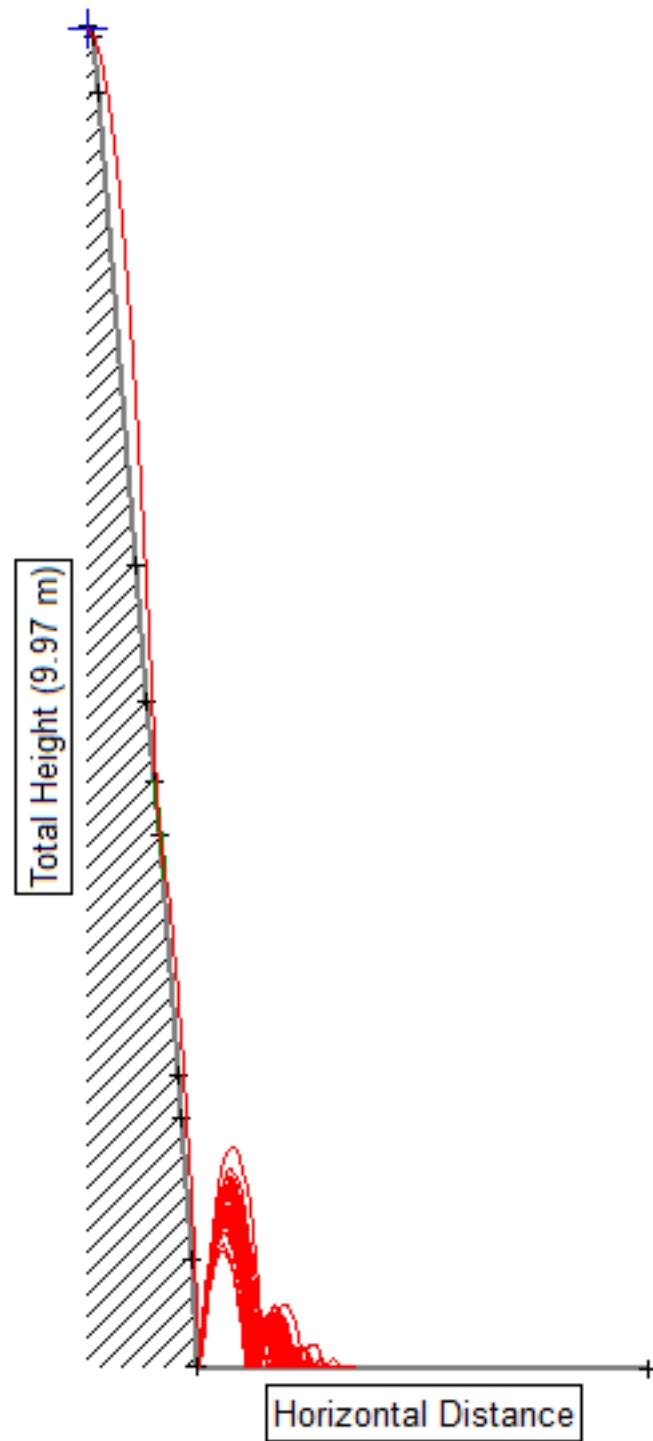


Fig. 4.67 Simulation of Rockfall trajectories detached from R2

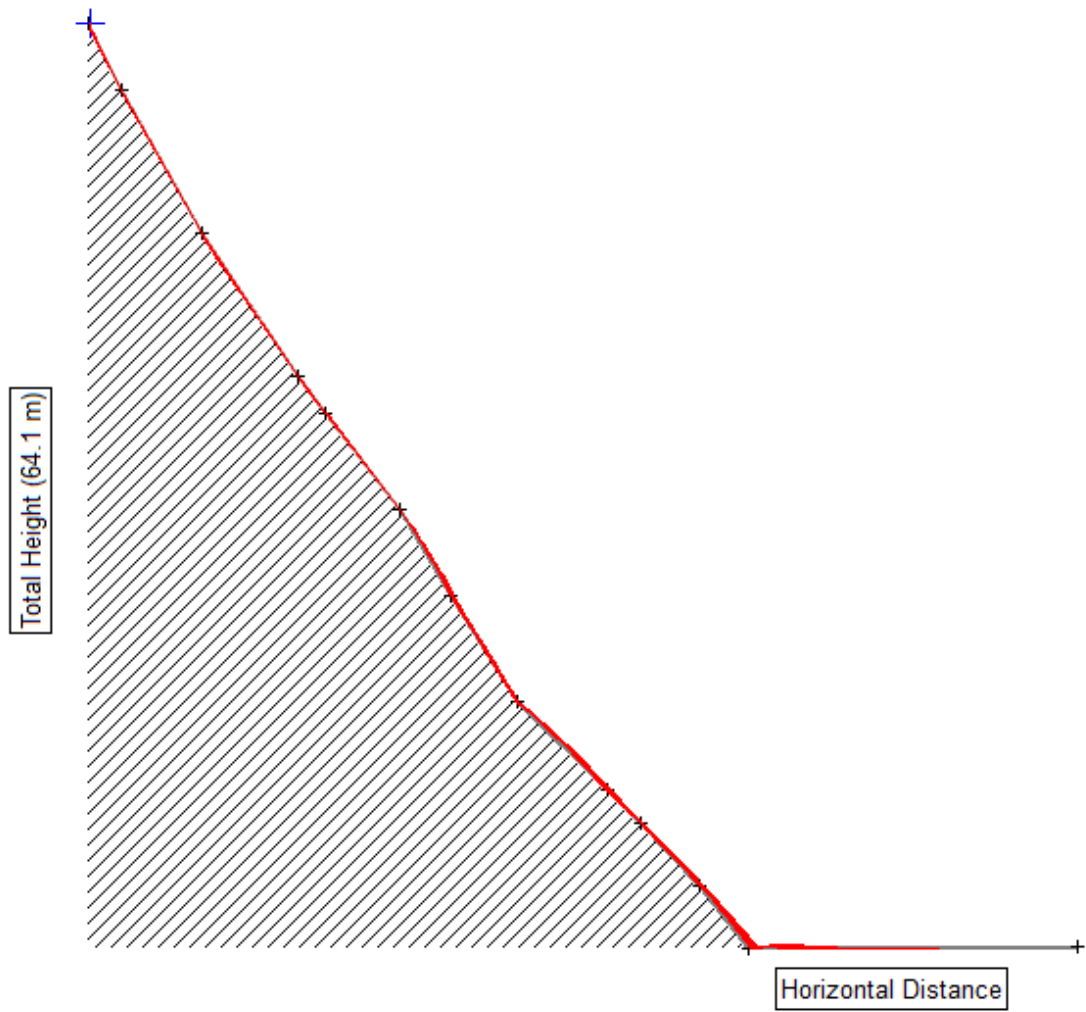


Fig. 4.68 Simulation of Rockfall trajectories detached from R3

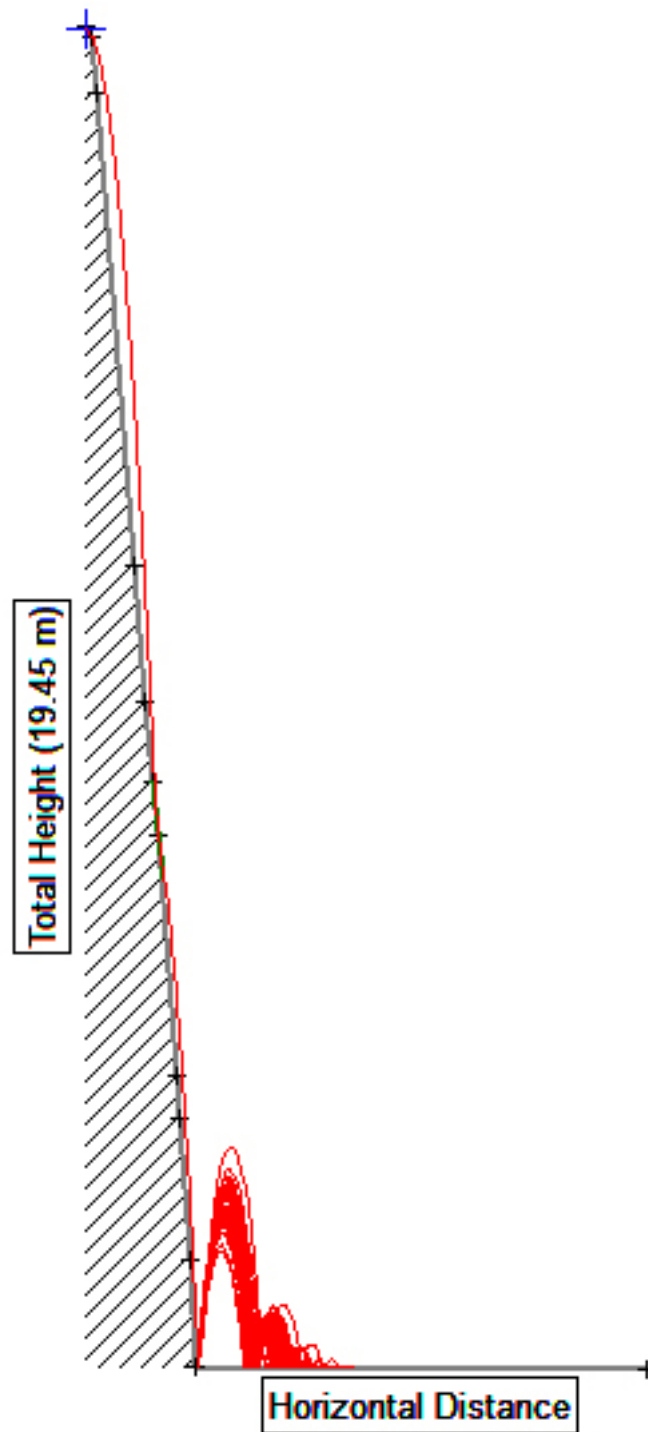


Fig. 4.69 Simulation of Rockfall trajectories detached from R4

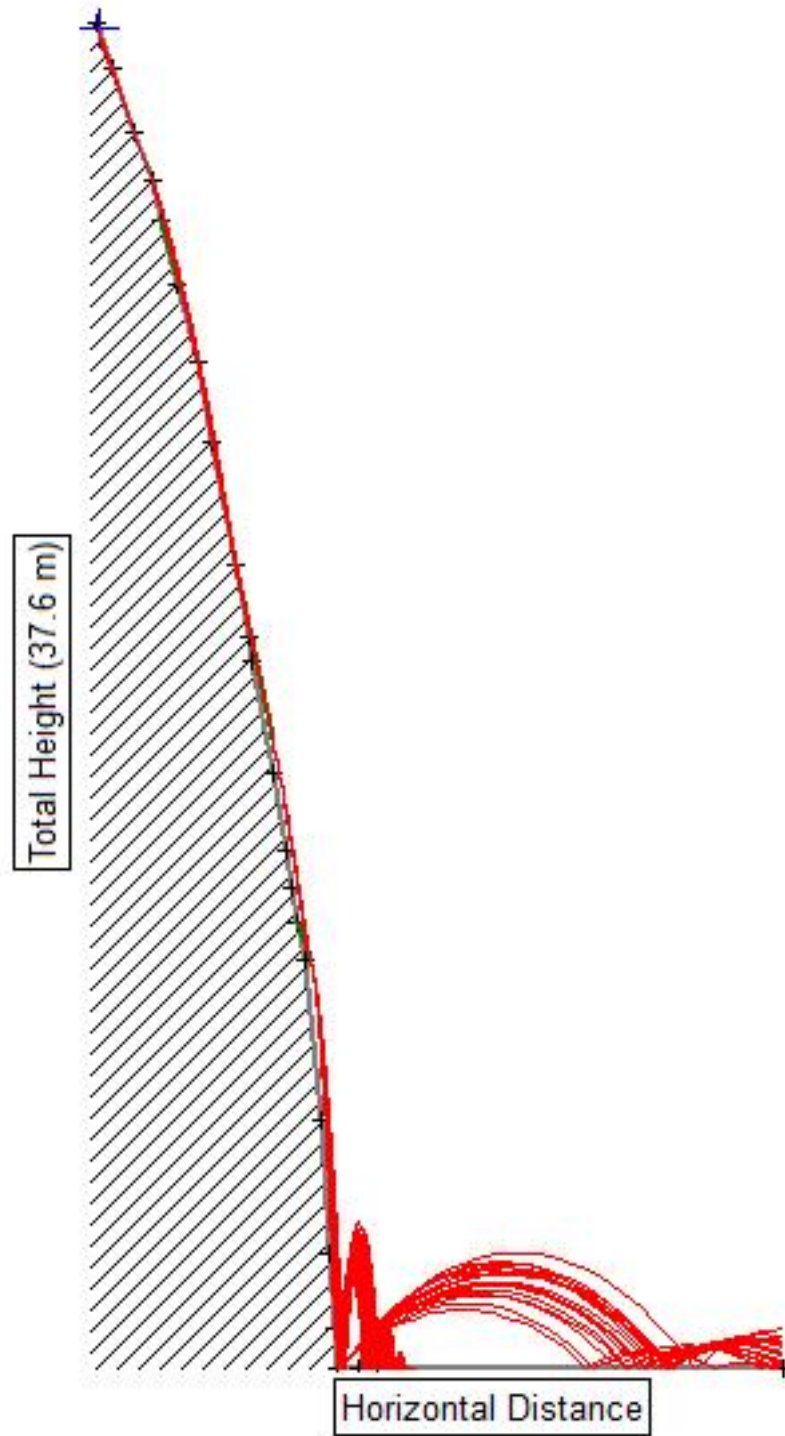


Fig. 4.70 Simulation of Rockfall trajectories detached from R5

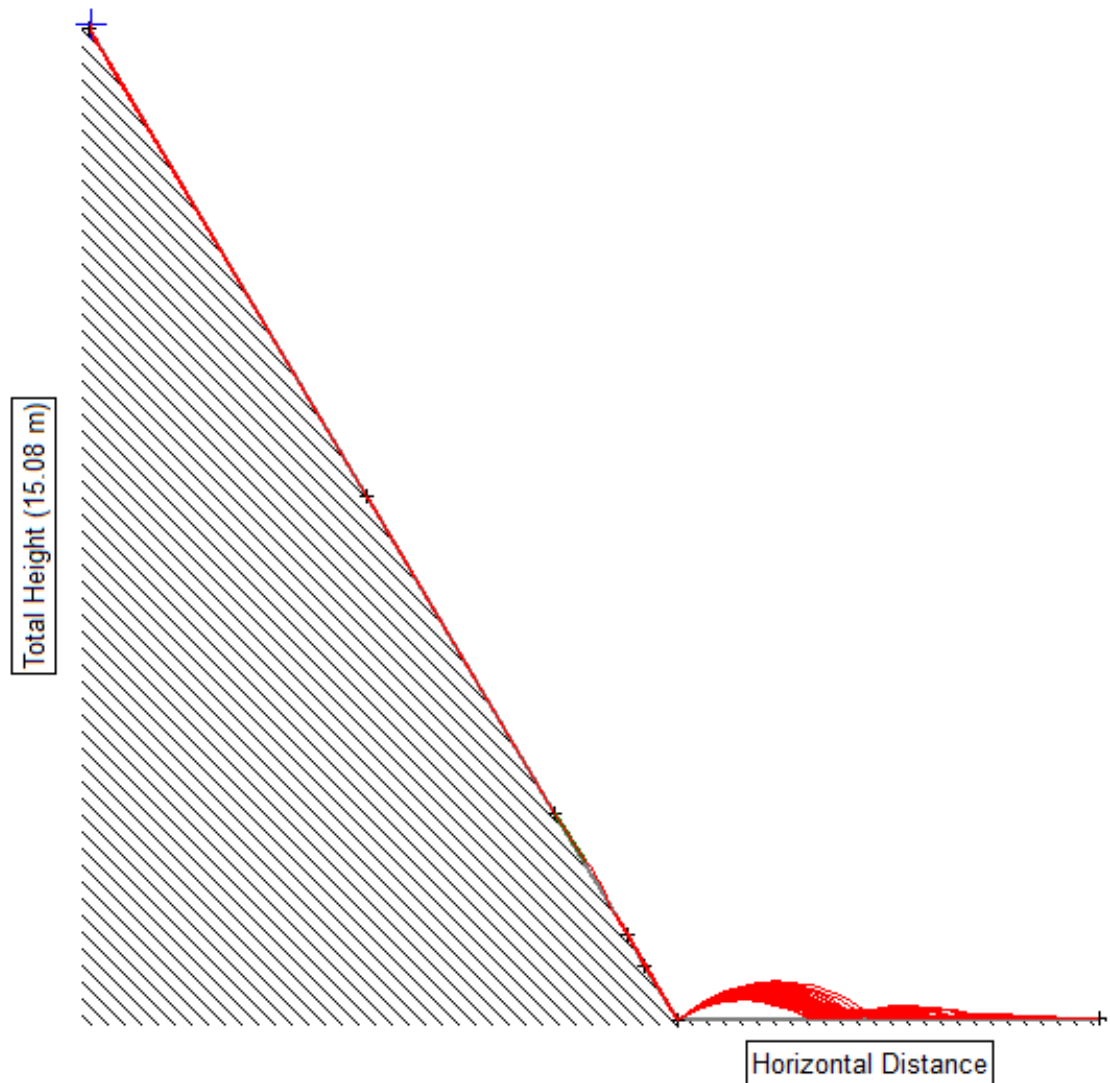


Fig. 4.71 Simulation of Rockfall trajectories detached from R6

For the field lithology, the coefficients of tangential restitution (R_t) and normal restitution (R_n) were chosen at 0.53 and 0.99, respectively. From the simulations, Figures 4.66, 4.67, and 4.68 present the numerical analysis for the bounce height, kinetic energy, and translational energy for each slope.

4.11.2. Bounce height and Run-out distance

As the free-falling blocks from the seeder at the head of the cliff fall with high velocity, the bounce height of rock blocks after hitting the ground surface is analyzed to be highest at R5 with 4.43 m above the ground at a horizontal distance of 6.71 along the roadway, and lowest at R6 of 0.57 m high at horizontal distance of 10.37 m along the roadway. Since, the run-out distance went down to the valley, except for R2, the entire width of the road is unsafe and made it critical, and may cause injuries.

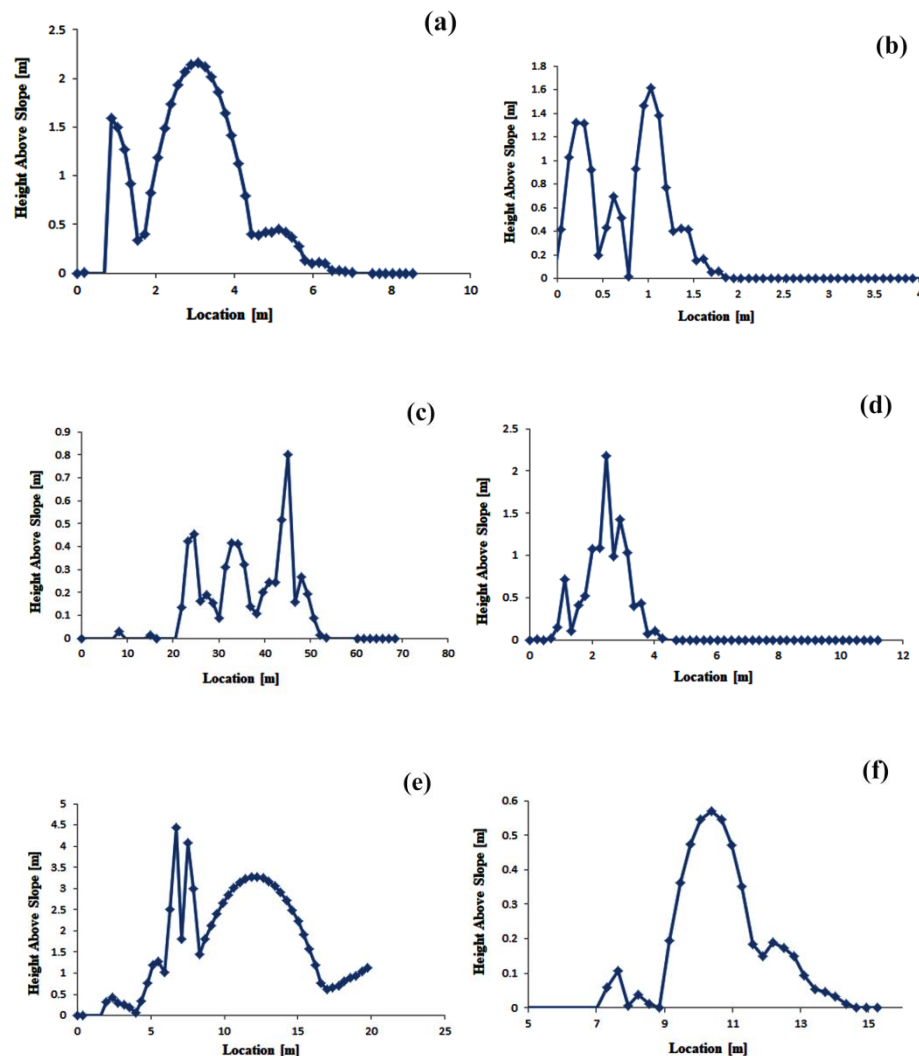


Fig. 4.72 Bouncing Height obtained from falling rocks after hitting the ground for each Slopes; (a) R1
(b) R2 (c) R3 (d) R4 (e) R5 (f) R6

4.11.3. Total Kinetic Energy and Translational Energy

The velocity of the falling rock is affected by the slope angle, the height of the slope on which the rock is detached, and the coefficient of friction of the slope-forming materials. During the fall, no barrier obstructs the velocity before bouncing onto the road. On colliding with the road, both the velocity and kinetic energy decrease. The total kinetic energy is found to be highest of 7036.31 Joule at the horizontal distance of 2.46 m on the road in R4, and translational velocity is analyzed to be highest of 23.58 m/s at 45.18 m, i.e, the rock block falls down the valley in R3.

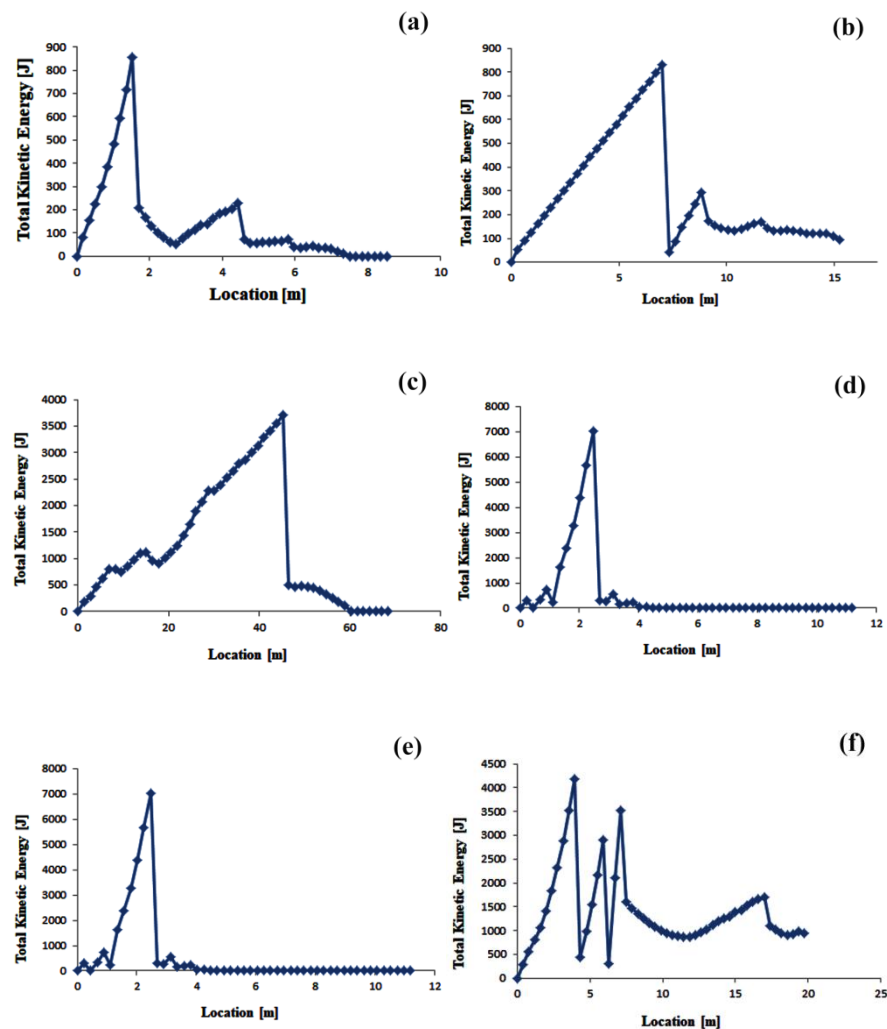


Fig. 4.73 Kinetic Energy obtained from falling rocks for each Slopes; (a) R1 (b) R2 (c) R3 (d) R4 (e) R5 (f) R6

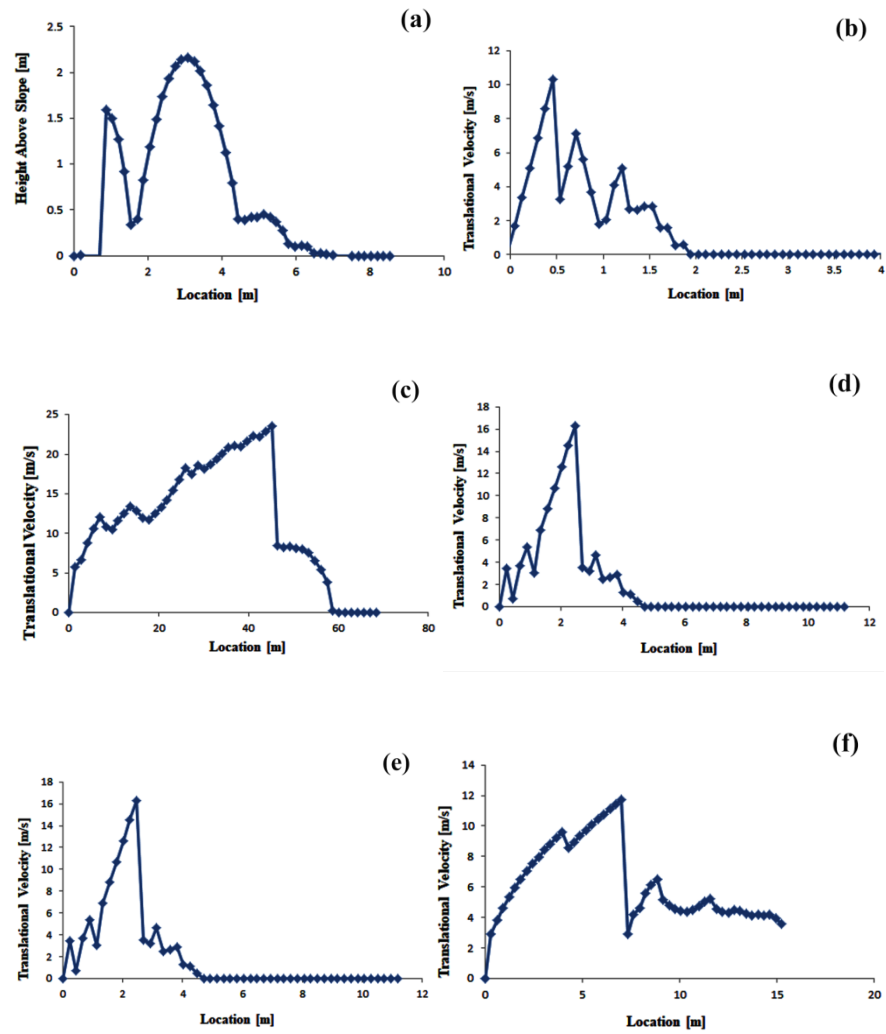


Fig. 4.74 Translational Velocity obtained from falling rocks for each Slopes; (a) R1 (b) R2 (c) R3 (d) R4 (e) R5 (f) R6

4.12. ANALYSIS OF CHAMPHAI DISTRICT RAINFALL DATA

The analysis of rainfall patterns is essential in understanding the recurring slope failures in Mizoram, particularly during the monsoon season. The region is highly susceptible to rainfall-induced landslides due to its steep terrain, weathered rock formations, and intensive land-use changes. In recent years, several slope failures have been reported across different parts of Mizoram, highlighting rainfall as a primary triggering factor.

To establish the correlation between precipitation and slope instability, rainfall data for Champhai District in the year 2021 was collected from the India Meteorological Department (IMD). This data is presented in Table 4.29 and Figure 4.75, showing the monthly rainfall distribution for the district.

Table 4.29 Champhai District Rainfall (in mm) in 2021

Months	Jan	Feb	Mar	Apr	May	June	July	Aug	Sept	Oct	Nov	Dec
Rainfall	4.67	0	26.8	32.11	129.32	192.04	252.94	329.59	239.85	105.1	44.3	60.54

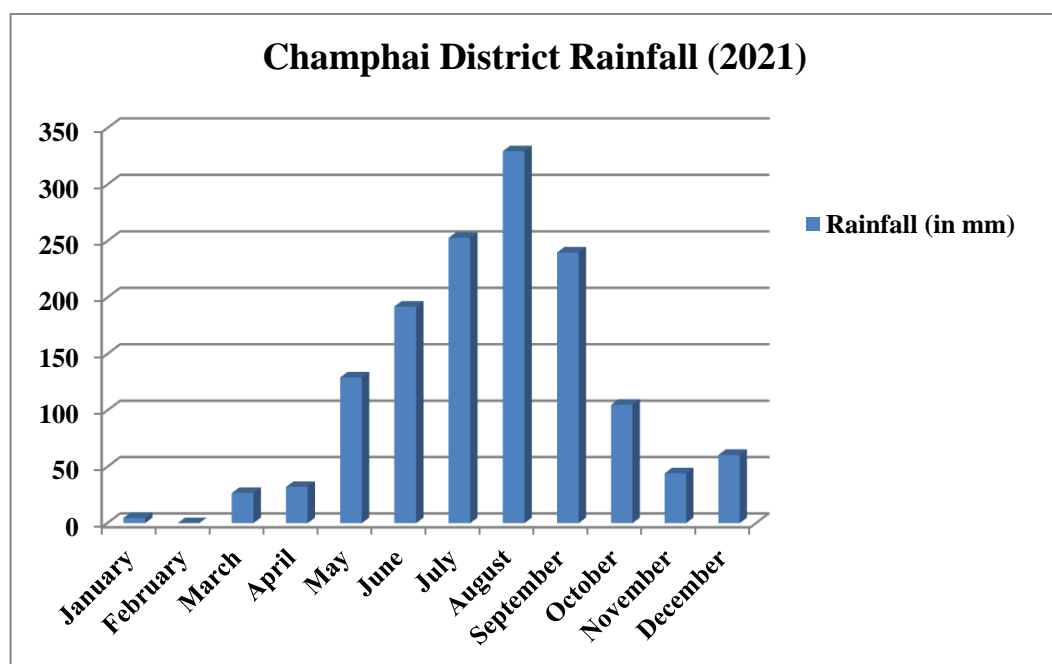


Fig. 4.75 Monthly Rainfall of Champhai District in 2021

In 2021, Champhai experienced continuous rainfall from March through December, with the intensity gradually increasing over the months. The precipitation peaked in August, recording 329.59 mm, marking it as the wettest month of the year. This trend reflects the typical monsoon pattern in Mizoram, where heavy and sustained rainfall occurs during the mid-monsoon period, often coinciding with a spike in reported landslide incidents.

Slope modifications expose the underlying soil and rock layers to atmospheric conditions, accelerating weathering and erosion. During heavy rainfall events, infiltration of rainwater into the soil profile increases significantly. As water percolates into the ground, it not only saturates the soil but also increases the pore water pressure within the soil matrix. This results in reduction of the soil's effective stress and shear strength, making it more prone to failure.

Furthermore, excess surface runoff during high-intensity rainfall events contributes to topsoil erosion and slope toe undercutting, both of which can trigger or exacerbate landslides. The process is further intensified in disturbed or deforested slopes, where vegetative cover is inadequate to retain soil moisture or stabilize the slope.

The daily rainfall data for Champhai in 2021, illustrated in Table 4.30 and Figure 4.76, provides a more granular view of rainfall distribution, which is crucial for identifying short-duration, high-intensity events that may have directly contributed to landslide occurrences.

The rainfall data analysis for Champhai District reinforces the understanding that rainfall plays a critical role in triggering slope failures in the region. The combination of steep slopes, modified terrain, and high rainfall intensity creates an environment highly vulnerable to landslides. Therefore, rainfall monitoring and early warning systems, coupled with land-use regulation and slope stabilization measures, are imperative for effective disaster risk reduction in Mizoram.

Table 4.30 Daily rainfall data of Champhai District in 2021

Day	Jan	Feb	Mar	Apr	May	June	July	Aug	Sep	Oct	Nov	Dec
1	0	0	0	6.07	17.36	3.32	13.96	3.84	49.1	3.39	0	0
2	0	0	0	0.2	0.62	5.62	6.99	26.45	5.57	0.32	0	0
3	0	0	0	0.44	3.36	7.47	1.47	58.12	0.27	6.13	0	0
4	0	0	1.89	0	2.74	0.44	1.29	5.34	21.6	1.84	0	0
5	0	0	0	0.26	4.74	9.03	1.08	7.01	2.89	1.98	0	0.02
6	0	0	0	0	0.09	18.2	0.71	12	0.29	0.43	0	8.38
7	0	0	0.47	0	0.28	6.06	3.09	25.39	3.85	0.75	0	36.32
8	0	0	1.79	0	0.82	0.82	8.64	5.24	14.46	0.64	0	12.34
9	0	0	3.69	0.7	0.33	0.9	4.99	9.05	29.2	7.03	0	0.09
10	0	0	0	0	3.18	12.12	18.92	4.96	10.18	3.55	0	2.59
11	0	0	0.08	0	3.4	26.57	6.88	2.89	5.07	2.42	0.06	0.19
12	0	0	0	0	21.27	10.38	2.44	2.83	0	3.14	0	0
13	0	0	0	0	12.63	17.06	38.21	1.93	0.21	1.66	2.62	0
14	0	0	0	0.31	11.07	11.79	6.15	2.25	4.22	0.49	10.06	0
15	0	0	0	0.01	11.35	10.91	5.06	0.87	4	0	22.55	0
16	0	0	0	0.18	1.12	11.67	11.63	21.82	15.39	0	8.46	0
17	0	0	0	3.8	3.88	13.66	41.24	19.05	15.74	0.12	0.55	0
18	0	0	0	0	5.98	5.06	12.07	3.07	9.42	0.96	0	0
19	0	0	0	7.99	3.79	6.52	8.79	3.65	16.43	11.43	0	0
20	0	0	0	3.49	1.32	6.08	1.57	3.08	0.57	16.62	0	0
21	4.67	0	0	0	0.38	2.77	7.2	4.34	6.61	34.3	0	0

22	0	0	0	0	0	0.71	5.59	5.25	4.21	4.71	0	0
23	0	0	0	0	7.99	3.13	2.05	1.93	0.32	0	0	0.61
24	0	0	0	0	0.98	1.75	0.19	2.76	1.82	0	0	0
25	0	0	0	0	1.63		11.91	2.35	0.1	0	0	0
26	0	0	0	0	3.2		14.82	1.22	0.21	0.16	0	0
27	0	0	0	0	3.04		7.62	11.55	0.24	2.12	0	0
28	0	0	0	2.97	1.73		1.3	30.77	0.23	0.53	0	0
29	0		0	5.69	1.04		7.08	19.1	13.75	0	0	0
30	0		5.73					23.97	3.9	0.14	0	0
31	0		13.15					7.51		0.24		0
Avg	0.151	0	0.86	1.10	4.45	8.00	8.72	10.63	7.99	3.39	1.47	1.95
Total	4.67	0	26.8	32.11	129.32	192.04	252.94	329.59	239.85	105.1	44.3	60.54

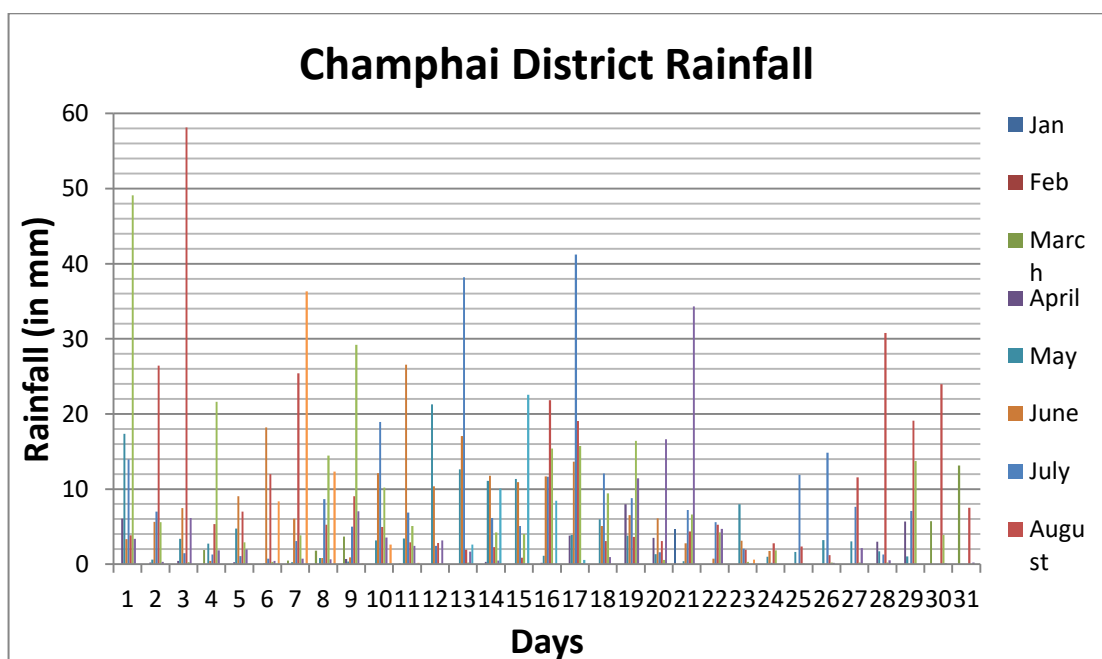


Fig. 4.76 Rainfall data of Champhai District in 2021

4.13. HAZARD ZONATION

From the analyses using Limit Equilibrium Method, Rock Mass Rating, Kinematic Analyses, Slope Mass Rating, and Rock fall Hazard Rating System, a hazard zonation map is generated based on the findings. It is classified into three; Low hazard zone, moderate hazard zone, and high hazard zone. The Hazard Zonation Map is displayed in figure 4.83.

The data suggests that locations LS1, LS4, LS5, S5, S6, R3, and R5 demand the most attention due to their unstable slopes, poor rock conditions, and high rockfall potential. All slope sections exhibit Factors of Safety (FoS) less than 1, indicating instability under saturated conditions. The lowest FoS (0.488) was recorded for LS1 using the Janbu Simplified Method, suggesting high susceptibility to failure. Variation in plasticity index and shear strength parameters indicates differing levels of slope stability. Samples of LS5 and LS6 exhibit medium plasticity and low shear strength, contributing to slope vulnerability. RMR values show a mix of fair (Class III) and poor to very poor (Classes IV–V) rock quality. Toppling and wedge failures are potential modes of rock slope failure at several locations. SMR scores indicate that some areas, especially Locations 6 and 7, fall into Class V (very bad rock mass), with up to 0.9 probability of failure. High slope angles (58° – 82°) and presence of undercutting increase the likelihood of rockfalls. Rockfall simulation shows high bounce height and kinetic energy, posing a significant hazard, especially at R4 and R5.

High Hazard Zones: LS1, LS4, LS5, R3, R5, S6, and S7 – marked by poor rock/soil properties, high failure probability, and critical energy outputs.

Moderate Hazard Zones: LS2, LS3, R1, R4, S1–S4 – show partial instability, fair rock masses, and moderate risk.

Low Hazard Zones: LS2 (partial), R2, S2 – relatively stable conditions with higher GSI/RMR and lower failure indicators.

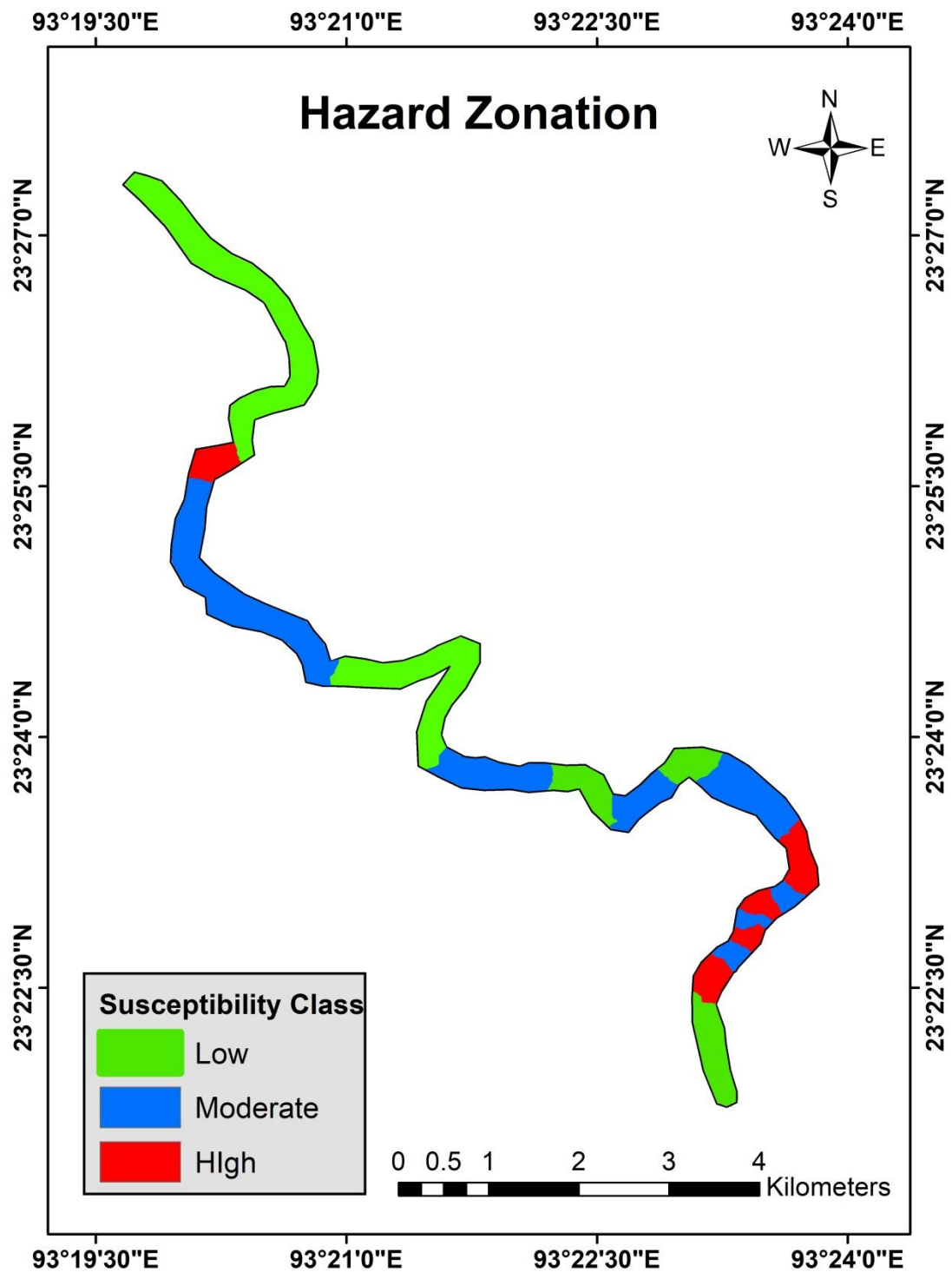


Fig. 4.77 Hazard Zonation Map of study sites

DISCUSSIONS

The findings from various techniques are presented, and they reflect the present condition and characteristics of the research area.

Natural moisture content of soil samples collected from six locations shows a variation, indicating that they have different compaction, strength, and stiffness. The liquid limit for sample 2 (LS2), i.e., location 2 has the lowest value of 20.23%, whereas sample 5 (LS5), i.e., location 5 has the highest value of 43.68. The plastic limit is lowest for sample 2 (LS2), i.e., location 2 at 17.70%, and maximum for sample 5 (LS5), i.e., location 5 with a value of 31.89%. From the liquid limit and plastic limit obtained from laboratory analyses, a plasticity index is obtained. Sample 2 (LS2) and sample 4 (LS4) are classified as slightly plastic, whereas the other samples, i.e. sample 1 (LS1), sample 3 (LS3), sample 5 (LS5), and sample 6 (LS6) are classified as medium plastic. Based on Sower's classification 1979, the liquidity index and consistency index are classified as medium stiff for sample 3 and sample 6, whereas stiff for sample 1, sample 2, sample 4, and sample 5.

The result obtained from the direct shear test shows that sample 4 (LS4) has the lowest cohesion of 0.27 kg/cm², while sample 3 (LS3) has the highest cohesion of 0.392 kg/cm². The other samples, i.e., sample 1 (LS1), sample 2 (LS2), sample 5 (LS5), and sample 6 (LS6) have a cohesion of 0.216 kg/cm², 0.163 kg/cm², 0.27 kg/cm², and 0.168 kg/cm², respectively. The angle of internal friction is lowest in sample 6 (LS6) having 7.26° and the maximum value is obtained in sample 5 (LS5) of 40.29°. The other four samples, i.e., LS1, LS2, LS3, and LS4 have an internal friction of 21.86°, 22.04°, 9.99°, and 17.84°, respectively.

From the slope stability analysis of the model slope using limit equilibrium methods considering the unit weight, strength type, cohesion, and angle of friction, the Factor of Safety for each cut-slope is less than 1, which indicates the research area is unstable, and highly vulnerable to sliding, when it is completely wet and fully saturated. From the analyses using different methods, the Janbu Simplified Method for slope LS1 has the lowest factor of safety of 0.488, while slope LS2 of Bishop Simplified Method has the highest factor of safety of 0.859. For LEM analyses using

different methods, the overall Factor of Safety for each slope, i.e., LS1, LS2, LS3, LS4, LS5, and LS6, Janbu Simplified Method has the lowest, whereas Bishop Simplified Method has the highest Factor of Safety.

For rock mass characterization using Rock Mass Rating, the analyses shows four locations, i.e., S1, S2, S3, and S7, have RMR values of 57, 59, 57, and 44, respectively. The four sites fall under class III of a fair rock description. The average stand-up time is 1 week for 5 meters span. From the RMR classification, the average cohesion and the angle of friction fall between 200-300 and 25-35, respectively. Locations 4, 5, and 6, having RMR values 28, 33, and 29, fall under class IV of poor rock description. The average stand-up time is 10 hours for 2.5 meters, having the cohesion between 100-200 and the angle of friction 23-35. The algebraic sum of the numerical values assigned for each parameter is low and corresponds to less favorable conditions for site development.

The overall observation values of Geological Strength Index based on Structure Ratings and Surface Condition Ratings falls between 42 and 54, with study site; spot 6 has the lowest GSI value, whereas, study site; spot 2 has the highest GSI value.

From the Kinematic Analysis, the probable slope failures were analyzed as wedge and direct toppling. S1, S2, and S4 show possible direct toppling failure, while S3, S5, S6, and S7 show possible wedge failure. The probability of slope failure is high due to the presence of weak joints and weak rock strength.

The overall Slope Mass Rating (SMR) score for locations S1, S2, and S3 are 51, 53, and 48, respectively. The three locations fall within class III with a normal rock mass description of 0.4 out of 1 probability of failure, having a planer along with some joints and many wedges. The overall SMR score for location S4 is 28 and, location S5 is 27, which falls within class IV with a bad rock description, having a planer or big wedge failure of 0.6 out of 1 probability of failure. Locations 6 and 7 have an overall SMR score of 20 and 19. The two locations fall within class V with a very bad rock description of 0.9 probability of failure.

From the Rockfall Hazard Rating System, the slope angle lies between 58° to 82° , indicating a high possibility of rocks falling along the road. Due to differential erosion, undercutting erosion is observed to a range in length from 0 to 0.6 meters. As a result, there is a greater risk that rock could fall if the undercutting is prolonged to weathering and erosion. In locations R1, R3, R5, and R6, there is no ditch catchment, and in locations R2 and R4, it is observed that the ditch length is relatively short, creating less possibility for rock blocks to be stopped after falling. With a mean score of 91.45% after the second cycle, the slake durability index is very high, indicating the rock is resistant to weathering. From the cumulative score, R2 is considered low urgency (i.e., <300), R1, R4 and R6 are considered to be of moderate urgency (i.e., $300\text{--}500$), while R3 and R5 are of high urgency (i.e., >500) and are at risk of rock falls.

The simulation studies determine the kinetic energy, translational energy, and bounce height of free-falling rock blocks. After striking the ground, R5 exhibits the largest bouncing height, measuring 4.43 meters. At R4, the highest translational energy is 23.59 m/s, and the maximum kinetic energy is 7036.31 joules. Heavy rock blocks carry more kinetic energy as they fall off the slope, causing greater risk to motor vehicles and people as well.

An analysis of Champhai District's 2021 rainfall data, sourced from the India Meteorological Department, shows continuous precipitation from March to December, peaking in August with 329.59 mm of rainfall. Heavy rainfall leads to increased soil saturation, which raises pore water pressure and reduces the shear strength of soil and rock, making slopes more vulnerable to failure. Additionally, slope modification and exposure to weathering accelerate erosion, especially during intense rain events. Runoff further removes topsoil and destabilizes slopes. Daily rainfall data reveals short-duration, high-intensity rainfalls that can directly trigger landslides. The pattern of rainfall aligns closely with the timing and frequency of past landslides in the region, confirming rainfall as a key contributing factor. This highlights the need for effective slope management, rainfall monitoring, and early warning systems to reduce landslide risks in Mizoram.

CHAPTER 5

CONCLUSIONS AND RECOMMENDATIONS

5.1. CONCLUSIONS

Based on the extensive field observations and the geotechnical analyses of soil and characterization of rock mass in the research area, the disaster vulnerability and the factors contributing to the instability of the slope can be concluded.

The research area mainly comprises loose soils and highly jointed rock mass, i.e, shales, siltstones, and intercalation of sandstones of Oligocene age. The majority of the rock mass is overlain by soil with thick vegetation. Due to slope modification for construction of highway, the soil and rock mass get exposed to daylight. The variation of the atmosphere enhanced the weathering process that weakened the strength of the soil and rock mass. Accumulation of surface water, excess runoff and infiltration of water into the ground due to heavy precipitation decreases the cohesiveness of the soil, and water penetrating through fractures and joints increases the pore pressure, which acts as an important triggering factor to slope failure. The newly constructed State Highway from Champhai town to Zokhawthar village was inaccessible after three months of its completion

For the disaster vulnerability and risk assessment, kinematic analysis is employed to analyze the type and potential failure of the rock slope. Road cut sections of different slope heights, slope angles, and aspects constitute the most suitable conditions for understanding the structural and geological properties, lithological variations, and discontinuity patterns. The potential failures analyzed were wedge failure for four selected slopes and direct toppling for three selected slopes. The discontinuities of the jointed rockmass intersected at two or more planes, making the rockmass vulnerable to detachment. The direct toppling failure shows that the discontinuity plane possesses a steep angle, leading to the outward and

downward movement of the rock mass. The potential wedge failure indicates that the jointed rock slopes have discontinuities where two planes intersect, forming a wedge-shaped rock mass. Therefore, the probability of rockfall is very high, which can cause casualties and even loss of life. The numerous joints and weak rock strength increase the probability of slope failure.

Based on the Atterberg limit, proctor compaction, and direct shear test, the geotechnical properties of soils concluded as slightly plastic to medium plastic. The natural moisture content of the soil varies for different soil samples between 17.98 % and 33.56 %. The consistency index classified the soil as medium stiff to stiff, indicating the soil bears medium resistance to deformation. The cohesion (c) ranges between 0.145 kg/cm² and 0.27 kg/cm², and the friction angles range between 7.26° and 40.29°. With each successive cycle of the slake durability test, the number of fragments increases with the decrease in the size of the rock fragments. It suggested that upon subjecting the rock to the atmosphere of continuous wetting and drying, the durability of the rock decreases. The changing of the atmosphere enhances the physical and chemical weathering of the rock, leading to disintegration. The geo-mechanical classification of rock based on the Rock Mass Rating assigned as fair to poor rock description. Four sites fall under class III, whereas three sites are within class IV. The low RMR value indicates poor rock quality and increased geotechnical engineering challenges. The GSI values shows that the study sites are blocky/ disturbed folded or faulted with angular blocks formed by many intersecting discontinuity sets. The blocks are disintegrated with heavily broken rock mass with a mixture of angular and rounded rock pieces. The SMR falls from partially stable to completely unstable, which indicates the rocks that constitute the slope are weak and are not suitable for development. Without implementing mitigation measures, slope modifications will likely result in slope failure.

The slope stability analysis using the Limit Equilibrium Method based on the Mohr-Coulomb criterion shows that the factor of safety obtained by different approaches for each site is less than 1. Since the factor of safety is less than 1, it implies the resisting forces exerted by the soil and rock to stabilize the slope are less than the forces exerted by pore water pressure and gravity that tend to result in slope

failure. The stress is below the allowable limit and is highly susceptible to slope failure. Consequently, the slope is vulnerable to failure under saturated conditions.

From the Rockfall Hazard Rating System, the steep and high angle slopes have greater possibility of rocks falling along the highway. The natural processes like sunlight, rainfall, weathering and erosion have contributed on the disintegration of rockmass on the slope, where undercutting is highly enhanced. The limited catchment area of falling rock increases the risk of the vehicles and pedestrians along the highway. With total score higher than 500, locations 3 and 5 falls under high urgency. The higher the cumulative score, the greater the risk of rock falls.

The bouncing height of the falling rocks after hitting the ground is controlled by their velocity, slope angle, roughness, shape and size, and the compaction of the detached rocks. Since the total kinetic energy of the rock falling down the slope depends on its mass, with the increase in the mass, the kinetic energy of the rock increases. Under the influence of gravity, the velocity of the vertical component increases with the increase of kinetic energy during the fall.

The research concludes that numerous landslides triggered by rainfall along the State highway from Champhai town to Zokhawthar Village are due to slope modification for highway improvements, expansion, widening, provision of cross-drainage facilities, curves, and gradient improvements. The high-angle slopes comprise poor rock mass covered by a loose thick soil, with a high probability of rockfall, and require mitigation measures to stabilize the area. Although numerous earthquakes occurred in the region, no earthquake-induced landslide is observed.

5.2. MITIGATION SUGGESTIONS

To reduce the hazard risk based on the investigation and results obtained, various mitigation measures are suggested to minimize the vulnerability as well as to improve the slope stability. The generalized slope stability measures are; modification of the high-angle slope with reinforced terrace sloping (benching $\leq 3\text{m}$) from the crown can reduce the driving force of the slope. To channelize runoff, each

bench should have catch water drainage. If the angle of slope is modified to gentle, it will reduce the translational energy as well as kinetic energy of the soil and rock blocks. Rock anchoring and wire meshing also help prevent the rocks from free-falling. It reduces the small rock fragments on reaching the road. A high-quality steel wire must be installed to cover the rock slope. Depending upon the curvature of the road, widening the ditch to arrest the free-falling blocks of rock from the slope can prevent more rocks from bouncing to the road and off towards the valley. Implementing geotextile to improve soil characteristics and planting shrubs at the benching level to minimize erosion. Construction of gabion walls at the toe along the road may reduce the overflow of soil on the road.

From the field observations and laboratory analyses of the selected study sites, remedial measures for each site are given in table 5.1

Table 5.1 Remedial Measures based on field observations and laboratory analyses

Study Site	Location	Types	Remedial Measures
LS1	23°23'34.22"N; 93°22'42.90"E	Debris Slide	Managing the drainage of both rainwater and household waste water, benching on slope with retaining wall.
LS2	23°23'43.00"N; 93°23'18.00"E	Debris Slide	Appropriate benching of slope with retaining barriers around the sliding area and channeling of the upslope surface runoff.
LS3	23°22'59.01"N; 93°23'25.37"E	Debris Slide	Repairing lined drainage along the road, benching the slope using contour drains along the slope, shotcreting the rock wall, channelizing the upslope running water.
LS4	23°22'51.72"N; 93°23'23.96"E	Debris Slide	Removal of slided debris, benching of the entire slope with concrete retaining walls with weep-holes along each bench, contour drains along the benches. Construction of lined hillside

			drains and road side drains, shotcrete and wire meshing the crown.
LS5	23°22'42.34"N; 93°23'20.02"E	Debris Slide	Slope easing, toe support, chanellization of water and hardening of overburden with vegetation.
LS6	23°22'35.15"N; 93°23'11.49"E	Debris Slide	Proper benching supported by retaining wall, channelizing the upslope running water
Rockfall Investigated Sites			
Study Site	Location	Remedial Measures	
R1	23°23'46.00"N, 93°21'47.00"E	Since the area has several joint sets that have led to unstable rock masses, trimming the highly jointed rock masses vulnerable to falling can be suggested as remedial measures.	
R2	23°23'47.67"N, 93°22'28.33"E	Trimming the highly jointed rocks and wire meshing help prevent the rocks from free-falling. It reduces the small rock fragments on reaching the road. A high-quality steel wire must be installed to cover the rock slope.	
R3	23°23'9.81"N, 93°23'43.01"E	A shotcrete with wire meshing to fill in the gaps in the cut slope can reduce the rolling and falling of rock. Maintaining the roadside drain can help to further toe erosion.	
R4	23°23'2.65"N, 93°23'37.53"E	Removal of overhanging rock blocks and wire meshing to arrest the fallen rock mass are suggested as remedial measures.	
R5	23°22'59.85"N; 93°23'31.10"E	Several overhanging rocks are seen in this area. Excess runoff and infiltration during monsoon, vibration caused by light and heavy machinery, and earthquakes can	

		quickly cause rocks to fall. As a result, it is necessary to scale down the overhanging rock by hand or machine. This will prevent more disasters.
R6	23°22'53.98"N; 93°23'25.58"E	Since the slope is composed of highly jointed rock mass, a tensioned rock anchor can be used to secure sliding blocks. Shotcreting the fractured zone can reduce erosion and weathering. Concrete buttresses can also be used to support rocks above the cavity.

5.3. LIMITATION

Slope stability is heavily influenced by the underlying geological framework, particularly in regions characterized by structural complexity. Features such as folds, faults, joints, fractures, and bedding planes create inherent planes of weakness within the rock mass. These discontinuities disrupt the rock's continuity and significantly reduce its overall strength and cohesion. When these structural features are oriented unfavorably with respect to the slope face, they become potential slip surfaces, increasing the likelihood of slope failure, especially under triggering conditions like intense rainfall, prolonged soil saturation, or seismic activity.

In the case of Mizoram, the geological setting is further complicated by the intercalation of diverse rock types—including sandstone, shale, siltstone, and claystone—often occurring within short lateral and vertical distances. This lithological heterogeneity leads to spatial variations in physical and mechanical properties such as shear strength, permeability, and weathering susceptibility. For instance, sandstone may remain relatively intact and resistant, while interbedded shale or clay-rich layers can become highly plastic and unstable when wet, resulting in differential movement and localized failure zones.

These geological complexities make it difficult to apply uniform slope stability models or hazard classifications across the region. Generalized empirical approaches that do not account for such site-specific variability often fail to capture

the true risk posed by localized structural and lithological conditions. As a result, slope stability assessments in Mizoram require a detailed, location-specific approach, incorporating field mapping of geological structures, laboratory testing of rock and soil samples, and advanced modeling techniques that reflect the unique geotechnical behavior of mixed lithologies.

The presence of complex structural features and lithological diversity in Mizoram significantly increases the challenges in evaluating slope stability. Effective assessment and mitigation must therefore be grounded in thorough geotechnical investigations, localized data, and a multidisciplinary understanding of how geological conditions interact with environmental triggers.

The Rockfall Hazard Rating System (RHRS) is a widely used method designed to evaluate the potential for rockfall hazards along transportation corridors and slopes. It operates through standardized tables and scoring systems based on general geological, topographic, and climatic assumptions. One such example is the differentiation of hazard ratings by slope aspect: west-facing slopes are typically assigned a relatively low hazard score of 3 points, while east-facing slopes are given a much higher score of 81 points, based on assumptions about sun exposure, freeze-thaw cycles, and moisture retention common to certain geographic contexts.

However, applying such generalized hazard ratings to a geologically complex and climatically unique region like Mizoram can lead to misrepresentations of actual slope stability conditions. Mizoram's terrain is characterized by frequent lithological changes, high rainfall, dense vegetation, and varied weathering profiles within short spatial intervals. As a result, the same slope aspect (e.g., east-facing) may behave very differently across multiple sites due to variations in rock type (e.g., sandstone vs. shale), intensity of weathering, drainage conditions, moisture infiltration, and vegetative cover.

Moreover, local microclimatic variations—driven by elevation, valley orientation, and vegetation density—can significantly alter evaporation rates, soil moisture retention, and runoff patterns, all of which affect slope behavior. In such a setting, assigning hazard ratings based solely on slope orientation without

considering site-specific geological and environmental factors may underestimate or overestimate the actual risk.

Therefore, while RHRS provides a useful initial framework for hazard assessment, there is a clear need to adapt or recalibrate the system for application in Mizoram. This involves incorporating localized geological data, detailed field observations, and terrain-specific modifications to the rating criteria. A more nuanced, context-sensitive approach would ensure more accurate hazard evaluations, leading to better-informed mitigation strategies and safer slope management practices in the region.

Given the unique geological, geomorphological, and environmental context of Mizoram, it is essential to adapt or recalibrate the Rockfall Hazard Rating System (RHRS) for more accurate and meaningful application in the region. The standard RHRS framework, while useful as a general tool, does not fully capture the complex interactions between slope orientation, lithology, weathering processes, rainfall intensity, and vegetation cover that define Mizoram's terrain.

By incorporating localized geological data, such as rock mass properties, structural orientations, and site-specific weathering conditions, the RHRS can be tailored to reflect the actual slope behavior and rockfall potential more precisely. Additionally, site-specific assessments, including detailed field surveys and hazard mapping, are critical to identify high-risk zones that may be overlooked by generalized rating systems.

This localized approach would enhance the accuracy of hazard evaluations and enable more effective, targeted risk mitigation strategies, thereby improving slope management, infrastructure safety, and disaster preparedness in Mizoram.

APPENDICES

- Research Photographs (Figure 1 to 20)



Fig. 1 Drone image of landslide



Fig. 2 Landslide debris blocking the road



Fig. 3 Landslide debris completely blocked the road



Fig. 4 Landslide debris blocking the road



Fig. 5 Panoramic view of collapsed slope



Fig. 6 Collapsed Road and slope



Fig. 7 Retaining wall collapsed due to slope failure



Fig. 8 Road, Curvert and Retaining collapsed



Fig. 9 Field investigation



Fig. 10 DGPS surveying



Fig. 11 Fragments of rocks falling on the road



Fig. 12 Outcrop along the road (*Scale Brunton Compass*)



Fig. 13 Field investigation



Fig. 14 Field investigation



Fig. 15 Data collection at the crown of landslide (*D.G.P.S. Rover*)



Fig. 16 Block of rock that detached from the slope bounced across the road



Fig. 17 Laboratory Investigation



Fig. 18 Ripple mark



Fig. 19 Trace fossil



Fig. 20 DGPS surveying at rockfall prone area

REFERENCES

- Abbas, Syed Muntazir & Konietzky, Heinz. (2015). Rock Mass Classification Systems.
- Arcaya, Mariana & Raker, Ethan & Waters, Mary. (2020). The Social Consequences of Disasters: Individual and Community Change. Annual Review of Sociology. 46. <https://doi.org/10.1146/annurev-soc-121919-054827>.
- Acharrya, S.K. (1997) Stratigraphy and tectonic history reconstruction of the Indo-Burma-Andaman mobile Belt. Indian Jour. Geol., v.69, pp. 211 - 234.
- Acharyya, Subhrangsu. (2008). Tectonic evolution of Indo-Burma Range with special reference to Naga-Manipur Hills. Geol. Soc. India Memoir. 75.
- Alam, Kazi & Abdullatif, Osman & El Husseiny, Ammar & Babalola, Lameed. (2021). Depositional and Diagenetic Controls on Reservoir Heterogeneity and Quality of the Bhuvan Formation, Neogene Surma Group, Srikail Gas Field, Bengal Basin, Bangladesh. Journal of Asian Earth Sciences. 223. 104985. <https://doi.org/10.1016/j.jseaes.2021.104985>.
- Alcántara-Ayala, Irasema; Sassa, Kyoji. 2023. Landslide risk management: from hazard to disaster risk reduction. Landslides 20, 2031–2037 (2023). <https://doi.org/10.1007/s10346-023-02140-5>
- Anbalagan, R., Kumar, R., Lakshmanan, K., Parida, S., & Neethu, S. (2015). Landslide hazard zonation mapping using frequency ratio and fuzzy logic approach, a case study of Lachung Valley, Sikkim. Geoenvironmental Disasters, 2(1). <https://doi.org/10.1186/s40677-014-0009-y>
- Ansari, M & Ahmad, M. & Singh, Rajesh & Singh, T.N.. (2016). Rockfall Slope Angle and its Effect on the Impact and Runout Distance of Falling Block: A Numerical.
- Ansari, Tariq & Kainthola, Ashutosh & Singh, K H & Singh, T.N. & Sazid, Mohammed. (2021). Geotechnical and micro-structural characteristics of

phyllite derived soil; implications for slope stability, Lesser Himalaya, Uttarakhand, India. CATENA. 196. 104906. <https://doi.org/10.1016/j.catena.2020.104906>.

Ansari, M & Ahmad, M. & Singh, Rajesh & Singh, T.N.. (2013). Rockfall Hazard Rating System for Indian Rockmass. International Journal of Earth Sciences and Engineering. 06. 18-27.

Antonini, G., & Romana, M. (1992). "Slope mass rating (SMR) for the design of rock slopes." Journal of the International Society for Rock Mechanics, 29(1), 81-88.

ASTM International. (2010). ASTM D4318-10: Standard Test Methods for Liquid Limit, Plastic Limit, and Plasticity Index of Soils. ASTM International.

ASTM. 2017. Standard practice for classification of soils for engineering 4 purposes (unified soil classification system). ASTM D2487. West Conshohocken, PA: ASTM.

ASTM International. (2020). ASTM D4644-20: Standard Test Method for the Determination of the Slake Durability of Rock Aggregate. ASTM International

Asthana, A.K.L. & Sah, M.P.. (2007). Landslides and cloudbursts in the Mandakini basin of Garhwal Himalaya. Himalayan Geology. 28. 59-67.

Atterberg, A. (1911). "Die physikalischen Eigenschaften der Tone." Jahrbuch der Preußischen Geologischen Landesanstalt, 31, 1-50.

Aven, Terje. (2015). Risk assessment and risk management: Review of recent advances on their foundation. European Journal of Operational Research. 253. <https://doi.org/10.1016/j.ejor.2015.12.023>.

Aydan, Ö., Ulusay, R. & Tokashiki, N. A New Rock Mass Quality Rating System: Rock Mass Quality Rating (RMQR) and Its Application to the Estimation of

- Geomechanical Characteristics of Rock Masses. *Rock Mech Rock Eng* 47, 1255–1276 (2014). <https://doi.org/10.1007/s00603-013-0462-z>
- Azeze, Azemeraw. (2020). Assessments of Geotechnical Condition of Landslide Sites and Slope Stability Analysis Using Limit Equilibrium Method in Goncha Siso Eneses Area, Northwestern Ethiopia. <https://doi.org/10.21203/rs.3.rs-97972/v1>.
- Azeze, Azemeraw. (2020). Assessments of Geotechnical Condition of Landslide Sites and Slope Stability Analysis Using Limit Equilibrium Method around Gundwin Town Area, Northwestern Ethiopia. <https://doi.org/10.21203/rs.3.rs-20574/v1>
- Barman, Jonmenjoy & Biswas, Brototi & Das, Jayanta. (2022). Mizoram, the Capital of Landslide: A Review of Articles Published on Landslides in Mizoram, India. https://doi.org/10.1007/978-3-031-15377-8_6.
- Baruah, M., & Pandey, N. (2019). Lithofacies, architectural elements and tectonic provenance of Mio-Pliocene Dupitila Formation in the Cachar Thrust Fold Belt, Northeast India. *SN Applied Sciences*, 1(3). <https://doi.org/10.1007/s42452-019-0263-4>
- Basu, A., & Dutta, P. (2017). "Geological and sedimentological characteristics of the Mizoram Fold Belt: Implications for the eastern Surma Basin." *Journal of Earth System Science*, 126(3), 46-59
- Basu, A., & Roy, S. (2016). "Sedimentary response to tectonic and eustatic controls in the Bengal Basin: Implications for the Barail Group." *Sedimentary Geology*, 342, 56-72
- Basyah, Nazaruddin & Syukri, Muhammad & Fahmi, Irham & Ali, Ismail & Rusli, Zulfadhli & Putri, Elva. (2023). Disaster Prevention and Management: A Critical Review of The Literature. *Jurnal Penelitian Pendidikan IPA*. 9. 1045-1051. <https://doi.org/10.29303/jppipa.v9i11.4486>.

- Bawri, Gautam Raj & Vanthangliana, V. & Koduri, Srinivasa & Mahanta, S. & Lalduhawma, K. & Bharali, Bubul. (2023). Petrographic characterization and diagenetic impact on Bhuban Sandstone of Surma Group, Aizawl, Mizoram: implications for provenance, tectonic setting, and reservoir quality. *Journal of Sedimentary Environments*. 9. 1-18. <https://doi.org/10.1007/s43217-023-00159-1>.
- Beyabanaki, S. Amir Reza. (2021). LEM Stability Analysis of Landslides Induced by Earthquakes: Impact of a Weak Layer. *American Journal of Engineering Research*. 10. 257-268.
- Bureau of Indian Standards. (1985). IS: 2720 (Part 5) - 1985: Methods of Test for Soils - Part 5: Determination of Liquid and Plastic Limits. New Delhi: BIS.
- Bhambri, Rakesh & Mehta, Manish & Singh, Shweta & Perumal, R & Gupta, Anil & Srivastava, Pradeep. (2017). Landslide inventory and damage assesment in the Bhagirathi valley, Uttarakhand, during June 2013 flood. *Himalayan Geology*. 38. 193-205.
- Bharali, B & Borgohain, Pradip. (2013). Few Characteristics of Tipam Sandstone Formation Within Oilfield Areas of Upper Assam – A Study Based on Wireline log Data. 2013. 36-45.
- Bharali, Bubul & Borgohain, Pradip & Bezbaruah, Devojit & Vanthangliana, V & Phukan, Parakh & Rakshit, Raghupratim. (2017). A geological study on Upper Bhuban Formation in parts of Surma Basin, Aizawl, Mizoram. *Science Vision*. 17. <https://doi.org/10.33493/scivis.17.03.02>.
- Bharali, Bubul & Hussain, M. Faruque & Borgohain, Pradip & Bezbaruah, Devojit & Vanthangliana, V. & Rakshit, Raghupratim & Phukan, Parakh. (2021). Reconstruction of Middle Miocene Surma Basin as Two Arcs Derived Sedimentary Model: Evidence from Provenance, Source Rock Weathering and Paleo-Environmental Conditions. *Geochemistry International*. 59. 264–289. <https://doi.org/10.1134/S0016702921030022>.

- Bhattacharya, A., & Gupta, S. (2005). "Stratigraphy and sedimentology of the Upper Eocene to Oligocene sequences of the Shillong Plateau, Northeast India." *Journal of Geological Society of India*, 65(2), 237-246
- Bhattacharya, A., & Ghosh, A. (2013). "Sedimentology of the Tipam Sandstone Formation in Northeast India: Textural and structural characteristics." *Journal of Geological Society of India*, 82(5), 877-885
- Bhaumik, S., & Ghosh, A. (2012). "Tectonic evolution of the Indo-Burman Orogenic belt: Insights from Mizoram." *Journal of Asian Earth Sciences*, 56, 81-93
- Bhaumik, S., & Mukhopadhyay, S. (2013). "Tectonic deformation in the Indo-Burman Orogenic belt: Insights from structural geology." *Tectonophysics*, 588, 25-38
- Bijoy, Sourov & Gazi, Md & Kabir, Sm. (2019). Geological and Geophysical Observations to Determine the Gas Seepage Source of Titas Gas Field Region, Bangladesh. 45. 93-109. <https://doi.org/10.3329/jasbs.v45i1.46572>.
- Bieniawski, Z.T., 1976, Rock Mass Classification in Rock Engineering, in Bieniawski, Z.T., ed., Symposium on exploration for rock engineering, Balkema: Rotterdam, p. 97-106.
- Bieniawski, Z. T. (1989). "Engineering Rock Mass Classifications." John Wiley & Sons.
- Bin Masood, Abdullah & Yuzuak, Ali. (2021). Mass Movements And it's Classifications. <https://doi.org/10.13140/RG.2.2.21266.99524>.
- Bishop, A. W. (1955). "The use of the slip circle in the stability analysis of slopes." *Geotechnique*, 5(1), 7-17.
- Bobrowsky, Peter. (2013). *Encyclopedia of Natural Hazards*.
- Borgohain, P., Hussain, M. F., Bezbaruah, D., Vanthangliana, V., Phukan, P. P., Gogoi, M. P., & Bharali, B. (2020). Petrography and whole-rock geochemistry of Oligocene Barail Sandstones of Surma basin: Implications

for tectono-provenance and paleoclimatic condition. Journal of Earth System Science <https://doi.org/10.1007/s12040-020-01431-y>

Borgohain, Kashyap & Sarmah, Ranjan Kr. (2022). Petrography and whole-rock geochemistry of the Miocene Bhuban Formation of Tripura Fold Belt, North District, Tripura, India: implications for provenance, tectonic setting and weathering intensity. Journal of Sedimentary Environments. 7. <https://doi.org/10.1007/s43217-022-00092-9>.

Brunner, M., & Varnes, D. J. (2006). "Rockfall hazard assessment and management." In Landslide Risk Management (pp. 85-99). Taylor & Francis

Cai, M.. (2011). Rock Mass Characterization and Rock Property Variability Considerations for Tunnel and Cavern Design. Rock Mechanics and Rock Engineering. 44. 379-399. <https://doi.org/10.1007/s00603-011-0138-5>

Chaudhary, Shipra & Gupta, Vikram & Sundriyal, Yaspal. (2010). Surface and sub-surface characterization of Byung landslide in Mandakini valley, Garhwal Himalaya. Himalayan Geology. 31. 125-132.

Chowdhury, R. (2009). "Slope stability analysis using limit equilibrium methods." Geotechnical Engineering, 162(2), 111-118.

Cheng, Yuanfang; Yan, Chuanliang; Han, Zhongying (2023). Strength and Deformation Characteristics of Rocks. In: Foundations of Rock Mechanics in Oil and Gas Engineering. Springer, Singapore. https://doi.org/10.1007/978-981-99-1417-3_4

Collins, Andrew. (2018). Advancing the Disaster and Development Paradigm. International Journal of Disaster Risk Science. 9.

Cardona, Omar & Aalst, Maarten & Birkmann, Joern & Fordham, Maureen & McGregor, Glenn & Perez, R & Pulwarty, R & Schipper, Lisa & Bach, Sinh. (2012). Determinants of risk: exposure and vulnerability.

- Chen, Y., Lin, H., Cao, R., & Zhang, C. (2021). Slope Stability Analysis Considering Different Contributions of Shear Strength Parameters. *International Journal of Geomechanics*, 21(3), 04020265. [https://doi.org/10.1061/\(asce\)gm.1943-5622.0001937](https://doi.org/10.1061/(asce)gm.1943-5622.0001937)
- Cruden, David. (2013). Landslide Types. In: Bobrowsky, P.T. (eds) *Encyclopedia of Natural Hazards*. Encyclopedia of Earth Sciences Series. Springer, Dordrecht. https://doi.org/10.1007/978-1-4020-4399-4_344
- Dahiya, Neeraj; Pandit, Koushik; Sarkar, Shananu; Pain, Anindya (2024). Various Aspects of Rockfall Hazards along the Mountain Roads in India: a Systematic Review. *Indian Geotech J* <https://doi.org/10.1007/s40098-024-01015-3>
- Dar, Roouf Un Nabi & Alam, Mehtab. (2020). Understanding Disaster Risk, its components and reduction.
- Dasgupta, Sujit. (1984). TECTONIC TRENDS IN SURMA BASIN AND POSSIBLE GENESIS OF THE FOLDED BELT. 58-61.
- Das, S., & Ghosh, A. (2015). "Stratigraphic analysis of the Barail Group in Northeast India: Sedimentological and lithological characteristics." *Journal of Geological Society of India*, 85(6), 1235-1245
- Devi, Salam. (2021). Geochemistry, Depositional and Tectonic setting of the Barail Group of the Indo-Myanmar Ranges. *Journal of The Indian Association of Sedimentologists*. 38. 13-22. <https://doi.org/10.51710/jias.v38i1.103>
- Devi, Salam & Mondal, Mohammad. (2008). Provenance and tectonic setting of Barail (Oligocene) and Surma (Miocene) Group of Surma-Barak basin, Manipur, India: Petrographic constraints. *Journal of the Geological Society of India*. 71. 459-467.
- Dinpuia, Lal. (2019). Cut Slope Stability Analysis of Rangvamuall Landslide Along Aizawl Airport Road, Northeast India: Proceedings of the 2nd GeoMEast International Congress and Exhibition on Sustainable Civil Infrastructures, Egypt 2018 – The Official International Congress of the Soil-Structure

- Interaction Group in Egypt (SSIGE). https://doi.org/10.1007/978-3-030-01941-9_16
- Duncan, J. M. (1996). "State of the Art: Limit Equilibrium and Finite Element Analysis of Slopes." *Journal of Geotechnical Engineering*, 122(7), 577-596.
- Duncan, J. M., & Wright, S. G. (2005). *Soil Strength and Slope Stability*. Wiley.
- Dutta, P., & Basu, A. (2015). "Structural and tectonic evolution of the Indo-Burman region: Evidence from the Mio-Pliocene." *Journal of Geological Society of India*, 86(4), 431-440
- Epada, Pouyon & Sylvestre, Ganno & Tabod, Tabod. (2012). Geophysical and Geotechnical Investigations of a Landslide in Kekem Area, Western Cameroon. *International Journal of Geosciences*. 3. 780-789. <https://doi.org/10.4236/ijg.2012.34079>
- Fookes, P. G. (1997). "The role of weathering in slope stability." *Proceedings of the International Symposium on Landslides*, 1, 33-48.
- Fredlund, D. G., & Rahardjo, H. (1993). *Soil Mechanics for Unsaturated Soils*. Wiley.
- Gajamer, Vineet & Kumar, Abhishek. (2023). A Comprehensive Review on Rainfall-Induced Slope Failures: Mechanism, Models, and Influencing Factors. 10.1007/978-981-19-7245-4_16. Jespen, Torben. (2016). Risk Assessment and Risk Reduction Methodologies. https://doi.org/10.1007/978-3-319-31361-0_5
- Ganesh. R, Gowtham. B, Manivel. T, Senthilkumar S, Sundrarajan, M. (2017). ISSN 2347-9523 (Print) Application of Resistivity Survey Method in Landslide Investigations along Mettupalayam to Coonoor Highway, Nilgiris District, Tamilnadu, India. *Scholars Journal of Engineering and Technology*. 5. 661-667. <https://doi.org/10.21276/sjet.2017.5.11.9>

- Ganju J L 1975 Geology of Mizoram; Geol. Mineralogy Metall. Soc. India, pp. 17–26.
- Gao, Wei. (2017). Investigating the critical slip surface of soil slope based on an improved black hole algorithm. *Soils and Foundations*. 57. <https://doi.org/10.1016/j.sandf.2017.08.026>
- Gazi, M. Y., Apu, S. I., Sharmili, N., & Rahman, M. Z. (2021). Origin and characterization of clay deposits in the Dupi Tila Formation of the Bengal Basin, Bangladesh. *Solid Earth Sciences*, 6(3), 313–327. <https://doi.org/10.1016/j.sesci.2021.07.001>
- Geertsema, Marten & Highland, Lynn & Vaugeouis, Laura. (2009). Environmental Impact of Landslides. https://doi.org/10.1007/978-3-540-69970-5_31
- Ghosh, A., & Saha, D. (2014). "Sedimentology and stratigraphy of the Miocene sedimentary sequences of Mizoram, Northeast India." *Journal of Earth System Science*, 123(5), 1069-1080.
- Ghosh, A., & Sarma, A. (2016). "Sedimentary characteristics and lithification processes in the Mizoram Fold Belt." *Journal of Geological Society of India*, 87(2), 245-258
- González, A., & Dussan, M. (2011). "Factors affecting the stability of slopes." In *Landslide Risk Management* (pp. 15-38). Taylor & Francis.
- Gougazeh, Mousa & Al-Shabatat, Ali. (2013). Geological and geotechnical properties of soil materials at Tannur dam, Wadi Al Hasa, South Jordan. *Journal of Taibah University for Science*. 7. <https://doi.org/10.1016/j.jtusci.2013.07.001>
- Guillard-Gonçalves, Clémence & Zêzere, José & Pereira, Susana & Garcia, Ricardo. (2016). Assessment of physical vulnerability of buildings and analysis of landslide risk at the municipal scale: Application to the Loures municipality, Portugal. *Natural Hazards and Earth System Sciences*. 16. 311-331. <https://doi.org/10.5194/nhess-16-311-2016>

- Gutiérrez, F., Gutiérrez, M. (2016). Slope Movements. In: Landforms of the Earth. Springer, Cham. https://doi.org/10.1007/978-3-319-26947-4_8
- Hauhnar, Malsawmtluangkima & Lalnunmawia, Jimmy & Dawngliana, Orizen. (2021). Geochemistry of Barail sandstone in Champhai, Mizoram: Implications on provenance and weathering history. Journal of Earth System Science. 130. 27. <https://doi.org/10.1007/s12040-020-01515-9>
- Holtz, R. D., & Kovacs, W. D. (1981). An Introduction to Geotechnical Engineering. Prentice-Hall.
- Hungr, O., & Evans, S. G. (1988). "Rockfalls." In Landslides: Causes, Consequences and Assessment (pp. 56-68). G. A. M. Scott & Associates.
- Hussain, M.Faruque; Bharali, Bubul (2019). Whole-rock geochemistry of Tertiary sediments of Mizoram Foreland Basin, NE India: implications for source composition, tectonic setting and sedimentary processes. Acta Geochim 38, 897–914. <https://doi.org/10.1007/s11631-019-00315-3>
- He, Manchao & Nie, W. & Zhao, Zhiye & Guo, Weihua. (2012). Experimental Investigation of Bedding Plane Orientation on the Rockburst Behavior of Sandstone. Rock Mechanics and Rock Engineering. 45. <https://doi.org/10.1007/s00603-011-0213-y>
- Hiller, K., & Elchi, M. (1984). Structural Development And Hydrocarbon Entrapment In The Surma Basin/Bangladesh (Northwest Indo Burman Fold Belt). Southeast Asia Show. <https://doi.org/10.2118/12398-ms>
- Hoeg, Kaare (2013). Slope Stability. In: Bobrowsky, P.T. (eds) Encyclopedia of Natural Hazards. Encyclopedia of Earth Sciences Series. Springer, Dordrecht. https://doi.org/10.1007/978-1-4020-4399-4_322
- Hoek, E., & Brown, E. T. (1980). "Empirical estimation of rock mass properties." Journal of the Soil Mechanics and Foundations Division, ASCE, 106(SM6), 1013-1035.

- Hoek, E., & Bray, J. W. (1981). Rock Slope Engineering. 3rd edition. Institute of Mining and Metallurgy.
- Hoek, E., & Brown, E. T. (1997). "Practical Estimates of Rock Mass Strength." International Journal of Rock Mechanics and Mining Sciences, 34(8), 1165-1186.
- Hoek, E., & Marinos, P. (2000). "The Geological Strength Index (GSI): A geotechnical classification for rock masses." In Proceedings of the 5th International Symposium on Landslides (pp. 1-12).
- Hong, Chang & Ryu, Hee-Hwan & Oh, Tae-Min & Cho, Gye-Chun. (2020). Probabilistic Rock Mass Rating Estimation Using Electrical Resistivity. KSCE Journal of Civil Engineering. 24. <https://doi.org/10.1007/s12205-020-1315-4>
- Hossain, H.M. & Roser, Barry & Kimura, Jun-Ichi. (2010). Petrography and whole-rock geochemistry of the Tertiary Sylhet succession, northeastern Bengal Basin, Bangladesh: Provenance and source area weathering. Sedimentary Geology. 228. 171-183. <https://doi.org/10.1016/j.sedgeo.2010.04.009>
- Hungr, Oldrich; Leroueil, Serge; Picarelli, Luciano. (2014). The Varnes classification of landslide types, an update. Landslides, 11(2), 167–194. <https://doi.org/10.1007/s10346-013-0436-y>
- Inan, Dedi & Beydoun, Ghassan & Othman, Siti. (2023). Risk Assessment and Sustainable Disaster Management. Sustainability. 15. 5254. <https://doi.org/10.3390/su15065254>
- Ip, Sabrina & Rahardjo, H. & Satyanaga, Alfrendo. (2020). Three-dimensional slope stability analysis incorporating unsaturated soil properties in Singapore. Georisk: Assessment and Management of Risk for Engineered Systems and Geohazards. 15. 1-15. <https://doi.org/10.1080/17499518.2020.1737880>
- Islam, M.S., Shijan, M.H.H., Saif, M.S. et al. Petrophysical and petrographic characteristics of Barail Sandstone of the Surma Basin, Bangladesh. J Petrol

Explor Prod Technol 11, 3149–3161 (2021). <https://doi.org/10.1007/s13202-021-01196-0>

Islam, Md. Shofiqul & Meshesha, Daniel & Shinjo, Ryuichi. (2014). Mantle source characterization of Sylhet Traps, northeastern India: A petrological and geochemical study. *Journal of Earth System Science*. 123. 1839-1855.

Jaeger, J. C., & Cook, N. G. W. (2009). *Fundamentals of Rock Mechanics*. Wiley-Blackwell.

Jahan, Shakura & Uddin, Ashraf & Pashin, Jack & Savrda, Charles. (2017). Petroleum source-rock evaluation of upper Eocene Kopili Shale, Bengal Basin, Bangladesh. *International Journal of Coal Geology*. 172. <https://doi.org/10.1016/j.coal.2017.02.002>

Johnson S Y and Alam A M N 1991 Sedimentation and tectonics of the Sylhet trough, Bangladesh; *Geol. Soc. Am. Bull.* 103 1513–1527.

Karunakaran, C. and Ranga Rao, A. (1979). Status of exploration for hydrocarbons in the Himalayan region contributions to stratigraphy and structure. In: *Himalayan Geology Seminar- 1976*, Geol. Surv. India, Misc. Pub., v.41, pp. 1-66.

Kainthola, Ashutosh & Singh, Prakash & Singh, T.N. (2014). Stability investigation of road cut slope in basaltic rockmass, Mahabaleshwar, India. *Geoscience Frontiers*. 6. <https://doi.org/10.1016/j.gsf.2014.03.002>

Kaiser, Md Shahidulla. (2021). *Land Degradation: Causes, Impacts and Interlinks with the SDGs*.

Kesari, G. K. 2011. *Geology and Mineral Resources of Manipur, Mizoram, Nagaland and Tripura*. Geological Survey of India Miscellaneous Publication No. 30 Pt 4, 1 (2): 103p.

Kesimal, Ayhan & Ercikdi, Bayram & Cihangir, Ferdi. (2008). Environmental impacts of blast-induced acceleration on slope instability at a limestone

quarry. *Environmental Geology*. 54. 381-389. <https://doi.org/10.1007/s00254-007-0825-4>

Khan, Saad & Shafi, Imran & Haider, Wasi & De la Torre Díez, Isabel & Flores, Miguel & Galán, Juan & Ashraf, Imran. (2023). A Systematic Review of Disaster Management Systems: Approaches, Challenges, and Future Directions. *Land*. 12. 1514. <https://doi.org/10.3390/land12081514>

Kumar, Akhilesh & Sharma, Ravi & Mehta, B.. (2020). Slope stability analysis and mitigation measures for selected landslide sites along NH-205 in Himachal Pradesh, India. *Journal of Earth System Science*. 129. <https://doi.org/10.1007/s12040-020-01396-y>

Kumar, S., & Dutta, P. (2017). "Rock mass characterization and its significance in engineering geology: A case study from Mizoram." *Engineering Geology*, 232, 1-12.

Kumar, S., & Mukherjee, P. (2014). "Tectonic controls on sedimentation in the Surma Basin: Implications for the Bhuban Formation." *Journal of Asian Earth Sciences*, 81, 74-87.

Kumar, Nikhil & Verma, Amit & Sardana, Sahil & Sarkar, Kripamoy & Singh, Trilok. (2017). Comparative analysis of limit equilibrium and numerical methods for prediction of a landslide. *Bulletin of Engineering Geology and the Environment*. 77. <https://doi.org/10.1007/s10064-017-1183-4>

Kumar, S., & Pandey, H. K. (2021). Slope Stability Analysis Based on Rock Mass Rating, Geological Strength Index and Kinematic Analysis in Vindhyan Rock Formation. *Journal of the Geological Society of India*, 97(2), 145–150. <https://doi.org/10.1007/s12594-021-1645-y>

Kumar, Sumit; Choudhary, Shiva Shankar; Burman, Avijit (2022). Recent advances in 3D slope stability analysis: a detailed review. *Model. Earth Syst. Environ.* 9, 1445–1462 (2023). <https://doi.org/10.1007/s40808-022-01597-y>

- Kumar, Surender & Srivastava, Jayahari. (2022). An Explained Typology of Natural Disasters in the State of Uttarakhand, India: Preparedness and Response Mechanism. 5(10). 2-9. <https://doi.org/10.4172/2573-458X.1000242>
- Kundu, Jagadish & Sarkar, Kripamoy & Singh, Prakash & Singh, T.N.. (2018). Deterministic and Probabilistic Stability Analysis of Soil Slope – A Case Study. Journal of the Geological Society of India. 91. 418-424. <https://doi.org/10.1007/s12594-018-0874-1>
- Laldinpuia, 2013. Geological investigation and mitigation suggestion of slumping localities in Saiha town, southern Mizoram, India. Sci Vis, 13:4.
- Laldinpuia, Kumar S. and Singh T.N., 2013. 11th May, 2013 Laipuitlang Rockslide, Aizawl, Mizoram, North-East India Landslide Science for a Safer Geo-environment, 2014 ISBN : 978-3-319-04995-3
- Laldinpuia, 2019. Geological investigation and monitoring of Ramhlun Sports Complex landslide, Aizawl, India. Science Vision, 19: 91-99. <https://doi.org/10.33493/scivis.19.03.03>
- Lalhlimpaia, H. & Zairemmawii, & Kumar, Shiva & Laldinpuia,. (2019). RMR and RHRS of Ngaizel Road cutting section, Aizawl, Mizoram. Senhri Journal of Multidisciplinary Studies. 4. 7-21. <https://doi.org/10.36110/sjms.2019.04.02.002>
- Lalnuntluanga, R., & Lalrinchhana, Z. (2020). "Climatic Analysis of Mizoram: A Study of Champhai District." Indian Journal of Geography and Environment, 25(2), 45-55.
- Lalrinawma, H., & Chhakchhuak, L. (2018). "Geographical and Socioeconomic Overview of Champhai District, Mizoram." Journal of North East India Studies, 8(1), 1-15
- Li, Y., & Mo, P. (2019). A unified landslide classification system for loess slopes: A critical review. Geomorphology. <https://doi.org/10.1016/j.geomorph.2019.04.020>

- Li, Charlie & Aure, Andreas & Knox, Greig. (2023). Experimental Study of the Effects of Borehole Size, Borehole Roughness, and Installation Pressure on the Pull Load Capacity of Inflatable Rockbolts. *Rock Mechanics and Rock Engineering*. 56. 1-17. <https://doi.org/10.1007/s00603-023-03492-z>
- Mathur L. P. & Evans P. (1964). Oil in India. 22nd session International Geological Congress New Delhi India 85
- Mirza Rezky, Danu & Irwan, Andesta & Saptono, Singgih. (2021). The effect of rock mass characterization on slope stability assessment. *AIP Conference Proceedings*. 2363. 030017. <https://doi.org/10.1063/5.0061098>.
- Munier, Nolberto. (2014). Risk Management for Engineering Projects: Procedures, Methods and Tools. <https://doi.org/10.1007/978-3-319-05251-9>
- Muralha, J., Lamas, L. (2023). Laboratory and Field Testing of Rock Masses for Civil Engineering Infrastructures. In: Chastre, C., Neves, J., Ribeiro, D., Neves, M.G., Faria, P. (eds) *Advances on Testing and Experimentation in Civil Engineering*. Springer Tracts in Civil Engineering . Springer, Cham. https://doi.org/10.1007/978-3-031-05875-2_3
- Nandy, D & Dasgupta, Sujit & Sarkar, Kalyan & Ganguly, Aniruddha. (1983). TECTONIC EVOLUTION OF TRIPURA-MIZORAM FOLD BELT, SURMA BASIN, NORTHEAST INDIA. *Quarterly Journal Geological Mining & Metallurgical Society of India*. 55. 186-194.
- Nichol, Susan & Hungr, Oldrich & Evans, Stephen. (2011). Large-scale brittle and ductile toppling of rock slopes. *Canadian Geotechnical Journal*. 39. 773-788. <https://doi.org/10.1139/t02-027>
- Oinam, Moni & Singh Rajkumar, Hemanta & Soibam, Ibotombi & Oinam, Nishila & Heni, Echeni. (2022). Sedimentary petrography and ichnology of the Barail Group along the Old Cachar road, Manipur, India. *Arabian Journal of Geosciences*. 15. 706. <https://doi.org/10.1007/s12517-022-09895-6>

- Olusegun, Aiyewunmi Temitope. 2021. Challenges and Potential Solutions to Pluvial Flood Risk in Urban Tropical African Communities: A Case study using Ijebu-Ode in South West Nigeria. The University of Liverpool, United Kingdom.
- Omidvar, Babak & Shirazi, Nazanin. (2023). Risk analysis and hazard probabilities. <https://doi.org/10.1016/B978-0-323-95163-0.00017-7>
- Osgoui, Reza & Ulusay, Resat & Unal, Erdal. (2010). An assistant tool for the Geological Strength Index to better characterize poor and very poor rock masses. International Journal of Rock Mechanics and Mining Sciences - INT J ROCK MECH MINING SCI. 47. 690-697. <https://doi.org/10.1016/j.ijrmms.2010.04.001>
- Park, Hyuck Jin & Lee, Jung-Hyun & Kim, Kang-Min & Um, Jeong-Gi. (2015). Assessment of rock slope stability using GIS-based probabilistic kinematic analysis. Engineering Geology. 203. <https://doi.org/10.1016/j.enggeo.2015.08.021>
- Perry, Ronald. (2018). Defining Disaster: An Evolving Concept. https://doi.org/10.1007/978-3-319-63254-4_1
- Pierson, L. A., Davis, S. A., and Van Vickie, R.: Rockfall Hazard Rating System – Implementation Manual, Federal Highway Administration (FHWA), Report FHWA-OR-EG-90-01, FHWA, U.S. Dep. of Transp., 1990.
- Pinho, Antonio.B; Andrade, Pedro Santarem; Duarte, Isabel.M.R. (2017). Physical Weathering. In: Bobrowsky, P., Marker, B. (eds) Encyclopedia of Engineering Geology. Encyclopedia of Earth Sciences Series. Springer, Cham. https://doi.org/10.1007/978-3-319-12127-7_219-1
- Piteau, D. R. (1993). "Rock slope stability analysis." Canadian Geotechnical Journal, 30(5), 869-876.
- Proctor, R. G. (1933). "Fundamental Principles of Soil Compaction." Transactions of the American Society of Civil Engineers, 98, 1627-1650.

- Qian, Z.G. & Li, A.J. & Chen, W.C. & Lyamin, Andrei & Jiang, J.C.. (2019). An artificial neural network approach to inhomogeneous soil slope stability predictions based on limit analysis methods. *Soils and Foundations*. 59. <https://doi.org/10.1016/j.sandf.2018.10.008>
- Rahman, M. & Sayem, Abu & Bhuiyan, Dr. Mohammad. (2014). Geochemistry of the Plio-Pleistocene Dupi Tila sandstones from the Surma Basin, Bangladesh: Implications for provenance, tectonic setting and weathering. *Himalayan Geology*. 35. 162-170.
- Rahman, Mohammad. (2022). Natural Hazard and Human induced Hazard: A Discourse of Disaster and Social Vulnerability Analysis. 2. 1-20.
- Rakshit, Raghupratim & Bezbaruah, Devojit & Bharali, Bubul. (2018). Oblique slip faulting associated with evolving central Indo-Burmese region from Early Pleistocene deformational sequences. *Solid Earth Sciences*. <https://doi.org/10.1016/j.sesci.2018.04.002>
- Ralte, Victor & Tiwari, R. & Lalchawimawii, & Malsawma, Jehova. (2011). Selachian fishes from Bhuban Formation, Surma Group, Aizawl, Mizoram. *Journal of the Geological Society of India*. 77. 328-348. <https://doi.org/10.1007/s12594-011-0036-1>.
- Rajkumar HS, Mustoe GE, Khaidem KS, Soibam I (2015) Crocodylian tracks from lower Oligocene flysch deposits of the Barail Group, Manipur, India. *Ichnos* 22:122–131
- Rao RA (1983) Geology and hydrocarbon potential of a part of Assam-Arakan basin and its adjacent region. *Petrol Asia J* 1:127–158
- Rao, Seshagiri. (2020). Characterization, Modelling and Engineering of Rocks and Rockmasses. *Indian Geotechnical Journal*. 50. 1-95. <https://doi.org/10.1007/s40098-020-00414-6>

- Ray, Saon & Jain, Samridhi & Thakur, Vasundhara. (2021). Financing India's Disaster Risk Resilience Strategy.
- Rocscience Inc. (2021). Slide 6.0 - Slope Stability Software User's Manual. Rocscience Inc. Available at: www.rocscience.com.
- Rovins, Jane & Wilson, Tom & Hayes, Josh & Jensen, Steven & Dohaney, Jacqueline & Mitchell, Jon & Johnston, David & Davies, Alistair. (2015). Risk Assessment Handbook.
- Rodriguez, Oscar & Albores, Pavel & Brewster, Christopher. (2018). Disaster preparedness in humanitarian logistics: A collaborative approach for resource management in floods. *European Journal of Operational Research*. 264. 978-993. <https://doi.org/10.1016/j.ejor.2017.01.021>.
- Romana, M. (1985). "New adjustment ratings for the slope mass rating system." *Proceedings of the International Symposium on Rock Slope Stability in Open Pit Mining and Civil Engineering*, 1, 53-64.
- Romana, Manuel & Tomás, Roberto & Serón, José. (2015). Slope Mass Rating (SMR) geomechanics classification: thirty years review.
- Sangeeta, A., Pandey, N., & Kingson, O. (2019). Petrography and tectonic provenance of the Miocene Surma Group in parts of the Naga-Manipur hills, in and around Nungba, Northeast India. *Acta Geochimica*. <https://doi.org/10.1007/s11631-019-00325-1>
- Santi, Paul & Russell, Christopher & Higgins, Jerry & Spriet, Jessica. (2009). Modification and statistical analysis of the Colorado Rockfall Hazard Rating System. *Engineering Geology - ENG GEOL*. 104. 55-65. <https://doi.org/10.1016/j.enggeo.2008.08.009>.
- Saraswat, A., & Choudhury, D. (2018). "Kinematic Analysis of Slope Stability Under Varying Conditions." *Journal of Engineering Geology*, 25(3), 215-228.

- Sardana, Sahil & Verma, Amit & Singh, Anand & Dinpuia, Lal. (2019). Comparative analysis of rockmass characterization techniques for the stability prediction of road cut slopes along NH-44A, Mizoram, India. *Bulletin of Engineering Geology and the Environment*. 78. 1-13. <https://doi.org/10.1007/s10064-019-01493-3>.
- Sardana, S., Verma, A. K., Singh, A., & Laldinpuia. (2019). Comparative analysis of rockmass characterization techniques for the stability prediction of road cut slopes along NH-44A, Mizoram, India. *Bulletin of Engineering Geology and the Environment*, 78(8), 5977–5989. <https://doi.org/10.1007/s10064-019-01493-3>
- Sarkar, S., & Bhattacharya, A. (2008). "Tectonic and sedimentary evolution of the Surma basin and its implications for Mizoram." *Journal of Earth System Science*, 117(1), 15-25
- Sarkar, S., & Choudhury, S. (2015). "Tectonic evolution and geodynamics of the Dauki Fault, Northeastern India." *Journal of Asian Earth Sciences*, 98, 186-196
- Sarkar, S., Kanungo, D.P. & Kumar, S. (2012) Rock Mass Classification and Slope Stability Assessment of Road Cut Slopes in Garhwal Himalaya, India. *Geotech Geol Eng* 30, 827–840. <https://doi.org/10.1007/s10706-012-9501-x>.
- Sarkar, Kripamoy & Buragohain, Bhritashree & Singh, T.N.. (2016). Rock Slope Stability Analysis along NH-44 in Sonapur Area, Jaintia Hills District, Meghalaya. *Journal of the Geological Society of India*. 87. 317-322. <https://doi.org/10.1007/s12594-016-0398-5>.
- Sarma, A., & Sharma, S. (2014). "Lithostratigraphy and depositional environments of the Bhuban Formation, Surma Group, Northeast India." *Journal of Geological Society of India*, 84(5), 719-730
- Sarma, A., & Sharma, S. (2016). "Stratigraphic framework of the Surma Group in Northeast India." *Journal of Earth System Science*, 125(6), 1121-1132

- Saulnier, Dell & Dixit, Amod Mani & Nunes, Ana. (2020). Disaster risk factors: hazards, exposure and vulnerability.
- Schlitz, Nicolas; Jany, Andrea, Saltiel; Saltiel, Rivka; Strüver, Anke (2023). Everyday Disasters in Everyday Lives—Rethinking SDG 11.5 in Times of Multiple Crises. In: Hummel, S., et al. Shaping Tomorrow Today – SDGs from multiple perspectives. Lernweltforschung, vol 39. Springer VS, Wiesbaden. https://doi.org/10.1007/978-3-658-38319-0_4
- Sharif, Amina. (2020). Disaster Types and Causes.
- Sharma, L. K. & Umrao, Ravi & Singh, Rajesh & Ahmad, M. & Singh, T.N.. (2017). Geotechnical Characterization of Road Cut Hill Slope Forming Unconsolidated Geo-materials: A Case Study. Geotechnical and Geological Engineering. 35. <https://doi.org/10.1007/s10706-016-0093-8>.
- Sharma, Pravin & Khandelwal, Manoj & Singh, T.N.. (2011). A correlation between Schmidt hammer rebound numbers with impact strength index, slake durability index and P-wave velocity. International Journal of Earth Sciences. 100. 189-195. <https://doi.org/10.1007/s00531-009-0506-5>.
- Shijoh, Chubala & Pebam, James & Vales, Savio & Singh, L. & Singh, C. & Shijoh, Vekhoto. (2023). Geochemistry and detrital geochronology of sandstones of Barail Group of Indo-Myanmar Range, NE India. Journal of Sedimentary Environments. 8. 1-20. <https://doi.org/10.1007/s43217-023-00142-w>.
- Shrivastava, B.P., Ramchandran, K.K. and Chaturvedi, J.G. (1979). Stratigraphy of Eastern Mizo-Hills/. Bull, ONGC, v.16(2), pp. 87-93.
- Siddique, Tariq & Alam, M. & Mondal, Mohammad & Vishal, Vikram. (2015). Slope mass rating and kinematic analysis of slopes along the national highway-58 near Jonk, Rishikesh, India. Journal of Rock Mechanics and Geotechnical Engin Siddique, T., Pradhan, S. P., & Vishal, V. (2018). Rockfall: A Specific Case of Landslide. Advances in Natural and

Technological Hazards Research, 61–81. https://doi.org/10.1007/978-3-319-77377-3_4eering.7.10.1016/j.jrmge.2015.06.007.

Singh, D. K., & Pati, S. (2014). "Stratigraphy and sedimentology of the Barail, Surma, and Tipam Groups in Northeast India." *Journal of Asian Earth Sciences*, 78, 177-187

Singh, M.Chandra; Kundal, P.; Kushwaha, R.A.S. (2010) Ichnology of Bhuvan and Boka Bil Formations, oligocene-miocene deposits of Manipur Western Hill, Northeast India. *J Geol Soc India* 76, 573–586. <https://doi.org/10.1007/s12594-010-0118-5>.

Singh, Zile. (2020). Disasters: Implications, mitigation, and preparedness. *Indian Journal of Public Health*. 64. 1. https://doi.org/10.4103/ijph.IJPH_40_20.

Sissakian, Varoujan & Jassim, Hamed & Vanarelli, Mark & Omer, Hassan. (2021). Slope Stability Analysis of Haibat Sultan Road Cut, Northern Iraq Using a Field Method. *Iraqi Geological Journal*. 54. <https://doi.org/10.46717/igj.54.1F.9ms-2021-06-29>.

Smith, J. V. (2015). A new approach to kinematic analysis of stress-induced structural slope instability. *Engineering Geology*, 187, 56–59. <https://doi.org/10.1016/j.enggeo.2014.12.015>.

Solanki, Ambar & Gupta, Vikram & Bhakuni, Surendra & Ram, Pratap & Joshi, Mallickarjun. (2019). Geological and geotechnical characterisation of the Khotila landslide in the Dharchula region, NE Kumaun Himalaya. *Journal of Earth System Science*. 128. <https://doi.org/10.1007/s12040-019-1106-9>.

Sonmez, H., & Ulusay, R. (1999). Modifications to the geological strength index (GSI) and their applicability to stability of slopes. *International Journal of Rock Mechanics and Mining Sciences*, 36(6), 743–760. [https://doi.org/10.1016/s0148-9062\(99\)00043-1](https://doi.org/10.1016/s0148-9062(99)00043-1).

Soufi, Amine & Bahi, Lahcen & Latifa, Ouadif & Kissai, Jamal. (2018). Correlation between Rock mass rating, Q-system and Rock mass index based on field

data. MATEC Web of Conferences. 149. 02030.
<https://doi.org/10.1051/mateconf/201714902030>

- Stead, D., & Wolter, A. (2015). A critical review of rock slope failure mechanisms: The importance of structural geology. *Journal of Structural Geology*, 74, 1–23. <https://doi.org/10.1016/j.jsg.2015.02.002>.
- Taheri, A., & Tani, K. (2010). Assessment of the stability of rock slopes by the slope stability rating classification system. *Rock Mechanics and Rock Engineering*, 43(3), 321–333. <https://doi.org/10.1007/s00603-009-0050-4>
- Thakur, V., L'Heureux, J.-S., & Locat, A. (2017). Landslide in Sensitive Clays – From Research to Implementation. *Advances in Natural and Technological Hazards Research*, 1–11. https://doi.org/10.1007/978-3-319-56487-6_1.
- Thiebes, Benni & Bell, Rainer & Glade, Thomas & Jäger, Stefan & Mayer, Julia & Anderson, Malcolm & Holcombe, Liz. (2013). Integration of a limit-equilibrium model into a landslide early warning system. *Landslides*. <https://doi.org/10.1007/s10346-013-0416-2>.
- Tiwari, B., Ajmera, B. (2023). Advancements in Shear Strength Interpretation, Testing, and Use for Landslide Analysis. In: Alcántara-Ayala, I., et al. *Progress in Landslide Research and Technology, Volume 2 Issue 2, 2023*. Progress in Landslide Research and Technology. Springer, Cham. https://doi.org/10.1007/978-3-031-44296-4_1.
- Tiwari, R. & Jauhri, A. Anil. (2014). Miocene Palaeobiology of Mizoram: Present Status and Future Prospect. Special Publication of the Palaeontological society of India.
- Tsuchida, T., Moriwaki, T., Nakai, S., & Athapaththu, A. M. R. G. (2019). Investigation and consideration on landslide zoning of multiple slope failures and debris flows of 2014 disaster in Hiroshima, Japan. *Soils and Foundations*. <https://doi.org/doi:10.1016/j.sandf.2018.12.012>.

- Turner, A. K. (2018). Social and environmental impacts of landslides. *Innovative Infrastructure Solutions*, 3(1). <https://doi.org/10.1007/s41062-018-0175-y>.
- UNDRO, 1980: Natural Disasters and Vulnerability Analysis. Report of Experts Group Meeting of 9-12 July 1979, UNDRO, Geneva, Switzerland. Vulnerability.
- UNDDR, & Dadvar, Maral. (2020). Hazard Definition and Classification Review. <https://doi.org/10.13140/RG.2.2.28232.34561>.
- Varnes, D. J. (1978). "Slope Movement Types and Processes." In *Landslides: Analysis and Control* (pp. 11-33). Transportation Research Board.
- Verma, Amit & Sardana, Sahil & Sharma, Pushpendra & Dinpuia, Lal & Singh, T.N.. (2018). Investigation of rockfall-prone road cut slope near Lengpui Airport, Mizoram, India. *Journal of Rock Mechanics and Geotechnical Engineering*. 11. <https://doi.org/10.1016/j.jrmge.2018.07.007>.
- White, G.F., 1973: Natural hazards research. In: *Directions in Geography* [Chorley, R.J. (ed.)]. Methuen and Co., London, UK, pp. 193-216.
- Xu, Jiancong. (2011). Debris slope stability analysis using three-dimensional finite element method based on maximum shear stress theory. *Environmental Earth Sciences - ENVIRON EARTH SCI*. 64. <https://doi.org/10.1007/s12665-011-1049-1>.
- Yalcin, Ali. (2011). Yalcin, A., —A geotechnical study on the landslides in the Trabzon Province, NE, Turkey, *Applied Clay Science*, 52, 11-19, (2011).. *Applied Clay Science*. 52. 11-19.
- Yang, H., Shi, P., Quincey, D. et al. A Heterogeneous Sampling Strategy to Model Earthquake-Triggered Landslides. *Int J Disaster Risk Sci* 14, 636–648 (2023). <https://doi.org/10.1007/s13753-023-00489-8>.
- Zairemmawii & Lalhlipui, H. & sangi, Lalhming & Vanthangliana, V. & puia, Laldin. (2021). Rockfall Analysis of State Highway along the Southern

Vicinity of Aizawl, Mizoram. Science & Technology Journal. 9.
<https://doi.org/100-112.10.22232/stj.2021.09.02.13>.

Zakaria, Adel. (2009). Hazard Analysis and Risk Assessment.
<https://doi.org/10.13140/RG.2.1.2144.1366>.

BRIEF BIO-DATA

PERSONAL DETAILS

Name : Lallawmsanga

Address : C-83, Zonuam, Aizawl, Mizoram

Email : lawmsanga93@gmail.com

Phone No. : +91 97740 68089

Father's Name : Lalnghakliana

Mother's Name : Lal̥thapuii

Language known : Mizo, English

Marital Status : Unmarried

EDUCATION

Year	Institution	Board	Class	Subject	Division	Percentage
2010	Govt. Mizo High School	MBSE	X	-	First	66.4
2012	Home Missions School	MBSE	XII	Science	Second	55.2
2016	Pachhunga University College	MZU	B.Sc.	Geology	First	74.8
2018	University of Mysore	UOM	M.Sc	Applied Geology	First	75.79
2021	Mizoram University	MZU	Ph.D. (Course Work)	Disaster Management	First	7.57 (SGPA)

PERFORMANCE :

1. Published a paper entitled “Determination of Geological Strength Index and Slake Durability Index of Jointed Rock Mass along Champhai to Zokhawthar Highway”. Science Vision. Vol. 24(2), pages 31–38. <https://doi.org/10.33493/scivis.24.02.02>.
2. Published a paper entitled “Characterization of Residual Soil of Changsari, Kamrup District of Assam, North East India”. Science Vision. Vol. 23 (1), pages 19–24. <https://doi.org/10.33493/scivis.23.01.04>.

PRESENTATIONS

1. Presented a research paper entitled “Assessment and Analysis of Geotechnical Properties Properties of Saron Veng Landslide, Aizawl, Mizoram”. North East Research Conclave (NERC) 2022.
2. Presented a research paper entitled “Rock Mass Characterization and Slope Stability Analysis along State Highway from Champhai to Zokhawthar”. Mizoram Science Congress 2022.
3. Presented a research paper entitled “Slope Stability Analysis along State Highway from Champhai to Zokhawthar Village, Mizoram, India. BEST PRESENTER. Earthquake Prediction- Forecast in Northeast India, 2023.
4. Presented a research paper entitled “Rockfall Hazard Rating System along State Highway from Champhai to Zokhawthar, Mizoram, India” at International Workshop on Geodynamics & Geophysical Methods for Exploration & Geohazards.
5. Presented a paper entitled “Assessment and Analysis of Geotechnical Properties of Landslide: A Case Study of Saron Veng Landslide, Aizawl, Mizoram” at the Online Interaction Programme for Ph.D. Scholars & Post-Doctoral Fellows organized by the UGC - Human Resource Development Centre, Mizoram University during 14th – 20th October, 2021.

TRAINING AND SEMINAR ATTEND

1. One Week Online Faculty Development Programme (FDP) on “Geo-Informatics In Disaster Management” organized by Civil Engineering Department of Jorhat Engineering College, Jorhat-785007, held during 18th – 22th June, 2024.
2. One Week Online Faculty Development Programme (FDP) on “Recent Advances In Structural Engineering And Material Science (RASEMS) on 25th – 29th June, 2024 organized by Civil Engineering Department of Jorhat Engineering College, Jorhat-785007.
3. Online International Conference on Geo-Disasters and Construction Engineering (ICGCE 2024) on June 07-08, 2024, Waterloo, Ontario, Canada.
4. One Week National Workshop on “Importance of Disaster Risk Reduction and Resilience” during 10th – 14th April, 2023 organized by Department of Civil Engineering, School of Engineering & Technology, Mizoram University.
5. Two Days International Workshop on “Psychosocial Adaptation, Disaster Mitigation and Preparedness of Climate Change Affected Communities” on 15th – 16th April, 2023 organized by Department of Social Work, Mizoram University.
6. Online training on "Rapid Urbanisation and Disaster Risk Reduction" from 27 March, 2023 to 29 March, 2023 organized by National Institute of Disaster Management, Ministry of Home Affairs, Govt. of India in collaboration with Central University of Himachal Pradesh.
7. Online Training on “Disaster Risk Reduction” from 21 Sep 2022 to 23 Sep 2022 organized by National Institute of Disaster Management, Ministry of Home Affairs, Govt. of India in collaboration with Research and Development Cell Central University of Jammu (J & K) Jammu.
8. Webinar on "Risk of Urbanisation on Heritage Understanding Impacts and Assessments" on 17 Feb 2023 organized by National Institute of Disaster Management, Ministry of Home Affairs, Govt. of India in collaboration with Intach Bengaluru Chapter.
9. training program on “Landslide Risk Mitigation & Detailed Project Report (DPR) Preparation” organized by Department of Geology, North- Eastern Hill University (NEHU), Shillong, Meghalaya from 23rd to 25th March, 2022.

10. Webinar on “Disaster Management in a Past Covid Society” held on 21st March, 2022 organized by University Grant Commission, Human Resource Development Centre, Mizoram University.
11. National level Webinar on Observing National Science Day 2022 and participated in the lecture of Prof. J.R. Kayal, Dy Director General, GSI (Rtd), Adjunct Professor, organized by Centre for Disaster Management (MZU) in collaboration with Mizoram Science, Technology & Innovation council (MISTIC) held on 1st March 2022.
12. Indo-Chile workshop on “Recent Advancements in Geotechnical Earthquake Engineering” held during 7 Sep – 9 Sep, 2021.
13. National Webinar on ‘Imperial Hegemony and Subaltern Resistance in Mizoram and Subaltern and India’s Freedom Struggle’ organized by Mizoram University on 2nd October, 2021.

PARTICULARS OF THE CANDIDATE

NAME OF THE CANDIDATE : **LALLAWMSANGA**

DEGREE : **Doctor of Philosophy (Ph.D.)**

DEPARTMENT : **Centre for Disaster Management**

TITLE OF THESIS : **Disaster Risk Assessment and Rock Mass
Characterization of State Highway from
Champhai to Zokhawthar, Champhai District,
Mizoram**

DATE OF ADMISSION : **19th August 2021**

APPROVAL OF RESEARCH PROPOSAL:

1. D.R.C : **21st March 2022**

2. B.O.S. : **27th May 2022**

3. SCHOOL BOARD : **10th June 2022**

MZU REGISTRATION : **2100107**

Ph.D. REGISTRATION NUMBER

& DATE : **MZU/Ph.D./1889 of 19.08.2021 Date 10th October 2022**

EXTENSION (IF ANY) :

Head

Department of Geography

ABSTRACT

**DISASTER RISK ASSESSMENT AND ROCK MASS
CHARACTERIZATION OF STATE HIGHWAY FROM
CHAMPHAI TO ZOKHAWTHAR, CHAMPHAI DISTRICT,
MIZORAM**

**AN ABSTRACT SUBMITTED IN PARTIAL FULFILLMENT OF
THE REQUIREMENTS FOR THE DEGREE OF DOCTOR OF
PHILOSOPHY**

LALLAWMSANGA

MZU REGISTRATION NO.: 2100107

Ph.D. REGISTRATION NO.: MZU/Ph.D./1889 of 19.08.2021



**CENTRE FOR DISASTER MANAGEMENT
SCHOOL OF EARTH SCIENCES AND NATURAL RESOURCES
MANAGEMENT**

JUNE, 2025

**DISASTER RISK ASSESSMENT AND ROCK MASS
CHARACTERIZATION OF STATE HIGHWAY FROM
CHAMPHAI TO ZOKHAWTHAR, CHAMPHAI DISTRICT,
MIZORAM**

By

LALLAWMSANGA

CENTRE FOR DISASTER MANAGEMENT

NAME OF SUPERVISOR

Dr. LALDINPUIA

Submitted

**In partial fulfillment of the requirement of the Degree of Doctor of
Philosophy in Disaster Management of Mizoram University, Aizawl**

ABSTRACT

Introduction

Risk assessment and evaluation are essential components of an all-encompassing, proactive risk management program. It speaks about risk transfer, risk minimization, and risk identification. In theory, a hazard is not considered a disaster unless it is triggered by a natural or man-made source. Engineering and management experts use the technical notion of risk to calculate potential losses and the likelihood that a disaster will occur. Although risk and hazard are sometimes interchangeable, risk also refers to the likelihood that a specific hazard may materialize. Disaster risk is the potential for a community to experience losses in terms of people, property, and services. Complex situations combined with man-made or natural hazards might result in losses. The likelihood that these interactions will have unfavorable consequences is ascertained by the risk assessment. Risk assessment includes evaluating the suggested risk reduction strategies from a cost-effectiveness perspective.

A landslide is the rapid movement of earth's material down a slope caused by gravity. It can consist of rock, soil, vegetation, or a combination of these, and it can be caused by either natural or man-made factors. When all of the components that constitute the slope are immobile and unaltered, the slope is said to be stable. Different types of landslides move at quite different rates. Compared to flows, slides move more slowly. Falls and topples happen suddenly and are connected to cliffs or steep grade slopes. The type of slope forming material used and the slip surface's geometry determine how quickly a slope fails. Significant acceleration of motions can happen on brittle material slopes when ground strains above the strain at which peak ground strength is reached. Other materials, like extra sensitive or rapid clays, lose nearly all of their strength when they are remolded, which causes extremely high movement speeds. One of the most harmful natural disasters we encounter in steep terrain is a rockfall, which has affected the slope's stability. A rockfall is defined as a fragment of rock or block that separates from the slope and drops vertically or sub-vertically by rolling on a debris slope or bouncing along trajectories. This can happen

via toppling, sliding, wedging, or falling. The block's dimensions might range from tiny pebbles to enormous cubic meters.

The process of identifying a matrix made up of rock discontinuities and other attitudes is known as rock mass characterization. Numerical, empirical, and analytical methods can be used to differentiate it. The empirical technique is frequently applied to the final design and is utilized for pre-design and feasibility studies. Bieniawski created the Rock Mass Rating classification scheme in 1976. It is regarded as the most trustworthy method for classifying rock masses and is frequently applied in geotechnical engineering to evaluate the quality of rock masses. It is composed of five fundamental parameters: groundwater condition, rock quality designation, discontinuity spacing, discontinuity orientation, and uniaxial compressive strength of intact rock. Based on the field observations and laboratory analysis, the values of Rock Mass Rating can be obtained using the formula where all the parameters are combined to provide a numerical rating score, ranging from 0 to 100. The stability of rock masses is determined by the values of RMR, indicating that the higher values have more stability.

Another method in geotechnical engineering for assessing the various slope collapse modes is kinematic analysis. The primary focus of this analysis is the displacement or movement of rock masses and soil along predetermined failure surfaces. Kinematic analysis aims to pinpoint possible reasons for failure. Planar, topple, and wedge slope failures are among the various types of probable slope collapses that are analyzed using the Rocscience program Dips 7.0.

Location of the Study Area

The study area; Champhai to Zokhawthar State Highway is located in the north-eastern part of Mizoram, India. It is an important route near the India-Myanmar border and serves as a hub for trade and commerce. The district is bounded to the north by the Churachandpur District of Manipur State, to the west by Aizawl and Serchhip District, and the south and east by Myanmar. It stretches from 23°27'22"N to 23°21'55"N latitudes and 93°19'44"E to 93°23'08"E longitudes. Champhai has a temperate climate all year round, with winter temperatures ranging

from 5 to 12 degrees Celsius and summer temperatures from 15 to 30 degrees Celsius. The primary trading hub for products imported from Myanmar via Zokhawthar is Champhai. It holds a significant position in the nation's international trade. The new State Highway alignment from Champhai to Zokhawthar via Melbuk was completed by August 2021 under the aid of World Bank funding. Several earthquake tremors and heavy rainfalls during and after affected the highway construction, which triggered the instabilities of the newly cut-slope. Several massive landslides occurred during October & November 2021 along the road. Thus, studies of cut slope instabilities, risk, and vulnerability assessment are the utmost needs for the safety of present and future Indo- Myanmar trade networks.

The Mizoram Fold Belt (MFB) of the Tertiary sedimentary sequence is the easternmost extension of the Surma basin. It is separated into three groups: the Tipam Group belonging to the late Miocene to Early Pliocene Age, the Barail Group belonging to the Oligocene Age, and the Surma Group belonging to the Upper Oligocene to Miocene Age. The longitudinal folds that make up MFB form a long, narrow anticline, while the broad, well-developed synclines that are connected with it. From Champhai to Zokhawthar, the lithology is part of the Barail group and is made up of alternating bands of sandstones, shales, and siltstones. The litho-units of the sedimentary structures indicate an environment of shallow marine depositional depths, and they are coarsening upward.

Scope of the Study

There have been numerous notable faults in this hilly region, which is situated in the Indo-Burmese plate's convergent plate border. Because it is young, the sedimentary strata is juvenile, and the folds have low lithification. Excessive precipitation results in a surface runoff of unchanneled water, most of which seeps into the soil and weakens the stability of the rock and soil. The land becomes susceptible to sliding as a result of the weakened cohesion of the soil caused by over-infiltration. The slope's strength has been diminished by the joints and local faults, making rockfall, rock slide, debris avalanche, earthflow, and creep—particularly on high-angle slopes—extremely vulnerable.

Anthropogenic activities, such as road construction, habitation, and other slope-management-related activities, are the main cause of landslides in mountainous regions. Studying the properties of the rock mass is so crucial. We can better comprehend the nature of topography and create sound recommendations for reducing and averting possible hazards by conducting a thorough investigation of the geotechnical characteristics of rock and soil.

In steep terrain, primary routes for importing requirements are the road and highway networks. An important route for international trade, specifically from India to Myanmar, runs through the study region along the State Highway from Champhai to Zokhawthar. Under World Bank Projects, the State Highway construction via Melbuk was finished in August 2021. However, a week of intense rain in November caused roughly fifteen large landslides to occur along the state highway's recently cut slopes, blocking the route. Because slope instability leads to issues with traffic, injury and even death in certain areas, and environmental degradation, cut slope stability around highways and roads is a major concern. A geotechnical investigation of landslides and a vulnerable area along the cut slope helps to understand the problem and give remedial measures for the stability of the slope.

Objective of the Research

1. To study the disaster vulnerability and risk assessment of the study area;
2. To determine the geotechnical properties of soil and rock mass characteristics;
3. To determine the cut slope stability analysis using numerical analyses;
4. To suggest mitigation and preventive measures for the study area.

Methodology

The foundation of every scientific investigation is its research technique, which offers an organized framework for data collection, analysis, and interpretation. This section explains the systematic technique used in this study to investigate the characteristics of the rock mass, the geotechnical properties of the soil, and areas of risk. In order to comprehend the research area, a combination of qualitative and quantitative methodologies is used. Combining these methods enables a

comprehensive investigation that yields rich, contextual insights and quantifies important variables.

As per IS: 2720 (Part 5), the Atterberg limit test is carried out. It is employed to ascertain the moisture content of the soil at which silty and clay soil move through distinct stages. It is employed to determine the soil sample's plastic limit (PL), liquid limit (LL), and shrinkage limit (SL). The Casagrande apparatus is used to determine the liquid limit. In order to determine the plastic limit of the soil, alternate rolling and kneading must be done until the thread collapses under pressure; this usually happens when the diameter is greater than 3 mm. The amount of water in the soil represented as a percentage of the total dry weight is what determines the soil's natural water content. The Plasticity Index is obtained by calculating the difference between the liquid limit and plastic limit of the soil.

As per IS: 2720 Part VII-1980, a laboratory test called the Proctor compaction test is performed to find the ideal moisture content (OMC) at which soil will become the most compact and reach its maximum dry density.

The direct shear test is performed as per IS: 2720 (Part 13)-1986. It is techniques for determining the soil's shear strength parameters, especially cohesion (c) and angle of internal friction (ϕ).

As per IS: 10050 -1981, slake durability test is to be carried out to measure the rock resistance to disintegration in a slaking fluid as a result of drying and wetting.

The Limit Equilibrium Method (LEM) is the basic method used in geotechnical engineering to ascertain slope and structural stability in soil mechanics. Determining whether the slope or structure is stable or unstable is the primary objective of this method. Rocscience Software Slide 6.0 can be used for LEM analysis. The study area can be analyzed using the GLE/Morgenstern Price Method, Janbu Method, Bishop Method, and Ordinary/Fellenius Method. The purpose of the analysis is to provide the safety factor. The total force acting along an assumed plane to prevent failure is compared to the total force acting to cause some areas of the slope to slide.

Rock Mass Rating (RMR) is a method used in geotechnical engineering and rock mechanics to evaluate the stability and quality of rock masses. It consists of five parameters for classifying the properties of rock masses; (a) Uniaxial Compressive Strength (UCS) of the Rock is the maximum axial compressive stress that a rock mass can withstand under zero confining stress, (b) Rock Quality Designation (RQD) is a qualitative evaluation of the degree of jointing in a rock mass for drilled core that is at least 10 cm in length. If coring is not possible, the Volumetric Joint Count (Jv) method can be used to determine the result, (c) Condition of discontinuities/ Joint condition assesses the nature of fractures, spacing, and condition of the discontinuities within rock masses, (d) Joint spacing is the spacing and nature of fractures, joints, and other discontinuities within the rock mass are described by this characteristic. It is divided into five categories, ranging from continuous and close to widely scattered and open. It is a measure taken in perpendicular of a distance between two adjacent discontinuities or between the joints of the same set. (e) Ground water condition is the existence and behaviour of groundwater within the rock mass is assessed.

Geological Strength Index (GSI) is a geomechanical classification scheme used to examine the quality and mechanical behavior of rock masses. It includes a numerical evaluation of the engineering properties and failure rate of a rock mass. Based on visual field examination, it is defined by two characteristics: surface condition rating (S.C.R.) and structure rating (S.R.). The roughness, weathering, and infilling ratings determine the SCR, whereas the volumetric joint count determines the SR.

Kinematic analysis is used to evaluate the safety and stability of slopes under different conditions and to identify probable slope failure mechanisms. This method of geotechnical engineering addresses slopes that are created naturally or artificially. It entails determining probable slope collapse triggers and observing the movement of rock masses and soil along predetermined failure surfaces.

Slope Mass Rating is a classification system for rock slopes that is used for stability analysis, slope design, and slope support. It is a tool for classifying slopes

according to their susceptibility to instability and for analyzing the stability of rock slopes. It is founded on a thorough field research that includes data gathering about the orientation of discontinuities pertaining to the slope and the technique used to excavate the cut-slope.

RockFall Hazard Rating System (RHRS) is an approach used to evaluate and categorize the risk posed by rockfalls in a particular location. This method aids in the identification of possible risk areas, the design of mitigation techniques, and the maintenance of infrastructure and staff safety. It is a systematic technique for evaluating the risk and possible outcomes of rockfall events in a specific location. Large boulders break free from cliffs and mountainous terrain in a rapid movement, creating natural rockfalls. These incidents endanger the lives of individuals as well as infrastructure and travel routes. Understanding potential risks and putting in place suitable mitigation measures are made easier with the aid of a rockfall hazard study.

The peak monsoon in Mizoram occurs from May to September. When saturated conditions of the soil arise, it leads to a decrease in the shear strength of the soil. The water seeps into the soil and fractures the rock, which increases the pore pressure that affects the stability of the slope. A comparative analysis of rainfall data and the frequency of landslides reveal that rainfall is another important cause. In Mizoram, the major landslides from the past are mainly rainfall-induced.

Results and Discussions

By performing in-depth visual assessments of the sites, field investigations were carried out in the area of interest to determine the failed slopes and vulnerable instability variables, such as topography, geology, vegetation, drainage patterns, and landslide evidence. Samples of rock and soil were taken from the field and examined in the laboratory. LS1, LS2, LS3, LS4, LS5, and LS6 are the locations of the six massive landslides that are examined using the limit equilibrium method (LEM). For the purposes of analyzing slope stability, vulnerability, and characterizing the rock mass, seven slopes (S1, S2, S3, S4, S5, S6, and S7) have been chosen. Various techniques, including Rock Mass Rating, Kinematic Analysis, and Slope Mass Ratings are used. Six slopes are assessed for the Rockfall Hazard Rating; R1, R2, R3,

R4, R5, and R6. The kinetic energy, translational energy, bounce height, and run-out distance of detached rock fragments are all examined using the Rocscience Software Rocfall 4.0.

For determining the Atterberg Limit, soil samples were taken from six different places, and their natural moisture content (NMC) varies, suggesting that the soils have varying compaction, strengths, and stiffness. Sample 2 (LS2), or location 2, has the lowest liquid limit of 20.23%, while sample 5 (LS5), or location 5, has the highest liquid limit of 43.68. Sample 2 (LS2), or location 2, has the lowest plastic restriction at 17.70%, whereas sample 5 (LS5), or location 5, has the highest plastic limit at 31.89%. The plasticity indices are derived from the plastics and liquid limits. While sample 1 (LS1), sample 3 (LS3), sample 5 (LS5), and sample 6 (LS6) are classed as medium plastic, samples 2 (LS2) and 4 (LS4) are classified as somewhat plastic. The liquidity index and consistency index are categorized as medium stiff for samples 3 and 6, whereas stiff for samples 1, 2, 4, and 5 based on Sower's (1979) classification.

From the direct shear test, sample 4 (LS4) has the lowest cohesion (0.27 kg/cm²), while sample 3 (LS3) has the highest cohesion (0.392 kg/cm²). The cohesion of the remaining samples, i.e., samples 1 (LS1), 2 (LS2), 5 (LS5), and 6 (LS6), is 0.216 kg/cm², 0.163 kg/cm², 0.27 kg/cm², and 0.168 kg/cm², in that order. Sample 6 (LS6) has the lowest internal friction angle (7.26°), whereas sample 5 (LS5) has the highest angle (40.29°). The internal friction values of the remaining four samples, LS1, LS2, LS3, and LS4, are 21.86°, 22.04°, 9.99°, and 17.84°, respectively.

The Limit Equilibrium analysis is performed based on the unit weight, strength type, cohesion, and angle of friction. Based on the observation, the factor of Safety for each cut-slope that is less than 1, indicating that the research area is unstable and highly susceptible to sliding when completely wet and saturated. The Janbu Simplified Method for slope LS1 has the lowest factor of safety (0.488) among the assessments performed using the various methods, whereas the Bishop Simplified Method's slope LS2 has the highest factor of safety (0.859). For LEM analyses using

different methods, the overall Factor of Safety for each slope, i.e., LS1, LS2, LS3, LS4, LS5, and LS6, Janbu Simplified Method has the lowest, whereas Bishop Simplified Method has the highest Factor of Safety.

From the Rock Mass Rating (RMR), four locations—S1, S2, S3, and S7—have RMR values of 57, 59, 57, and 44, respectively, where Class III of a fair rock description were assigned to the four locations. One week is the average stand-up time for a five-meter span. The average cohesiveness and the angle of friction fall into the 200–300 and 25–35 ranges, respectively. Locations S4, S5, and S6 are classified as having poor rock description (class IV) with RMR values of 28, 33, and 29, respectively. For 2.5 meters, the average stand-up period is 10 hours, with a cohesiveness of 100–200 and an angle of friction of 23–35. The algebraic sum of the numerical values assigned for each parameter is low and corresponds to less favorable conditions for site development.

The Geological Strength Index ranges from 42 to 54, based on Structure Ratings and Surface Condition Ratings. From the overall observation, the study site spot 2 has the greatest, while study site spot 6 has the lowest GSI value.

From the Kinematic Analysis using Dips 7.0, the probable slope failures were examined as wedge and direct toppling. While S3, S5, S6, and S7 indicate a potential wedge failure, S1, S2, and S4 demonstrate a potential direct toppling failure. Weak joints and weak rock strength increase the likelihood of slope failure.

The overall Slope Mass Rating (SMR) scores for locations S1, S2, and S3 are 51, 53, and 48, respectively. The three areas are classified as class III, with a standard rock mass description of 0.4 out of 1 probability of failure, having a planar, along with several joints, and wedges. Location S5 has an overall SMR score of 27 and S4 has a score of 28, both of which fall into class IV with a poor rock description and a planar or big wedge failure probability of 0.6 out of 1. The total SMR scores for locations 6 and 7 are 20 and 19, respectively. The two places have an extremely unsatisfactory rock description of 0.9 chance of failure and are classified as class V.

From the Rockfall Hazard Rating System, the slope angles which ranges from 58° to 82°, suggests that there is a good chance that rocks will fall along the road.

Undercutting erosion is observed to a length ranging from 0 to 0.6 meters as a result of differential erosion. As a result, there is a greater risk that rock could fall if the undercutting is prolonged to weathering and erosion. There is no ditch catchment at locations R1, R3, R5, and R6, and the ditch length is comparatively short at sites R2 and R4, which reduces the likelihood that falling rock blocks would halt. The resistance of rock to weathering is demonstrated by the slake durability index, which shows a very high mean score of 91.45% following the second cycle. From the cumulative score, R2 is considered low urgency (i.e., <300), R1, R4 and R6 are considered to be of moderate urgency (i.e., 300–500), while R3 and R5 are of high urgency (i.e., >500) and are at risk of rock falls.

From the numerical simulation, the kinetic energy, translational energy, and bounce height of rock blocks falling freely are determined. R5 has the highest bouncing height, measuring 4.43 meters, after hitting the ground. At R4, the maximum kinetic energy is 7036.31 joules, and the highest translational energy is 23.59 m/s. As they tumble down the slope, heavy granite blocks have more kinetic energy, which puts both people and vehicles at risk.

Limitations

Slope stability can be greatly affected by the complex geological structures, which includes numerous folding, joints and fractures. The existence and intercalations of many geological formations and rock types could hinder assessments and make it difficult to generalize the conclusions to different areas.

The ratings in the RHRS tables are based on generalizations that could not apply to particular geology and climate. Slope aspect toward the west is rated with 3 points, whereas slope aspect toward the east is rated with 81 points. The ratings might not apply to a given set of geological and climatic conditions of Mizoram, since lithological variations over short distances can result in notable differences in rock stability and behavior. It could be necessary to modify or adjust the RHRS in order to better fit the unique geological and environmental conditions of Mizoram.